WITS
UNIVERSITY

# Discovering potential inhibitors for *Plasmodium falciparum* and *vivax* glutathione transferases through systematic integration of empirical with theoretical studies

---


**by**

**Onisuru Olalekan**

**Student number: 2430435**


**Thesis**

submitted in fulfilment of the requirements for the degree of a

**Doctor of Philosophy**

in

**Molecular and Cell Biology**


in the Faculty of Science, University of the Witwatersrand, Johannesburg, South Africa

Supervisor: Prof Ikechukwu Achilonu


August 2024

## Declaration

I, Olalekan Onisuru (student number 2430435) who is submitting for a PhD (Doctor of Philosophy) in Biochemistry and Cell Biology, from the Protein Structure-Function Research Unit (PSFRU) of the School of Molecular and Cell Biology (MCB), Faculty of Science, at the University of the Witwatersrand, South Africa

I hereby declare the following

- I am in full knowledge of the meaning, implications, and consequences of plagiarism, which is the unauthorized or unpermitted use of another person's work without acknowledging it.
- I affirm that this thesis being submitted for examination in respect of the above degree is my original and unsupported work.
- I have complied with the required referencing format while referencing the thoughts and ideas of others in buttressing mine.
- I am fully aware that the University of the Witwatersrand seriously frowns at plagiarism and may take disciplinary action against me on the ground that I have consciously or unconsciously failed to acknowledge the source of my idea or word while writing.

Signature: ----------

Date: August 2, 2024

## Dedication

This study is dedicated to the All-Sufficient and Almighty God for providentially enabling me to undertake this program successfully. To my dear wife and best friend, Dr (Mrs) Oluwatayo Racheal Onisuru for making this journey a worthy one. To Anthony and Glory of God Onisuru, God's precious gifts to me as children, who paid the most incredible price of denial of my full presence and attention as a father. To my irreplaceable God's family, Deeper Life Campus Fellowship, South Africa, for prayerfully and financially standing by me. To my loving parents, whose fervent prayers and immense show of love from home kept me going.

**Acknowledgements**

Foremostly, I want to express my deepest appreciation to the only wise God, the giver of salvation, wisdom, strength, and success. Without your grace and blessings Lord, this feat would not have been possible. So, it is with humility and gladness of heart that I say thank you Lord for the hope of the possibility of successfully completing this degree.

My sincere appreciation goes to my supervisor, Prof Ikechukwu Achilonu for being a worthy mentor, supervisor, and role model. I will always be grateful for your selfless and sacrificial financial support throughout the course of my study. I particularly acknowledge your guidance, care, and patience in providing robust supervision. Your supervisory model and training are exceptional. Thank you, sir.

I truly acknowledge my graduate advisor and the director of Protein Structure-Function Research Unit (PSFRU), Prof Yasien Sayed, for providing an enabling environment for first-class research in the unit. I appreciate his leadership skills and express the same deep appreciation to the unit's management committee for always ensuring students' research is seamlessly carried out with excellent results as the ultimate goal.

I want to profoundly acknowledge and deeply appreciate my jewel of inestimable value and dear wife, Dr(Mrs) Oluwatayo Racheal Onisuru. I will be eternally grateful to God for you as my wife. I am more than blessed to always have you and your love as a bedrock, your simplicity in selflessly giving yourself to this union God himself instituted. God bless you for always looking after my well-being, and success, excellently taking care of the home front and our priceless gifts of children from God, Anthony Ayomilekan Onisuru and Glory of God Olaoluwatayo Onisuru. Their love, understanding, sacrifices, prayers, and kind words always brightened the way in making my research a historic one.

To this warm and loving family of God's people, I met and know here in South Africa, Deeper Life Campus Fellowship and Deeper Life Bible Church, your generous show of love and demonstration of biblical brotherliness further entrenched my faith in the veracity of the scriptures and heaven. I particularly acknowledge Pastor (Prof) Oyerinde and his amazing wife Dr (Mrs)

Rebecca Oyerinde for their selfless and sacrificial support to me, my program, and my family. In the same breath, I heartily appreciate the care and warmth of Pastor (Prof) Adelowotan and his lovely wife Dr (Mrs) Adelowotan for their prayers, support, and solidarity all the way. To Pastor (Dr) Peter Olukanmi and his preciously loving wife, Dr(Mrs) Olukanmi, I say a big thank you sir and ma. Your prayers and support form an integral part of this achievement. I am deeply appreciative of all members of DLCF Wits, DLCF UJ and DLBC South Africa. Words and space will fail me to singly acknowledge and appreciate everyone's immense contribution and support towards the success of my PhD.

To my biological family, my heartfelt gratitude and appreciation goes to you all. You all made me proud of the family I come from. The individual and collective support, tangibly and intangibly, goes a long way in bringing me to this pivotal point in my studies. A special mention is worthy of note of my dear father (Mr Zebulon Ojo Onisuru) and mother (Mrs Olufunmilayo Florence Onisuru), who has been my pillar of support all the way. May the good Lord bless you with sound health and long life. A special thanks to my mother-in-law, Deaconess Agnes Owolabi, and my brothers and sisters-in-law, I will always cherish your support and the incredible show of love and support to me and my immediate family. My dear brother and best friend, Suleiman Ahmed, his lovely wife, Mrs Foluke Ahmed, and their lovely children are not just a family but are treasurable, priceless and an integral part of this PhD journey. Time will fail me to thank and appreciate Prof Adeyemi and Mrs Ajibike's family for their immense support; thank you a million times, sir/ma.

To all members of teaching and non-teaching staff of the School of Molecular and Cell Biology. I heartily acknowledge and express my sincere appreciation to you all. My undeniable appreciation goes to all PSFRU family and friends. You taught me, showed me love and cared for me most professionally. Special thanks to Mrs Olamide Jeje and Ms Marushka Soobben who are my dependable research group members and mates, Dr Blessing, Dr Aloke, Dr Sarah, and Dr Emmanuel for their support.

**Keywords**

*Plasmodium falciparum* Glutathione *S*-Transferase; *Plasmodium vivax* Glutathione *S*-Transferase; malaria; antimalarial; parasite; artemisinin-based combination therapy; drugs; binding; inhibitors; inhibition; bromosulfophthalein; natural compounds; flavonoids; ligand; ligandin; spectroscopy; fluorescence; protein expression; structure; target; empirical studies; molecular dynamics simulation; molecular docking; stability; high-throughput virtual screening.

## List of Publication and manuscripts under review

**Olalekan Onisuru and Ikechukwu Achilonu**, Describing the ligandin properties of *Plasmodium falciparum* and *vivax* glutathione transferase towards Bromosulfophthalein from empirical and computational modelling viewpoints. *Journal of Biomolecular Structure and Dynamics*, March 2024 (Published)

**Olalekan Onisuru and Ikechukwu Achilonu**, Targeting Phase II Detoxification Enzyme Inhibitor in *Plasmodium* for Malaria Treatment. (Manuscript under review at Molecular and Biochemical Parasitology).

**Olalekan Onisuru and Ikechukwu Achilonu**, Characterizing the ligandin properties of *Plasmodium falciparum* and *vivax* glutathione transferase towards selected antimalarial drugs. (Manuscript under review at Molecular and Biochemical Parasitology)

**Olalekan Onisuru and Ikechukwu Achilonu**, Discovery of probable inhibitors of *Plasmodium falciparum* and *vivax* glutathione transferase through high-throughput virtual screening of a flavonoid library using bromosulfophthalein as the benchmark ligand. (Manuscript in preparation to be submitted to Computational Biology and Chemistry)

## Table of Contents

Table of Contents

Declarations ……..i

Dedication ……ii

Acknowledgements ……iii

Keywords ……v

List of Publication and manuscripts under review ……vi

Table of Contents ……vii

List of Figures ……xxi

List of Tables ……xviii

Abbreviations ……xix

Abstract ……1

Chapter I: Introduction ……3

1.1: Problem statement…… 5

1.2: Rationale……6

1.3: Aim and objectives……7

1.5: Thesis outline……8

References……9

Chapter 2: Literature review……...14

2.1. Malaria: Africa and Global burden …….14

2.2. Malaria Parasite Life Cycle: Complexities and Pathogenesis……...……..17

2.3. Malaria: Treatment and Resistance…….18

References…… 19

Introduction to manuscript 1…… 26

Targeting Phase II Detoxification Enzyme Inhibitor in *Plasmodium* for Malaria Treatment…...27

Challenge of Unmitigated Malaria Burden……..28

Contemporaneity of Malaria Treatment……30

Complexity associated with Malaria Treatment and Elimination…….32

Criticality of GSTs in *Plasmodium falciparum* and *Plasmodium vivax*……...34

Concept of Biotransformation and Phase II Detoxification in *Plasmodium* Parasite……...36

Containing malaria through Phase II Detoxification enzyme inhibition in *Plasmodium* Parasite..38

Conclusion on the significance of targeting Phase II Detoxification enzyme in *Plasmodium*…...39

References……..41

Chapter 3: Transformation, Recombinant Expression, Purification, Quantification, and Characterization of *Plasmodium falciparum* and *Plasmodium vivax* Glutathione *S*-Transferase……56

3.1.Introduction……..57

3.2 Materials……. 57

3.3 Methods…….. 58

3.3.1 *Pf*GST and *Pv*GST's Transformation and Recombinant Expression.……59

3.3.2 Chromatographic Purification of *Pf*GST Protein……59

3.3.3 Spectrophotometric and Electrophoretic Quantification of *Pf*GST and *Pv*GST Proteins...60

References……61

Chapter 4. Introduction to manuscript 2.…….…….65

Characterizing the ligandin properties of *Plasmodium falciparum* and *vivax* glutathione transferase towards selected antimalarial drugs……..66

Abstract…….. 67

1. Introduction……... .68

2. Materials and methods…….. .70

2.1 Materials……70

2.2. Recombinant overexpression of *Pf*GST, *Pv*GST in *E.coli* and purification……....70

2.3. *Pf*GST and *Pv*GST's enzymatic and inhibitory assay with antimalarials……....71

2.4. Antimalarial drug biotransformation assay with Glutathione, *Pf*GST, and *Pv*GST…….72

2.5. Antimalarial's ligandin and binding to *Pf*GST and *Pv*GST……72

2.6. Antimalarials' effect on the thermal stability of *Pf*GST and *Pv*GST by thermal shift assay…….72

3. Results…….....74

4. Conclusion……..90

References……...91

Chapter 5. Introduction to manuscript 3.…….……97

Describing the ligandin properties of *Plasmodium falciparum* and *vivax* glutathione transferase towards Bromosulfophthalein from empirical and computational modelling viewpoints…....98

Abstract…….....99

1. Introduction…… 100
2. Materials and methods…….102
2.1. Materials……..102
2.2. Methods……...102
2.2.1. Recombinant overexpression of *Pf*GST, *Pv*GST in *E.coli* and purification…….102
2.2.2. Enzymatic and inhibitory assay of *Pf*GST and *Pv*GST……103
2.2.3. Extrinsic ANS fluorescence spectroscopic analysis of *Pf*GST, *Pv*GST, and BSP complex…….103
2.2.4. Stability elucidation of *Pf*GST, *Pv*GST, and BSP complex by thermal shift assay..104
2.2.5. *Pf*GST and *Pv*GST's Steady-state kinetics determination……105
2.3 Computational studies……...105
2.3.1. Computational software and hardware....…….105
2.3.2 Apo *Pf*GST, *Pv*GST, and ligand preparation……105
2.3.3. Computational-based drug-likeness and ADMET predictions…….106
2.3.4. Induced fit ligand docking...…….107
2.3.5. Molecular dynamic simulation...……..107
2.3.6. Post dynamic analyses...……...108
2.3.7. Post-simulation MM/GBSA binding free energy calculations…….109
2.3.8. Principal component analysis……...…110
3. Results and discussions…….110
3.1. Recombinantly heterologous overexpression of *Pf*GST, *Pv*GST and purification...110
3.2. Enzymatic and inhibitory assay of *Pf*GST and *Pv*GST……111
3.3. Extrinsic ANS fluorescence spectroscopic analysis of *Pf*GST, *Pv*GST, and BSP complex…….112
3.4. Stability elucidation of *Pf*GST and *Pv*GST in the presence of BSP and/or GSH by thermal shift assay……..114
3.5. *Pf*GST and *Pv*GST's Steady-state kinetics studies……115
3.6. Computational studies result and discussion…….....117
4.0. Conclusion…….....130
References……..132
Chapter 6: Discovery of probable inhibitors of *Plasmodium falciparum* and *vivax* glutathione transferase through high-throughput virtual screening of a flavonoid library using bromosulfophthalein as the benchmark ligand

Abstract……..……141
1. Introdduction……..142
2. Materials and methods…… ..144
2.1. Computational studies……...144
2.1.1 Computer hardwares……...144
2.2. Ligand and protein preparation…….144
2.3. High-throughput virtual screening……145
2.4. Induced-fit ligand docking……146
2.5. Molecular dynamics simulations and post-dynamic analyses……..146
2.6. Molecular mechanics/generalized born and surface area solvation (MMGBSA) calculations……147
3. Results and discussion……...148
3.1. HTVS analysis of flavonoid compound's potential inhibitor of *Pf*GST and *Pv*GST.148
3.2. Induced fit docking of BA and TTMF respectively to *Pf*GST and *Pv*GST……151
3.3. Molecular dynamics simulation and post-dynamic analysis of *Pf*GST, *Pv*GST, *Pf*GST:BA, and *Pv*GST:TTMF……..152
3.4. Molecular mechanics/generalized born and surface area solvation (MMGBSA) Analysis……..156
4. Discussion……...157
References……158
Chapter 7: Summary and conclusion of the study……164
Limitation of the study…….166
Future Perspective……166

## List of Figures

### Chapter 1

Figure 1. The World Health Organization, World Malaria Report for the year 2023's statistical representation of global malaria morbidity and mortality rate between the year 2019 – 2022 showing slight decline in mortality rate but 5 million increment in the mortality rate.

Figure 2. The World Health Organization, World Malaria Report for the year 2023's statistical representation of global malaria morbidity and mortality rate for the year 2022 showing (A). morbidity rate per country, and (B). 608,000 mortality rate distribution across countries.

### Chapter 2

Figure 1: Pictorial summary of different antimalarials that has been developed and the enzymes/genes they respectively target.

Figure 2: A schematic illustration of biotransformation/detoxification of xenobiotics through phase I and phase II reaction mechanisms

### Chapter 4

Fig. 1. Schematic description of the transformation procedure, recombinant overexpression, and purification processes of *Pf*GST and *Pv*GST. The construct's transformation in BL21(DE3) competent cells were successful as evident from the yield of single and distinct colonies on the LB plates. The 0.50 mM IPTG overexpressed protein was successfully purified using a one-step IMAC procedure. The *Pf*GST and *Pv*GST proteins were found to be pure, and their sizes correspond to the approximately 25 kDa theoretical sizes.

Fig. 2A. Characterizing *Pf*GST and *Pv*GST with respect to their specific enzymatic activities through a GSH-CDNB conjugation model assay characteristics of GST in a reaction buffer containing 100 mM $NaH_2PO_4$ at pH 7.2, 1 mM EDTA, 1 mM DTT,

5 mM GSH at pH 6.5, 30 mM CDNB. Each sample with varying concentrations were spectroscopically monitored. *Pf*GST's specific enzymatic activity (**black**) and *Pv*GST's specific enzymatic activity (**green**) were determined to be 37.90 µmol/min/mg and 35.33 µmol/min/mg respectively. The $R^2$ value of approximately 1 attest to the validity of the standard curve.

Fig. 2B-2I. Characterizing the respective *Pf*GST and *Pv*GST's specific enzymatic activities with respect to artemisinin (B and C), artesunate (D and E), artemether (F and G), and pyrimethamine (H and I). These characterizations similarly followed a GSH-CDNB conjugation model assay, which is typical of a GST enzyme activity assay. A 1 mM constant concentration of artemisinin, artesunate, artemether, and pyrimethamine alongside varying concentration of *Pf*GST and *Pv*GST in evaluating the inhibitory effect of the specific enzymatic activities. The reaction buffer similarly contains 100 mM $NaH_2PO_4$ at pH 7.2, 1 mM EDTA, 1 mM DTT, 5 mM GSH at pH 6.5, 30 mM CDNB. The plots show the spectroscopic monitoring of *Pf*GST's specific enzymatic activity (**black**), *Pf*GST's specific enzymatic activity in the presence of the drugs (**red**), *Pv*GST's specific enzymatic activity (**green**), and *Pv*GST's specific enzymatic activity in the presence of the drugs (**blue**). The $R^2$ value of approximately 1 attest to the validity of the standard curves.

Fig. 3. A UV-Vis spectrophotometric characterization of *Pf*GST and *Pv*GST's respective biotransformation potential towards artemisinin (**A** and **B**), artemether (**C** and **D**), artesunate (**E** and **F**), amodiaquine (**G** and **H**), lumefantrine (**I** and **J**), mefloquine (**K** and **L**), and pyrimethamine (**M** and **N**). The respective drug spectra measurements (orange) and the spectra measurements of PfGST and PvGST (dotted grey lines) showing light absorption at 280 nm are also revealed. The spectra measurements of GSH-drug incubated samples **(purple),** *Pf*GST or *Pv*GST incubated drug samples (**black**) and *Pf*GST or *Pv*GST and GSH incubated drug samples (**red**) are herein figuratively represented.

Fig. 4. Ligandin activity of *Pf*GST and *Pv*GST through ANS fluorescence spectroscopy towards artemisinin (**A** and **B**), artemether (**C** and **D**), artesunate (**E**

and **F**), amodiaquine (**G** and **H**), lumefantrine (**I** and **J**), mefloquine (**K** and **L**), and pyrimethamine (**M** and **N**) and their effect on *Pf*GST and *Pv*GST's tertiary structural conformation. A spectrofluorometric monitored ANS fluorescence emission at 395 nm excitation showing the emission spectrum of free ANS **(grey dotted lines)**, ANS bound *Pf*GST **(black)** and ANS bound *Pv*GST **(green)**. The respective antimalarial complexed *Pf*GST's emission spectrum is represented in **(red),** and *Pv*GST complexed antimalarials are **(blue)**. A reduced GSH was added as a *Pf*GST and *Pv*GST protein in all the samples monitored.

**Chapter 5**

Fig. 1. Schematic description of the recombinant overexpression and purification processes of *Pf*GST and *Pv*GST. The construct's transformation in BL21(DE3) competent cells were successful as evident from the yield of single and distinct colonies on the LB plates. The 0.50 mM overexpressed was successfully purified using a one-step IMAC procedure. The *Pf*GST and *Pv*GST proteins were found to be pure, and their sizes correspond to the approximately 25 kDa theoretical sizes.

Fig. 2. Characterization of *Pf*GST and *Pv*GST in terms of their enzymatic specific activity in the presence and absence of BSP through a GSH-CDNB conjugation assay (100 mM $NaH_2PO_4$ pH 7.2, 1 mM EDTA, 1 mM DTT, 5 mM GSH pH 6.5, 30 mM CDNB, and 1 mM BSP) monitored spectroscopically showing *Pf*GST's specific activity **(black)**, *Pv*GST's specific activity **(green),** *Pf*GST:BSP's specific activity **(red)**, and *Pv*GST:BSP's specific activity **(blue)**.

Fig. 3. Ligandin activity of *Pf*GST and *Pv*GST through ANS fluorescence spectroscopy towards BSP and its effect on their tertiary structural conformation. A spectrofluorometric monitored ANS fluorescence emission at 395 nm excitation showing (A) emission spectrum of free ANS **(grey)**, ANS bound *Pf*GST **(black)** and ANS bound *Pv*GST **(green)**, (B) BSP complexed proteins' emission spectrum of *Pf*GST:BSP **(red)** and *Pv*GST:BSP **(blue)**, (C) reduced GSH incubated protein's emission spectrum of *Pf*GST-GSH **(black)** and *Pv*GST-GSH **(green)**, and (D) BSP

complexed and GSH incubated proteins' emission spectrum for *Pf*GST:GSH:BSP **(red)** and *Pv*GST:GSH:BSP **(blue)**

Fig. 4. Profiles for the thermal stability using melting peak temperature of *Pf*GST and *Pv*GST in the presence and absence of GSH and BSP at temperatures between 25 – 65 °C using a qPCR differential scanning fluorimetry evaluation. The fluorescence thermal shift assay was carried out in 100 mM $NaH_2P0_4$, 1 mM DTT, and 1 mM EDTA, pH ± 1 mM GSH, ± BSP, with the sample monitored in triplicate. The derived -d(RFU)/dT against temperature (◦C) plots showing melting peak temperature *Tm* in ºC of (A) *Pf*GST (**black**) and *Pv*GST (**green**), (B) *Pf*GST:GSH (**black**) and *Pv*GST:GSH (**green**), (C) *Pf*GST:BSP (**red**) and *Pv*GST:BSP (**blue**), and (D) *Pf*GST:GSH:BSP (red) and *Pv*GST:GSH:BSP (**blue**).

Fig. 5. Plots towards the determination of the steady-state kinetic parameters of *Pf*GST and *Pv*GST towards GSH in the presence and absence of BSP using Michaelis-Menten and Lineweaver-Burke models at varying GSH concentrations. (A). A Michaelis-Menten plot of 300 nM *Pf*GST (**black**) and *Pv*GST (**green**), (B). A Lineweaver-Burke straight line steady-state kinetics plot of *Pf*GST (**black**) and *Pv*GST (**green**), (C). Michaelis-Menten plot of 300 nM *Pf*GST in the presence of 0.5 mM BSP (**red**) and *Pv*GST in the presence of 0.5 mM BSP (**blue**), and (D). A Lineweaver-Burke straight-line steady-state kinetics plot of *Pf*GST in the presence of 0.5 mM BSP (**red**) and *Pv*GST in the presence of 0.5 mM BSP (**blue**),

Fig. 6. Protein-Ligand complex ribbon representation of the induced fit docking best pose for (A) *Pf*GST:BSP complex, (B) *Pv*GST:BSP, showing BSP binding at the dimer interphase of *Pf*GST and *Pv*GST. The image is a snapshot from the induced fit ligand docking algorithm implemented in Schrodinger Maestro v13.0.

Fig. 7. 2-D ligand interaction plot highlighting the side chains involved in the binding between the interaction of (A) IFD docking pose of BSP with *Pf*GST and (B) amino acid residue's position of BSP with *Pf*GST over 500 ns simulation. (C) IFD docking of BSP with *Pv*GST and (D) amino acid residue's position of BSP

with *Pv*GST over 500 ns simulation. Tyr108 is seen as the only non-polar amino side chains (**green**) involved in π-π* interaction with BSP's phenyl moiety in both *Pf*GST and *Pv*GST, while similar amino residues' involvement was seen during docking and the average simulation time. These Images were snapshots from the Maestro 2D interaction diagram implemented in Schrödinger Maestro 13.0

Fig. 8. *Pf*GST and *Pv*GST's structural alignment and sequence analysis reveal the similarity in positions of the amino acid residues taking part in the bonding and simulation interactions using Expresso™. Lys15, Gln 71, Gln 73, Ser72, Cys101, Asp105, Tyr108, and Asn111 were all conserved in both proteins.

Fig. 9. Simulation event analysis generated profile showing (A) the radius of gyration (Rg) of the apo systems of *Pf*GST (black) and *Pv*GST (green). (B) the radius of gyration (Rg) of the protein-ligand complex *Pf*GST:BSP (red) and *Pv*GST:BSP (blue) throughout the 500 ns simulation time plotted in picoseconds (ps)

Fig. 10. Analysis of the simulation trajectory showing (A) the RMSD of the Cα atoms and (B) the RMSF of the side chains as a function of the 500 ns simulation time for apo-*Pf*GST (black), apo-*Pv*GST (green), *Pf*GST:BSP complex (red), *Pf*GST:BSP complex (blue).

Fig. 11. The interaction of BSP with *Pf*GST and *Pv*GST in respect of their (A) MolSA quantitatively revealing BSP's interaction at both proteins' molecular environment, with *Pf*GST:BSP's trajectory (red) showing a higher MolSA than *Pv*GST:BSP (blue) and (B) global SASA showing similar binding dynamics of BSP in the two proteins. The *Pf*GST:BSP's SASA (red) is however higher than that of *Pv*GST:BSP (blue).

Fig. 12. Amino acid side chains interactions and types of interactions stacked bar charts between (A) *Pf*GST:BSP and (B) *Pv*GST:BSP, throughout the 500 ns simulation. The interaction diagram showed H-bonds are categorized into backbone

acceptor, backbone donor, side-chain acceptor, and side-chain donor. Hydrophobic interactions are categorized into π-cation, π-π*, and other non-specific interactions. The stacked bar charts are normalized throughout the 500 ns trajectory. The images were obtained with the use of the Ligand Interaction Algorithm implemented in Maestro v13.0.

Fig. 13. The subspace trajectories projections of the first two principal components (PC1 and PC2) in respect of their (A) Cα RMSD of *Pf*GST and *Pf*GST:BSP and (B) Cα *Pv*GST and *Pv*GST:BSP, (C) Cα RMSF of *Pf*GST and *Pf*GST:BSP and (D) Cα *Pv*GST and *Pv*GST:BSP.

**Chapter 6**

Fig. 1. The 2D chemical structure description of (A) Baicalin, BA and (B) 5,7,3'—Trihydroxy—6,4',5'—trimethoxyflavone, TTMF, respectively, obtained from the PubChem database with CID numbers 64982 for BA and 5496475.

Fig. 2. Induced fit docking analysis of the protein-ligand complex ribbon representation of (A) *Pf*GST:BA complex, (B) *Pv*GST:TTMF, showing BA and TTMF respectively binding and sitting tightly at the dimer interphase of *Pf*GST and *Pv*GST. The image is a snapshot from the induced fit ligand docking algorithm implemented in Schrodinger Maestro v13.0.

Fig. 3. 2-D ligand interaction plot highlighting the side chains involved in the binding between the interaction of (A) IFD docking pose of BA with *Pf*GST and (B) IFD docking of TTMF with *Pv*GST. HID107 is seen as the only amino side chain involved in π-π* interaction with BA's phenyl moiety in *Pf*GST and not in TTMF interaction with *Pv*GST. Not too similar amino acid residues' involvement were seen in the induced fir docking process. These Images were snapshots from the Maestro 2D interaction diagram implemented in Schrödinger Maestro 13.0

Fig. 4. Analysis of the simulation trajectory showing (A) the Cα-RMSD of *Pf*GST (**black**), *Pf*GST:BA (**red**) and (B) Cα-RMSD of *Pv*GST (**green**), and *Pv*GST:TTMF (**blue**). Also, the RMSF of the side chains as a function of the 500 ns simulation time for (C) apo-*Pf*GST (**black**), *Pf*GST:BA complex (**red**), and (D) apo-*Pv*GST (**green**), *Pv*GST:TTMF complex (**blue**).

Fig. 5. Amino acid side chains interactions and types of interactions stacked bar charts between (A) *Pf*GST:BA and (B) *Pv*GST:TTMF, throughout the 500 ns simulation. The interaction diagram showed that H-bonds are categorized into backbone acceptor, backbone donor, side-chain acceptor, and side-chain donor. Hydrophobic interactions are categorized into π-cation, π-π*, and other non-specific interactions. The stacked bar charts are normalized throughout the 500 ns trajectory. The images were obtained with the use of the Ligand Interaction Algorithm implemented in Maestro v13.0.

## List of Tables

**Chapter 1**

**Chapter 2**

Table 1 Approved traditional antimalaria drugs, year of introduction, and report of resistance

**Chapter 3**

Table 3.1 Experimental methods, non-standard reagents, and materials used, with their specific manufacturer

**Chapter 4**

Table 1. The thermal stability melt peak of *Pf*GST:GSH and *Pv*GST:GSH with respect seven selected antimalarials

**Chapter 5**

Table 1. Summary of the melt peaks showing the stability of PfGST and PvGST in the Presence of GSH and BSP

Table 2. Steady-state kinetic evaluation of PfGST and PvGST in the presence and absence of BSP

Table 3. BSP's predicted physicochemical descriptors, ADMET parameters, pharmacokinetic properties, and its' drug-like nature.

Table 4. Simulation Quality Analysis parameters and data of the four systems of the 500 ns MDS

Table 5. Calculated MM/GBSA binding energy of BSP interaction with *Pf*GST and *Pv*GST

**Chapter 6**

Table 1. HTVS computed binding affinity scores of the BA and TTMF to *Pf*GST and *Pv*GST's binding site

Table 2. Calculated MM/GBSA energy binding of BA and TTMF's respective interaction with *Pf*GST and *Pv*GST

## Abbreviations

| | |
|---|---|
| °C | Degree Celsius |
| λ | Wavelength |
| Δ*G*sol | Solvation free energy |
| 3D | Three-dimensional |
| ACT | Artemisinin Combination Therapy |
| AL | Artemether-lumefantrine |
| ANS | 8-anilino-1-naphthalenesulfonic acid |
| ARG | Antibiotic resistance gene |
| ASAQ | Artesunate-amodiaquine |
| ASMQ | Artesunate-mefloquine |
| ASSP | Artesunate plus sulfadoxine-pyrimethamine |
| BSP | Bromosulfophthalein |
| CADD | Computer-aided drug discovery |
| cDNA | Complementary deoxyribonucleic acid |
| CDNB | 1-chloro-2,4-dinitrobenzene |
| CPT1 | Carnitine palmityl transferase 1 |
| DHP | Dihydroartemisinin-piperaquine |
| DMSO | Dimethyl sulfoxide |
| EDTA | Ethylenediaminetetraacetic acid |
| $E_{gas}$ | Gas phase energy |
| $E_{int}$ | Sum of the internal energy |
| $E_{ele}$ | Coulomb energy |
| $E_{vdW}$ | Van der Waals energies |
| FP's | Ferriprotoporphyrin IX's |
| $G_{GB}$ | Energy from the polar states |
| $G_{SA}$ | Energy from Non-polar states |
| GSH | Glutathione |
| GPx | Glutathione peroxidase |
| GST | Glutathione *S*-Transferase |
| IDA | Iminodiacetic acid |

| | |
|---|---|
| IFD | Induced-fit docking |
| HTVS | High-throughput virtual screening |
| IMAC | Immobilized metal affinity chromatography |
| IPTG | Isopropyl β-D-1-thiogalactopyranoside |
| LB | Lysogeny broth |
| LB | Luria-Bertani |
| MCE | MedChemExpress |
| MDS | Molecular dynamics simulations |
| nm | Nanometer |
| NTA | Nitriloacetic acid |
| $OD_{600}$ | Optical density |
| OPLS | Optimized potentials for liquid simulations |
| ORF | Open reading frame |
| PAGE | Polyacrylamide gel electrophoresis |
| PCA | Principal Component Analysis |
| PC | Principal component |
| PCR | P*olymerase chain reaction* |
| *Pf* | *Plasmodium falciparum* |
| *Pv* | *Plasmodium vivax* |
| *Pf*GST | *Plasmodium falciparum* Glutathione S-Transferase |
| *Pv*GST | *Plasmodium vivax* Glutathione S-Transferase |
| *qPCR* | *quantitative polymerase chain reaction* |
| RCSB PDB | Research Collaboration for Structural Bioinformatics Protein Data Bank |
| RFU | Relative fluorescence unit |
| Rg | Radius of gyration |
| RMSD | Root-mean-square-deviation |
| RMSF | Root-mean-square fluctuations |
| ROS | Reactive oxygen species |
| SASA | Solvent accessible surface area |
| SDF | Structure data files |
| *SDS-PAGE* | Sodium dodecyl-sulfate polyacrylamide gel electrophoresis |
| SP | Standard protocol or precision |

| | |
|---|---|
| $T_m$ | Melting temperature |
| TSA | Thermal shift assay |
| TTMF | 5,7,3'-Trihydroxy-6,4',5'-trimethoxyflavone |
| UV-vis | Ultra-violet visible |
| WHO | World Health Organization |
| XP | Extended protocol |

## Abstract

*Plasmodium falciparum* (*Pf*) and *Plasmodium vivax* (*Pv*) are parasites that have progressively resisted existing antimalarial drugs by evading their current therapeutic mode of action. This has thereby necessitated research into novel therapeutics with a distinct and unique mode of action. The rapid development of resistance to prophylactic and interventional malaria drugs has undeniably been a thing of concern to researchers and healthcare practitioners. Glutathione S-Transferase (GST) as an adept enzyme has been brought to the limelight as a potential target for developing antimalarial drugs. This is connected to GST's significant involvement in cellular processes leading to metabolizing or detoxifying carcinogens, chemotherapeutic drugs, environmental pollutants, and oxidative stress products. Hence, the accelerated effort to target GST as a potential drug target in *Plasmodium falciparum* and *Plasmodium vivax*, are parasites which had progressively resisted existing antimalarial drugs. Although, the artemisinin derivatives antimalarials known as Artemisinin Combination Therapy (ACT) are currently one of the World Health Organization (WHO) approved drugs against *Pf* and *Pv*. Artemisinin-based combination therapies are currently used as the frontline treatment for malaria, thanks to their rapid action and high efficacy against *Plasmodium* parasites. However, the growing problem of drug resistance necessitates the study of ACTs in the context of protein-ligand interactions to discover their activity towards the drug target under consideration. It's also to gain new antimalarial strategies and enhance existing therapies. The seven selected ACTs used in this study were based on their reported efficacy and availability. Both *Plasmodium falciparum* and *Plasmodium vivax* possess a versatile enzyme which are respectively known as *Plasmodium falciparum* Glutathione S-Transferase (*Pf*GST) and *Plasmodium vivax* Glutathione S-Transferase (*Pv*GST). This class of enzyme exogenously and endogenously inactivates toxic molecules, metabolizing, and detoxifying carcinogens, and chemotherapeutic drugs. This has made these two enzymes catch the attention of many researchers for drug discovery. This is because the inhibition of *Pf*GST and *Pv*GST will reduce both *Plasmodium falciparum's* and *Plasmodium vivax's* detoxification abilities and weakened their antioxidant ability. Hence, this makes these targets represent a potential target for developing antimalarial drugs. The biochemistry of the protective role (detoxification of xenobiotics) being exerted by *Pf*GST and *Pv*GST was thus explored as a potential target for antimalarial drug development. In this study, the interactions, binding, stability, and inhibition

potentials by seven selected antimalarials, bromosulfophthalein (BSP) and natural products (flavonoids) are in this study insightfully considered as potential inhibitors. Computational studies novelly support all the biophysical characterizations employed in this study.

Spectroscopic analysis of the selected antimalarial drugs for biotransformation by GSH conjugation of the targets revealed that all the antimalarials are GSH-glutathionylated and GST biotransformed. Expectedly, while the GSH-CDNB conjugation assay showed that the antimalarials weakly inhibited the enzymatic activities of *Pf*GST and *Pv*GST, the ANS extrinsic fluorescence spectrophotometric analysis also revealed the weak binding to the targets. The quantitative polymerase chain reaction (qPCR) thermal shift stability elucidation shows that the antimalarial drugs moderately cause thermal instability of the targets. The ligandin properties of *Pf*GST and *Pv*GST towards the steady-state kinetics and molecular modelling-induced fit docking all showed that BSP binds more strongly to *Pf*GST and *Pv*GST than the selected ACTs. Steady-state kinetics evaluation and all the post-dynamic analysis from molecular dynamics simulations of *Pf*GST and *Pv*GST with BSP are in tandem in demonstrating BSP's drug-likeness. All the spectroscopic and spectrofluorometric techniques showed that the selected antimalarials were less effective as an inhibitor compared to BSP. The various results of molecular dynamics simulations and other computational studies reveal that BSP impacts the compactness of *Pf*GST and *Pv*GST in a decreasing manner and decreases their conformational dynamics accordingly more than the selected antimalarials. On the other hand, the high-throughput virtual computational studies screening selected baicalin and 5,7,3'-Trihydroxy-6,4',5'-trimethoxyflavone to outperform BSP and ellagic acid in binding and a better inhibitor of *Pf*GST and *Pv*GST. This study insightfully elucidated and positioned BSP's ability as a potential drug candidate to be further developed as an efficacious antimalarial and advanced a further study on two flavonoids, baicalin and 5,7,3'-Trihydroxy-6,4',5'-trimethoxyflavone as a better inhibitor of *Pf*GST and *Pv*GST respectively.

## Chapter I: Introduction

The infectivity of malaria as an annual three million people-killing disease, has continued to necessitate the search for new therapeutics with swift efficacy, affordability, and minimal toxicity. This is because malaria remains both a health burden economically challenging, and thereby causing significant morbidity cum mortality with grave economic losses (Singh and Rathi, 2023; Siqueira-Neto *et al.*, 2023). Malaria's global endemicity, as reported by the World Health Organization (WHO) in its World Malaria Report for the year 2023, is estimated to be 249 million malaria cases as of the year 2022 spreading across 84 malaria-endemic countries (World Health Organization, 2023). This stupefying statistic is unconnected to the COVID-19 pandemic interruption between 2019-2021, which posed a significant challenge to malaria control efforts. Other factors include the waning potency of stakeholders' primary malaria-fighting resources, climate change, and increased resistance to malaria's insecticide-treated nets. Most important is the multidrug resistance phenomenon confronting the front-line antimalarials (Hussein *et al.*, 2022; Li and Managi, 2022; Li *et al.*, 2022; World Health Organization, 2022). As malaria burden and its global endemicity linger despite multidimensional and multistakeholder concerted efforts towards finding treatment, researchers continue to find new drug targets. This is to grapple with the enormous burden malaria's morbidity and mortality places on man.

Malaria remains disproportionally high, an infectious disease burden with *Plasmodium falciparum* (*Pf*) and *Plasmodium vivax* (*Pv*) causing most morbidity and mortality in sub-Saharan Africa and Asia, respectively (Loy *et al.*, 2017; Larson, 2019). The ongoing threat of malaria, which kills three million people annually, continues to drive researchers in the search for new therapeutics. Also, this search for new therapeutics is necessitated by the discovery of resistant and multidrug-resistant malaria-causing *Plasmodium*, first to the traditional quinolone, antifolate antibiotics, and later to the gold standard artemisinin combination therapy (ACTs) approved by the WHO. Hence, searching for new and effective antimalaria and drug targets in *Plasmodium* has become more compelling to researchers (Chigorimbo-Murefu *et al.*, 2012; Zhan *et al.*, 2015). Understandably, and paying closer attention to the *Plasmodium* parasite's survival mechanism vis-à-vis its biochemical mechanism process, therapeutics targeting new targets will not be out of place. Therefore, studying targets that are found to be fundamental to malaria parasite survival will indeed be a worthy effort geared towards exploring new and novel designs of potent antimalaria therapies (Soni *et al.*, 2017).

*Plasmodium falciparum* Glutathione S-Transferase (*Pf*GST) and *Plasmodium vivax* Glutathione S-Transferase (*Pv*GST) have been found to exert protective roles in the form of detoxification of xenobiotics in *Plasmodium falciparum* and *Plasmodium vivax* respectively. This is thus one main reason they are both considered unique drug targets towards the development of novel and potent antimalarials (Mangoyi *et al.*, 2010; Quesada-Soriano *et al.*, 2013, 2014; Dasari *et al.*, 2018; Dasari *et al.*, 2018). Consequentially, inhibiting these *Pf*GST and *Pv*GST will have therapeutic implications. This is because the inhibition of *Pf*GST and *Pv*GST will wither *Plasmodium falciparum* and *Plasmodium vivax*'s detoxification ability and bring down their antioxidant ability. Several artemisinin-based combination therapies (ACTs) and chloroquine in combination with either primaquine or tafenoquine have been used for the treatment of uncomplicated *Plasmodium falciparum* and *Plasmodium vivax* causing malaria. However, the emergence and development of resistance and multi-drug resistance occurrence to these drugs have reversed the hitherto once-celebrated gains in the antimalarial fight and effort towards effective treatment and eradication of malaria (Wicht, Mok and Fidock, 2020; Rasmussen, Alonso and Ringwald, 2022; Siqueira-Neto *et al.*, 2023).

Historically, natural products have often been used to source for antimalarials. This is as researchers recognize their potency which is attributable to their structural diversity and complexities (Conrad and Rosenthal, 2019; Tse, Korsik and Todd, 2019; Kingston and Cassera, 2022). While numerous natural products have been isolated and modified for use as key antimalarial agents, this process is not without its challenges. The development of natural products such as antimalarials faces significant obstacles, making them less appealing as a primary focus for drug discovery. One major issue is the inherent complexity and variability of natural compounds, which can complicate the process of isolating and modifying them into effective drugs. Additionally, the lack of complimentary high-throughput phenotypic screening techniques and the unexplored potential of target-based screening have hindered progress in utilizing natural products as reliable antimalarial scaffolds. These challenges make it difficult to systematically explore and exploit the vast diversity of natural compounds, leading researchers to consider other approaches in their quest for effective antimalarial therapies. As a result, the pursuit of natural products for antimalarial drug development remains a challenging endeavour that requires innovative solutions and methodologies. (Guantai and Chibale, 2011; Korsik and Todd, 2019;

Siqueira-Neto *et al.*, 2023). Flavonoids represent a group of naturally occurring polyphenolic compounds found in plants which have emerged as promising alternative candidates for malaria treatment (Boniface and Ferreira, 2019). Their potential as antimalarial agents is supported by several factors, including their ability to target multiple stages of the *Plasmodium* parasite's life cycle. Flavonoids have been reported (*in vivo*) to demonstrate inhibitory effects on the parasite's growth and replication within red blood cells, as well as their ability to interfere with the metabolic pathways essential for the parasite's survival (Okoduwa *et al.*, 2024). The prospect of flavonoids as antimalarial agents not only provides a complementary approach to existing treatments but also offers a pathway to overcoming the growing challenge of drug resistance, ultimately contributing to more effective and sustainable malaria control strategies. While the search for new therapeutic compounds has historically relied on empirical experimentation, advancements in computational techniques now offer a promising avenue for the systematic identification of potential inhibitors (Ou-Yang *et al.*, 2012; Thomford *et al.*, 2018). Virtual screening, in particular, enables the rapid evaluation of vast chemical libraries, significantly expediting the drug discovery process (Sadybekov and Katritch, 2023).

Similarly, bromosulfophthalein (BSP), an anionic phthalein, triphenylmethane dye with two sulfonic acid groups and often greatly used in diagnosing liver injury through a liver function test, has also been found to inhibit some protozoans (Padi *et al.*, 2021; Pooe *et al.*, 2022). While BSP's use transcends liver function clinical diagnosis and some protozoic inhibition, it has not, however, been explored as a potent inhibitor in malaria parasites to date. The paradigm shift in focus towards finding and utilizing cost-effective, safe, and potent small molecules for malaria treatment forms the basis of this study approach. This study has investigated the novel use of bromosulfophthalein and natural compounds as an effective treatment option for malaria.

Hence, this study systematically integrates both empirical approaches and computation studies to discover potential inhibitors of *Pf*GST and *Pv*GST. While the empirical approach employed several biophysical principles and techniques in the characterization of the targets, computational studies are utilized to validate the results and vice versa. Also, because of the need to address the urgent need for novel antimalarial agents, this study employs a cutting-edge approach—high throughput virtual screening of a natural product library, to discover potent antimalaria that targets *Pf*GST and *Pv*GST.

## 1.1 . Problem Statement

As malaria caused by *Plasmodium falciparum* (*Pf*) and *Plasmodium vivax* (*Pv*) remains disproportionally high an infectious disease burden with most morbidity and mortality in sub-Saharan Africa and Asia, respectively, it then becomes imperative to find new drugs for their treatment. Though significant efforts have been directed toward global malaria treatment and eradication, nevertheless, these efforts have proved insufficient. Therapeutically, these insufficiencies result from drug and multidrug resistance towards the antimalarials in use, including the Artemisinin-based Combination Therapy (ACT), also known as the "gold standard" drugs used as the first-line treatment of malaria cases globally. Since these gold-standard antimalarials have been limited and rendered inefficacious by the resistance developed towards them, it becomes imperative to scientifically look out for ways of modifying and repurposing them or developing entirely new and potent antimalarials to combat this endemic parasitic disease. The ease at which some established antimalarial drug targets are prone to mutation thereby leading to resistance which ultimately culminates in the withering of the therapeutic effectiveness of drugs for malaria treatment necessitating the exploration of new targets. Given that the mechanism of drug target vis-à-vis its understanding and application has become pivotal in the effort aimed at developing target-based, novel and potent antimalarials, will inhibitors of *Pf*GST and *Pv*GST not prove a compound to be looked at as potent antimalarials? Understanding the mechanism behind the inhibition of these targets will help clarify how structural modifications can be made to antimalarial drugs that have reached late-stage preclinical development, especially those that have been made ineffective by resistance and multidrug resistance. Research indicates that a thorough understanding of drug target mechanisms is essential for rapidly advancing the development of target-based antimalarials from the initial stages to the final structural modifications. Will discovering potent inhibitors of *Pf*GST and *Pv*GST not be proven to be the needed solution to malaria treatment?

## 1.2. Rationale

The phenomenal emergence and spread of resistance and multi-drug resistance to current traditional, front-line, and low-cost antimalaria drugs available have made efforts to combat the world's most devastating parasitic disease, malaria, a glaring necessity. Since malaria parasites

have developed resistance against nearly all commonly used chemotherapeutics, hence this brings about the imperativeness to characterize alternative novel drug targets. *Plasmodium falciparum* and *Plasmodium vivax* harbour exclusively one distinct type and similar Glutathione-S-Transferase. The inhibition of *Plasmodium falciparum* Glutathione-S-Transferase (*Pf*GST) and *Plasmodium vivax* Glutathione-S-Transferase (*Pf*GST) is anticipated to alter the Glutathione-dependent conjugation process, increase cytotoxic peroxides' level, and toxic ferriprotoporphyrin IX's (FP's) concentration. This then will ultimately show that both *Pf*GST and *Pv*GST are novel drug targets and that their inhibition would be a worthy route to designing new and effective antimalarials. It becomes equally imperative to consider and study *Plasmodium falciparum* and *Plasmodium vivax*, both of which are etiological agents of most malaria cases recorded in the continent of Africa and Asia respectively. Owing to the novelty in class that *Pf*GST and *Pv*GST stand for among GST isoenzymes and isoforms, *Pf*GST and *Pv*GST have since been adjudged highly important drug targets for the development of new antimalarials. This novelty of *Pf*GST and *Pv*GST is in their substrate binding sites which significantly differ architecturally. Also, since *Pf*GST and *Pv*GST share substantial sequence identities and functionalities as important drug targets, discovering common or different compounds (synthetic or natural) will be advantageous to developing antimalarials against the most causative agents of malaria. The rationality of the study approach is combining *in silico* High-throughput virtual screening (HTVS) and molecular dynamics simulation (MDS) alongside empirical studies becomes imperative. This is because computational studies and empirical studies continue to play a significant role as employable techniques in designing new inhibitors against new targets such as *Pf*GST and *Pv*GST. Owing to the importance of systemically integrating these two approaches in new treatment discovery, empirical-based biophysical tools and *in-silico* or computational modelling studies are hence employed in this study to elucidate the discovery of potent inhibitors of *Pf*GST and *Pv*GST as antimalarials drugs.

### 1.3. Aim and objectives

This study aims to systematically integrate empirical and theoretical studies in discovering potent inhibitors of two druggable proteins (*Pf*GST and *Pv*GST) as antimalaria drugs capable of

mitigating the health burden, which remains a challenge in malaria-laden Africa and Asia respectively. This aim will be achieved through the following proposed objectives:

1. Expression and purification of recombinant *Pf*GST and *Pv*GST using pET 11a vector and one-step Immobilized metal affinity Chromatography (IMA)C affinity chromatography respectively.
2. Quantitatively and qualitatively assessing *Pf*GST and *Pv*GST using Ultraviolet-visible (UV-Vis) spectrophotometry and Sodium dodecyl-sulfate polyacrylamide gel (SDS-PAGE).
3. Biophysical characterization of the expressed and purified recombinant *Pf*GST and *Pv*GST in terms of inhibition, binding, and stability studies using spectrophotometrically determined enzymatic activity, spectrofluorometric, and thermal shift techniques, respectively
4. High-throughput virtual screening of flavonoid library for probable natural compound inhibitors of *Pf*GST and *Pv*GST.
5. Molecular dynamics simulation validation study of BSP and flavonoid compound as probable natural compound inhibitors of *Pf*GST and *Pv*GST.
6. Determining the effect of seven antimalarials, BSP, and flavonoid compounds on the structure, function, and stability of *Pf*GST and *Pv*GST.
7. Determining the ligandin properties of *Pf*GST and *Pv*GST towards the seven antimalarials

### 1.4. Novelty of the study

The design of novelly acting drugs as antimalarial with new mechanisms of action has become imperatively necessary to combat the *Plasmodium* parasite's resistance to drugs. To this end, the discovery of potential inhibitors of *Pf*GST and *Pv*GST, being two important detoxification enzymes found in *Plasmodium falciparum* and *Plasmodium vivax* respectively is novelly imperative. This is because this study's scope of simultaneously studying both parasites will be far-reaching in the problem-solving component of the research while also broadly contributing to knowledge. Similarly, the systematic integration of empirical studies and computational modelling

alongside a high throughput virtual screening approach to discover probable inhibitors of *Pf*GST and *Pv*GST in one pot is equally novel. The study's novelty is equally expressed in starting from what is known about the current antimalarials to empirically and computationally aiming to discover new antimalarial candidates. This systematic integration makes the study robust and scientifically validatable. To the best of my knowledge, no study has been undertaken computationally or empirically to probe a rich flavonoid library with BSP and the selected antimalarials as potential inhibitors against these unique drug targets (*Pf*GST and *Pv*GST) in this regard. Similarly, because no study has been conducted on BSP (empirically and computationally) as a potential antimalarial, shows the novelty that characterizes this study

### 1.5. Thesis outline

Chapter 1. Introduction

Chapter 2. Literature review

Chapter 3. Transformation, Recombinant Expression, Purification, Quantification, and Characterization of *Plasmodium falciparum* and *Plasmodium vivax* Glutathione *S*-Transferase

Chapter 4. Characterizing the ligandin properties of *Plasmodium falciparum* and *vivax* glutathione transferase towards selected antimalarial drugs (Paper 1, under review)

Chapter 5. Describing the ligandin properties of Plasmodium falciparum and vivax glutathione transferase towards Bromosulfophthalein from empirical and computational modelling viewpoints (Paper 2, Published)

Chapter 6. Discovery of probable inhibitors of *Plasmodium falciparum* and *vivax* glutathione transferase through high-throughput virtual screening of a flavonoid library using bromosulfophthalein as the benchmark ligand (Paper 3, under review)

Chapter 7. Conclusion

**References**

Boniface, P.K. and Ferreira, E.I. (2019) 'Flavonoids as efficient scaffolds: Recent trends for malaria, leishmaniasis, Chagas disease, and dengue', *Phytotherapy Research*, 33(10), pp. 2473–2517. Available at: https://doi.org/10. 1002/ptr.6383.

Chigorimbo-Murefu, N.T.L. *et al.* (2012) 'Biotransformation and biocatalysis: roles and applications in the discovery of antimalarials', *Future Medicinal Chemistry*, 4(18), pp. 2325–2336. Available at: https://doi.org/10.4155/fmc.12.173.

Conrad, M.D. and Rosenthal, P.J. (2019) 'Conrad, M. D., & Rosenthal, P. J. (2019). Antimalarial drug resistance in Africa: the calm before the storm? The Lancet Infectious Diseases, 19(10), e338–e351.Antimalarial drug resistance in Africa: the calm before the storm?', *The Lancet Infectious Diseases*, 19(10), pp. 338–351. Available at: https://doi.org/10.1016/S1473-3099(19)30261-0.

Dasari, S., Swamy, M., *et al.* (2018) 'Chemico-Biological Interactions Role of glutathione S-transferases in detoxi fi cation of a polycyclic aromatic hydrocarbon , methylcholanthrene', *Chemico-Biological Interactions*, 294(August), pp. 81–90. Available at: https://doi.org/10.1016/j.cbi.2018.08.023.

Dasari, S., Ganjayi, M.S., *et al.* (2018) 'Role of glutathione S-transferases in detoxification of a polycyclic aromatic hydrocarbon, methylcholanthrene', *Chemico-Biological Interactions*, 294(January), pp. 81–90. Available at: https://doi.org/10.1016/j.cbi.2018.08.023.

Guantai, E. and Chibale, K. (2011) 'How can natural products serve as a viable source of lead compounds for the development of new/novel anti-malarials?', *Malaria Journal*, 10(1), pp. 1–8. Available at: https://doi.org/10.1186/1475-2875-10-S1-S2.

Hussein, R. *et al.* (2022) 'Impact of COVID-19 and malaria coinfection on clinical outcomes: a retrospective cohort study', *Clinical Microbiology and Infection*, 28(8), pp. 1152-e1. Available at: https://doi.org/10.1016/j.cmi.2022.03.028.

Kingston, D.G.I. and Cassera, M.B. (2022) *Antimalarial natural products*. Springer. Available at: https://doi.org/10.1007/978-3-030-89873-1_1.

Larson, B. (2019) 'Origin of Two Most Virulent Agents of Human Malaria: Plasmodium falciparum and Plasmodium vivax', *Malaria*, 4, pp. 1–16. Available at: https://doi.org/10.5772/intechopen.84481.

Li, C. and Managi, S. (2022) 'Global malaria infection risk from climate change', *Environmental Research*, 214, p. 114028. Available at: https://doi.org/10.1016/j.envres.2022.114028.

Li, Z. *et al.* (2022) 'Temporal trends in the burden of non-communicable diseases in countries with the highest malaria burden, 1990–2019: Evaluating the double burden of non-communicable and communicable diseases in epidemiological transition', *Globalization and Health*, 18(1), pp. 1–9. Available at: https://doi.org/10.1186/s12992-022-00882-w.

Loy, D.E. *et al.* (2017) 'Out of Africa: origins and evolution of the human malaria parasites Plasmodium falciparum and Plasmodium vivax', *International Journal for Parasitology*, 47(2–3), pp. 87–97. Available at: https://doi.org/10.1016/j.ijpara.2016.05.008.

Mangoyi, R. *et al.* (2010) 'Glutathione transferase from Plasmodium falciparum - Interaction with malagashanine and selected plant natural products', *Journal of Enzyme Inhibition and Medicinal Chemistry*, 25(6), pp. 854–862. Available at: https://doi.org/10.3109/14756366.2010.486793.

Okoduwa, S.I.R. *et al.* (2024) 'Multi-therapeutic potential of flavonoids as an essential component in nutraceuticals for the treatment and management of human diseases', *Phytomedicine Plus*, p. 100558. Available at: https://doi.org/10.1016/j.phyplu.2024.100558.

Organization, W.H.O. (2023) *World malaria report 2023*, *World malaria report 2023*.

Ou-Yang, S. *et al.* (2012) 'Computational drug discovery', *Acta Pharmacologica Sinica*, 33(9), pp. 1131–1140. Available at: https://doi.org/10.1038/aps.2012.109.

Padi, N. *et al.* (2021) 'Engineering a pseudo-26-kda schistosoma glutathione transferase from bovis/haematobium for structure, kinetics, and ligandin studies', *Biomolecules*, 11(12). Available at: https://doi.org/10.3390/biom11121844.

Pooe, K. *et al.* (2022) 'Biophysical description of Bromosulfophthalein interaction with the 28-kDa glutathione transferase from Schistosoma japonicum', *Molecular and Biochemical Parasitology*, 252, p. 111524. Available at: https://doi.org/10.1016/j.molbiopara.2022.111524.

Quesada-Soriano, I. *et al.* (2013) 'Calorimetric studies of ligands binding to glutathione S-transferase from the malarial parasite Plasmodium falciparum', *Biochemistry*, 52(11), pp. 1980–1989. Available at: https://doi.org/10.1021/bi400007g.

Quesada-Soriano, I. *et al.* (2014) 'Asn112 in Plasmodium falciparum glutathione S-transferase is essential for induced reversible tetramerization by phosphate or pyrophosphate', *Biochimica et Biophysica Acta - Proteins and Proteomics*, 1844(9), pp. 1427–1436. Available at: https://doi.org/10.1016/j.bbapap.2014.04.017.

Rasmussen, C., Alonso, P. and Ringwald, P. (2022) 'Current and emerging strategies to combat antimalarial resistance', *Expert Review of Anti-infective Therapy*, 20(3), pp. 353–372. Available at: https://doi.org/10.1080/14787210.2021.1962291.

Sadybekov, A. V. and Katritch, V. (2023) 'Computational approaches streamlining drug discovery', *Nature*, 616(7958), pp. 673–685. Available at: https://doi.org/10.1038/s41586-023-05905-z.

Singh, A.P. and Rathi, B. (2023) 'Advances in Anti-Malarial Drug Discovery', *Frontiers in Drug Discovery*, 3, pp. 1–2. Available at: https://doi.org/10.3389/fddsv.2023.1335842.

Siqueira-Neto, J.L. *et al.* (2023) 'Antimalarial drug discovery: progress and approaches', *Nature Reviews Drug Discovery*, 22(10), pp. 807–826. Available at: https://doi.org/10.1038/s41573-023-00772-9.

Soni, R. *et al.* (2017) 'Signaling strategies of malaria parasite for its survival, proliferation, and infection during erythrocytic stage', *Frontiers in immunology*, 8, p. 349.

Thomford, N.E. *et al.* (2018) 'Natural products for drug discovery in the 21st century: innovations for novel drug discovery', *International journal of molecular sciences*, 19(6), p. 1578. Available at: https://doi.org/10.3390/ijms19061578.

Tse, E.G., Korsik, M. and Todd, M.H. (2019) 'The past, present and future of anti-malarial medicines', *Malaria journal*, 18(1), pp. 1–21. Available at: https://doi.org/10.1186/s12936-019-2724-z.

Wicht, K.J., Mok, S. and Fidock, D.A. (2020) 'Molecular mechanisms of drug resistance in Plasmodium falciparum malaria', *Annual review of microbiology*, 74, pp. 431–454. Available at: https://doi.org/10.1146/annurev-micro-020518- 115546.

World Health Organization (2022) *World malaria report 2022*. World Health Organization.

Zhan, Y. *et al.* (2015) 'Biotransformation of artemisinin by Aspergillus niger', *Applied microbiology and biotechnology*, 99, pp. 3443–3446. Available at: https://doi.org/10.1007/s00253-015-6464-x.

## Chapter 2: Literature Review

Glutathione S-Transferase or Glutathione Transferase (GST) is an adept enzyme family that occurs copiously in nearly all organisms. They are responsible for detoxifying many substances intracellularly by inactivating and converting diverse exogenous and endogenous toxic molecules to less toxic soluble compounds (which are metabolized partially and hence can be eliminated easily) via glutathione (GSH) conjugation [1–4]. Currently, GSTs have caught the attention of many researchers for drug discovery, nanotechnology, and biotechnology and this is due to GST's significant involvement in cellular processes. This GST cellular processes have been attributed to GST's ability in metabolizing and detoxifying carcinogens, chemotherapeutic drugs, environmental pollutants, and oxidative stress products [5]. This enzyme is predominantly located within the cytosol (hence the name cytosolic GST), where they function as peroxidase and isomerase, protecting cells against $H_2O_2$-induced cell death [6]. The versatility of GSTs (E.C.2.5.1.18) as a class of enzyme is in its functionality as an inactivator and transformer of a broad miscellany of exogenous and endogenous toxic molecules to water-soluble compounds [3]. Also, as a phase II biotransformation detoxification enzyme, GST primarily catalyzes glutathione sulfur atom's attack of the nucleophile in the substrate's second electrophilic groups. This then leads to GSTs capacity to detoxify mutagens, carcinogenic, and several chemical substances [5,7]. They are also known as bi-substrate detoxification enzymes primarily involved in catalyzing the hydrophobic site (H-site) xenobiotics binding to the glutathione site (G-site) of the substrates of the endogenous glutathione [8]. GSTs also add to the GSH nucleophilically toxic compounds, reduce hydroperoxides, and functionally act as protein (ligandins) carriers of distinct organic nucleophiles, resulting in these molecules' inactivation and immobilization [4].

*Plasmodium falciparum* and *Plasmodium vivax* parasites had progressively been resistant to existing antimalarial drugs by evading the current therapeutic mode of action, necessitating research into novel therapeutics with a distinct mode of action [4,9]. There has been tremendous call and demand for the development of potent, promising, and novel drug targets that could help suppress malaria occasioned by the rapid development of resistance to prophylactics and interventional drugs [10–12]. *Plasmodium falciparum* and *Plasmodium vivax* parasites had progressively been resistant to existing antimalarial drugs by evading the current therapeutic mode of action [4]. The *Plasmodium falciparum* Glutathione S-Transferase (*Pf*GST) and *Plasmodium vivax* Glutathione S-Transferase (*Pv*GST) are distinctively different, existing singularly in the

cytosol different from the multiple GSTs found in eukaryotic organisms [4]. While these two GSTs do not only respectively constitute about 0.1-1% of *Plasmodium falciparum* (*Pf*) and *Plasmodium vivax* (*Pv*) total protein component, but they are indispensable for these protozoan's survival [7]. Consequentially and generally, GSTs' inhibitory ability have therapeutic, anthelmintic, antiparasitic, and anti-cancer applications. This is as the inhibition of *Pf*GST and *Pv*GST will wither *Pf* and *Pv* detoxification ability and bring down their antioxidant ability. Also, the functionalities of GSTs have also been attributed to the drug resistance being developed against cancer therapy like the alkylating agents, and as well as the corresponding overexpression of GST in cells. The bodily process of GST is also found to step up in chloroquine-resistant cells, hence making it a good representation of ligandin for parasitotoxic hemin and an enzyme of a possible target for the development of antimalaria drug [1]. Hence, it is not surprising that *Pf*GST and *Pv*GST represent a potential target for developing antimalaria drugs [1,3,7,8].

## 2.1. Malaria: Africa and Global Burden

The world since time immemorial has been plagued with diseases, with one of such being Malaria, which is highly dominant in the sub-Saharan Africa. Globally, malaria burdensomeness was hiked after the year 2020 global pandemic as the global malaria cases reported in year 2022 increase to 249 million from 244 million in year 2021 [13,14]. The global 5 million increase recorded were attributed to increases in malaria cases in three African, one Oceania, and one South Asia continent as highlighted in Figure 1.

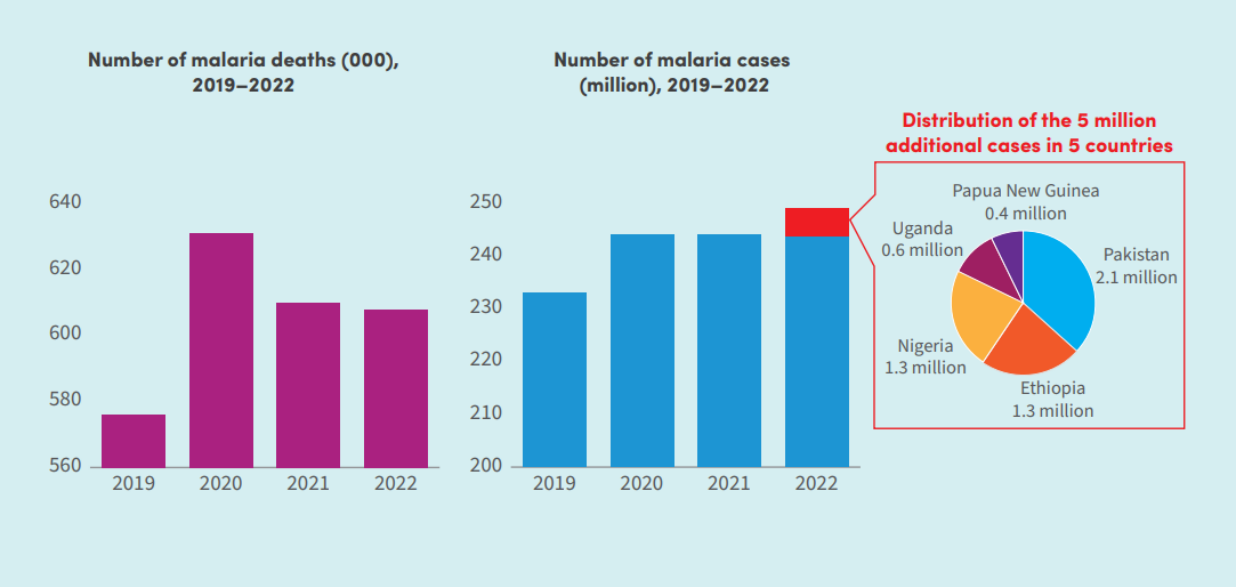


Figure 1. The World Health Organization, World Malaria Report for the year 2023's statistical representation of global malaria morbidity and mortality rate between the year 2019 – 2022 showing slight decline in mortality rate but 5 million increment in the mortality rate.

Malaria, being an acute febrile illness, is also a highly varied endemic infection in southern African countries. It is still a significant disease in South Africa too, more so that its incidence rate dramatically increased from the year 2016 in the north and north-eastern delimitation of South Africa [3,7,15]. The global malaria morbidity and mortality rates, as shown in Figure 2A and 2B, respectively, are somewhat similar with respect to countries being affected, according to the World Malaria Report of the year 2023. It is imperative to state that the African region or the African continent continues to bore the brunt of the burden of malaria, which includes the economic loss and negative social impact. Succinctly put, there are five known species of malaria-causing *Plasmodium* parasites in humans which include *Plasmodium falciparum*, *Plasmodium vivax*, *Plasmodium ovale*, *Plasmodium malariae*, and *Plasmodium knowelsi*. While the *Plasmodium falciparum* and *Plasmodium vivax* are the most prominent in human, the *Plasmodium falciparum* result in the most devastating malaria and *Plasmodium vivax* causes the most complicated to treat malaria, due to its' tendency to lead to recurrent infections [16,17]. The burden of malaria is significant in the South-East Asia, Eastern Mediterranean, and Western Pacific, with *Plasmodium vivax* being largely implicated to almost 46% of the all cases there [14]. Malaria remains disproportionally high, an infectious disease burden with *Plasmodium falciparum* and *Plasmodium vivax* causing most morbidity and mortality in sub-Saharan Africa and Asia, respectively [18,19]. Malaria is a vector-carrying disease etiologically originating from the Apicomplexan unicellular

parasite belonging to the *Plasmodium* genius usually accounts for the highest fatality and drug-resistant rate [15,20].

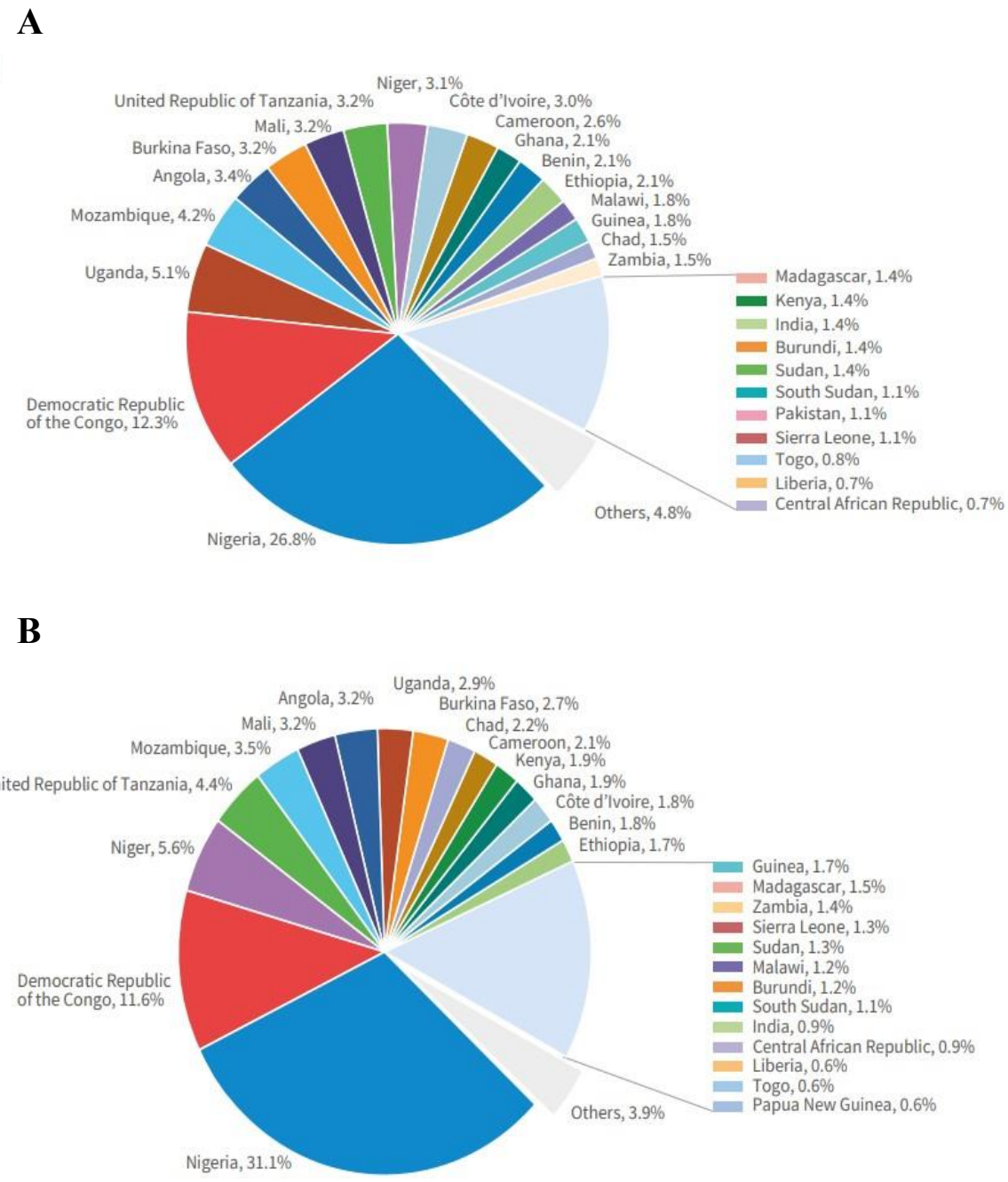


Figure 2. The World Health Organization, World Malaria Report for the year 2023's statistical representation of global malaria morbidity and mortality rate for the year 2022 showing (A). morbidity rate per countries and (B). 608,000 mortality rate distribution across countries.

Of the well-known species that are disease-causing in humans are the *Plasmodium falciparum* and *Plasmodium vivax*, which the WHO, in its global World Malaria Report for 2023, stated that *Plasmodium falciparum* and *Plasmodium vivax* are responsible for 99.7% and 46% of estimated malaria cases in the African and Asia Region respectively [14]. The report also implicated the Africa continent as taking a relatively high 95 % share of the global 229 million malaria morbidity and 608,000 mortality cases reported to date [14,21].

### 2.2. Malaria Parasite Life Cycle: Complexities and Pathogenesis

The malaria parasite's complex life cycle, especially the human infecting *Plasmodium* species, has been attributed to sharing mosquito and human host. This knowledge stems from the *Plasmodium* species growth and development propensity in human host and the blood feed mosquitoes [22,23]. The *Plasmodium* parasite many stages of development both within the human host and the mosquito vector, gives the *Plasmodium* exceptional adaptation ability, which in turn contributes to its' pathogenicity [23–25]. The life cycle is made up of the asexual stages and sexual stages, with the asexual stage of the parasite's life cycle taking place inside human host. Specifically, the human host liver cells (hepatocytes) and the red blood cells (erythrocytes) house the asexual stage of the life cycle. While the hepatocytes stage is asymptomatic in nature being an initial development phase, the clinical symptoms of malaria as a disease however begin to manifest when the proliferation begins in the erythrocytes [26]. Figure 3 shows the human (host) asexual stage is divided into the pre-erythrocytic and erythrocytic stages, while the sexual stage takes place in the mosquito vector [22]. In terms of the parasites' pathogenicity, while the hepatocyte stage is essential in for infection establishment and subsequently in the blood stage, however, the intraerythrocytic stages is very critical, as the characteristic symptoms of malaria, including fever, anemia, organ damage, and potentially fatal complications takes place. This understanding of the malaria parasites' intricate life cycle is essential for developing effective prevention strategies, treatments, and vaccines to combat this deadly disease.

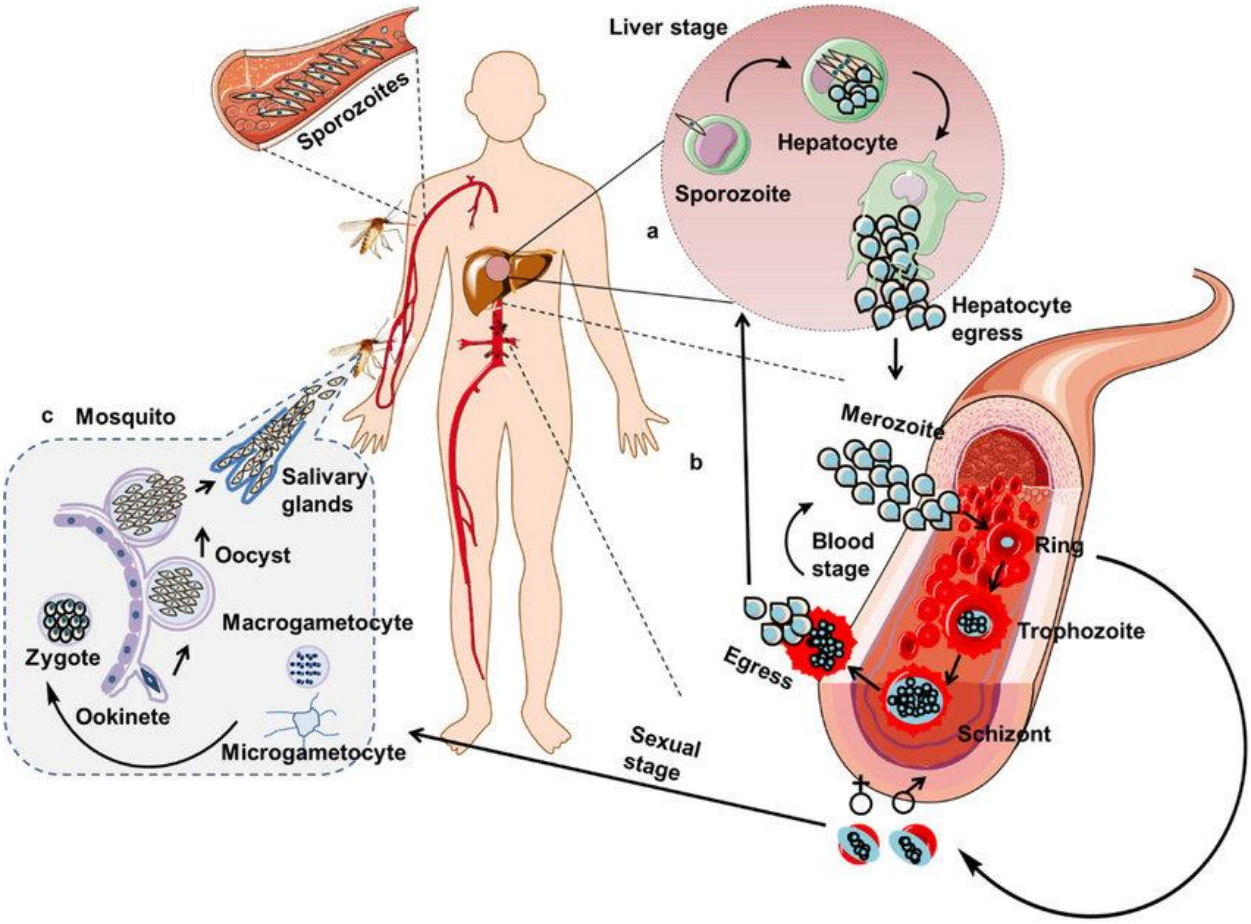


Figure 3. Malaria parasite (*Plasmodium falciparum*) life cycle showing the complexity of the stages divided into a. liver (pre-erythrocytic) stage, b. the red blood cell (erythrocytic stage) stage and c. mosquito (sexual) stage This image is adapted from [22].

### 2.3. Malaria: Treatment and Resistance

Malaria's withering consequences are not unconnected to the phenomenal emergence and spread of resistance to the traditional and low-cost antimalarial drugs available. The resistance of *Plasmodium* parasites to an antimalaria drug is delineated to mean the quality or power of a *Plasmodium* parasite strain to withstand or circumvent chemotherapeutics and grow in its host irrespective of doses of administered and absorbed specific antimalarial drugs [21]. In that regard, a parasitic *Plasmodium falciparum* or *Plasmodium vivax* is said to be resistant to antimalarial drug when the parasite possesses an ability to continue to live, proliferate irrespective of the antimalaria dosage (equal or higher) administered or absorbed. A number of factors which include; rate of parasitic mutation, parasite load, potency and dosage of drug used, compliance of or poor adherence to antimalarials, among others, contribute to the development of resistance to antimalarials [17]. The emergence of multidrug-resistant *Plasmodium falciparum* and

*Plasmodium vivax* to the commonly available front-line drugs has made efforts to combat this world's most devastating parasitic disease not only plateaued but also come to a frightening and worrisome regression [4,21]. Though significant efforts have been directed towards global malaria eradication, nevertheless, these efforts have proved insufficient. Therapeutically, these insufficiencies are as a result of drug and multidrug resistance towards the antimalarials in use. This insufficiency is however compounded by the lack of novelly new mechanism of action drugs [27]. This has resulted in *Plasmodium falciparum* and *Plasmodium vivax* resistance to almost all current antimalarial drugs currently in use, including the 'gold standard' Artemisinin-based Combination Therapy (ACT) used as first-line treatment [28]. ACTs, which are the current antimalaria drugs in use, can be broadly classified into three groups, namely the aryl amino alcohol compounds, antifolate compounds, and the artemisinin compounds [17,29]. The WHO recommends artemisinin-based combination therapies (ACTs) for uncomplicated malaria treatment because artemisinin rapidly and significantly reduces most malaria parasites, while the partner drug, on the other hand, clears the few parasites remaining [30,31]. The WHO recommended ACTs for use in uncomplicated malaria treatment of malaria include artemether-lumefantrine (AL), artesunate-amodiaquine (ASAQ), artesunate-mefloquine (ASMQ), artesunate plus sulfadoxine-pyrimethamine (ASSP), and dihydroartemisinin-piperaquine (DHP) [31–34]. However, the efficacy and continuous use of these ACTs are continuously threatened by resistance mediated by kelch (K13) protein mutation in *Plasmodium falciparum*, chloroquine, and other drugs resistance in *Plasmodium vivax* [21,35–39]. The existing antimalarials are mainly targeted at the erythrocyte invading and replicating parasite stages in the bloodstream. This is because the development inside the erythrocyte protects the pathogen from the host's immune response while limiting access to nutrients, among other solutes in plasma [17]. Also, *Plasmodium falciparum* and *Plasmodium vivax*'s ability to temporarily enter a state of inactivity upon drug intake which is a metabolically reduced non-proliferative phase makes it resistant to artemisinin. And once treatment is removed, the parasites can proliferate. This phenomenon results in inefficient parasite clearance, which ultimately lead to treatment failure [28,37,40,41].

## References


[1] K. Fritz-Wolf, A. Becker, S. Rahlfs, P. Harwaldt, R.H. Schirmer, W. Kabsch, K. Becker, X-ray structure of glutathione S-transferase from the malarial parasite Plasmodium falciparum, Proc. Natl. Acad. Sci. U. S. A. 100 (2003) 13821–13826. https://doi.org/10.1073/pnas.2333763100.

[2] N. Hiller, K. Fritz-Wolf, M. Deponte, W. Wende, H. Zimmermann, K. Becker, Plasmodium falciparum glutathione S -transferase-Structural and mechanistic studies on ligand binding and enzyme inhibition , Protein Sci. 15 (2006) 281–289. https://doi.org/10.1110/ps.051891106.

[3] R. Mangoyi, R. Hayeshi, B. Ngadjui, F. Ngandeu, M. Bezabih, B. Abegaz, S. Razafimahefa, P. Rasoanaivo, S. Mukanganyama, Glutathione transferase from Plasmodium falciparum - Interaction with malagashanine and selected plant natural products, J. Enzyme Inhib. Med. Chem. 25 (2010) 854–862. https://doi.org/10.3109/14756366.2010.486793.

[4] E.E. Colón-Lorenzo, D.D. Colón-López, J. Vega-Rodríguez, A. Dupin, D.A. Fidock, A. Baerga-Ortiz, J.G. Ortiz, J. Bosch, A.E. Serrano, Structure-Based Screening of Plasmodium berghei Glutathione S-Transferase Identifies CB-27 as a Novel Antiplasmodial Compound, Front. Pharmacol. 11 (2020) 1–17. https://doi.org/10.3389/fphar.2020.00246.

[5] S. Dasari, M.S. Ganjayi, P. Yellanurkonda, S. Basha, B. Meriga, Role of glutathione S-transferases in detoxification of a polycyclic aromatic hydrocarbon, methylcholanthrene, Chem. Biol. Interact. 294 (2018) 81–90. https://doi.org/10.1016/j.cbi.2018.08.023.

[6] D. SHEEHAN, G. MEADE, V.M. FOLEY, C.A. DOWD, Structure, function and evolution of glutathione transferases: implications for classification of non-mammalian members of an ancient enzyme superfamily, Biochem. J. 360 (2001) 1–16. https://doi.org/10.1042/bj3600001.

[7] I. Quesada-Soriano, C. Barón, R. Téllez-Sanz, F. García-Maroto, L. García-Fuentes, Asn112 in Plasmodium falciparum glutathione S-transferase is essential for induced reversible tetramerization by phosphate or pyrophosphate, Biochim. Biophys. Acta - Proteins Proteomics. 1844 (2014) 1427–1436.

https://doi.org/10.1016/j.bbapap.2014.04.017.

[8] M.N. Al-Qattan, M.N. Mordi, S.M. Mansor, Assembly of ligands interaction models for glutathione-S-transferases from Plasmodium falciparum, human and mouse using enzyme kinetics and molecular docking, Comput. Biol. Chem. 64 (2016) 237–249. https://doi.org/10.1016/j.compbiolchem.2016.07.007.

[9] T. Tripathi, B.-K. Na, W.-M. Sohn, K. Becker, V. Bhakuni, Structural, functional and unfolding characteristics of glutathione S-transferase of Plasmodium vivax, Arch. Biochem. Biophys. 487 (2009) 115–122. https://doi.org/10.1016/j.abb.2009.05.011.

[10] J. Huttu, B.K. Singh, S.P. Bhargav, J.M. Sattler, H. Schüler, I. Kursula, Crystallization and preliminary structural characterization of the two actin-depolymerization factors of the malaria parasite, Acta Crystallogr. Sect. F Struct. Biol. Cryst. Commun. 66 (2010) 583–587. https://doi.org/10.1107/S1744309110011589.

[11] C. Burmeister, M. Perbandt, C. Betzel, R.D. Walter, E. Liebau, Crystallization and preliminary X-ray diffraction studies of the glutathione S-transferase from Plasmodium falciparum, Acta Crystallogr. - Sect. D Biol. Crystallogr. 59 (2003) 1469–1471. https://doi.org/10.1107/S0907444903011090.

[12] K.N. Olafson, T.Q. Nguyen, J.D. Rimer, P.G. Vekilov, Antimalarials inhibit hematin crystallization by unique drug–surface site interactions, Proc. Natl. Acad. Sci. U. S. A. 114 (2017) 7531–7536. https://doi.org/10.1073/pnas.1700125114.

[13] World Health Organization, World malaria report 2022, World Health Organization, 2022.

[14] W.H.O. Organization, World malaria report 2023, 2023.

[15] R. Maharaj, I. Seocharan, B. Qwabe, M. Mkhabela, S. Kissoon, Decadal epidemiology of malaria in KwaZulu - Natal , a province in South Africa targeting elimination, Malar. J. (2019) 1–7. https://doi.org/10.1186/s12936-019-3001-x.

[16] J. Popovici, L. Pierce-Friedrich, S. Kim, S. Bin, V. Run, D. Lek, K.H.D. Hee, L. Lee Soon-U, M. V Cannon, D. Serre, Recrudescence, reinfection, or relapse? A more rigorous framework to assess chloroquine efficacy for Plasmodium vivax malaria, J. Infect. Dis. 219 (2019) 315–322. https://doi.org/10.1093/infdis/jiy484.

[17] M.A. Shibeshi, Z.D. Kifle, S.A. Atnafie, Antimalarial drug resistance and novel targets for antimalarial drug discovery, Infect. Drug Resist. 13 (2020) 4047–4060. https://doi.org/10.2147/IDR.S279433.

[18] B. Larson, Origin of Two Most Virulent Agents of Human Malaria: Plasmodium falciparum and Plasmodium vivax, Malaria. 4 (2019) 1–16. https://doi.org/10.5772/intechopen.84481.

[19] D.E. Loy, W. Liu, Y. Li, G.H. Learn, L.J. Plenderleith, S.A. Sundararaman, P.M. Sharp, B.H. Hahn, Out of Africa: origins and evolution of the human malaria parasites Plasmodium falciparum and Plasmodium vivax, Int. J. Parasitol. 47 (2017) 87–97. https://doi.org/10.1016/j.ijpara.2016.05.008.

[20] G. Boumis, G. Giardina, F. Angelucci, A. Bellelli, M. Brunori, D. Dimastrogiovanni, F. Saccoccia, A.E. Miele, Crystal structure of Plasmodium falciparum thioredoxin reductase, a validated drug target, Biochem. Biophys. Res. Commun. 425 (2012) 806–811. https://doi.org/10.1016/j.bbrc.2012.07.156.

[21] F.A. Siddiqui, X. Liang, L. Cui, Plasmodium falciparum resistance to ACTs: Emergence, mechanisms, and outlook, Int. J. Parasitol. Drugs Drug Resist. 16 (2021) 102–118. https://doi.org/10.1016/j.ijpddr.2021.05.007.

[22] S.R. Bonam, L. Rénia, G. Tadepalli, J. Bayry, H.M.S. Kumar, Plasmodium falciparum malaria vaccines and vaccine adjuvants, Vaccines. 9 (2021) 1072. https://doi.org/10.3390/vaccines9101072.

[23] K. Venugopal, F. Hentzschel, G. Valkiūnas, M. Marti, Plasmodium asexual growth and sexual development in the haematopoietic niche of the host, Nat. Rev. Microbiol. 18 (2020) 177–189. https://doi.org/10.1038/s41579-019-0306-2.

[24] S. Cebrián-Camisón, J. Martínez-de la Puente, J. Figuerola, A literature review of host feeding patterns of invasive Aedes mosquitoes in Europe, Insects. 11 (2020) 848. https://doi.org/10.3390/insects11120848.

[25] P. Chandley, R. Ranjan, S. Kumar, S. Rohatgi, Host-parasite interactions during Plasmodium infection: Implications for immunotherapies, Front. Immunol. 13 (2023) 1091961. https://doi.org/10.3389/fimmu.2022.1091961.

[26] N.A. Counihan, J.K. Modak, T.F. de Koning-Ward, How malaria parasites acquire nutrients from their host, Front. Cell Dev. Biol. 9 (2021) 649184. https://doi.org/10.3389/fcell.2021.649184file:///C:/

[27] H. Madhav, N. Hoda, An insight into the recent development of the clinical candidates for the treatment of malaria and their target proteins, Eur. J. Med. Chem. 210 (2021) 112955. https://doi.org/10.1016/j.ejmech.2020.112955.

[28] C.O. Egwu, J.M. Augereau, K. Reybier, F. Benoit-Vical, Reactive oxygen species as the brainbox in malaria treatment, Antioxidants. 10 (2021) 1–20. https://doi.org/10.3390/antiox10121872.

[29] M. Adigo Shibeshi, E. Fentahun Enyew, G. Mequanint Adinew, T. Jemere Aragaw, Antimalarial Activity of Methanolic Extracts and Solvent Fractions of Combretum molle Leaves in Plasmodium berghei Infected Mice, J. Exp. Pharmacol. (2021) 69–89.

[30] M.R. Rosenthal, C.L. Ng, Plasmodium falciparum Artemisinin Resistance: The E ff ect of Heme, Protein Damage, and Parasite Cell Stress Response, 6 (2020) 1599–1614. https://doi.org/10.1021/acsinfecdis.9b00527.

[31] C. Naing, M.A. Whittaker, N.H. Htet, S.N. Aye, J.W. Mak, Efficacy of antimalarial drugs for treatment of uncomplicated falciparum malaria in Asian region: A network meta-analysis, PLoS One. 14 (2019) 1–16. https://doi.org/10.1371/journal.pone.0225882.

[32] C. Naing, V. Racloz, M.A. Whittaker, K. Aung, S.A. Reid, J.W. Mak, M. Tanner, Efficacy and safety of dihydroartemisinin-piperaquine for treatment of Plasmodium vivax malaria in endemic countries: meta-analysis of randomized controlled studies, PLoS One. 8 (2013) e78819. https://doi.org/10.1371/journal.pone.0078819.

[33] W. Satimai, P. Sudathip, S. Vijaykadga, A. Khamsiriwatchara, S. Sawang, T. Potithavoranan, A. Sangvichean, C. Delacollette, P. Singhasivanon, J. Kaewkungwal, Artemisinin resistance containment project in Thailand. II: Responses to mefloquine-artesunate combination therapy among falciparum malaria patients in provinces bordering Cambodia, Malar. J. 11 (2012) 1–13. https://doi.org/10.1186/1475-2875-11-300.

[34] D.A. Mekonnen, G.S. Abadura, S.W. Behaksra, H.S. Taffese, G.A. Bayissa, M.G. Bulto,

T.S. Tessema, F.G. Tadesse, E. Gadisa, Treatment of uncomplicated Plasmodium vivax with chloroquine plus radical cure with primaquine without G6PDd testing is safe in Arba Minch, Ethiopia: assessment of clinical and parasitological response, Malar. J. 22 (2023) 1–11. https://doi.org/10.1186/s12936-023-04562-x.

[35] F.A. Siddiqui, R. Boonhok, M. Cabrera, H.G.N. Mbenda, M. Wang, H. Min, X. Liang, J. Qin, X. Zhu, J. Miao, Role of Plasmodium falciparum Kelch 13 protein mutations in P. falciparum populations from northeastern Myanmar in mediating artemisinin resistance, MBio. 11 (2020) 10–1128. https://doi.org/10.1128/mbio.01134-19 f

[36] R.N. Price, L. Von Seidlein, N. Valecha, F. Nosten, J.K. Baird, N.J. White, Global extent of chloroquine-resistant Plasmodium vivax: a systematic review and meta-analysis, Lancet Infect. Dis. 14 (2014) 982–991.

[37] R.N. Price, R.J. Commons, K.E. Battle, K. Thriemer, K. Mendis, Plasmodium vivax in the era of the shrinking P. falciparum map, Trends Parasitol. 36 (2020) 560–570. https://doi.org/10.1016/j.pt.2020.03.009.

[38] D. Menard, A. Dondorp, Antimalarial drug resistance: a threat to malaria elimination, Cold Spring Harb. Perspect. Med. 7 (2017). https://doi.org/10.1101/cshperspect.a025619.

[39] A. Uwimana, E. Legrand, B.H. Stokes, J.-L.M. Ndikumana, M. Warsame, N. Umulisa, D. Ngamije, T. Munyaneza, J.-B. Mazarati, K. Munguti, Emergence and clonal expansion of in vitro artemisinin-resistant Plasmodium falciparum kelch13 R561H mutant parasites in Rwanda, Nat. Med. 26 (2020) 1602–1608. https://doi.org/10.1038/s41591-020-1005-2.

[40] C.O. Egwu, P. Pério, J.M. Augereau, I. Tsamesidis, F. Benoit-Vical, K. Reybier, Resistance to artemisinin in falciparum malaria parasites: A redox-mediated phenomenon, Free Radic. Biol. Med. 179 (2022) 317–327. https://doi.org/10.1016/j.freeradbiomed.2021.08.016.

[41] L. Van Dorp, P. Gelabert, A. Rieux, M. De Manuel, T. De-Dios, S. Gopalakrishnan, C. Carøe, M. Sandoval-Velasco, R. Fregel, I. Olalde, Plasmodium vivax malaria viewed through the lens of an eradicated European strain, Mol. Biol. Evol. 37 (2020) 773–785. https://doi.org/10.1093/molbev/msz264.

The literature review component has been put together, submitted and under review as a manuscript entitled "**Targeting Phase II Detoxification Enzyme Inhibitor in *Plasmodium* for Malaria Treatment**" by Olalekan Onisuru and Ikechukwu Achilonu in **Molecular and Biochemical Parasitology**. This review insightfully and novelly provides for the first time the scientific significance of targeting the inhibition of phase II detoxification enzymes (*Plasmodium falciparum* Glutathione S transferase, *Pf*GST and *Plasmodium vivax* Glutathione S transferase, *Pv*GST) in *Plasmodium* parasite. Since the management and treatment approach of malaria through drug targeting detoxification pathway and their enzymatic inhibition in *Plasmodium* has not been fully explored, this review paper will awaken research aimed at the development of novel antimalarials in this direction and serves to immensely benefit readers of this Journal. To the best of our knowledge, there has not been a published research or review paper on the inhibition of *Pf*GST and *Pv*GST in *Plasmodium falciparum* and *Pf*GST and *Plasmodium vivax* respectively.

Both authors support and are aware of submitting this manuscript to **Molecular and Biochemical Parasitology**. Also, no part or the whole of this manuscript is under consideration for publication by other journals.

# Targeting Phase II Detoxification Enzyme Inhibitor in *Plasmodium* for Malaria Treatment

Olalekan Onisuru and Ikechukwu Achilonu*

Protein Structure-Function and Research Unit, School of Molecular and Cell Biology, Faculty of Science, University of the Witwatersrand, Braamfontein, Johannesburg 2000, South Africa

***Correspondence to Ikechukwu Achilonu*** (Ikechukwu.Achilonu@wits.ac.za): Protein Structure-Function and Research Unit, School of Molecular and Cell Biology, Faculty of Science, University of the Witwatersrand, Braamfontein, Johannesburg 2000, South Africa

**Authors**

Olalekan Onisuru: 2430435@students.wits.ac.za

Ikechukwu Achilonu: Ikechukwu.Achilonu@wits.ac.za

## Review Outline

Challenge of Unmitigated Malaria Burden

Contemporaneity of Malaria Treatment

Complexity associated with Malaria Treatment and Elimination

Criticality of GSTs in *Plasmodium falciparum* and *Plasmodium vivax*

Concept of Biotransformation and Phase II Detoxification in *Plasmodium* Parasite

Containing malaria through Phase II Detoxification enzyme inhibition in *Plasmodium* Parasite

Conclusion on the significance of targeting Phase II Detoxification enzyme in *Plasmodium*

**Abstract**

As malaria burden and its global endemicity linger despite multidimensional and multistakeholder concerted efforts towards finding treatment, researchers continue to find new drug targets in order to grapple with the enormous burden malaria's morbidity and mortality places on man. *Plasmodium* parasite had progressively been resistant to previous and existing antimalarial drugs by evading their therapeutic mode of action, necessitating research into novel therapeutics with a distinct mode of action. There has however been tremendous call and demand for the development of potent, promising, and novel drug targets that could help suppress malaria occasioned by the rapid development of resistance to prophylactics and interventional drugs. Drug discovery in the face of resistant/multi drug resistant *Plasmodium* parasite essentially requires the need to characterize the enzyme(s) implicated in the parasite's xenobiotic (drug) metabolism. This is in addition to the enzyme implicated in the parasite's detoxification ability and knowing its biotransformation pathways. Considering this importance, it then becomes imperative to explore the inhibition of these detoxification enzymes. Glutathione *S*-Transferase (GST) is being implicated in this function. Their unique role in the parasite's survival includes the involvement in cellular processes leading to the metabolizing and detoxification of carcinogens, chemotherapeutic drugs, environmental pollutants, and oxidative stress products. Therefore, targeting the inhibition of this enzyme then becomes imperative in a novel drug discovery effort. In this review paper, the established understanding of GSTs' use in *Plasmodium* for detoxifying many substances intracellularly is copiously presented. The inactivation and conversion of diverse exogenous and endogenous toxic molecules through phase II biotransformation/detoxification process to less toxic soluble compounds is here explored as a potential antimalarial drug discovery route. This process of *Plasmodium falciparum* and *vivax*'s GSTs of metabolizing/detoxifying compounds to easily get rid of ones via glutathione (GSH) conjugation has been reexamined. To this end and in this review, we look at the significance and different approaches targeting the GST's inhibition in both *Plasmodium falciparum* and *Plasmodium vixax*. These two parasites are the two most responsible malaria-causing parasites in Africa and Asia, respectively. This is because the management and treatment approach of malaria through a drug-targeting detoxification pathway and their enzymatic inhibition in *Plasmodium* have not been fully explored.

**Keywords:** Malaria, Detoxification, Glutathione *S*-Transferase (GST), *Plasmodium*, Inhibition

**Challenge of Unmitigated Malaria Burden**

Malaria's global endemicity as reported by the World Health Organization (WHO) in her World Malaria Report for the year 2022 is estimated to be 247 million malaria cases as at the year 2021. This is spread across 84 malaria endemic countries with four countries namely Nigeria (27%), the Democratic Republic of the Congo (12%), Uganda (5%) and Mozambique (4%) accounting for approximately half of all cases globally [13]. Although, twenty-nine countries accounted for the 96% of the 619,000 global malaria deaths, four countries namely Nigeria (31%), Democratic Republic of the Congo (13%), Niger (4%), and United Republic of Tanzania (4%) accounted for more than halve of this deaths [13,42]. In the same vein, COVID-19 pandemic interruption between 2019-2021 posed a significant challenge to malaria control efforts. Other factors such as waning potency of stakeholders' primary malaria fighting resources and climate change also contributed to increased resistance to malaria's prevention [43–45]. Most importantly the multidrug resistance phenomenon being confronted by front line antimalarials, also contributed to the challenge of unmitigated malaria burden in a world where about half of its inhabitant are threatened by malaria [13,42,46,47]. Also, emerging challenge posed by *Anopheles stephensi*, a relatively new malaria vector which is originally native to South Asia and has now been progressively detected in Djibouti (2012), Ethiopia and Sudan (2016), Somalia (2019), and Nigeria (2020), has been reported. This has contributed to the challenge of malaria burden in the already malaria-traumatized world region [13,48–50]. This malaria global burden keeps being a notable public health concern due to malaria's associated and prevalent high morbidity and mortality, with most impact toll on children and pregnant women. Poor infrastructure and overall failing effectivity or failed health systems especially in low income countries in Sub-Saharan Africa who are the most hit have been contribute to the malaria burden [51]. The severity of socioeconomic impact of malaria is seen in the way it negatively impacts individuals, families, and entire communities. For instance, individuals affected by the disease are often immobilized, disengaged from social or economic activities, and ultimately reduce their productivity [52,53]. The costs associated with malaria treatment and prevention further exacerbate the economic burden, placing strain on already fragile health systems and household finances. Additionally, malaria-related expenditures divert resources away from other essential health services and development priorities, perpetuating a cycle of poverty and disease in endemic areas [54].

**Contemporaneity of Malaria Treatment**

Over time, antimalarial drugs such as quinolines (quinine, chloroquine, and mefloquine), naphthoquinones, 8-aminoquilonines, endoperoxides, antifolates (sulfadoxine and pyrimethamine), and the artemisinin derivatives [55–57] have been deployed as the main classes of antimalarials in the tropical and subtropical Sub-Saharan continent. It is widely recognized that the effectiveness of these drugs has significantly decreased due to the emergence of multidrug resistance, which has increasingly weakened efforts in malaria prophylaxis, treatment, and eradication. As a result, the battle against malaria is becoming more challenging, with fewer reliable options to prevent and treat the disease effectively [55]. In practical terms, the enormous pressure faced by these drugs which are not only occasioned by resistance but by the quality of the drugs, poor pharmacokinetic and drug pharmacodynamics among other factors have made the search and development of new generation drugs to be used as effective antimalarials not only imperative but urgent[55]. In contemporary times, a significant proportion of the antimalarial drug classes have been developed with the parasites' asexual stage in view. This is as this complex and cyclic process proceeds and continues only in the host where the parasite exerts its devastating and degrading action on the host by degrading its erythrocytes (hemoglobin) and utilize same for its growth and development [55]. This important metabolic pathway and that of nucleic acid synthesis have been deem significant and explored as targets for the development of some antimalarials [58].

The antimalarial drug discovery process, which was previously based on phenotypic screening and natural products with over seven million compounds tested against the malarial parasites' asexual stage, has now shifted to a process that is target-based [59,60]. This is owing to the high rate of attrition and cost of drug design coupled with the limitations associated with phenotypic screenings and also because of the advantages that the target-based approach has over it. Owing to these reasons, research into resistance's molecular marker and development of transmission-blocking antimalaria drugs have been explored. These efforts, alongside vaccine development, among other strategies, are all being pooled into the drive towards finding and using novelly potent small molecules for malaria treatment [61–63]. Contemporaneously and in addition to target-based drug discovery, both rational and computational drug design approaches towards the development of new and effective antimalarial is also being explored [60]. The understanding that the discovery of traditional drug approaches relies on existing agents and regimens' modification and optimization, respectively, alongside the idea of natural products testing,

chemical libraries screening, and repositioning of other disease-used drugs, are all currently employed in the search and efforts towards effective malaria treatment [64,65]. Over times and in the course of different antimalarial developments, different protein or genes in *Plasmodium* parasite has been explored as targets with some antimalarials targeting more than one protein or gene. Figure 1 shows different antimalarials that has been developed and their respective targets.

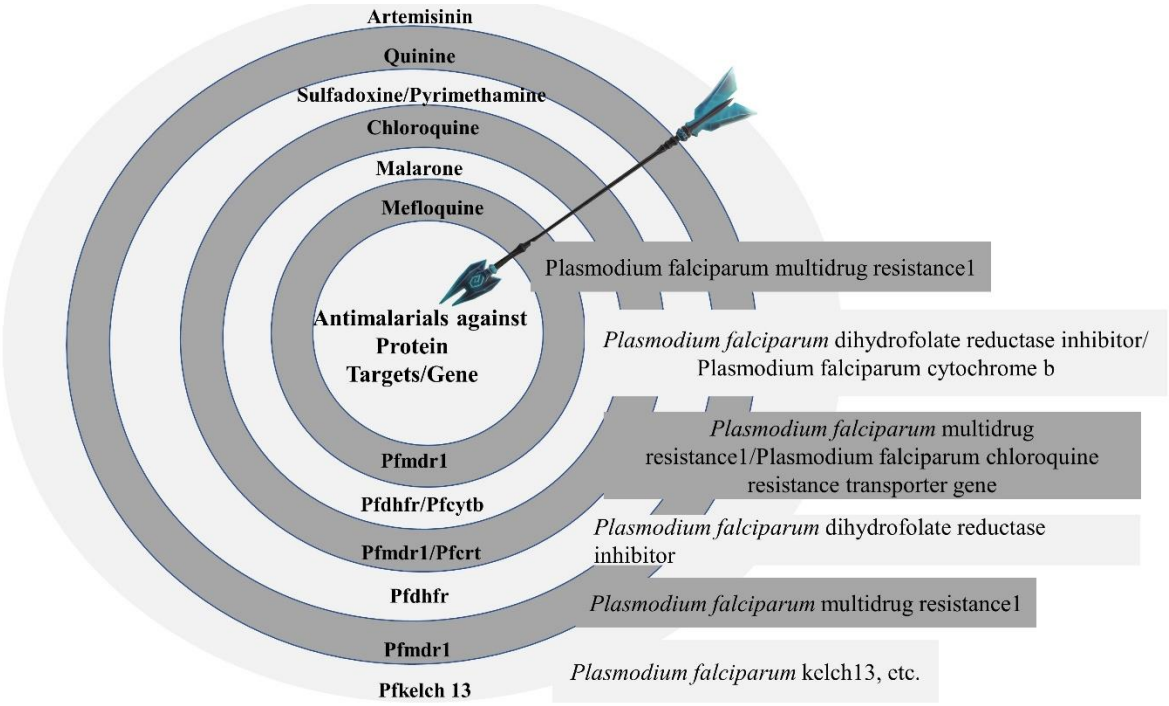


Figure 1: Pictorial summary of different antimalarials that have been developed and the enzymes/genes they respectively target.

The currently used antimalarial drugs can be broadly categorized into three groups (based on their combination with partner drugs), namely the aryl amino alcohol compounds, antifolate compounds, and the artemisinin compounds [66]. The aryl amino compounds that have been found to possess antimalarial properties include quinine, lumefantrine, chloroquine, amodiaquine, and mefloquine, among others. This is owing to the fact these aryl amino compounds possess an aromatic and amino alcohol portion linked by a carbon chain of two or three atoms in length, which is a structural requirement for a compound to possess an antiplasmodial activity. These aryl amino alcohols represent a versatile class of compounds with diverse pharmacological activities with applications in medicinal chemistry and general drug development [67,68]. On the other hand, the antifolates drug's use as antimalarial is owing to their ability to disrupt and inhibit

*Plasmodium*'s folate metabolism, synthesis, and use as cofactors. They are often used as combination therapies to enhance efficacy and prevent resistance [66,69]. However, due to genetic mutations leading to lowered binding, efficacy and resistance susceptibility, the other group of the antimalarial were then discovered [67,70–73]. The artemisinin compounds/drugs include artemisinin, dihydroartemisinin, artesunate, artemether, and arteether [74]. The WHO recommends artemisinin-based combination therapies (ACTs) for uncomplicated malaria treatment due to their dual mechanism of action: artemisinin acts quickly to substantially reduce the majority of malaria parasites, while the partner drug is responsible for eliminating any remaining parasites. This combination ensures a more complete and effective treatment, reducing the risk of resistance and recurrence by targeting the parasite population from multiple angles [30,31]. The WHO recommended ACTs for use in uncomplicated malaria treatment include artemether-lumefantrine (AL), artesunate-amodiaquine (ASAQ), artesunate-mefloquine (ASMQ), artesunate plus sulfadoxine-pyrimethamine (ASSP), and dihydroartemisinin-piperaquine (DHP) [31]. Similarly, an approach closely related to this combination therapy is the covalent biotherapy approach which involves the combination of two distinctly or analogous pharmacophores with their respective mechanism of actions to make a composite molecule [75,76]. This approach is also among those being contemporaneously explored as possible novel and effective antimalaria agents, although it remains uncertain if it will not be spontaneously or later welcome with resistance as the ACTs.

**Complexity associated with Malaria Treatment and Elimination**

Since the discovery of resistance and multidrug resistance malaria-causing *Plasmodium*, first to the traditional quinolone, antifolate antibiotics, and until recently to the gold standard WHO-approved artemisinin-based combination therapy (ACTs), the search for new and effective antimalaria has been brought to the front burner. The complexity involved in the life cycle of malaria parasites contributes to the challenge of its elimination, making available more and more platforms for intervention. This is because the host's pathological symptoms are primarily due to the malaria parasite's intra-erythrocytic stage [30,77]. *Plasmodium falciparum* and *Plasmodium vivax* possess complex biochemical action which remains puzzling or rather unclear, and hence making efforts aimed at combatting them difficult [78]. For example, both *Plasmodium falciparum* and *Plasmodium vivax* have the ability to evade host's immune response as they undergo antigenic

variation. This is because they can change the surface proteins expressed on their outer membrane and this hence making it difficult for the immune system to recognize and eliminate them effectively [79,80]. Similarly, both parasites have sophisticated mechanisms for invading host red blood cells, which is a critical step in the parasite's life cycle. These invasion mechanisms involve interactions between parasite surface proteins and receptors on red blood cells. Hence, targeting these invasion mechanisms with drugs is challenging due to the complexity of the interactions involved [81–84]. Also, *Plasmodium falciparum* has more recently developed a mechanism of circumventing the action of ACTs with resistance being associated with mutations in the Kelch13 gene, which encodes a protein involved in the parasite's response to artemisinin. This is in addition to the quiescence mechanism, which allows *Plasmodium falciparum* to survive in the red blood cells upon treatment and continues to grow after the withdrawal of the artemisinin derivatives treatment [38,85–88]. Furthermore, the short half-life associated with artemisinin and its derivatives also contributes to the treatment complexity of malaria as the parasites proliferate and lead to increased parasitemia and blood-stage infection [89]. *Plasmodium vivax,* on the other hand has a unique feature of temporarily entering a dormant state (hypnozoites) in the liver, leading to relapse and repeated clinical attacks. This the parasite does by continuing its regular cycle irrespective of drug administration [90,91]. This phenomenon, among others, results in inefficient parasite clearance, which ultimately leads to treatment failure [28]. This is because the speedy proliferation rate of *Plasmodium falciparum* and *Plasmodium vivax* in an infected patient and the severity of malaria corresponds to how many red blood cells have been infected. Moreover, because it is in the course of these widespread proliferation both in the mosquito midget, human liver, and RBC that malaria pathogenesis takes place, makes the malaria treatment complicated [92,93]. Similarly, the ease at which some established antimalarial drug targets are prone to mutation and thereby leading to resistance which ultimately culminate in withering of the therapeutic effectiveness of drugs for malaria treatment calls for attention.

In Table 1 below which succinctly highlights the time interval for resistance to be detected to some antimalarials and their targets (as per the WHO), it also shows the multiplicity of drugs designed targeting same or similar drug target. This similarly underscores the complexity in malarial drug design and treatment [61,94,95]. Till date there has not been any antimalaria drug produced or currently undergoing clinical trials as at May 2023 [61], that targets the inhibition of

phase II detoxification enzymes in both *Plasmodium falciparum* and *Plasmodium vivax*. However, we have started a study in this regard which has since been accepted for publication.

Table 1 Approved traditional and conventional antimalaria drugs, year of introduction, and report of resistance

| Antimalarial Agents | Year of introduction | Year resistance was reported | Year interval to resistance report | Therapy type | Reference(s) |
|---|---|---|---|---|---|
| Quinine | 1632 | 1910 | 278 | Single therapy | [87,96] |
| Artemisinin | 1980 | 2006 | 26 | Single therapy | [57,97] |
| Chloroquine | 1945 | 1957 | 12 | Single therapy | [87,96] |
| Mefloquine | 1977 | 1982 | 5 | Single therapy | [87] |
| Sulfadoxine+Pyrimethamine (Antifolates) | 1967 | 1967 | Same year | Combination therapy | [57,96] |
| Malarone (Atovaquone + Proguanil) | 1996 | 1996 | Same year | Combination therapy | [57,98] |
| Artemisinin based Combination Therapy (ACTs) | 2001 | 2007* | 6* | Combination therapy | [89,99,100] |

NB: * signifies that this first reported year and the time interval for it to be reported is as per the WHO guidelines towards partial artemisinin resistance.

**Criticality of GSTs in *Plasmodium falciparum* and *Plasmodium vivax***

Understanding and paying closer attention to *Plasmodium* parasite's survival mechanism vis-viz its biochemical mechanism process that is found to be fundamental to its survival, is indeed a requisite effort geared towards exploring new and novel potential targets for the design of potent antimalaria therapies [101]. Glutathione (GSH)'s functionality is seen as a co-factor for several antioxidants and detoxification enzymes, with GST and glutathione peroxidase (GPx) being the prominent examples [77]. Glutathione S-Transferase (GST, EC2.5.1.18), as a multi-functionally acting enzyme belonging to a superfamily, catalyzes the conjugation of GSH to multi-structural

electrophilic compounds such as xenobiotics (including drugs) and physiological substances [102]. Glutathione S-Transferase' presence in *Plasmodium* has been deemed not only an essentially multifunctional enzyme but also to possess peroxidase and isomerase capabilities. Depending directly on GSH, GST's in *Plasmodium* through a mercapturic acid pathway detoxify xenobiotics after catalyzing the conjugation of electrophilic substrates to GSH [103]. GSTs have conferred ability and resistance development against organisms ranging from simple prokaryotes to the most complex eukaryotes, with this resistance being against antibiotics, among other endogenous and exogenous compounds like insecticides, herbicides, environmental pollutants, chemical carcinogens, among others [104,105]. In addition to the highlighted significance of GSTs play, it's bodily process also found to step up in chloroquine-resistant cells, hence making it a good representation of ligandin for parasitotoxic hemin and an enzyme of a possible target for the development of antimalaria drug [1].

*Plasmodium falciparum* Glutathione S-Transferase (*Pf*GST) analyses had earlier been classified by Colón-Lorenzo phylogenetically and structurally as per their three-dimensional (3D) structures to be sigma class existing in a dimer-tetramer equilibrium regulated by GSH. Characteristically and exceptionally too, *Pf*GSTs are different from other GSTs in that they exist as tetramer and dimer in the absence and presence of GSH, respectively. This is unlike other GSTs, which exist as dimers in the presence of GSH [4,106]. Although there has not been a three-dimensional structure for *Plasmodium vivax* Glutathione-S-Transferase (*Pv*GST) solved yet, however available literature shows that *Pv*GST shares substantial sequence identity of about 85%, evolutionary similarity, structurally and with the same biochemical functionalities as *Pf*GST, and hence the reason why it is also being positioned as an important drug target for the treatment of *Plasmodium vivax* caused malaria [9,107,108].

Interestingly, only one GST has been identified in the *Plasmodium falciparum* parasite. This GST shares merely 37% sequence identity with known GST family members, indicating that it belongs to a novel class. This uniqueness highlights its potential as a new target for antimalarial drug development, emphasizing the need for further research to explore its structure and function within the context of combating malaria [106]. Another phenomenon of exclusivity to *Plasmodium* is that only *Pf*GST has the dimer-to-tetramer transition, a feature that confers the ability to inactivate enzymes [4]. The GSTs of *Plasmodium falciparum* are differentiated structurally from those of other GSTs in that they possess an extra loop that converts the alpha helix 4 to alpha helix

5 (residue 113-120). However, these residues have been found to participate in the formation of dimer and enzyme activity [4].

**Concept of Biotransformation and Phase II Detoxification in *Plasmodium***

Biotransformation and phase II detoxification processes are two essential routes towards the elimination of xenobiotics, such as toxins and drugs from living organisms' body [109,110]. These processes are employed in the *Plasmodium* parasites to modify drugs (antimalarials), adapt well and interplay with the host environment, and among others. Hence, elucidating *Plasmodium falciparum* and *Plasmodium vivax*'s biotransformation and detoxification pathway will be essential towards the development of new antimalarials [111,112]. This is as the understanding of drug target mechanism has become pivotal towards every scientifical efforts aimed at developing target-based, novel, and potent antimalarials. This becomes imperative as insight into this mechanism will help to elucidate possible structural modifications of late-stage preclinical development of antimalarials. It will also help postulate possible structural modifications to existing antimalarials that has hitherto been confronted and rendered ineffective by resistance phenomenon [113]. Although metabolism and biotransformation are words often used interchangeably especially in relation to drugs, they are however different in their meaning. Metabolism depicts the breaking down mechanisms of drugs, biotransformation on the other hand describes living organisms' biochemical alteration or modification of drugs (pharmaceutical substances) with the aid of particularize enzymatic systems [114–116].

Biotransformation and detoxification as a defence process by *Plasmodium falciparum* and *Plasmodium vivax* are made possible by Glutathione S-Transferase, which is a ubiquitous enzyme which also plays a significant role in all living organisms. Specifically, in *Plasmodium falciparum* and *Plasmodium vivax*, while biotransformation as a process involves the inactivation of active compounds to one which is pharmacologically less active than the parent compound, it can also lead to a metabolic product with more activity or toxicity, otherwise [115,117,118]. However, when this biotransformation process of xenobiotics (drugs) produces a less toxic or non-toxic product which is water soluble and excretable, it is then termed a detoxification process and entotoxification process if the product is rather more toxic [119]. While these detoxification processes are usually in two phases (I and II), the phase I detoxification reaction, which is mainly

(oxidation, reduction, and hydrolysis reaction) will, however, still need a complementary effort of a phase II reaction to completely produce a pharmacologically inactive product as seen in figure 2, and hence making the inhibition of this process an ideal route for the development of novel antimalarials. Again, while this phase I drug biotransformation process or reaction has previously been explored in the development of different drugs or prodrugs, not so much clinical research has been conducted with phase II detoxification pathway inhibition in view, especially in antimalaria drug developments.

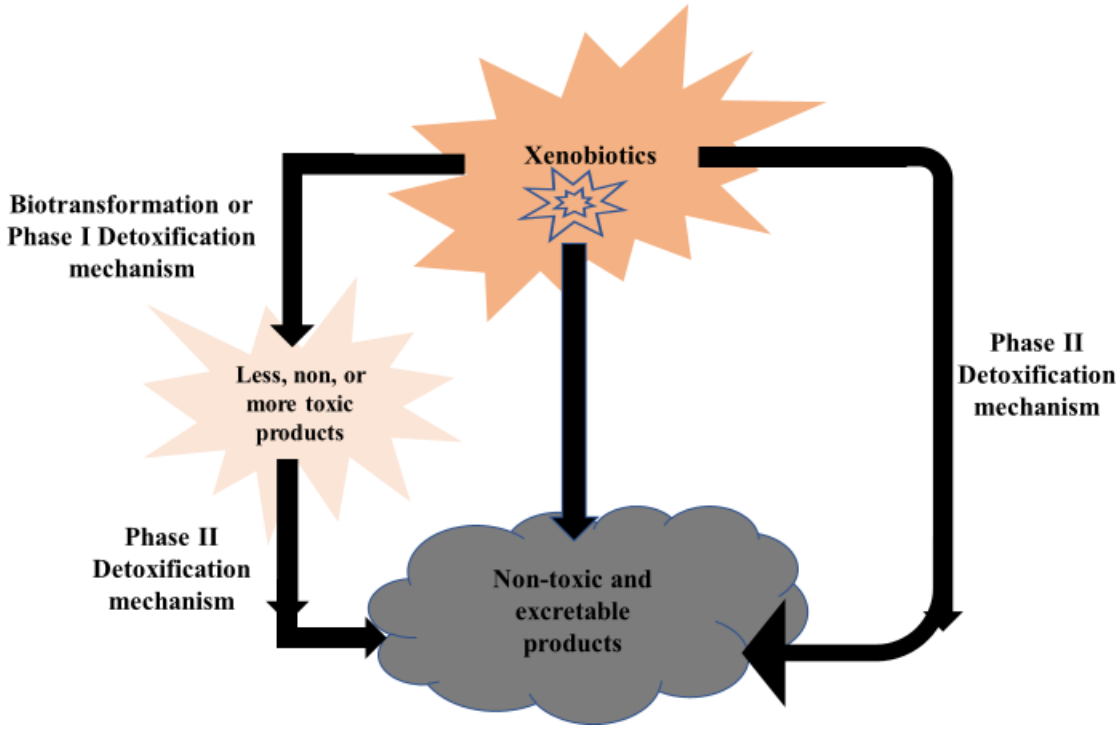


Figure 2: A schematic illustration of biotransformation/detoxification of xenobiotics through phase I and phase II reaction mechanisms

It is however worthy of note that while only few xenobiotic metabolism and drug detoxification are excreted in urine or feces unchanged, most pass through a number of metabolic conversions. These conversions in living cells change xenobiotics' physical properties from being lipophilic to hydrophilic, thereby reducing the therapeutic effect(s) of such xenobiotics [118]. While the GSH's conjugation process catalyzed by *Plasmodium's* GST to xenobiotics (drugs) may occur after the phase I reaction or directly by phase II reaction (as seen in figure 2), they however lead to the production of water-soluble, excretable, and pharmacologically inactive compound, thereby laying credence on the significance of this phase II reaction. Given this insight and in the

face of resistance and multidrug-resistant phenomenon that has made the search for new druggable targets and pathways in antimalaria development drive imperative, the novel look into the concept of inhibition of essential functionalities (such as the phase II detoxification ability) in malaria parasite might be the game changer in the effort to finding effective antimalarial with novel mechanism of action totally different form the existing malaria drugs.

**Containing Malaria through Phase II Detoxification Enzyme Inhibition**

Given the importance of malaria parasites' GST in the detoxification of endogenous and xenobiotic compounds, among other functionalities which has been shown to enhance drug resistance ability to anti-parasitic and insecticides, the inhibition of this detoxification ability is thus worth targeting as a novel and effective antimalarial [120]. Also, studies have shown that GSH vis-à-vis GST activities significantly increases chloroquine resistance malaria parasites [121–123]. Previously, the detoxification pathway of heme, an iron containing molecule and hemoglobin digestion toxic byproduct has been mostly explored as drug target malaria treatment but with limitations, owing to the uncertainty around the mechanism of heme detoxification. This is as this mechanism has been found to have likelihood of increasing malaria parasites reactive oxygen species (ROS) and nitric oxide (NO), which are both harmful to the parasite [124,125]. Specifically, both *Pf*GST and *Pv*GST have been reported to be very important in protecting their cells from ROS-induced oxidative stress through this phase II detoxification process, thereby laying credence to the importance of targeting its inhibition as a means of developing novel antimalarial with a broader aim of containing malaria.

Since studies have shown that the two gene families/enzymes commonly linked to mosquito resistance are cytochrome P450s and glutathione s-transferase and with studies already exploring P450s as a drug target [126,127], looking into the inhibition of GSTs' detoxification ability in the parasite with the view of exploring clinical entities that could inhibit *Pf*GST and *Pv*GST will be a major step in scaffolding new antimalarial design and development. Studies currently ongoing and being concluded at the Protein Structure-Function Research Unit (PSFRU) of the University of the Witwatersrand has shown through biochemical and structural characterization that the inhibition of phase II detoxification enzymes (namely *Pf*GST and *Pv*GST in both Plasmodium falciparum and Plasmodium vivax respectively

**Conclusion on the significance of targeting Phase II Detoxification enzyme in *Plasmodium***

Drug target mechanisms have become pivotal in the effort to develop target-based, novel and potent antimalarials. Understanding the mechanism of antimalarial drug action is crucial for identifying structural modifications in drugs that have reached late-stage preclinical development but have been rendered ineffective by resistance and multidrug resistance. This knowledge allows researchers to pinpoint where and how these drugs can be improved to combat resistant strains of the malaria parasite. By elucidating the drug's interaction with its target, scientists can design modifications that enhance efficacy and overcome resistance, thereby extending the lifespan of existing treatments and improving their effectiveness against malaria. This approach is vital for developing more robust and sustainable antimalarial therapies in the future. Also, given the enormous pressure faced by current antimalarials, which are occasioned by resistance alongside the quality of these drugs, poor pharmacokinetic and drug pharmacodynamics among others, the search and development of new generation drugs that can be used as effective antimalarials is therefore not only imperative but urgent. Given the scientifically proven elucidated facts in this review, the inhibition of *Pf*GST and *Pv*GST will wither both *Plasmodium falciparum's* and *Plasmodium vivax's* detoxification abilities respectively and bring down their antioxidant ability. Remarkably so and given the understanding that the inhibition of *Plasmodium falciparum* Glutathione-S-Transferase (*Pf*GST) and *Plasmodium vivax* Glutathione-S-Transferase (*Pv*GST) is not only anticipated to alter the Glutathione-dependent conjugation process, but also increase cytotoxic peroxides' level, and toxic ferriprotoporphyrin IX's (FP's) concentration, which then promisingly makes *Pf*GST and *Pv*GST novel drug targets. It has become equally imperative to consider and always include *Plasmodium vivax* (an etiological agent of most malaria cases recorded in the continent of Asia, which has also gradually found its way to Africa) in the drive aimed at developing novel and effective antimalarials. This is as *Plasmodium vivax* Glutathione S-Transferase (*Pv*GST) which shares substantial sequence identities and functionalities as *Pf*GST, as an important drug target will ultimately respond to inhibition activity through the same mechanism as *Pf*GST. We therefore surmise that owing to the novelty in class that *Plasmodium falciparum's* GST and *Plasmodium vivax's* GST stand for among GST isoenzymes and isoforms, *Pf*GST and *Pv*GST have hence not only been adjudged a highly drug target for the development of new antimalarials but targeting their inhibition ability will be the very effective in malaria treatment with no spontaneous resistance likely to be recorded.

## Declarations

### Ethical Approval

Not applicable to this work.

### Competing Interests

The authors declare that they have no competing interests.

### Authors Contribution

Olalekan Onisuru wrote this manuscript, figures, and table formatting were also done by him.

Ikechukwu Achilonu conceptualized this research, provides guidance, and supervision.

### Funding

This work receives no funding of any kind.

### Availability of data materials

Not applicable to this work

## References


[1] K. Fritz-Wolf, A. Becker, S. Rahlfs, P. Harwaldt, R.H. Schirmer, W. Kabsch, K. Becker, X-ray structure of glutathione S-transferase from the malarial parasite Plasmodium falciparum, Proc. Natl. Acad. Sci. U. S. A. 100 (2003) 13821–13826. https://doi.org/10.1073/pnas.2333763100.

[2] N. Hiller, K. Fritz-Wolf, M. Deponte, W. Wende, H. Zimmermann, K. Becker, Plasmodium falciparum glutathione S -transferase-Structural and mechanistic studies on ligand binding and enzyme inhibition , Protein Sci. 15 (2006) 281–289. https://doi.org/10.1110/ps.051891106.

[3] R. Mangoyi, R. Hayeshi, B. Ngadjui, F. Ngandeu, M. Bezabih, B. Abegaz, S. Razafimahefa, P. Rasoanaivo, S. Mukanganyama, Glutathione transferase from Plasmodium falciparum - Interaction with malagashanine and selected plant natural products, J. Enzyme Inhib. Med. Chem. 25 (2010) 854–862. https://doi.org/10.3109/14756366.2010.486793.

[4] E.E. Colón-Lorenzo, D.D. Colón-López, J. Vega-Rodríguez, A. Dupin, D.A. Fidock, A. Baerga-Ortiz, J.G. Ortiz, J. Bosch, A.E. Serrano, Structure-Based Screening of Plasmodium berghei Glutathione S-Transferase Identifies CB-27 as a Novel Antiplasmodial Compound, Front. Pharmacol. 11 (2020) 1–17. https://doi.org/10.3389/fphar.2020.00246.

[5] S. Dasari, M.S. Ganjayi, P. Yellanurkonda, S. Basha, B. Meriga, Role of glutathione S-transferases in detoxification of a polycyclic aromatic hydrocarbon, methylcholanthrene, Chem. Biol. Interact. 294 (2018) 81–90. https://doi.org/10.1016/j.cbi.2018.08.023.

[6] D. SHEEHAN, G. MEADE, V.M. FOLEY, C.A. DOWD, Structure, function and evolution of glutathione transferases: implications for classification of non-mammalian members of an ancient enzyme superfamily, Biochem. J. 360 (2001) 1–16. https://doi.org/10.1042/bj3600001.

[7] I. Quesada-Soriano, C. Barón, R. Téllez-Sanz, F. García-Maroto, L. García-Fuentes, Asn112 in Plasmodium falciparum glutathione S-transferase is essential for induced reversible tetramerization by phosphate or pyrophosphate, Biochim. Biophys. Acta - Proteins Proteomics. 1844 (2014) 1427–1436. https://doi.org/10.1016/j.bbapap.2014.04.017.

[8] M.N. Al-Qattan, M.N. Mordi, S.M. Mansor, Assembly of ligands interaction models for glutathione-S-transferases from Plasmodium falciparum, human and mouse using enzyme kinetics and molecular docking, Comput. Biol. Chem. 64 (2016) 237–249. https://doi.org/10.1016/j.compbiolchem.2016.07.007.

[9] T. Tripathi, B.-K. Na, W.-M. Sohn, K. Becker, V. Bhakuni, Structural, functional and unfolding characteristics of glutathione S-transferase of Plasmodium vivax, Arch. Biochem. Biophys. 487 (2009) 115–122. https://doi.org/10.1016/j.abb.2009.05.011.

[10] J. Huttu, B.K. Singh, S.P. Bhargav, J.M. Sattler, H. Schüler, I. Kursula, Crystallization and preliminary structural characterization of the two actin-depolymerization factors of the malaria parasite, Acta Crystallogr. Sect. F Struct. Biol. Cryst. Commun. 66 (2010) 583–587. https://doi.org/10.1107/S1744309110011589.

[11] C. Burmeister, M. Perbandt, C. Betzel, R.D. Walter, E. Liebau, Crystallization and preliminary X-ray diffraction studies of the glutathione S-transferase from Plasmodium falciparum, Acta Crystallogr. - Sect. D Biol. Crystallogr. 59 (2003) 1469–1471. https://doi.org/10.1107/S0907444903011090.

[12] K.N. Olafson, T.Q. Nguyen, J.D. Rimer, P.G. Vekilov, Antimalarials inhibit hematin crystallization by unique drug–surface site interactions, Proc. Natl. Acad. Sci. U. S. A. 114 (2017) 7531–7536. https://doi.org/10.1073/pnas.1700125114.

[13] World Health Organization, World malaria report 2022, World Health Organization, 2022.

[14] W.H.O. Organization, World malaria report 2023, 2023.

[15] R. Maharaj, I. Seocharan, B. Qwabe, M. Mkhabela, S. Kissoon, Decadal epidemiology of malaria in KwaZulu - Natal , a province in South Africa targeting elimination, Malar. J. (2019) 1–7. https://doi.org/10.1186/s12936-019-3001-x.

[16] J. Popovici, L. Pierce-Friedrich, S. Kim, S. Bin, V. Run, D. Lek, K.H.D. Hee, L. Lee Soon-U, M. V Cannon, D. Serre, Recrudescence, reinfection, or relapse? A more rigorous framework to assess chloroquine efficacy for Plasmodium vivax malaria, J. Infect. Dis. 219 (2019) 315–322. https://doi.org/10.1093/infdis/jiy484.

[17] M.A. Shibeshi, Z.D. Kifle, S.A. Atnafie, Antimalarial drug resistance and novel targets for

antimalarial drug discovery, Infect. Drug Resist. 13 (2020) 4047–4060. https://doi.org/10.2147/IDR.S279433.

[18] B. Larson, Origin of Two Most Virulent Agents of Human Malaria: Plasmodium falciparum and Plasmodium vivax, Malaria. 4 (2019) 1–16. https://doi.org/10.5772/intechopen.84481.

[19] D.E. Loy, W. Liu, Y. Li, G.H. Learn, L.J. Plenderleith, S.A. Sundararaman, P.M. Sharp, B.H. Hahn, Out of Africa: origins and evolution of the human malaria parasites Plasmodium falciparum and Plasmodium vivax, Int. J. Parasitol. 47 (2017) 87–97. https://doi.org/10.1016/j.ijpara.2016.05.008.

[20] G. Boumis, G. Giardina, F. Angelucci, A. Bellelli, M. Brunori, D. Dimastrogiovanni, F. Saccoccia, A.E. Miele, Crystal structure of Plasmodium falciparum thioredoxin reductase, a validated drug target, Biochem. Biophys. Res. Commun. 425 (2012) 806–811. https://doi.org/10.1016/j.bbrc.2012.07.156.

[21] F.A. Siddiqui, X. Liang, L. Cui, Plasmodium falciparum resistance to ACTs: Emergence, mechanisms, and outlook, Int. J. Parasitol. Drugs Drug Resist. 16 (2021) 102–118. https://doi.org/10.1016/j.ijpddr.2021.05.007.

[22] S.R. Bonam, L. Rénia, G. Tadepalli, J. Bayry, H.M.S. Kumar, Plasmodium falciparum malaria vaccines and vaccine adjuvants, Vaccines. 9 (2021) 1072. https://doi.org/10.3390/vaccines9101072.

[23] K. Venugopal, F. Hentzschel, G. Valkiūnas, M. Marti, Plasmodium asexual growth and sexual development in the haematopoietic niche of the host, Nat. Rev. Microbiol. 18 (2020) 177–189. https://doi.org/10.1038/s41579-019-0306-2.

[24] S. Cebrián-Camisón, J. Martínez-de la Puente, J. Figuerola, A literature review of host feeding patterns of invasive Aedes mosquitoes in Europe, Insects. 11 (2020) 848. https://doi.org/10.3390/insects11120848.

[25] P. Chandley, R. Ranjan, S. Kumar, S. Rohatgi, Host-parasite interactions during Plasmodium infection: Implications for immunotherapies, Front. Immunol. 13 (2023) 1091961. https://doi.org/10.3389/fimmu.2022.1091961.

[26] N.A. Counihan, J.K. Modak, T.F. de Koning-Ward, How malaria parasites acquire nutrients

from their host, Front. Cell Dev. Biol. 9 (2021) 649184. https://doi.org/10.3389/fcell.2021.649184

[27] H. Madhav, N. Hoda, An insight into the recent development of the clinical candidates for the treatment of malaria and their target proteins, Eur. J. Med. Chem. 210 (2021) 112955. https://doi.org/10.1016/j.ejmech.2020.112955.

[28] C.O. Egwu, J.M. Augereau, K. Reybier, F. Benoit-Vical, Reactive oxygen species as the brainbox in malaria treatment, Antioxidants. 10 (2021) 1–20. https://doi.org/10.3390/antiox10121872.

[29] M. Adigo Shibeshi, E. Fentahun Enyew, G. Mequanint Adinew, T. Jemere Aragaw, Antimalarial Activity of Methanolic Extracts and Solvent Fractions of Combretum molle Leaves in Plasmodium berghei Infected Mice, J. Exp. Pharmacol. (2021) 69–89.

[30] M.R. Rosenthal, C.L. Ng, Plasmodium falciparum Artemisinin Resistance: The E ff ect of Heme, Protein Damage, and Parasite Cell Stress Response, 6 (2020) 1599–1614. https://doi.org/10.1021/acsinfecdis.9b00527.

[31] C. Naing, M.A. Whittaker, N.H. Htet, S.N. Aye, J.W. Mak, Efficacy of antimalarial drugs for treatment of uncomplicated falciparum malaria in Asian region: A network meta-analysis, PLoS One. 14 (2019) 1–16. https://doi.org/10.1371/journal.pone.0225882.

[32] C. Naing, V. Racloz, M.A. Whittaker, K. Aung, S.A. Reid, J.W. Mak, M. Tanner, Efficacy and safety of dihydroartemisinin-piperaquine for treatment of Plasmodium vivax malaria in endemic countries: meta-analysis of randomized controlled studies, PLoS One. 8 (2013) e78819. https://doi.org/10.1371/journal.pone.0078819.

[33] W. Satimai, P. Sudathip, S. Vijaykadga, A. Khamsiriwatchara, S. Sawang, T. Potithavoranan, A. Sangvichean, C. Delacollette, P. Singhasivanon, J. Kaewkungwal, Artemisinin resistance containment project in Thailand. II: Responses to mefloquine-artesunate combination therapy among falciparum malaria patients in provinces bordering Cambodia, Malar. J. 11 (2012) 1–13. https://doi.org/10.1186/1475-2875-11-300.

[34] D.A. Mekonnen, G.S. Abadura, S.W. Behaksra, H.S. Taffese, G.A. Bayissa, M.G. Bulto, T.S. Tessema, F.G. Tadesse, E. Gadisa, Treatment of uncomplicated Plasmodium vivax

with chloroquine plus radical cure with primaquine without G6PDd testing is safe in Arba Minch, Ethiopia: assessment of clinical and parasitological response, Malar. J. 22 (2023) 1–11. https://doi.org/10.1186/s12936-023-04562-x.

[35] F.A. Siddiqui, R. Boonhok, M. Cabrera, H.G.N. Mbenda, M. Wang, H. Min, X. Liang, J. Qin, X. Zhu, J. Miao, Role of Plasmodium falciparum Kelch 13 protein mutations in P. falciparum populations from northeastern Myanmar in mediating artemisinin resistance, MBio. 11 (2020) 10–1128. https://doi.org/10.1128/mbio.01134-19 file:///C:/Users/Administrator/Downloads/scholar - 2024-01-27T122352.713.ris.

[36] R.N. Price, L. Von Seidlein, N. Valecha, F. Nosten, J.K. Baird, N.J. White, Global extent of chloroquine-resistant Plasmodium vivax: a systematic review and meta-analysis, Lancet Infect. Dis. 14 (2014) 982–991.

[37] R.N. Price, R.J. Commons, K.E. Battle, K. Thriemer, K. Mendis, Plasmodium vivax in the era of the shrinking P. falciparum map, Trends Parasitol. 36 (2020) 560–570. https://doi.org/10.1016/j.pt.2020.03.009.

[38] D. Menard, A. Dondorp, Antimalarial drug resistance: a threat to malaria elimination, Cold Spring Harb. Perspect. Med. 7 (2017). https://doi.org/10.1101/cshperspect.a025619.

[39] A. Uwimana, E. Legrand, B.H. Stokes, J.-L.M. Ndikumana, M. Warsame, N. Umulisa, D. Ngamije, T. Munyaneza, J.-B. Mazarati, K. Munguti, Emergence and clonal expansion of in vitro artemisinin-resistant Plasmodium falciparum kelch13 R561H mutant parasites in Rwanda, Nat. Med. 26 (2020) 1602–1608. https://doi.org/10.1038/s41591-020-1005-2.

[40] C.O. Egwu, P. Pério, J.M. Augereau, I. Tsamesidis, F. Benoit-Vical, K. Reybier, Resistance to artemisinin in falciparum malaria parasites: A redox-mediated phenomenon, Free Radic. Biol. Med. 179 (2022) 317–327. https://doi.org/10.1016/j.freeradbiomed.2021.08.016.

[41] L. Van Dorp, P. Gelabert, A. Rieux, M. De Manuel, T. De-Dios, S. Gopalakrishnan, C. Carøe, M. Sandoval-Velasco, R. Fregel, I. Olalde, Plasmodium vivax malaria viewed through the lens of an eradicated European strain, Mol. Biol. Evol. 37 (2020) 773–785. https://doi.org/10.1093/molbev/msz264.

[42] Z. Li, J. Shi, N. Li, M. Wang, Y. Jin, Z. Zheng, Temporal trends in the burden of non-

communicable diseases in countries with the highest malaria burden, 1990–2019: Evaluating the double burden of non-communicable and communicable diseases in epidemiological transition, Global. Health. 18 (2022) 1–9.

[43] A. Zawawi, M. Alghanmi, I. Alsaady, H. Gattan, H. Zakai, K. Couper, The impact of COVID-19 pandemic on malaria elimination, Parasite Epidemiol. Control. 11 (2020) e00187. https://doi.org/10.1016/j.parepi.2020.e00187.

[44] S.J. Rogerson, J.G. Beeson, M. Laman, J.R. Poespoprodjo, T. William, J.A. Simpson, R.N. Price, Identifying and combating the impacts of COVID-19 on malaria, BMC Med. 18 (2020) 1–7. https://doi.org/10.1186/s12916-020-01710-x.

[45] W.H. Organization, The potential impact of health service disruptions on the burden of malaria: a modelling analysis for countries in sub-Saharan Africa, (2020) 1–44.

[46] R. Hussein, M. Guedes, N. Ibraheim, M.M. Ali, A. El-Tahir, N. Allam, H. Abuakar, R. Pecoits-Filho, P. Kotanko, Impact of COVID-19 and malaria coinfection on clinical outcomes: a retrospective cohort study, Clin. Microbiol. Infect. 28 (2022) 1152-e1.

[47] C. Li, S. Managi, Global malaria infection risk from climate change, Environ. Res. 214 (2022) 114028.

[48] T.E. Carter, S. Yared, A. Gebresilassie, V. Bonnell, L. Damodaran, K. Lopez, M. Ibrahim, S. Mohammed, D. Janies, First detection of Anopheles stephensi Liston, 1901 (Diptera: culicidae) in Ethiopia using molecular and morphological approaches, Acta Trop. 188 (2018) 180–186.

[49] A. Ahmed, R. Khogali, M.-A.B. Elnour, R. Nakao, B. Salim, Emergence of the invasive malaria vector Anopheles stephensi in Khartoum State, Central Sudan, Parasit. Vectors. 14 (2021) 1–5. https://doi.org/10.1186/s13071-021-05026-4.

[50] M.K. Faulde, L.M. Rueda, B.A. Khaireh, First record of the Asian malaria vector Anopheles stephensi and its possible role in the resurgence of malaria in Djibouti, Horn of Africa, Acta Trop. 139 (2014) 39–43.

[51] E. Sarpong, D.O. Acheampong, G.N.R. Fordjour, A. Anyanful, E. Aninagyei, D.A. Tuoyire, D. Blackhurst, G.B. Kyei, M. Ekor, N.E. Thomford, Zero malaria: a mirage or reality for

populations of sub-Saharan Africa in health transition, Malar. J. 21 (2022) 314.

[52] S.T. Wafula, T. Habermann, M.A. Franke, J. May, D.I. Puradiredja, E. Lorenz, J. Brinkel, What are the pathways between poverty and malaria in sub-Saharan Africa? A systematic review of mediation studies, Infect. Dis. Poverty. 12 (2023) 13–30. https://doi.org/10.1186/s40249-023-01110-2.

[53] O.O. John, F. Atewologun, D.E. Lucero-Prisno III, O.A. Adigun, O.T. Adebimpe, E. Manirambona, O.N. Olabode, G. Eshun, A.O. Agboola, I.I. Okon, Bridging the Gap to Malaria Vaccination in Africa: Challenges and Opportunities, J. Med. Surgery, Public Heal. (2024) 100059. https://doi.org/10.1016/j.glmedi.2024.100059.

[54] S. Alonso, C.J. Chaccour, E. Elobolobo, A. Nacima, B. Candrinho, A. Saifodine, F. Saute, M. Robertson, R. Zulliger, The economic burden of malaria on households and the health system in a high transmission district of Mozambique, Malar. J. 18 (2019) 1–10. https://doi.org/10.1186/s12936-019-2995-4.

[55] S. Rout, R.K. Mahapatra, Plasmodium falciparum: Multidrug resistance, Chem. Biol. Drug Des. 93 (2019) 737–759.

[56] N.A. Bispo, R. Culleton, L.A. Silva, P. Cravo, A systematic in silico search for target similarity identifies several approved drugs with potential activity against the Plasmodium falciparum apicoplast, PLoS One. 8 (2013) e59288.

[57] K. Haldar, S. Bhattacharjee, I. Safeukui, Drug resistance in Plasmodium, Nat. Rev. Microbiol. 16 (2018) 156–170. https://doi.org/10.1038/nrmicro.2017.161.

[58] K.T. Andrews, G. Fisher, T.S. Skinner-Adams, Drug repurposing and human parasitic protozoan diseases, Int. J. Parasitol. Drugs Drug Resist. 4 (2014) 95–111.

[59] T. Yang, S. Ottilie, E.S. Istvan, K.P. Godinez-Macias, A.K. Lukens, B. Baragaña, B. Campo, C. Walpole, J.C. Niles, K. Chibale, K.J. Dechering, M. Llinás, M.C.S. Lee, N. Kato, S. Wyllie, C.W. McNamara, F.J. Gamo, J. Burrows, D.A. Fidock, D.E. Goldberg, I.H. Gilbert, D.F. Wirth, E.A. Winzeler, MalDA, Accelerating Malaria Drug Discovery, Trends Parasitol. 37 (2021) 493–507. https://doi.org/10.1016/j.pt.2021.01.009.

[60] B. Forte, S. Ottilie, A. Plater, B. Campo, K.J. Dechering, F.J. Gamo, D.E. Goldberg, E.S.

Istvan, M. Lee, A.K. Lukens, C.W. McNamara, J.C. Niles, J. Okombo, C.F.A. Pasaje, M.G. Siegel, D. Wirth, S. Wyllie, D.A. Fidock, B. Baragaña, E.A. Winzeler, I.H. Gilbert, Prioritization of Molecular Targets for Antimalarial Drug Discovery, ACS Infect. Dis. 7 (2021) 2764–2776. https://doi.org/10.1021/acsinfecdis.1c00322.

[61] T. Umumararungu, J.B. Nkuranga, G. Habarurema, J.B. Nyandwi, M.J. Mukazayire, J. Mukiza, R. Muganga, I. Hahirwa, M. Mpenda, A.N. Katembezi, Recent developments in antimalarial drug discovery, Bioorg. Med. Chem. (2023) 117339.

[62] J. Okombo, K. Chibale, Recent updates in the discovery and development of novel antimalarial drug candidates, Medchemcomm. 9 (2018) 437–453. https://doi.org/10.1039/C7MD00637C.

[63] M. Mishra, V.K. Mishra, V. Kashaw, A.K. Iyer, S.K. Kashaw, Comprehensive review on various strategies for antimalarial drug discovery., Eur. J. Med. Chem. 125 (2017) 1300–1320. https://doi.org/10.1016/j.ejmech.2016.11.025.

[64] Y. Chen, C. Murillo-Solano, M.G. Kirkpatrick, T. Antoshchenko, H.W. Park, J.C. Pizarro, Repurposing drugs to target the malaria parasite unfolding protein response, Sci. Rep. 8 (2018) 1–12. https://doi.org/10.1038/s41598-018-28608-2.

[65] Y. Le Govic, S. Houzé, N. Papon, Repurposing Anticancer Drugs To Tackle Malaria, ChemMedChem. 16 (2021) 2192–2194.

[66] M.A. Shibeshi, Z.D. Kifle, S.A. Atnafie, Antimalarial drug resistance and novel targets for antimalarial drug discovery, Infect. Drug Resist. 13 (2020) 4047. https://doi.org/10.2147/IDR.S279433.

[67] M. Quiliano, A. Mendoza, K.Y. Fong, A. Pabón, N.E. Goldfarb, I. Fabing, A. Vettorazzi, A.L. de Cerain, B.M. Dunn, G. Garavito, Exploring the scope of new arylamino alcohol derivatives: Synthesis, antimalarial evaluation, toxicological studies, and target exploration, Int. J. Parasitol. Drugs Drug Resist. 6 (2016) 184–198. https://doi.org/10.1016/j.ijpddr.2016.09.004.

[68] H. Madhav, N. Hoda, An insight into the recent development of the clinical candidates for the treatment of malaria and their target proteins, Eur. J. Med. Chem. 210 (2021) 112955.

https://doi.org/10.1016/j.ejmech.2020.112955.

[69] C. Pethrak, N. Posayapisit, J. Pengon, N. Suwanakitti, A. Saeung, M. Shorum, K. Aupalee, K. Taai, Y. Yuthavong, S. Kamchonwongpaisan, New insights into antimalarial chemopreventive activity of antifolates, Antimicrob. Agents Chemother. 66 (2022) e01538-21. https://doi.org/10.1128/aac.01538-21.

[70] S. Sridaran, S.K. McClintock, L.M. Syphard, K.M. Herman, J.W. Barnwell, V. Udhayakumar, Anti-folate drug resistance in Africa: meta-analysis of reported dihydrofolate reductase (dhfr) and dihydropteroate synthase (dhps) mutant genotype frequencies in African Plasmodium falciparum parasite populations, Malar. J. 9 (2010) 1–22. https://doi.org/10.1186/1475-2875-9-247.

[71] R. Capela, R. Moreira, F. Lopes, An overview of drug resistance in protozoal diseases, Int. J. Mol. Sci. 20 (2019) 5748. https://doi.org/10.3390/ijms20225748.

[72] A. Heinberg, L. Kirkman, The molecular basis of antifolate resistance in Plasmodium falciparum: looking beyond point mutations, Ann. N. Y. Acad. Sci. 1342 (2015) 10–18. https://doi.org/10.1111/nyas.12662.

[73] S. Kumar, T.R. Bhardwaj, D.N. Prasad, R.K. Singh, Drug targets for resistant malaria: Historic to future perspectives, Biomed. Pharmacother. 104 (2018) 8–27. https://doi.org/10.1016/j.biopha.2018.05.009.

[74] J. Golenser, J.H. Waknine, M. Krugliak, N.H. Hunt, G.E. Grau, Current perspectives on the mechanism of action of artemisinins, Int. J. Parasitol. 36 (2006) 1427–1441. https://doi.org/10.1016/j.ijpara.2006.07.01117005183.

[75] F.W. Muregi, A. Ishih, Next-generation antimalarial drugs: hybrid molecules as a new strategy in drug design, Drug Dev. Res. 71 (2010) 20–32. https://doi.org/10.1002/ddr.20345.

[76] N.S. Tibon, C.H. Ng, S.L. Cheong, Current progress in antimalarial pharmacotherapy and multi-target drug discovery, Eur. J. Med. Chem. 188 (2020) 111983.

[77] S. Tiwari, N. Sharma, G.P. Sharma, Redox interactome in malaria parasite Plasmodium falciparum, (2021) 423–434.

[78] L. Anton, D.W. Cobb, C.-M. Ho, Structural parasitology of the malaria parasite Plasmodium falciparum, Trends Biochem. Sci. 47 (2022) 149–159. https://doi.org/10.1016/j.tibs.2021.10.006file:///C:/Users/Administrator/Downloads/scholar - 2024-03-11T090146.310.ris file:///C:/Users/Administrator/Downloads/scholar - 2024-03-11T090229.627.ris.

[79] M.U. Ferreira, B.C. Carlos, G. Wunderlich, Antigenic diversity and immune evasion in malaria parasites, Rev. Da Biol. 6 (2011) 26–31.

[80] L.A. Kirkman, K.W. Deitsch, Antigenic variation and the generation of diversity in malaria parasites, Curr. Opin. Microbiol. 15 (2012) 456–462. https://doi.org/10.1016/j.mib.2012.03.003.

[81] A.S. Paul, E.S. Egan, M.T. Duraisingh, Host–parasite interactions that guide red blood cell invasion by malaria parasites, Curr. Opin. Hematol. 22 (2015) 220–226. https://doi.org/10.1097/MOH.0000000000000135.

[82] A.L. Burns, M.G. Dans, J.M. Balbin, T.F. de Koning-Ward, P.R. Gilson, J.G. Beeson, M.J. Boyle, D.W. Wilson, Targeting malaria parasite invasion of red blood cells as an antimalarial strategy, FEMS Microbiol. Rev. 43 (2019) 223–238. https://doi.org/10.1093/femsre/fuz005.

[83] P. V Groomes, U. Kanjee, M.T. Duraisingh, RBC membrane biomechanics and Plasmodium falciparum invasion: probing beyond ligand–receptor interactions, Trends Parasitol. 38 (2022) 302–315. https://doi.org/10.1016/j.pt.2021.12.005.

[84] C.A. Ezema, I.U. Okagu, T.P.C. Ezeorba, Escaping the enemy's bullets: an update on how malaria parasites evade host immune response, Parasitol. Res. 122 (2023) 1715–1731.

[85] F. Teuscher, M.L. Gatton, N. Chen, J. Peters, D.E. Kyle, Q. Cheng, Artemisinin-induced dormancy in Plasmodium falciparum: duration, recovery rates, and implications in treatment failure, J. Infect. Dis. 202 (2010) 1362–1368. https://doi.org/10.1086/656476.

[86] M.A. Phillips, J.N. Burrows, C. Manyando, Malaria, Nat. Rev. Dis. Prim. 3 (2017) 17050. https://doi.org/10.1038/nrdp.2017.50.

[87] L. Paloque, A.P. Ramadani, O. Mercereau-Puijalon, J.-M. Augereau, F. Benoit-Vical,

Plasmodium falciparum: multifaceted resistance to artemisinins., Malar. J. 15 (2016) 149. https://doi.org/10.1186/s12936-016-1206-9.

[88] B. Witkowski, J. Lelievre, M.J. López Barragán, V. Laurent, X. Su, A. Berry, F. Benoit-Vical, Increased tolerance to artemisinin in Plasmodium falciparum is mediated by a quiescence mechanism, Antimicrob. Agents Chemother. 54 (2010) 1872–1877. https://doi.org/10.1128/aac.01636-09.

[89] J.T. Lin, J.J. Juliano, C. Wongsrichanalai, Drug-resistant malaria: the era of ACT, Curr. Infect. Dis. Rep. 12 (2010) 165–173.

[90] Q. Bassat, M. Velarde, I. Mueller, J. Lin, T. Leslie, C. Wongsrichanalai, J.K. Baird, Key knowledge gaps for Plasmodium vivax control and elimination, Am. J. Trop. Med. Hyg. 95 (2016) 62. https://doi.org/10.4269/ajtmh.16-0180.

[91] C. Schäfer, G. Zanghi, A.M. Vaughan, S.H.I. Kappe, Plasmodium vivax latent liver stage infection and relapse: biological insights and new experimental tools, Annu. Rev. Microbiol. 75 (2021) 87–106. https://doi.org/10.1146/annurev-micro-032421-061155.

[92] V.S. Stuermer, S. Stopper, P. Binder, A. Klemmer, N.B. Becker, J. Guizetti, Malaria parasite proliferation implicates a resource-dependent counter mechanism, BioRxiv. (2023) 2001–2023.

[93] S. Klaus, P. Binder, J. Kim, M. Machado, C. Funaya, V. Schaaf, D. Klaschka, A. Kudulyte, M. Cyrklaff, V. Laketa, Asynchronous nuclear cycles in multinucleated Plasmodium falciparum facilitate rapid proliferation, Sci. Adv. 8 (2022) eabj5362.

[94] J.M. Mwangi, L.C. Ranford-Cartwright, Genetic and genomic approaches for the discovery of parasite genes involved in antimalarial drug resistance, Parasitology. 140 (2013) 1455–1467.

[95] D.J. Bacon, A.M. McCollum, S.M. Griffing, C. Salas, V. Soberon, M. Santolalla, R. Haley, P. Tsukayama, C. Lucas, A.A. Escalante, Dynamics of malaria drug resistance patterns in the Amazon basin region following changes in Peruvian national treatment policy for uncomplicated malaria, Antimicrob. Agents Chemother. 53 (2009) 2042–2051.

[96] A.M. Thu, A.P. Phyo, J. Landier, D.M. Parker, F.H. Nosten, Combating multidrug-resistant

Plasmodium falciparum malaria., FEBS J. 284 (2017) 2569–2578. https://doi.org/10.1111/febs.14127.

[97] T. Mita, S.-I. Tachibana, M. Hashimoto, M. Hirai, Plasmodium falciparum kelch 13: a potential molecular marker for tackling artemisinin-resistant malaria parasites., Expert Rev. Anti. Infect. Ther. 14 (2016) 125–135. https://doi.org/10.1586/14787210.2016.1106938.

[98] C. Severini, M. Menegon, Resistance to antimalarial drugs: An endless world war against Plasmodium that we risk losing, J. Glob. Antimicrob. Resist. 3 (2015) 58–63. https://doi.org/https://doi.org/10.1016/j.jgar.2015.02.002.

[99] Y. Lubell, A. Dondorp, P.J. Guérin, T. Drake, S. Meek, E. Ashley, N.P.J. Day, N.J. White, L.J. White, Artemisinin resistance–modelling the potential human and economic costs, Malar. J. 13 (2014) 1–10. https://doi.org/10.1186/1475-2875-13-452.

[100] World Health Organization, Antimalarial drug combination therapy: report of a WHO technical consultation, 4–5 April, 2001, WHO, Geneva, 2001.

[101] R. Soni, D. Sharma, P. Rai, B. Sharma, T.K. Bhatt, Signaling strategies of malaria parasite for its survival, proliferation, and infection during erythrocytic stage, Front. Immunol. 8 (2017) 349.

[102] H. Gao, X. Lin, B. Yang, Z. Liu, The roles of GSTs in fipronil resistance in Nilaparvata lugens : Over-expression and expression induction, Pestic. Biochem. Physiol. 177 (2021) 104880. https://doi.org/10.1016/j.pestbp.2021.104880.

[103] G. Kapoor, Oxidative stress in Plasmodium: Role of glutathione revisited, Bull. Pure Appl. Sci. 41 (2022) 149–157.

[104] N. Pavlidi, J. Vontas, T. Van Leeuwen, The role of glutathione S-transferases (GSTs) in insecticide resistance in crop pests and disease vectors, Curr. Opin. Insect Sci. 27 (2018) 97–102. https://doi.org/10.1016/j.cois.2018.04.007.

[105] E. Hilario, S. De Keyser, L. Fan, Structural and biochemical characterization of a glutathione transferase from the citrus canker pathogen Xanthomonas research papers, (2020) 778–789. https://doi.org/10.1107/S2059798320009274.

[106] I. Valenzuela-Chavira, C.A. Contreras-Vergara, A.A. Arvizu-Flores, H. Serrano-Posada,

A.A. Lopez-Zavala, K.D. García-Orozco, J. Hernandez-Paredes, E. Rudiño-Piñera, V. Stojanoff, R.R. Sotelo-Mundo, M.A. Islas-Osuna, Insights into ligand binding to a glutathione S-transferase from mango: Structure, thermodynamics and kinetics, Biochimie. 135 (2017) 35–45. https://doi.org/10.1016/j.biochi.2017.01.005.

[107] B.K. Na, J.M. Kang, T.S. Kim, W.M. Sohn, Plasmodium vivax: Molecular cloning, expression and characterization of glutathione S-transferase, Exp. Parasitol. 116 (2007) 414–418. https://doi.org/10.1016/j.exppara.2007.02.005.

[108] C. Aurrecoechea, J. Brestelli, B.P. Brunk, J. Dommer, S. Fischer, B. Gajria, X. Gao, A. Gingle, G. Grant, O.S. Harb, PlasmoDB: a functional genomic database for malaria parasites, Nucleic Acids Res. 37 (2009) D539–D543.

[109] S. Phang-Lyn, V.A. Llerena, Biochemistry, biotransformation, (2019).

[110] G.G. Gibson, P. Skett, Introduction to drug metabolism, Springer, 2013.

[111] P. Matoušková, I. Vokřál, J. Lamka, L. Skálová, The role of xenobiotic-metabolizing enzymes in anthelmintic deactivation and resistance in helminths, Trends Parasitol. 32 (2016) 481–491. https://doi.org/10.1016/j.pt.2016.02.004.

[112] R.L. Davis, Mechanism of action and target identification: a matter of timing in drug discovery, Iscience. 23 (2020). https://doi.org/file:///C:/Users/Administrator/Downloads/scholar - 2024-03-01T161417.412.ris file:///C:/Users/Administrator/Downloads/scholar - 2024-03-01T161511.163.ris 10.1016/j.isci. 2020.101487.

[113] P.P.S. Calic, M. Mansouri, P.J. Scammells, S. McGowan, Driving antimalarial design through understanding of target mechanism, Biochem. Soc. Trans. 48 (2020) 2067–2078. https://doi.org/10.1042/BST20200224.

[114] M.F. Hoffmann, S.C. Preissner, J. Nickel, M. Dunkel, R. Preissner, S. Preissner, The Transformer database: biotransformation of xenobiotics, Nucleic Acids Res. 42 (2014) D1113–D1117.

[115] P.K. Gupta, Fundamentals of toxicology: essential concepts and applications, Academic Press, 2016.

[116] G. Zdesenko, F. Mutapi, Drug metabolism and pharmacokinetics of praziquantel: A review of variable drug exposure during schistosomiasis treatment in human hosts and experimental models, PLoS Negl. Trop. Dis. 14 (2020) e0008649.

[117] M.A. Correia, Drug biotransformation, Basic Clin. Pharmacol. (2018) 53.

[118] M. Đanić, M. Mikov, Biotransformation of Xenobiotics in Living Systems—Metabolism of Drugs: Partnership of Liver and Gut Microflora, in: Pharm. Biocatal., Jenny Stanford Publishing, 2020: pp. 129–166.

[119] D.M. Vasudevan, S. Sreekumari, K. Vaidyanathan, Textbook of biochemistry for medical students, Jaypee brothers Medical publishers, 2019.

[120] A. Sadeghi Tafreshi, S. Sadeghi, M. Hekmatipour, S. Shams, M. Mohammadi, F. Vahabi, M. Arjmand, Z. Zamani, The effect of some antimalarial drugs on Plasmodium berghei glutathione-S-transferase enzyme, J. Microb. World. 12 (2019) 84–90.

[121] N. Lumjuan, L. McCarroll, L. Prapanthadara, J. Hemingway, H. Ranson, Elevated activity of an Epsilon class glutathione transferase confers DDT resistance in the dengue vector, Aedes aegypti, Insect Biochem. Mol. Biol. 35 (2005) 861–871. https://doi.org/10.1016/j.ibmb.2005.03.008.

[122] H. Ginsburg, J. Golenser, Glutathione is involved in the antimalarial action of chloroquine and its modulation affects drug sensitivity of human and murine species of Plasmodium, Redox Rep. 8 (2003) 276–279. https://doi.org/file:///C:/Users/Administrator/Downloads/scholar - 2024-03-11T180624.590.ris file:///C:/Users/Administrator/Downloads/scholar - 2024-03-11T180652.929.ris 10.1179/135100003225002907.

[123] A.M. Lehane, C.A. McDevitt, K. Kirk, D.A. Fidock, Degrees of chloroquine resistance in Plasmodium–Is the redox system involved?, Int. J. Parasitol. Drugs Drug Resist. 2 (2012) 47–57. https://doi.org/10.1016/j.ijpddr.2011.11.001.

[124] S. Kapishnikov, D. Grolimund, G. Schneider, E. Pereiro, J.G. McNally, J. Als-Nielsen, L. Leiserowitz, Unraveling heme detoxification in the malaria parasite by in situ correlative X-ray fluorescence microscopy and soft X-ray tomography, Sci. Rep. 7 (2017) 1–12.

[125] M. Gupta, S. Kumar, R. Kumar, A. Kumar, R. Verma, M.P. Darokar, P. Rout, A. Pal, Inhibition of heme detoxification pathway in malaria parasite by 3-hydroxy-11-keto-β-boswellic acid isolated from Boswellia serrata, Biomed. Pharmacother. 144 (2021) 112302.

[126] C.R. Chamboko, W. Veldman, R.B. Tata, B. Schoeberl, Ö. Tastan Bishop, Human cytochrome P450 1, 2, 3 families as pharmacogenes with emphases on their antimalarial and antituberculosis drugs and prevalent African alleles, Int. J. Mol. Sci. 24 (2023) 3383.

[127] N. Awasthi, R. Yadav, D. Kumar, Metabolism of 8-aminoquinoline (8AQ) primaquine via aromatic hydroxylation step mediated by cytochrome P450 enzyme using density functional theory, J. Organomet. Chem. 957 (2022) 122154.

# Chapter 3

# Transformation, Recombinant Expression, Purification, Quantification, and Characterization of *Plasmodium falciparum* and *Plasmodium vivax* Glutathione *S*-Transferase

## 3.1 Introduction

Recombinant protein expression is possible using prokaryotic systems like *Escherichia coli* (*E.coli*) since it is readily manipulatable, culturable in an inexpensive manner, and can also proliferate (Jia and Jeon, 2016). This is so because *Escherichia coli* is an essential genetic tool used to synthesize various bioproducts, large complex molecules like antibodies, or its fragments (Gupta and Shukla, 2017). To achieve the above, numerous procedures are being followed: cloning, optimization of expression condition, solubility enhancement, and purification (Kondo and Yumura, 2020). This is preceded by a procedure in which the recombinant vector from a mixture or vector solution gets into competent *E.coli* cells in order to propagate and store the plasmid. This procedure first entails the cloning of the open reading frame (ORF) cDNA into an appropriate vector (pET 11a) and subsequent insertion into the competent cells, in a process called or referred to as transformation (Rédei, 2008). Additionally, a non-cleavable 6×His-tag was added upstream of the open reading frame (ORF). The gene was synthesized and cloned into a pET-11a vector (pET11-*Pf*GST and pET11a-*Pv*GST), which includes ampicillin selection, a T7 polymerase promoter for expression control, and NdeI and BamHI sites for targeted gene insertion. The transformation process is completed with the mixture of competent cells and the plasmid being briefly incubated and grown in a nutrient-rich super optimal broth with a catabolite repression (SOC) medium to obtain a maximal transformation efficiency. This is seen after the solution has been plated on a dish lysogeny broth (LB) agar supplemented with appropriate antibiotics and incubated overnight. The importance of supplementing the LB agar with an antibiotic cannot be overemphasized as its selection for cells that have taken up the plasmid containing the antibiotic resistance gene (ARG) and the ORF. Protein overexpression is followed by inducing an overnight culture of single colony growth in a fresh 2XYT medium with an appropriate concentration of isopropyl β-D-1-thiogalactopyranoside (IPTG). This step becomes significant as bacterially expressed proteins are employed for function elucidation, and crystal structure studies, among others. Purified proteins are essential reagents for conducting downstream biophysical and structural studies. Therefore, obtaining these proteins is a crucial step in the research process.

Without purified proteins, it's impossible to perform the detailed analyses necessary for understanding molecular interactions and structures at a high level of precision and accuracy. This allows for subsequent diagnostic and therapeutic applications (Langlais and Korn, 2006; Raynal *et al.*, 2010, 2014). The assessment of recombinant protein qualitatively and quantitatively post-purification step is essential. This is to allow for ascertainment of the recombinant protein free from (i) nucleic acid contamination, (ii) aggregation, and (iii) other protein contaminants. In this context, the UV-Vis absorbance spectrum and polyacrylamide gel electrophoresis (PAGE) with sodium dodecyl sulfate (SDS) are valuable tools for assessing the purity and concentration of recombinant proteins. UV-Vis absorbance provides insight into the protein's concentration by measuring light absorption. At the same time, SDS-PAGE separates proteins based on size, allowing researchers to determine the protein's purity and molecular weight. Together, these methods offer a comprehensive analysis essential for ensuring high-quality protein samples for further studies. In this study, the *Pf*GST and *Pv*GST genes were transformally inserted into a pET11a vector alongside a His-tag, forming pET11a-*Pf*GST and pET11a-*Pv*GST constructs. Transformation of T7 Express$^{TM}$ *E.coli* and BL21(DE3) competent cells was achieved with the respective pET11-*Pf*GST and pET11a-*Pv*GST vectors. Successful expression and one-step purification were achieved chromatographically using Immobilized Metal Affinity Chromatography (IMAC). This is possible because of the non-cleavable 6×His-tag added upstream of the ORF. Electrophoretically and spectrophotometrically, recombinant *Pf*GST and pET11a-*Pv*GST's quantification were performed using SDS-PAGE and UV-Vis spectrophotometer, respectively. These techniques are discussed in detail below.

## 3.2 Materials

Table 3.1 Experimental methods, non-standard reagents, materials used, and with their specific manufacturer

| Research Method | Material | Manufacturer |
|---|---|---|
| Transformation | pET11a plasmid | GenScript, USA |
| and expression | Ampicillin | Melford, UK |
| | T7 Express$^{TM}$ *E.coli* cells | New England Biolab, USA |
| | Isopropyl β-D-1-thiogalactopyranoside | Melford, UK |

| | | |
|---|---|---|
| Purification | ÄKTAPrime plus FPLC Purifier<br>HisTrap Column | Cytiva Life Sciences, USA<br>GE Healthcare, Sweden |
| Quantification<br>Glycine SDS-PAGE | JascoV-550 UV-Vis Spectrophotometer<br>BLUeye Prestained Protein Ladder<br>A Bio-Rad Mini Protein II® gel-casting unit | Jasco, Japan<br>Sigma, USA<br>Bio-Rad, USA |

### 3.3 Methods

#### 3.3.1 *Pf*GST and *Pv*GST's Transformation and Recombinant Expression

High transformation efficient BL21(DE3) competent cell and nutrient-rich SOC media [2% (w/v) tryptone, 0.5% (w/v) yeast, 10 mM NaCl, 2.5 mM KCl, 10 mM $MgCl_2$, and 20 mM glucose] taken from -80 ºC freezer were first thawed on ice. After this, the BL21(DE3) cell in the eppendorf tubes were supplemented with 1 µL of *Pf*GST_pET11a and *Pv*GST_pET11a plasmids respectively, after which 30 minutes incubation on ice followed. Afterward, incubated cells containing the respective *Pf*GST_pET11a and BL21(DE3), *Pv*GST_pET11a, and BL21(DE3) were heat-shocked at 42 ºC for 45 seconds. This enables the BL21(DE3) competent cells to take up the *Pf*GST_pET11a and *Pv*GST_pET11a genes in a process called transformation. The recombinant sample cells were then chilled on ice for 10 minutes, after which 900 µL of nutrient-rich SOC media was first added before incubation on a shaker incubator for 1 hour (37 ºC, 250 rpm). The incubated recombinant samples were then first centrifuged for 2 minutes at 3000 rpm, and then 800 µL of the supernatant was discarded before resuspending the pellet in the remaining solution. This transformation process was concluded by respectively spreading 100 µL of the resuspended recombinant solutions on an LB agar plates supplemented appropriately with 100 µL of ampicillin. The sample plates were then (round to prevent contamination), sealed, and grown in an incubator for approximately 16 hours, after which the plates were observed for transformants.

Recombinant expression of the transformants was carried out by first growing a single and distinct colony from the respective plates in a 2 × yeast tryptone (2XYT) media [1% (v/v) yeast, 1.6% (w/v) tryptone, 0.5% (w/v) NaCl] appropriately supplemented with 100 µL ampicillin and then

incubated overnight (37 ºC, 250 rpm). A freshly made (2XYT) media [1% (v/v) yeast, 1.6% (w/v) tryptone, 0.5% (w/v) NaCl] was then supplemented with 2 mL of the overnight culture solution and then grown (37 ºC, 250 rpm) until it reached an optical density 0.6. This quickly returns the cells to logarithmic growth and optimal density in preparation for induction. The samples were then first chilled on ice for 10 minutes and later induced with 0.5 mM IPTG for protein overexpression. Cells from the samples were then first centrifugally (5000×g, 15 minutes, 4 ºC) harvested before being resuspended in sodium phosphate buffer solution [50 mM sodium phosphate (monobasic), 0.01% (w/v) $NaN_3$; pH 7.2]. These resuspended cells were then kept in a -20 ºC freezer for the purification procedure.

### 3.3.2 Chromatographic Purification of *Pf*GST Protein

Recombinant proteins are highly and efficiently purified when affinity tags are used as tools for structural and functional proteomics. Immobilized metal affinity chromatography (IMAC) is a method of choice when the purification of proteins made up of short affinity tags composed of polyhistidine residues are involved (Cheung *et al*., 2012; Walls *et al.*, 2017; Loughran and Milne, 2023). This method involves the use and immobilization of ions such as nickel [Ni(II)] and cobalt [Co(II)] on fractionating support to purify soluble proteins. This is so as proteins can specifically bind to the coordination sites on the metal ion using certain amino acid side chains like histidine. The reason for this is the strongest ability possessed by this amino acid (histidine) to interact with the matrices of the metal ion. This protein serves as an electron donor on the histidine imidazole ring attached to the chromatographic support and thereby bonds with the immobilized metal ions and produce metal chelates ( Cheung *et al*., 2012; Loughran and Milne, 2023). To immobilize the metal ions to agarose, two chelation adsorbents are usually used for metal-chelate affinity chromatography. They include tetradentate nitriloacetic acid (NTA) and iminodiacetic acid (IDA).

The IMAC purification procedure started with the room temperature thawing of the expressed frozen cells from the - 20 ºC freezer and subsequent disruption of the cells by sonication on ice using Qsonica Sonicators, USA. The sonicated cells were then centrifuged (18000xg, 30 minutes, 4 ºC) to separate the insoluble fraction from the soluble fraction, which was later purified. A 5 mL (1.6 × 2.5 cm) Ni-NTA [$Ni(II^+)$] charged HisTrap® column, GE Healthcare, Sweden was used in this procedure. A 20-column volume equilibration buffer [50 mM sodium phosphate, 0.01 % (w/v) $NaN_3$, pH 7.2] was used to equilibrate (5 mL/min) the column used to purify the *Pf*GST and *Pv*GST

using an instrument ÄKTAPrime plus FPLC Purifier, Cytiva life sciences, USA. After performing a system wash of the instrument, washing the super loop with 20 % (v/v) ethanol, and equilibrating the column, the filtered soluble fractions were allowed to flow through the column after being injected into the column, and flow-through collected. This process was followed by washing the column with a 20-column volume equilibration buffer. This ensures that non-specifically bound protein is washed off, leaving only the bound protein. The bound proteins were subsequently eluted [50 mM sodium phosphate, 500 mM imidazole, 0.01 % (w/v) $NaN_3$, pH 7.2] from the column using a one-step elution. The different eluted fragments were collected into different eppendorf tubes from the time elution profile rises till when it peaks and declines to baseline. The protein fractions and the flow-through alongside the supernatant and pellet after the previous centrifugation were run on a glycine SDS-PAGE gel to check for the presence, solubility, and purity of the expressed proteins.

### 3.3.3 Spectrophotometric and Electrophoretic Quantification of *Pf*GST and *Pv*GST Proteins

Understanding the protein content in a sample requires the accurate quantification qualitatively and quantitatively. This is so as critical assays, subsequent downstream applications, and drug development process require not only pure but precise total protein content to generate data that will be used for in depth biophysical and structural characterization. The quantification of protein qualitatively and quantitatively gives the basis for the right interpretation of many experiments involving biophysical and structural characterization. According to Bertrand Raynal *et al*., 2014, this characterization depends on (i) the purity and homogeneity of the protein sample (ii) accurate determination of protein concentration (iii) solubility of the active protein sample in native state (Raynal *et al.*, 2014). For this study, UV-Vis absorbance spectrum and SDS-PAGE were employed to evaluate the *Pf*GST protein sample

A Glycine-SDS-PAGE otherwise known as Laemmli-SDS-PAGE which was formulated by Laemmli in 1970 [4% (w/v) stacking and 10% (w/v) separating] was assembled for the purpose of determining the successfulness of the overexpression and purity of the recombinant *Pf*GST and *Pv*GST proteins. This electrophoretic technique uses SDS for protein denaturation and noncontinuous polyacrylamide gel as a support medium to separate protein. Upon treatment with SDS, the protein molecule's secondary, tertiary and quaternary structure gets disrupted producing

a linear polypeptide chains which are coated with negatively charged SDS molecules. SDS-PAGE examines charged molecules movement in an electric field. The movement of the SDS-Protein complexes is influenced by the applied electric field, gel matrix, shape, charge and primarily the size of the protein to be separated. While the smaller protein molecule have greater mobility and hence reached base of the gel, the larger protein molecules are retarded by the sieving effect of the polyacrylamide gel (Roy *et al*., 2012; Mesapogu *et al*., 2013). Hence, this electrophoretic technique was used to determine the purity and molecular mass of the *Pf*GST and *Pv*GST protein samples.

The fractionated *Pf*GST and *Pv*GST protein samples collected were solubilized in reducing sample buffer [125 mM Tris-HCl, 4% (w/v) SDS, 10% (v/v) β-mercaptoethanol, 20% (v/v) glycerol; pH 6.8] in ratio 1:1 (50 µL: 50 µL) and then heated up to 100 ºC for 15 minutes. This is to ensure the protein samples were denatured. The respective *Pf*GST and *Pv*GST protein samples (5 µL) were ran using a Bio-Rad Mini-PROTEAN Tetra Vertical Electrophoresis Cell with tank buffer [250 mM Tris-HCl, 192 mM Glycine, 0.1% (w/v) SDS, pH 8.3] poured in. Upon applying current at constant voltage (120 V) on a discontinuous gel made up of 12.5% (w/v) separating gel [1.5 M Tris-HCl, pH 8.8] and 4% (w/v) stacking gel [500 mM Tris-HCl, pH 6.8], the samples and molecular weight marker loaded alongside were separated according to their sizes until the separation bands were 0.1 cm from the bottom of the gel casting unit. The gel was subsequently removed, stained and destained with Coomassie Blue R 250 staining solution [0.1% (w/v) Coomassie dye in 1:5:4 (v/v/v) acetic acid-methanol water solution] and destaining solution [1:5:4 (v/v/v) acetic acid-methanol-water solution] respectively. The destained gel image was captured in order to graphically estimate the molecular weight of the recombinant *Pf*GST and *Pv*GST proteins. This is because the migration rate of the *Pf*GST and *Pv*GST protein samples coated with SDS is inversely proportional to the logarithm of its molecular weight. The destained gel image and the molecular weight of the protein were shown in the respective chapters where they were reported.

The procedure above was followed by the spectrophotometric purity evaluation and concentration quantification of the purified protein according to methods previously reported (Oliveira and Domingues, 2018; Raynal *et al.*, 2021; Loughran and Milne, 2023). In doing this, *Pf*GST and *Pv*GST's protein fractions were pooled for centrifugation. The centrifugation (10 000×g, 10 min)

was carried out to remove aggregates if present. With the use of a JascoV-550 UV-Vis Spectrophotometer machine, a UV-Vis absorbance spectrum of the proteins (*Pf*GST and *Pv*GST) at wavelength of between 250 to 340 nm were respectively run to ascertain the proteins' purity and freeness of aggregates and nucleic acid contaminations. This is usually confirmed by a characteristic trough and peak at 260 and 280 respectively, with zero absorbance at 340 nm. In evaluating protein's purity, a 260/280 ratio of $\sim 0.57$ indicate a near 100% pure protein sample while a ratio > 0.57 is indicative nucleic acid contaminations.

In spectroscopically quantifying the *Pf*GST and *Pv*GST protein samples, a 280 nm absorbance measurements of the serial diluted protein samples were taken and evaluated using the Beer-Lambert law given below:

$$A = \varepsilon c l$$

while A represents the absorbance of the samples, ε is the molar extinction coefficient ($M^{-1}cm^{-1}$), c is the molar concentration (M) of the protein samples in solution and l represents the light's path length (cm) passing through the solution. The samples' absorbance readings were plotted against the dilutions after which the slopes of the plots were used for the concentration determination.

**References**

Cheung, R.C.F., Wong, J.H. and Ng, T.B. (2012) 'Immobilized metal ion affinity chromatography: A review on its applications', *Applied Microbiology and Biotechnology*, 96(6), pp. 1411–1420. Available at: https://doi.org/10.1007/s00253-012-4507-0.

Gupta, S.K. and Shukla, P., 2017. Microbial platform technology for recombinant antibody fragment production: a review. *Critical reviews in microbiology*, *43*(1), pp.31-42.

Jia, B. and Jeon, C.O. (2016) 'High-throughput recombinant protein expression in Escherichia coli: Current status and future perspectives', *Open Biology*, 6(8). Available at: https://doi.org/10.1098/rsob.160196.

Kondo, T. and Yumura, S. (2020) 'Strategies for enhancing gene expression in Escherichia coli', *Applied Microbiology and Biotechnology*, 104(9), pp. 3825–3834. Available at: https://doi.org/10.1007/s00253-020-10430-4.

Langlais, C. and Korn, B. (2006) 'Recombinant protein expression in bacteria', *Encyclopedic Reference of Genomics and Proteomics in Molecular Medicine, Springer, Berlin Heidelberg*, pp. 1609–1616.

Loughran, S.T. and Milne, J.J. (2023) *Protein chromatography: methods and protocols*. Springer Nature. Available at: https://doi.org/10.1007/3-540-29623-9_4800.

Mesapogu, S., Jillepalli, C.M. and Arora, D.K. (2013) 'Agarose Gel Electrophoresis and Polyacrylamide Gel Electrophoresis: Methods and Principles', pp. 73–91. Available at: https://doi.org/10.1007/978-3-642-34410-7_5.

Oliveira, C. and Domingues, L. (2018) 'Guidelines to reach high-quality purified recombinant proteins', *Applied microbiology and biotechnology*, 102, pp. 81–92.

Raynal, B. *et al.* (2010) 'Quality assessment and optimization of purified protein samples: Why and how?', *Microbial Cell Factories*, 13(1), pp. 1–10. Available at: https://doi.org/10.1186/s12934-014-0180-6.

Raynal, B. *et al.* (2014) 'Quality assessment and optimization of purified protein samples: why and how?', *Microbial cell factories*, 13, pp. 1–10. Available at: https://doi.org/10.1186/s12934-014-0180-6.

Raynal, B. *et al.* (2021) 'Assessing and improving protein sample quality', *Protein-ligand interactions: methods and applications*, pp. 3–46. Available at: https://doi.org/10.1007/978-1-0716-1197-5_1.

Rédei, G.P. (2008) *Encyclopedia of genetics, genomics, proteomics, and informatics*. Springer

Science & Business Media.

Roy, V.K., Kumar, N.S. and Gurusubramanian, G. (2012) 'Proteins – Structure, Properties and Their Separation by SDS- Polyacrylamide Gel Electrophoresis', *Science Vision*, 12(4), pp. 170–181. Available at: https://pdfs.semanticscholar.org/a0b2/abe0fd6b3139342cfdc3c16bafccb491f25b.pdf.

Walls, D. *et al.* (2017) *Protein chromatography*. Springer. Available at: https://doi.org/10.1007/978-1-4939-6412-3.

# CHAPTER 4

This chapter has been put together as a manuscript. It is currently under review as "**Characterizing the ligandin properties of *Plasmodium falciparum* and *vivax* glutathione transferase towards selected antimalarial drugs**" by Olalekan Onisuru and Ikechukwu Achilonu for publication as an original research article in Molecular and Biochemical Parasitology. This article combinatorially reports for the first time the experimental characterization of *Plasmodium falciparum* Glutathione *S*-transferase (*Pf*GST) and *Plasmodium vivax* Glutathione *S*-transferase (*Pv*GST) towards seven selected existing antimalarials. Since the management and drug treatment of malaria through glutathione-conjugation and biotransformation enzyme inhibition vis-à-vis the binding by antimalarial drugs has not been fully explored, this article therefore systematically characterize *Pf*GST and *Pv*GST's ligandin properties towards some existing potent antimalarials. To the best of our knowledge, there has not been a published comparative experimental characterization on the inhibition of both *Pf*GST and *Pv*GST by the selected antimalarials. We believe this article will benefit all readers of Molecular and Biochemical Parasitology.

# Characterizing the ligandin properties of *Plasmodium falciparum* and *vivax* glutathione transferase towards selected antimalarial drugs

Olalekan Onisuru and Ikechukwu Achilonu*

Protein Structure-Function and Research Unit, School of Molecular and Cell Biology, Faculty of Science, University of the Witwatersrand, Braamfontein, Johannesburg 2000, South Africa

***Correspondence to Ikechukwu Achilonu*** (Ikechukwu.Achilonu@wits.ac.za): Protein Structure-Function and Research Unit, School of Molecular and Cell Biology, Faculty of Science, University of the Witwatersrand, Braamfontein, Johannesburg 2000, South Africa

**Authors**

Olalekan Onisuru: 2430435@students.wits.ac.za

Ikechukwu Achilonu: Ikechukwu.Achilonu@wits.ac.za

**Abstract**

The ligandin properties of *Plasmodium falciparum* Glutathione *S*-Transferase (*Pf*GST) and *Plasmodium vivax* Glutathione *S*-Transferase (*Pv*GST) have been reported in the literature as enzymes possessing the ability to bind endogenous and exogenous substrates via a glutathione (GSH) detoxification process. While this has aroused research interest towards *Pf*GST and *Pf*GST as potential antimalarial drug targets, their binding and inhibition by existing antimalarials has not however been characterized. The artemisinin-based combination therapies (ACTs) and other antimalarials that have hitherto proved potent as therapeutics against malarial, have unfortunately been confronted with resistance and rendered inefficacious against their targets. Hence, this study, for the first time, characterized the ligandin properties of *Pf*GST and *Pf*GST towards seven existing potent antimalarials. Specifically, antimalarial drugs, which include artemisinin, artemether, artesunate, amodiaquine, lumefantrine, mefloquine, and pyrimethamine's binding and inhibition of *Pf*GST and *Pf*GST were characterized. While all the drugs showed insufficiently proven inhibition of *Pf*GST and *Pf*GST's specific enzymatic activities, with artemisinin having the highest inhibition at 27 %, they all however showed different degrees of binding. The characterization also shows that while not all antimalarials are glutathionylated, all are biotransformed by *Pf*GST and *Pf*GST, but they however elicited differential manner in making *Pf*GST and *Pf*GST less stable. This study provided novel insights into the selected class of antimalarial's targeting *Pf*GST and *Pv*GST and experimentally and rightly proved the need to target the binding and inhibition of these enzymes for the development of potent antimalarials.

## Introduction

Malaria, an infection caused by a parasitic protozoan remains a prevalently deadly disease despite the concerted effort aimed at its control and treatment. This, in addition to its high morbidity and mortality burden, makes the search for novel antimalarials with potent mechanism of actions continue to be pressing [1,2]. Of the several *Plasmodium* species known to humans, the five known to be predominantly infectious include *Plasmodium falciparum*, *Plasmodium vivax*, *Plasmodium ovale*, *Plasmodium malarie*, and *Plasmodium knowelsi*. While *Plasmodium falciparum* (*Pf*) is the deadliest, *Plasmodium vivax* (*Pv*), on the other hand, is the most widely distributed of the parasite [3–5]. Malaria continues to be a significant global health issue, with its impact varying by region. Specifically, *Plasmodium falciparum* is the leading cause of morbidity and mortality in sub-Saharan Africa, while *Plasmodium vivax* is the primary contributor to these issues in Asia. The disease burden remains disproportionately high in these regions, highlighting the critical need for targeted interventions and strategies to address the differing challenges posed by these two major malaria parasites [6,7]. The complexity of the life cycle of these parasites contributes to the challenge of their elimination, making available more and more platforms for intervention. This is because the host's pathological symptoms are primarily due to the malaria parasite's intra-erythrocytic stage [8,9].

Over times and in the course of different antimalarial developments, different proteins in *Plasmodium* parasite has been explored as targets with some antimalarials targeting more than one protein [10–13]. Glutathione *S*-Transferase or Glutathione Transferase (GST) is an adept enzyme family that occurs copiously in nearly all organisms. They are responsible for detoxifying many substances intracellularly by inactivating and converting diverse exogenous and endogenous toxic molecules to less toxic soluble compounds. These are metabolized partially and hence can be easily gotten rid of via glutathione (GSH) conjugation [14–17]. Currently, GSTs have caught the attention of many researchers for drug discovery, nanotechnology, and biotechnology and this is due to GST's significant involvement in cellular processes. The *Plasmodium falciparum* Glutathione *S*-Transferase (*Pf*GST) and *Plasmodium vivax* Glutathione *S*-Transferase (*Pv*GST) are distinctively different, existing singularly in the cytosol different from the multiple GSTs found in eukaryotic organisms [17]. While these two GSTs do not only respectively constitute about 0.1-1% of *Plasmodium falciparum* (*Pf*) and *Plasmodium vivax* (*Pv*) total protein component, they are however, indispensable for these protozoan's survival [18]. Consequentially and generally, GSTs'

inhibitory ability have therapeutic, anthelmintic, antiparasitic, and anti-cancer applications. This is as the inhibition of *Pf*GST and *Pv*GST will wither *Pf* and *Pv* detoxification ability and bring down their antioxidant ability

There are many World Health Organization (WHO) approved antimalarial drugs in use either as prophylaxis for malaria or to treat and prevent malaria infection worldwide. In providing a primary line of defense against malaria, many of the current antimalarials in use, aim to primarily kill the parasites in the host's infected RBCs and thereby provide timely treatment to infected individuals [19–21]. This will then anticipatorily bring relief of malaria's symptoms in the infected person and help to prevent the spread of the disease within communities. In the management of malaria, artemisinin-based combination therapies (ACTs) has become the prime drug approved by the WHO for the treatment of uncomplicated *Pf* and chloroquine-resistant *Pv*. This is as ACTs have demonstrated the capacity to rapidly bring about the parasite density's significant reductions [22–26]. These ACTs as approved by the WHO, include artemether-lumefantrine, artesunate-amodiaquine, artesunate-mefloquine, dihydroartemisinin-piperaquine, artesunate-sulfadoxine/pyrimethamine, and artesunate-pyronaridine [27,28]. The existing antimalarials are mainly targeted at the erythrocyte invading and replicating parasite stages in the bloodstream. This is because the development inside the erythrocyte protects the pathogen from the host's immune response while limiting access to nutrients, among other solutes in plasma [29]. However, given the high reported treatment failure rate associated with ACTs, which are the WHO-approved first-line treatment for malaria, the search for novel antimalarials has become urgently necessary [30]. Antimalaria drug discovery process which was previously based on phenotypic screening and natural products with over seven million compounds tested against the malarial parasites' asexual stage has now shifted to a process that is target-based [31,32]. In addition, the parasitic mutation responsible for artemisinin resistance found in some African countries has imperatively made novel targets-driven alternative malaria treatment becomes indispensable [33].

It has been reported that both *Pf*GST and *Pv*GST are known to possess ligandin properties. This is as these two enzymes possess ability to bind to a wide range of hydrophobic ligands. They also possess the wherewithal to bind to endogenous and exogenous substrates via a glutathione (GSH) detoxification process [34–36]. Aside from the fact that this binding capacity may contribute to sequestration and transport of hydrophobic molecules within the parasite (aiding in their metabolism or removal from the cell), it can also inhibit their functionalities [37,38]. This is

as ligand binding has been reported to bring about structural and conformational modification of proteins [39]. Given the importance of malaria parasites' GST in the detoxification of endogenous and xenobiotic compounds, among other functionalities which has been shown to enhance drug resistance ability to anti-parasitic and insecticides, the inhibition of this detoxification ability is thus worth targeting as a novel and effective antimalarial [40]. In view of this, we present for the first time the characterization of the *Pf*GST and *Pv*GST's ligandin abilities towards some seven selected antimalarials. This becomes novel as this is the first time (based on our knowledge) current ACTs will be studied for their binding and inhibitory potential targeting a detoxification enzyme from both *Plasmodium falciparum* and *Plasmodium vivax*.

## 2. Materials and Methods

### 2.1. Materials

A New England BioLabs BL21(DE3) competent cells were purchased for transformation use while GenScript Biotech, USA synthesized *Pf*GST_pET11a and *Pv*GST_pET11a plasmids were also purchased for use in this study. The following materials like glutathione reduced (GSH), 1-chloro-2,4-dinitrobenzene (CDNB), and 8-anilino-1-naphthalenesulfonic acid (ANS) were all purchased from Sigma-Aldrich (St. Louis, Missouri, USA). Similarly, the other materials which were equally purchased from Sigma-Aldrich include isopropyl β-D-1-thiogalactopyranoside (IPTG), dimethyl sulfoxide (DMSO), ampicillin, and GSH-agarose. On the other hand, SYPRO Orange dye was purchased from Thermo Fisher Scientific, USA. The seven selected antimalarials namely artemisinin, artemether, artesunate, amodiaquine hydrochloride, lumefantrine, mefloquine hydrochloride, and pyrimethamine were all purchased from Angene Chemical, India.

### 2.2. Recombinant overexpression of *Pf*GST, *Pv*GST in *E.coli* and purification

A high transformation efficient chemically competent *E.coli* BL21(DE3) cells were respectively mixed with *Pf*GST_pET11a and *Pv*GST_pET11a (GenScript) plasmids expression vectors, using a heat shock treatment procedure. The spread of 100 µL of the resuspended recombinant solution on a Luria-Bertani (LB) agar plate supplemented appropriately with 100 µL of ampicillin (100 µg/mL) completed the transformation process. A singularly distinct colony from

the respective overnight (16 hours) incubated plates were separately inoculated into a 2 × yeast tryptone (2XYT) media [1% (v/v) yeast, 1.6% (w/v) tryptone, 0.5% (w/v) NaCl] which has been appropriately supplemented with 100 µL ampicillin (100 µg/mL). This was then allowed for overnight incubation (37 ºC, 250 rpm) on a shaker incubator. An optical density ($OD_{600}$) of 0.6 was allowed before the addition of 0.5 mM IPTG, 6 hrs to induce protein overexpression. The solubility of the protein was ascertained using an SDS-PAGE gel, and soluble protein was harvested by centrifugation at 5000xg for 15 minutes. A one-step purification was carried out using an immobilized metal affinity chromatography (IMAC) purification procedure on the two proteins. This employed the use of a separate 5 mL (1.6 × 2.5 cm) cobalt [Co(II)] charged HisTrap® column, GE Healthcare, Sweden connected to the ÄKTA Start Purifier, Cytiva Life Sciences, USA. A 50 mM sodium phosphate, 500 mM imidazole, 0.01 % (w/v) NaN3, and pH 7.2 elution buffer was employed to obtain purified *Pf*GST and *Pv*GST used for the different characterizations.

## 2.3. *Pf*GST and *Pv*GST's enzymatic and inhibitory assay with antimalarials

Utilizing the previously described assay of GSTs' conjugation ability exhibitable by reduced glutathione towards l-chloro-2,4-dinitrobenzene (CDNB), the enzymatic specific activity of *Pf*GST and *Pv*GST's were spectrophotometrically determined [41]. This assay measures the dinitrophenyl thioether chromophore conjugation product of 1-(S-glutathionyl)-2,4 dinitrobenzene formed. This product was sequentially monitored in triplicates at 20 ºC for 60 s on a Jasco V-730 BIO spectrophotometer with a 3 mL glass quartz cuvette. The $\varepsilon_{340}$ of 9600 $M^{-1}.cm^{-1}$ and 340 nm absorbance were parameters observed when this activity was monitored spectrophotometrically. The reaction buffer contains 100 mM sodium phosphate, 5 mM GSH, 1 mM CDNB (3% (v/v) ethanol), 1 mM EDTA, 5 mM DTT, and 0.02% $NaN_3$, at pH 7.2. Varying concentrations of *Pf*GST and *Pv*GST were used in the presence and absence of 1 mM concentrations of the seven antimalarials. The results were subsequently corrected for linear progress curves and background non-enzymatic reaction rates.

## 2.4. Antimalarial drug biotransformation assay with Glutathione, *Pf*GST, and *Pv*GST

Understanding the significance of glutathionylation as a biochemical process where GSH becomes attached to another molecule for drug metabolism or undertakes a significant

biotransformation route [42,43], a biotransformation assay of the antimalarials was carried out. This is the biotransformation of the drugs with GSH, and *Pf*GST or *Pv*GST, will have altering pharmacokinetics and pharmacodynamics effects on the drugs, including altering their function, localization, or stability [43]. This assay looks at the possibility of the biotransformation of artemisinin, artemether, artesunate, amodiaquine, lumefantrine, mefloquine, and pyrimethamine by GSH and or *Pf*GST or *Pv*GST. Hence, using a Jasco V-730 BIO spectrophotometer, UV-Vis scan for these drugs were carried out to check if there were they were GSH-glutathionylated or GST biotransformed. This is as changes in absorbance can indicate the formation of new chemical entities or alterations in the electronic structure of the drugs during biotransformation reactions. The assay was carried in a freshly prepared 100 mM sodium phosphate at pH 7.2 buffer, 2 mg/mL concentration of *Pf*GST and *Pv*GST, 5 mM GSH, and 1 mM concentration of each of the drugs. Four reaction mixtures (the drugs, GSH incubated drug samples, *Pf*GST or *Pv*GST incubated samples, and *Pf*GST or *Pv*GST, and GSH 30 minutes incubated samples) were spectrophotometrically measured for absorbance alteration of light at wavelength range of between 240 – 350 nm. An agarose resin was added to the *Pf*GST or *Pv*GST, and GSH 30 minutes incubated samples to stop the reaction by trapping the GST, after that it was briefly spun down to remove the GST. This was done so that the GST does not affect the correctness of the spectra measurements.

### 2.5. Antimalarial's ligandin and binding to *Pf*GST and *Pv*GST

The tertiary structural conformation of *Pf*GST and *Pv*GST proteins and their respective complexes with GSH and the antimalarials were evaluated using a JASCO FP-6300 spectrofluorometer machine with installed Spectra Manager software v1.5.00 (Jasco Inc., Tokyo, Japan). This was done by employing the ability of 8-anilino-1-naphthalenesulfonic acid (ANS)'s as an extrinsic probe to fluorescently bind to protein's hydrophobic pockets. The structural conformation and interaction of *Pf*GST and *Pv*GST in the presence of GSH and when incubated with the antimalarials as ligands was carried out. With 5 µM each of *Pf*GST and *Pv*GST samples in 10 mM sodium phosphate, 1 mM EDTA, 2 mM DTT, 0.02 % (w/v) NaN3, pH 7, a 200 µM ANS as extrinsic fluorescence probe, the ligandin and binding was spectroscopically analyzed. These spectroscopic analysis was done in a 10 mm pathlength quartz cuvette at 20°C, with a fluorescence emission spectra at an excitation of 395 nm and wavelength of between 400 and 650 nm. Other parameters set in the spectrofluorometer machine include an excitation bandwidth of 5 nm, 2.5 nm

emission with data pitch of 1 nm, 1 cm path length, and scanning speed of 200 nm/min. The fluorescence absorbance readings were recorded in triplicate with the buffer corrected before being averaged.

Specifically, the antimalaria ligandin and binding effect on both *Pf*GST and *Pv*GST's hydrophobic cleft was separately carried out using a 1 mM concentration of artemisinin, artemether, artesunate, amodiaquine, lumefantrine, mefloquine, and pyrimethamine. Before spectra measurement, 1 mM of each of the antimalarials were separately incubated with 5 µM *Pf*GST and *Pv*GST in the presence and absence of 5 mM GSH for 30 min. In this monitored spectroscopic analysis, spectra signals at three accumulations were averaged and recorded. Recorded spectra were buffer corrected before the fluorescence intensities in the presence of the antimalarials were also corrected for the inner filter effect to account for any absorption of excitation (primary) and emission (secondary) light.

2.6. Antimalarials' effect on the thermal stability of *Pf*GST and *Pv*GST by thermal shift assay

The *Pf*GST and *Pv*GST's native protein stability in the presence of glutathione (substrate) and their interaction with each of the seven antimalarials (ligand) was evaluated using a thermal shift assay (TSA). The thermal denaturation of *Pf*GST and *Pv*GST was separately and individually evaluated in the presence of the antimalarials. This was done using a CFX96 Touch-Real-Time qPCR detection system (Bio-Rad Laboratories, Inc., Hercules, CA, USA). A 1.5 mg/mL protein concentration of *Pf*GST and *Pv*GST were separately and individually incubated with 1mM concentration of artemisinin, artemether, artesunate, amodiaquine, mefloquine, and pyrimethamine. This thermal stability was studied using a naturally quenched fluorescent dye (SYPRO Orange dye) as a probe on an environment-sensitive 96-well PCR plate. The 96-well plate was prepared with each well containing a triplicate sample mix of 1.5 mg/mL *Pf*GST or *Pv*GST in 100 mM $NaH_2P0_4$, 1 mM DTT, 1 mM EDTA, ± 5 mM GSH, ± 1 mM antimalarials. Before the commencement of the assay, 5 µL of diluted 5000 X SYPRO Orange dye was added into each of the 96 wells which was then briefly but thoroughly spun down on a microplate centrifuge to ensure mixing. The plate was then put in the qPCR machine and set at temperature range of 20 ºC – 90 ºC, with 0.5 ºC increments for 10 s each, to allow the dye to interact with the sample's hydrophobic core. This interaction becomes visible upon denaturation leading to the dye's fluorescence quantum yield increasing when bound to exposed hydrophobic patches on a thermally denatured *Pf*GST and *Pv*GST. Each sample's melt peak was resolved using the CFX

Maestro software and plotted as sample's melting temperature (*Tm*). This represents the lowest point of the melting curve derived from the plot (-d(RFU)/dT). The replicates samples were averaged and corrected with buffer blanks before plotting.

**3. Results**

In characterizing the ligandin properties of *Pf*GST and *Pv*GST towards the seven selected antimalarials, the proteins were first recombinantly and heterologously overexpressed and purified. This was done after the heat-shock transformation procedure yielding a transformed plates with distinct and clear colonies without contamination, which is an indication that the transformation was successful. For the 6 hours, 30ºC, and 250 rpm overexpression procedure, a 0.50 mM IPTG was separately added to the transformed mix of *Pf*GST and *Pv*GST to induce protein overexpression of the recombinant protein. This yields soluble protein which were subsequently subjected to a one-step immobilized metal affinity chromatography (IMAC) purification procedure using an ÄKTA Start Purifier, Cytiva Life Sciences, USA. The spectrophotometric quantification of the protein using a UV-Vis spectrophotometer V-730, JASCO Europe, showed that the purified *Pf*GST and *Pv*GST were 13 mg and 10 mg per litre of uncontaminated, soluble, and active proteins respectively. Qualitatively, the purity of *Pf*GST and *Pv*GST were confirmed by sodium dodecyl-sulfate polyacrylamide gel electrophoresis (SDS-PAGE). Similarly, the experimentally determined sizes of *Pf*GST and *Pv*GST were calculated to be approximately 25 kDa and 24.50 kDa, respectively, which corresponds to their sub-unit's theoretical molecular weights. These results revealed a high-yield soluble and pure protein free from DNA and other contaminants that can be used for further downstream characterization. The entire process from transformation, overexpression, and purification to quantitative and qualitative assessment of *Pf*GST and *Pv*GST were pictorially represented in Fig.1.

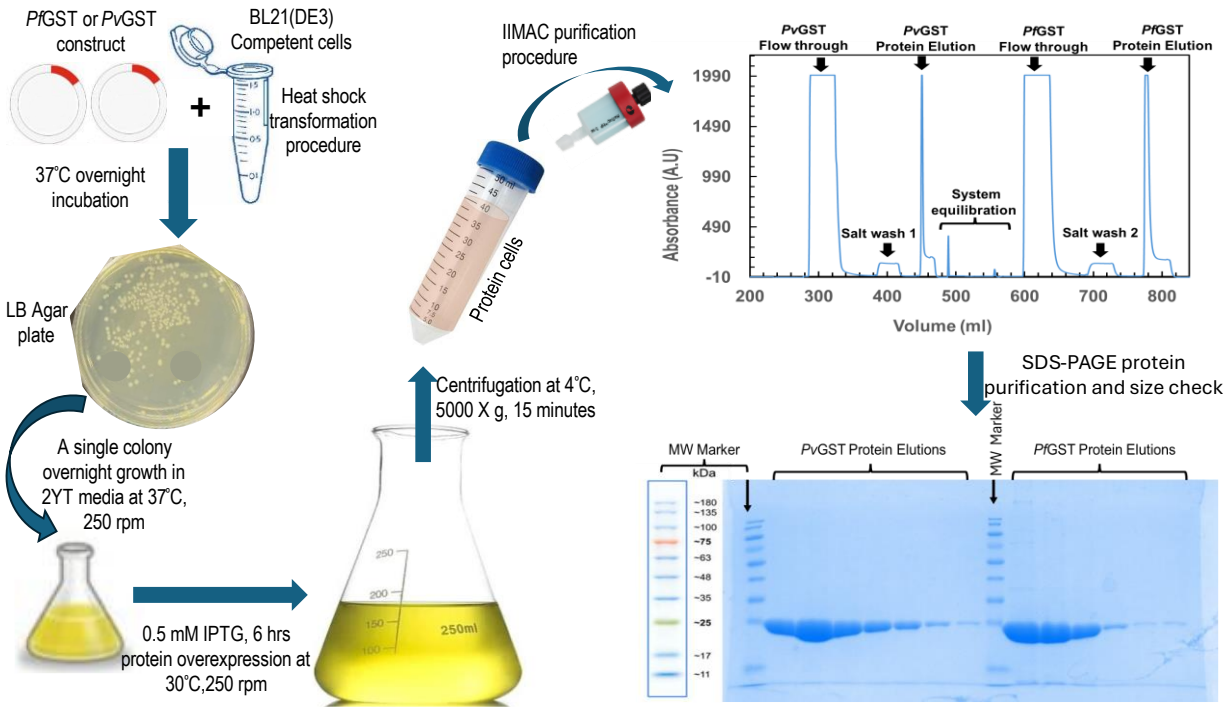


Fig. 1. Schematic description of the transformation procedure, recombinant overexpression, and purification processes of *Pf*GST and *Pv*GST. The construct's transformation in BL21(DE3) competent cells were successful as evident from the yield of single and distinct colonies on the LB plates. The 0.50 mM overexpressed was successfully purified using a one-step IMAC procedure. The *Pf*GST and *Pv*GST proteins were found to be pure, and their sizes correspond to the approximately 25 kDa theoretical sizes.

Similarly, the enzymatic specific activity of *Pf*GST and *Pv*GST were spectrophotometrically determined according to the method described in Section 2.3. While both proteins were found to be catalytically and enzymatically active, *Pf*GST's specific activity was evaluated to be 37.90 µmol/min/mg, and *Pv*GST was 35.33 µmol/min/mg (Fig.2A). This result attests to *Pf*GST and *Pv*GST's having similar structural and functional similarities. This result also correlates with the SDS-PAGE result which showed the two proteins had similar protein band yields.

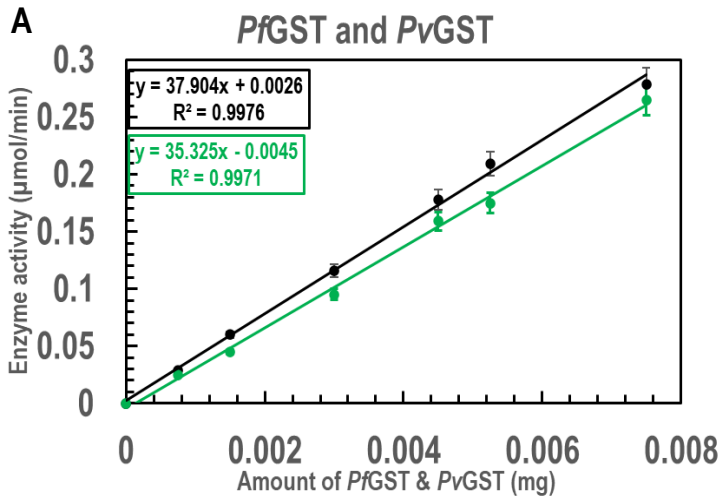


Fig. 2A. Characterizing *Pf*GST and *Pv*GST with respect to their specific enzymatic activities through a GSH-CDNB conjugation model assay characteristics of GST in a reaction buffer containing 100 mM $NaH_2PO_4$ at pH 7.2, 1 mM EDTA, 1 mM DTT, 5 mM GSH at pH 6.5, 30 mM CDNB. Each sample with varying concentrations were spectroscopically monitored. *Pf*GST's specific enzymatic activity (**black**) and *Pv*GST's specific enzymatic activity (**green**) were determined to be 37.90 µmol/min/mg and 35.33 µmol/min/mg respectively. The $R^2$ value of approximately 1 attest to the validity of the standard curve.

The inhibitory effect of artemisinin, artemether, artesunate, amodiaquine, lumefantrine, mefloquine, and pyrimethamine towards the enzymatic activities of *Pf*GST and *Pv*GST were subsequently evaluated. While the inhibitory activities of amodiaquine, lumefantrine, and mefloquine could not be reliably evaluated owing to their color effect on the spectrophotometric absorbance, those of artemisinin, artemether, artesunate, and pyrimethamine were reliably evaluated with standard curve $R^2$ value approximately 1, indicating the validity of the assay. Artemisinin inhibited the specific enzymatic activities of *Pf*GST and *Pv*GST from 37.90 µmol/min/mg and 35.33 µmol/min/mg to 31.46 µmol/min/mg and 25.58 µmol/min/mg respectively, representing a 16.99 % and 26.58 % inhibition (Fig. 2B and C). Similarly, artesunate also inhibited the specific enzymatic activity of *Pf*GST and *Pv*GST to 28.77 µmol/min/mg and 33.79 µmol/min/mg respectively (Fig. 2D and 2E). This represents a 24.09 % and 4.36 % inhibition respectively. There is a 11.66 % and 7.56 % inhibitory potency of artemether in the specific enzymatic activities of *Pf*GST and *Pv*GST's specific enzymatic activities respectively. This brings *Pf*GST's specific enzymatic activities to 33.48 µmol/min/mg and *Pv*GST's specific enzymatic activities to 32.66 µmol/min/mg (Fig. 2F and 2G). In the same breath, pyrimethamine exert it's inhibitory potency on both *Pf*GST and *Pv*GST's specific enzymatic activity. While pyrimethamine

inhibited *Pf*GST's specific to 34.21 µmol/min/mg (Fig 2H), which is a 9.74 % inhibition, on the other hand, it inhibited the specific enzymatic activity of *Pv*GST to 29.21 µmol/min/mg, corresponding to 17.32 % inhibition (Fig. 2I)

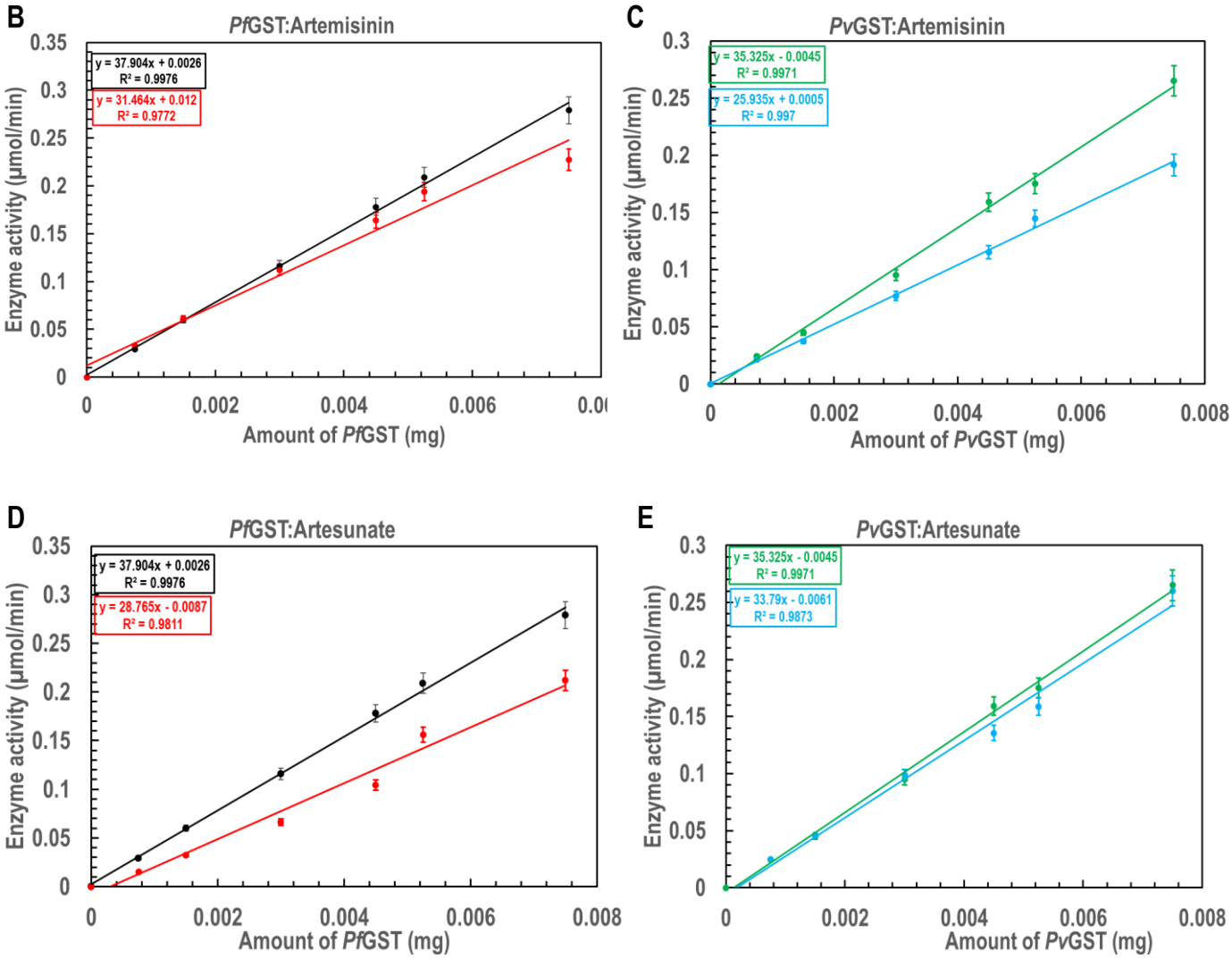

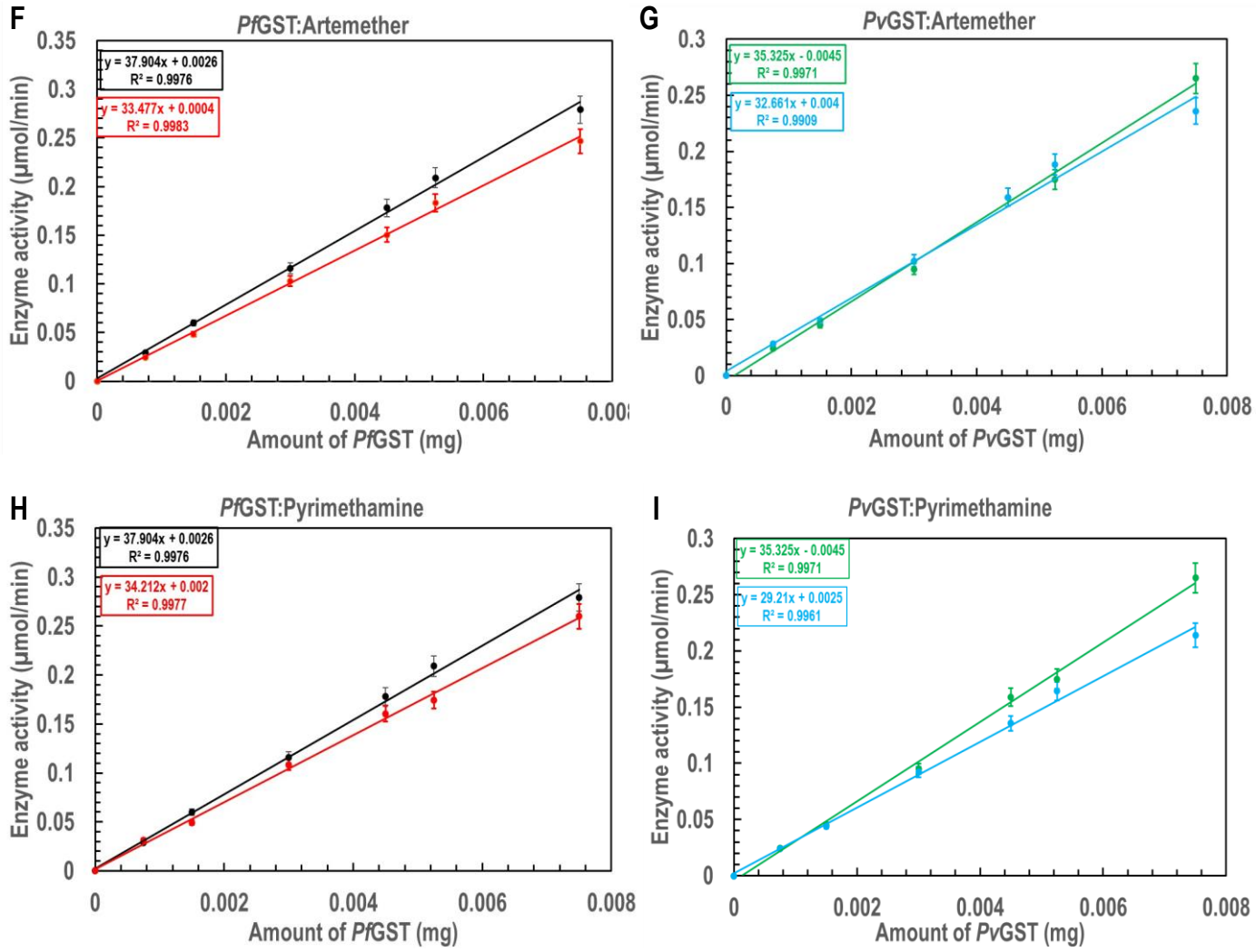


Fig. 2B-2I. Characterizing the respective *Pf*GST and *Pv*GST's specific enzymatic activities with respect to artemisinin (B and C), artesunate (D and E), artemether (F and G), and pyrimethamine (H and I). These characterizations similarly followed a GSH-CDNB conjugation model assay, which is typical of a GST enzyme activity assay. A 1 mM constant concentration of artemisinin, artesunate, artemether, and pyrimethamine alongside varying concentration of *Pf*GST and *Pv*GST in evaluating the inhibitory effect of the specific enzymatic activities. The reaction buffer similarly contains 100 mM $NaH_2PO_4$ at pH 7.2, 1 mM EDTA, 1 mM DTT, 5 mM GSH at pH 6.5, 30 mM CDNB. The plots show the spectroscopic monitoring of *Pf*GST's specific enzymatic activity (**black**), *Pf*GST's specific enzymatic activity in the presence of the drugs (**red**), *Pv*GST's specific enzymatic activity (**green**), and *Pv*GST's specific enzymatic activity in the presence of the drugs (**blue**). The $R^2$ value of approximately 1 attest to the validity of the standard curves.

Utilizing the ability of UV-Vis spectroscopy to provide valuable information about the kinetics and mechanisms of drug metabolism by GST enzymes and GSH, hence GSH, and or *Pf*GST and *Pv*GST were characterized for their biotransformation ability. This is as observable changes (such as the appearance of new peaks or shifts in absorbance maxima) in the spectra over time are

indicative of drug conjugation or metabolic transformation. In Fig. 3A, 3B, 3C, 3D, 3E, 3F, 3I, and 3J the spectra representative of artemisinin, artemether, artesunate, and lumefantrine vis-à-vis their GSH-incubated samples revealed no significant difference either in shift or intensity. This shows that there is no GSH conjugation with or glutathionylation of artemisinin, artemether, artesunate, and lumefantrine. This similar spectra pattern of artemisinin, artemether, and artesunate confirms their similarities in belonging to the same class (artemisinin) and having similar chemical structures made up of a sesquiterpene lactone structure with an endoperoxide bridge [44,45]. However, the spectra measurement of the GSH-incubated amodiaquine (Fig. 3G and H), mefloquine (Fig. 3K and L), and pyrimethamine significantly reduced in intensity. While this is indicative of GSH-conjugation or glutathionylation, they however follows different spectra pattern from each other. This is not unexpected as the three drugs differ in their chemical structures and mechanism of actions. From the observed spectra measurements, *Pf*GST and *Pv*GST respectively biotransformed artemisinin (Fig. 3A and B), artemether (Fig. 3C and D), artesunate (Fig. 3E and F), and lumefantrine (Fig. 3I and J). This is seen in the spectra shift and absorbance increase (compared to the drugs and the apo *Pf*GST and *Pv*GST) at 250 nm. However, the biotransformation reaction of these drugs improved in the presence of GSH. This shows that an enzyme-substrate interactions taking place leading to enhance biotransformation of the respective drugs. Similarly, the shifts in absorbance maxima and appearance of new peaks are not respectively conclusive of *Pf*GST and *Pv*GST biotransformation of amodiaquine (Fig. 3G and H), mefloquine (Fig. 3K and L), and pyrimethamine (Fig. 3M and N). This may however be indicative of a metabolic transformation taking place.

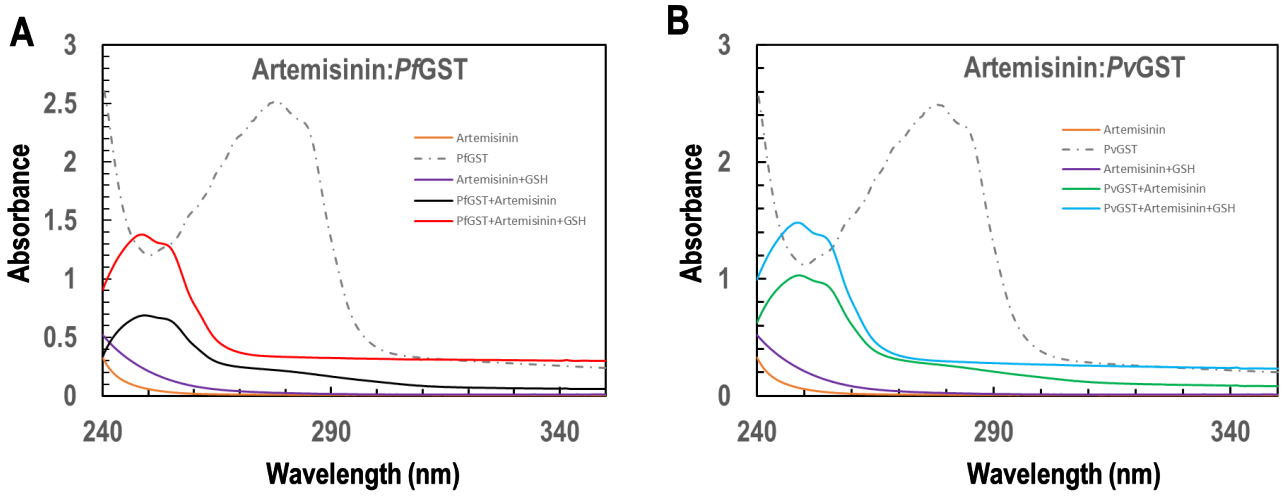

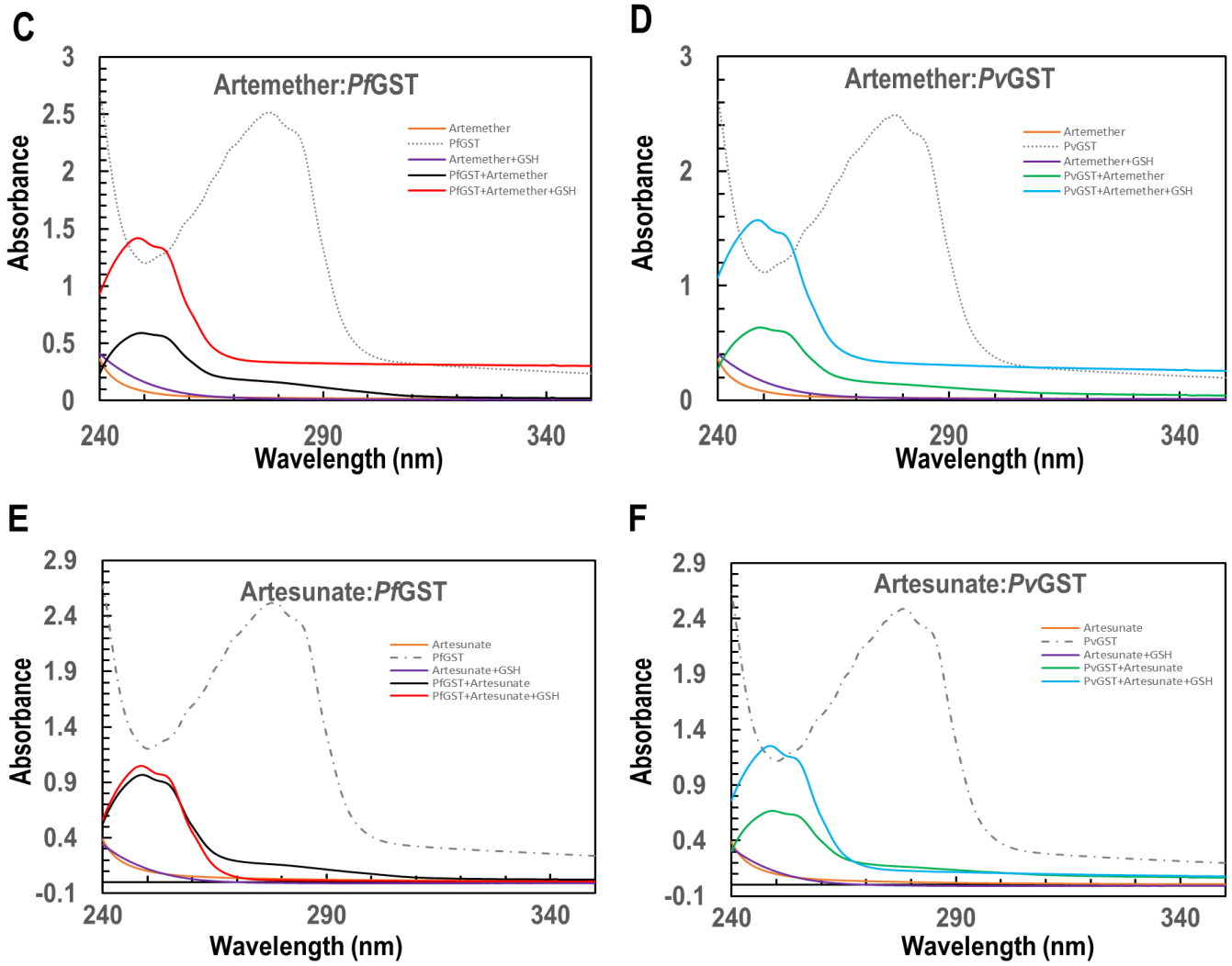
C
Artemether:PfGST
Artemether
PfGST
Artemether+GSH
PfGST+Artemether
PfGST+Artemether+GSH
Absorbance
Wavelength (nm)
D
Artemether:PvGST
Artemether
PvGST
Artemether+GSH
PvGST+Artemether
PvGST+Artemether+GSH
Absorbance
Wavelength (nm)
E
Artesunate:PfGST
Artesunate
PfGST
Artesunate+GSH
PfGST+Artesunate
PfGST+Artesunate+GSH
Absorbance
Wavelength (nm)
F
Artesunate:PvGST
Artesunate
PvGST
Artesunate+GSH
PvGST+Artesunate
PvGST+Artesunate+GSH
Absorbance
Wavelength (nm)

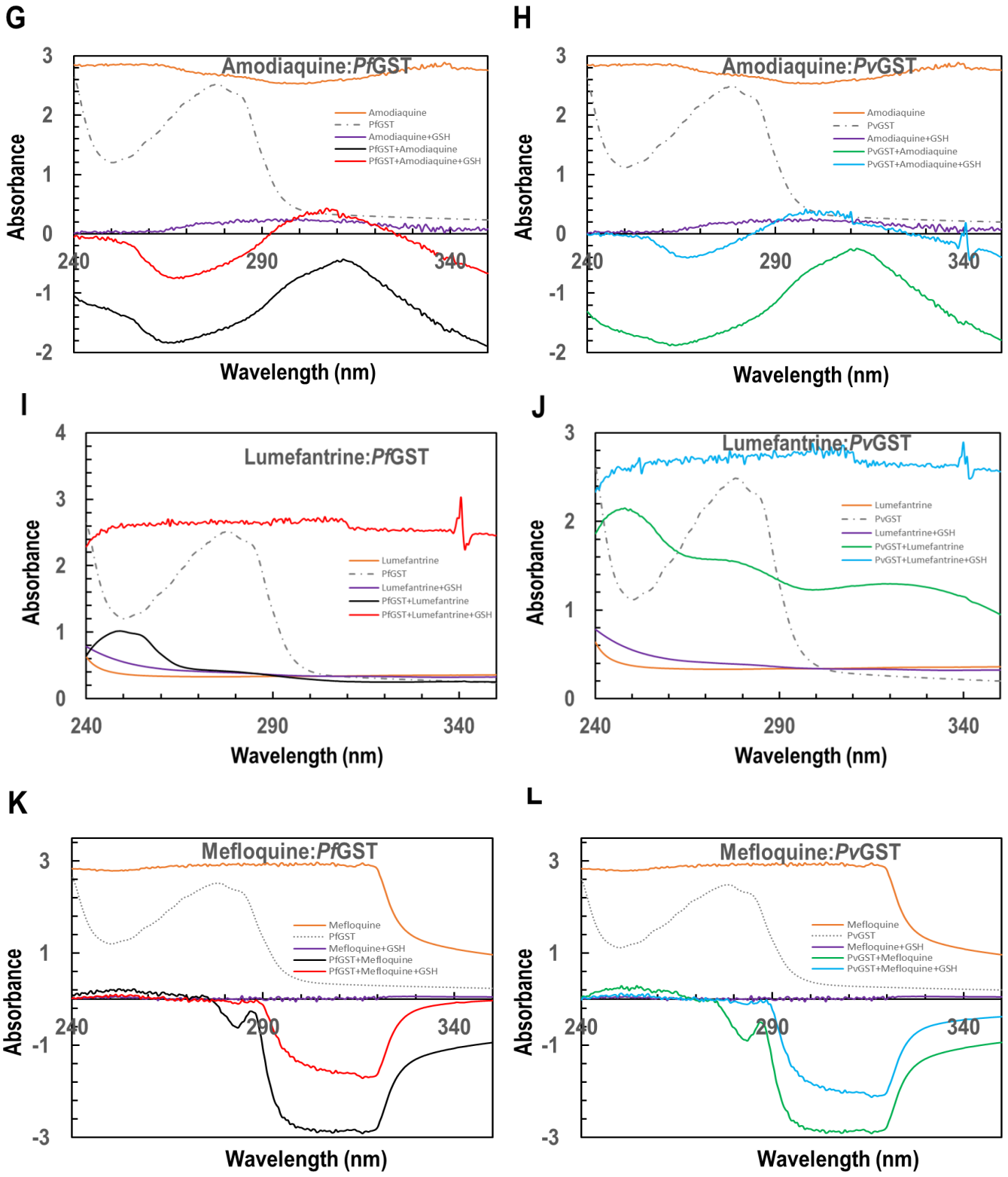
G
Amodiaquine:PfGST
Amodiaquine
PfGST
Amodiaquine+GSH
PfGST+Amodiaquine
PfGST+Amodiaquine+GSH
Absorbance
Wavelength (nm)
H
Amodiaquine:PvGST
Amodiaquine
PvGST
Amodiaquine+GSH
PvGST+Amodiaquine
PvGST+Amodiaquine+GSH
Absorbance
Wavelength (nm)
I
Lumefantrine:PfGST
Lumefantrine
PfGST
Lumefantrine+GSH
PfGST+Lumefantrine
PfGST+Lumefantrine+GSH
Absorbance
Wavelength (nm)
J
Lumefantrine:PvGST
Lumefantrine
PvGST
Lumefantrine+GSH
PvGST+Lumefantrine
PvGST+Lumefantrine+GSH
Absorbance
Wavelength (nm)
K
Mefloquine:PfGST
Mefloquine
PfGST
Mefloquine+GSH
PfGST+Mefloquine
PfGST+Mefloquine+GSH
Absorbance
Wavelength (nm)
L
Mefloquine:PvGST
Mefloquine
PvGST
Mefloquine+GSH
PvGST+Mefloquine
PvGST+Mefloquine+GSH
Absorbance
Wavelength (nm)

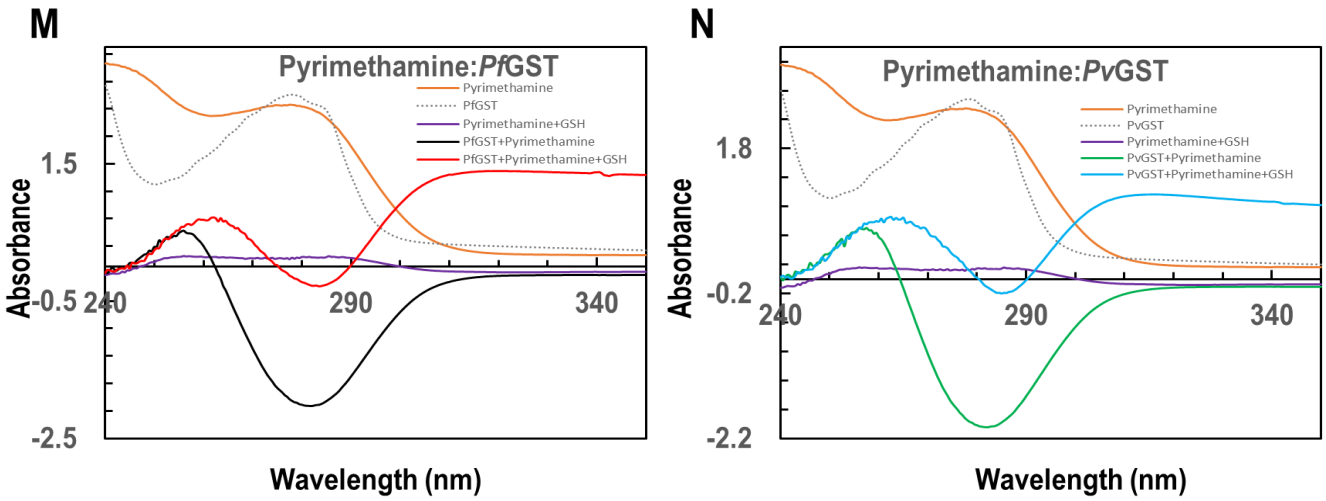


Fig. 3. A UV-Vis spectrophotometric characterization of *Pf*GST and *Pv*GST's respective biotransformation potential towards artemisinin (**A** and **B**), artemether (**C** and **D**), artesunate (**E** and **F**), amodiaquine (**G** and **H**), lumefantrine (**I** and **J**), mefloquine (**K** and **L**), and pyrimethamine (**M** and **N**). The respective drugs spectra measurements (**orange**) and the spectra measurements of *Pf*GST and *Pv*GST (**dotted grey lines)** showing light absorption at 280 nm, are also revealed. The spectra measurements of GSH-drug incubated samples **(purple),** *Pf*GST or *Pv*GST incubated drug samples (**black**) and *Pf*GST or *Pv*GST and GSH incubated drug samples (**red**) are herein figuratively represented.

In characterizing the ligandin properties of *Pf*GST and *Pv*GST towards artemisinin, artemether, artesunate, amodiaquine, lumefantrine, mefloquine, and pyrimethamine, the extrinsic anionic dye, ANS was employed in a fluorospectrophotomtetric analysis. The ANS, which is solvatochromic fluorophore was used to monitor the tertiary structural conformational differences of the proteins upon binding of the antimalarial. This is as the accessibility of the ANS to the proteins' hydrophobic pockets bring about an observable emission spectra shifts and changes, which show the protein tertiary structural features [46,47]. On that basis, a 395 nm (λ) excitation fluorescence emission maxima of free ANS from 525 nm to 490 nm and 485 nm for ANS bound *Pf*GST:GSH and *Pv*GST:GSH respectively can be observed as shown in all of Fig. 4 as a reference to the complexes. The fluorescence intensity of ANS-bound *Pv*GST:GSH is significantly higher than that of bound *Pf*GST:GSH, an indication that *Pv*GST's hydrophobic pockets were more accessible for the ANS than that of *Pf*GST. Artemisinin, artemether, and artesunate complexed *Pf*GST:GSH and *Pv*GST:GSH were blue shifted to 500 nm, they however had a varying degree of significant fluorescent intensity reduction (Fig 4A-F). These observed blue-shifts and reduced fluorescent intensity is an indication of artemisinin, artemether, and artesunate's binding to the H-site hydrophobic clefts of *Pf*GST and *Pv*GST. While these shifts speaks to the alteration in the

proteins' tertiary structure conformational integrity alteration, the decreased fluorescent intensity gives an indication of the displacement of the ANS by the binding of these antimalarials. On the other hand, amodiaquine and lumefantrine did cause a noisy, blue-shifted emission at 525 nm for *Pf*GST and *Pv*GST (Fig. 4G-J) with an almost complete quenching of fluorescent intensity below that of the free ANS. While this is not conclusive of binding, it may however be as a result of precipitation or aggregation elicited by insolubility of these antimalarials. This aggregation induced blue-shift assertion is supported by literature [48–50]. In the same vein, mefloquine's interaction with *Pf*GST and *Pv*GST as seen in Fig. 4K and L respectively, results in an excitation fluorescence emission maxima similar to that of free ANS. This is also not indicative of binding but rather causing an alteration in macromolecular environment of the proteins which subsequently shields the proteins' hydrophobic pockets from the surrounding solvent molecules, leading to reduced fluorescence emission. On the other hand, pyrimethamine's interaction with *Pf*GST and *Pv*GST give different spectra pattern different from all previously antimalarial result. Pyrimethamine result in a red-shift with a significant increase in fluorescence intensity. In *Pf*GST (Fig 4M), it was red-shifted to excitation fluorescence emission maxima of 485 nm while *Pv*GST was with excitation fluorescence emission maxima of 482 nm. This could be attributed to a decrease in the protein's binding site hydrophobicity with an ANS restricted mobility. This assertion is also supported by literature [51].

In characterizing *Pf*GST and *Pv*GST's thermal stability with respect to the antimalarials, a fluorescence thermal shift assay that measures and detects protein-ligand interaction were carried out using the CFX96 Touch Real-Time PCR Detection System (BIO-RAD).

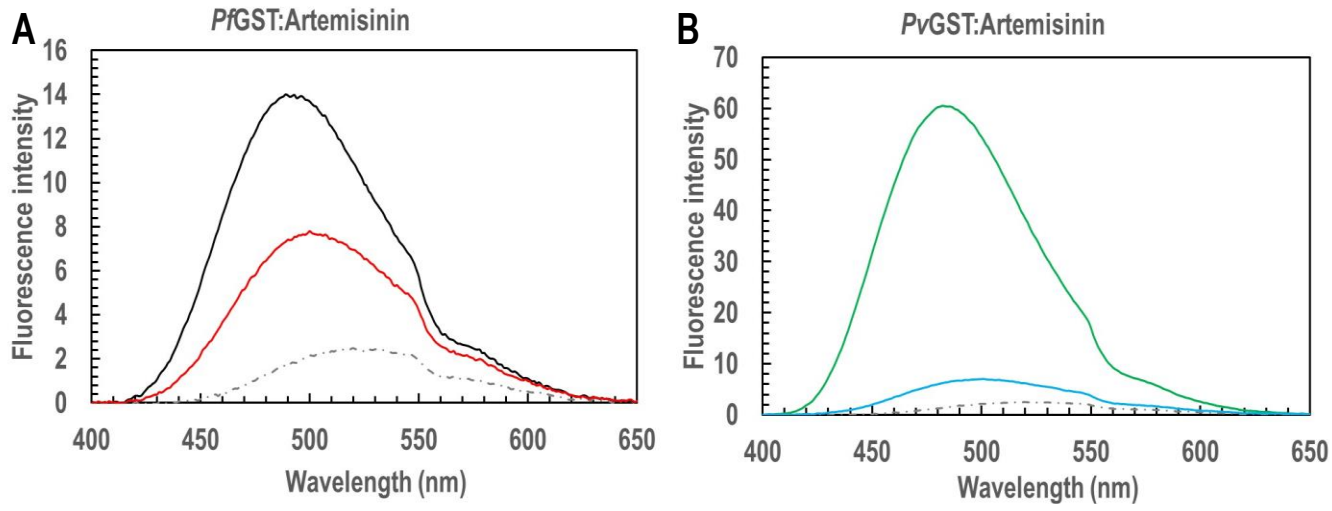

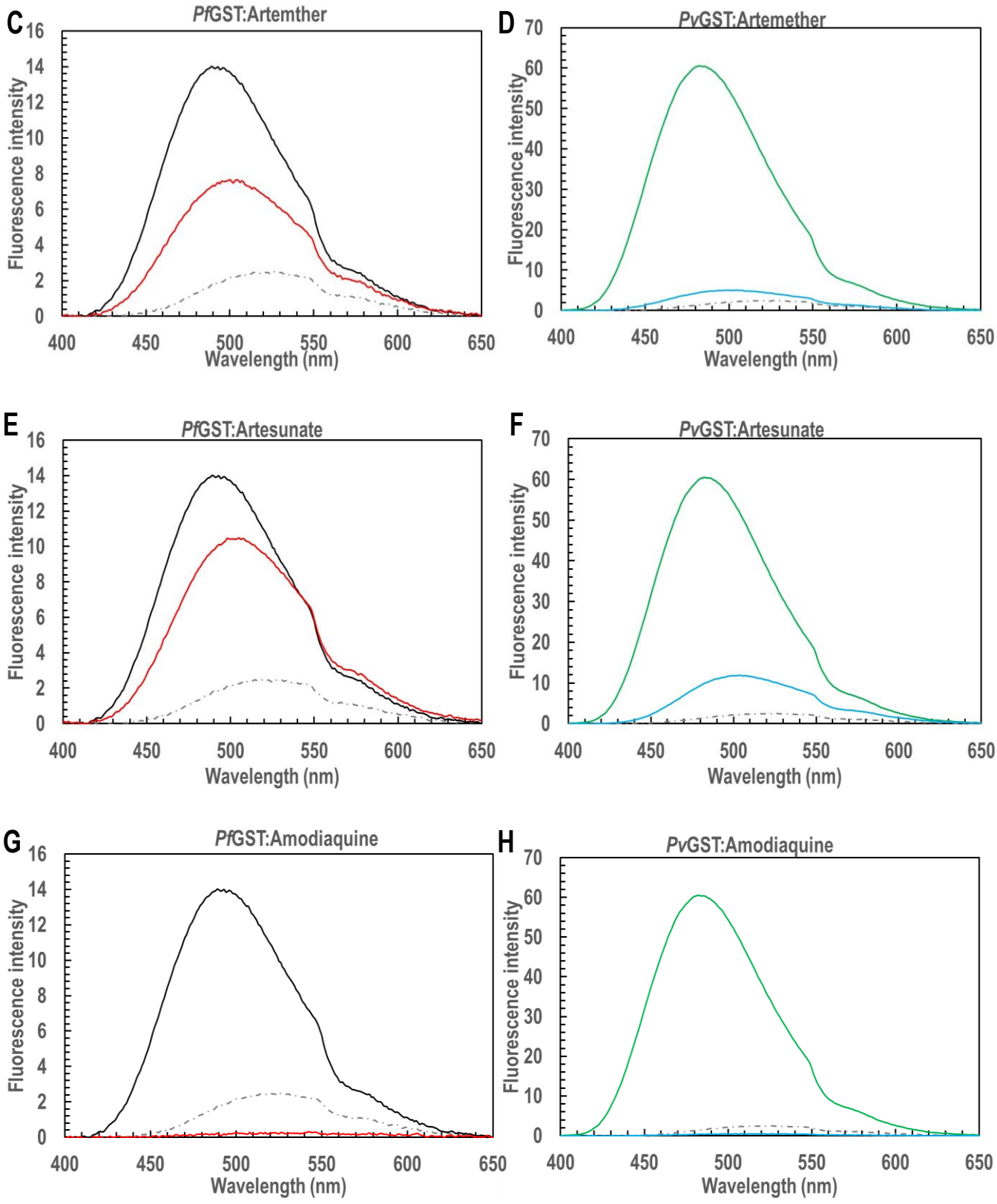
C
PfGST:Artemther
Fluorescence intensity
Wavelength (nm)
D
PvGST:Artemether
Fluorescence intensity
Wavelength (nm)
E
PfGST:Artesunate
Fluorescence intensity
Wavelength (nm)
F
PvGST:Artesunate
Fluorescence intensity
Wavelength (nm)
G
PfGST:Amodiaquine
Fluorescence intensity
Wavelength (nm)
H
PvGST:Amodiaquine
Fluorescence intensity
Wavelength (nm)

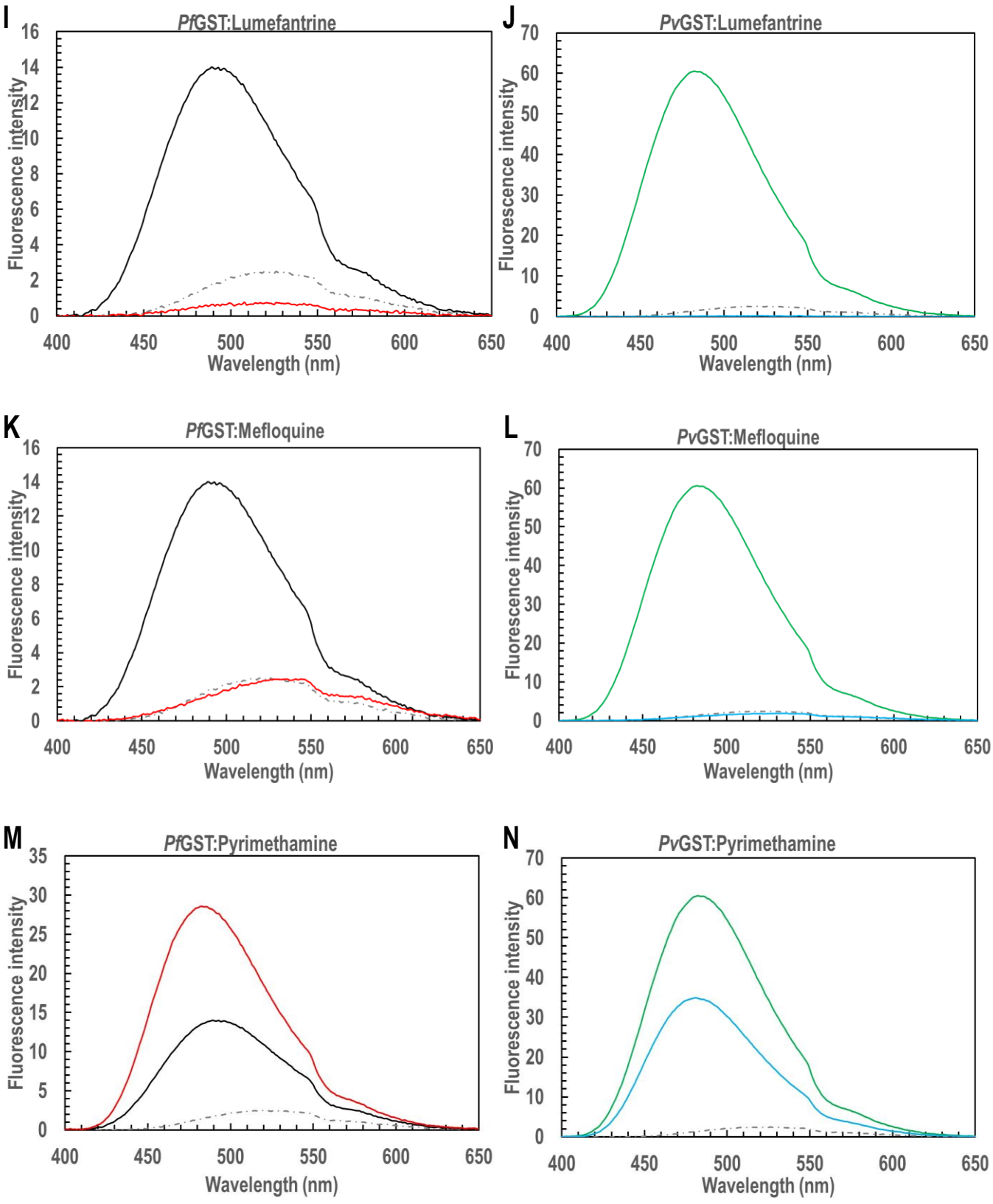


Fig. 4. Ligandin activity of *Pf*GST and *Pv*GST through ANS fluorescence spectroscopy towards artemisinin (**A** and **B**), artemether (**C** and **D**), artesunate (**E** and **F**), amodiaquine (**G** and **H**), lumefantrine (**I** and **J**), mefloquine (**K** and

**L**), and pyrimethamine (**M** and **N**) and their effect on *Pf*GST and *Pv*GST's tertiary structural conformation. A spectrofluorometric monitored ANS fluorescence emission at 395 nm excitation showing emission spectrum of free ANS **(gray dotted lines)**, ANS bound *Pf*GST **(black)** and ANS bound *Pv*GST **(green)**. The respective antimalarial complexed *Pf*GST's emission spectrum are represented in **(red)** and *Pv*GST complexed antimalarials are **(blue)**. A reduced GSH were added as a *Pf*GST and *Pv*GST proteins in all the samples monitored.

The stability of the apo form of *Pf*GST and *Pv*GST, *Pf*GST:GSH, and *Pv*GST:GSH and their complexes with artemisinin, artemether, artesunate, amodiaquine, lumefantrine, mefloquine, and pyrimethamine were all evaluated. This technique utilizes the ability and propensity of the binding of SYPRO Orange dye to bind to the protein's hydrophobic patches when it gets thermally denatured, and this is seen in increased quantum yield. The melting temperature of the unbound and antimalarial-complexed samples were recorded during the denaturation at an increasing temperature range of between 25 ºC to 65 ºC. The melting temperature ($T_m$) of *Pf*GST and *Pv*GST were evaluated to be 56.0 ± 0.5 ºC and 58.0 ± 0.5 ºC respectively, and this is consistent and characteristics of the $T_m$ of other GSTs previously reported [52,53]. Expectedly, GSH an essential GST substrate induces a more conformational stability when incubated with the two *Pf*GST and *Pv*GST with *Pf*GST:GSH and *Pv*GST:GSH's $T_m$ evaluated to 61.5 ± 0.2 ºC and 60.0 ± 0.2 ºC respectively. This is so as GSH's specificity and binding to *Pf*GST and *Pv*GST's G-site do not displace the SYPRO Orange dye (which binds to the H-site) and thereby enhancing the stability of the two proteins. These results were represented in all of Fig. 5 to serve as reference and comparison with the liganded samples. However, while artemisinin seems not to induce conformational instability in *Pf*GST:GSH (Fig. 5A) with $T_m$ of 55.0 ± 0.2 ºC, it however made *Pv*GST:GSH significantly less stable with $T_m$ of 48.5 ± 0.5 ºC (Fig 5B). This result correlates with the level of artemisinin inhibited specific enzymatic activities reported in Fig 2C. Similarly, artemether and artesunate also induce less conformational instability in *Pf*GST:GSH (Fig 5C and 5E) with $T_m$ of 52.5 ± 0.2 ºC compared to that of the respective artemether and artesunate complexed *Pv*GST:GSH (Fig. 5D and 5F) with same $T_m$ of 48.0 ± 0.2 ºC. While amodiaquine seems not to also induce conformational instability in *Pf*GST:GSH (Fig. 5G), as these complex has same $T_m$ with unbound *Pf*GST:GSH, it however bound and lowered the stability of *Pv*GST:GSH to $T_m$ of 50.0 ± 0.2 ºC (Fig 5H). The thermal stability of mefloquine and pyrimethamine complexed *Pf*GST:GSH were evaluated to be $T_m$ of 52.0 ± 0.2 ºC and 54.5 ± 0.2 ºC respectively (Fig. 5I and 5K). On the other hand, the mefloquine and pyrimethamine bound *Pf*GST:GSH were evaluated to be $T_m$ of 42.0 ± 0.2 ºC and 48.50 ± 0.5 ºC respectively (Fig. 5I

and 5K). These observable differential binding elicited thermal conformational stability or instability summarized in Table 1 below show that while GSH's specificity and binding to the proteins' G-site do not displace the SYPRO Orange dye, it however stabilize the protein. It also show the antimalarials behaves differently in making *Pf*GST:GSH and *Pv*GST:GSH less stable.

Table 1. The thermal stability melt peak of *Pf*GST:GSH and *Pv*GST:GSH with respect seven selected antimalarials

| | **Samples' Melt Peak (°C)** | |
|---|---|---|
| **Drugs** | ***Pf*GST:GSH @ $T_m$ of 61.5 ± 0.2** | ***Pv*GST:GSH @ $T_m$ of 60.0 ± 0.2** |
| Artemisinin | 55.0 ± 0.2 | 48.5 ± 0.5 |
| Artemether | 52.5 ± 0.2 | 48.5 ± 0.2 |
| Artesunate | 52.5 ± 0.2 | 48.0 ± 0.2 |
| Amodiaquine | 56.0 ± 0.5 | 50.0 ± 0.2 |
| Lumefantrine | ---- | --- |
| Mefloquine | 52.0 ± 0.2 | 42.0 ± 0.2 |
| Pyrimethamine | 54.5 ± 0.2 | 48.5 ± 0.5 |

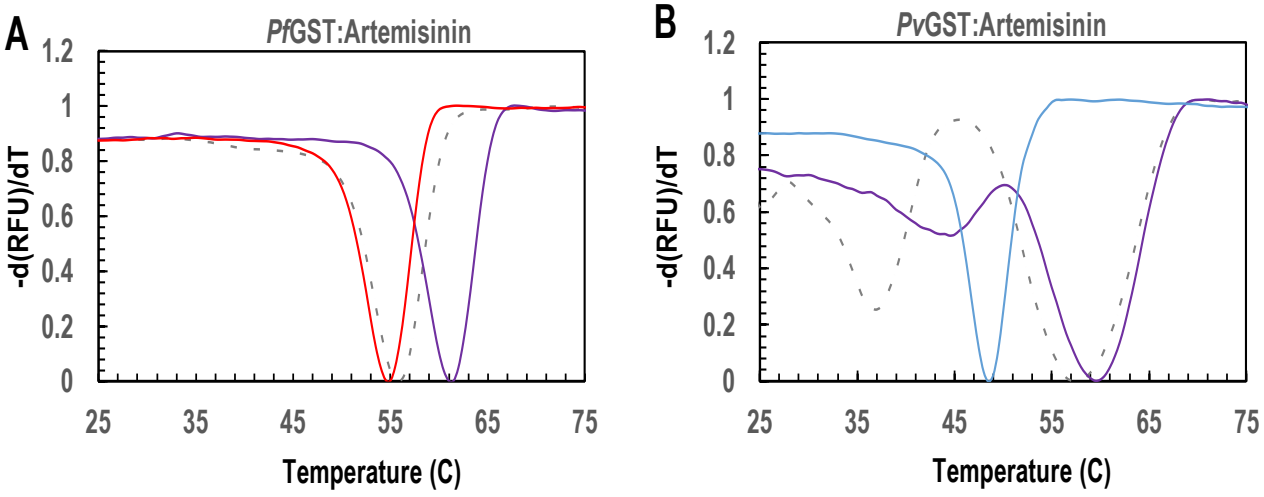

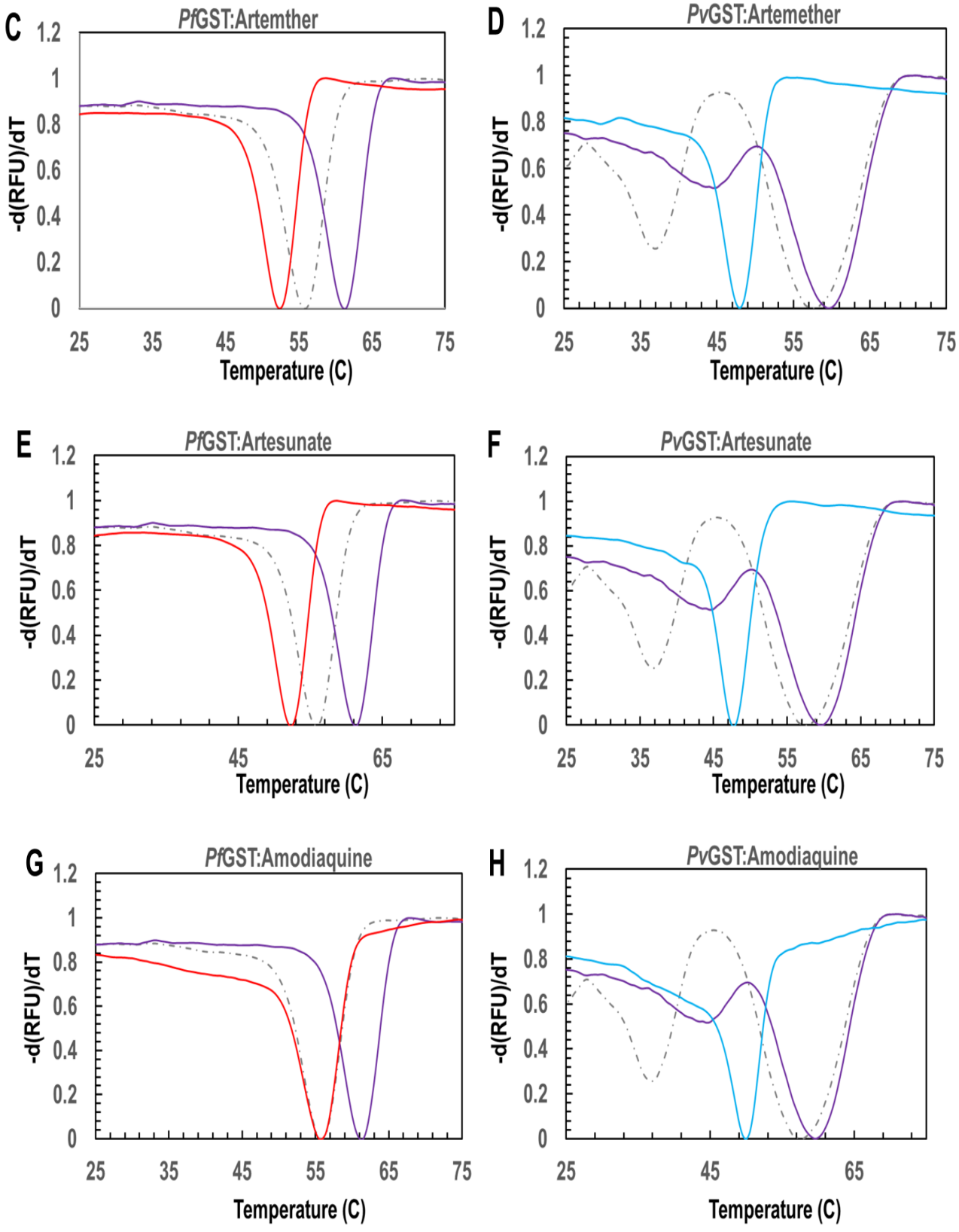
C
PfGST:Artemther
D
PvGST:Artemether
E
PfGST:Artesunate
F
PvGST:Artesunate
G
PfGST:Amodiaquine
H
PvGST:Amodiaquine
-d(RFU)/dT
Temperature (C)

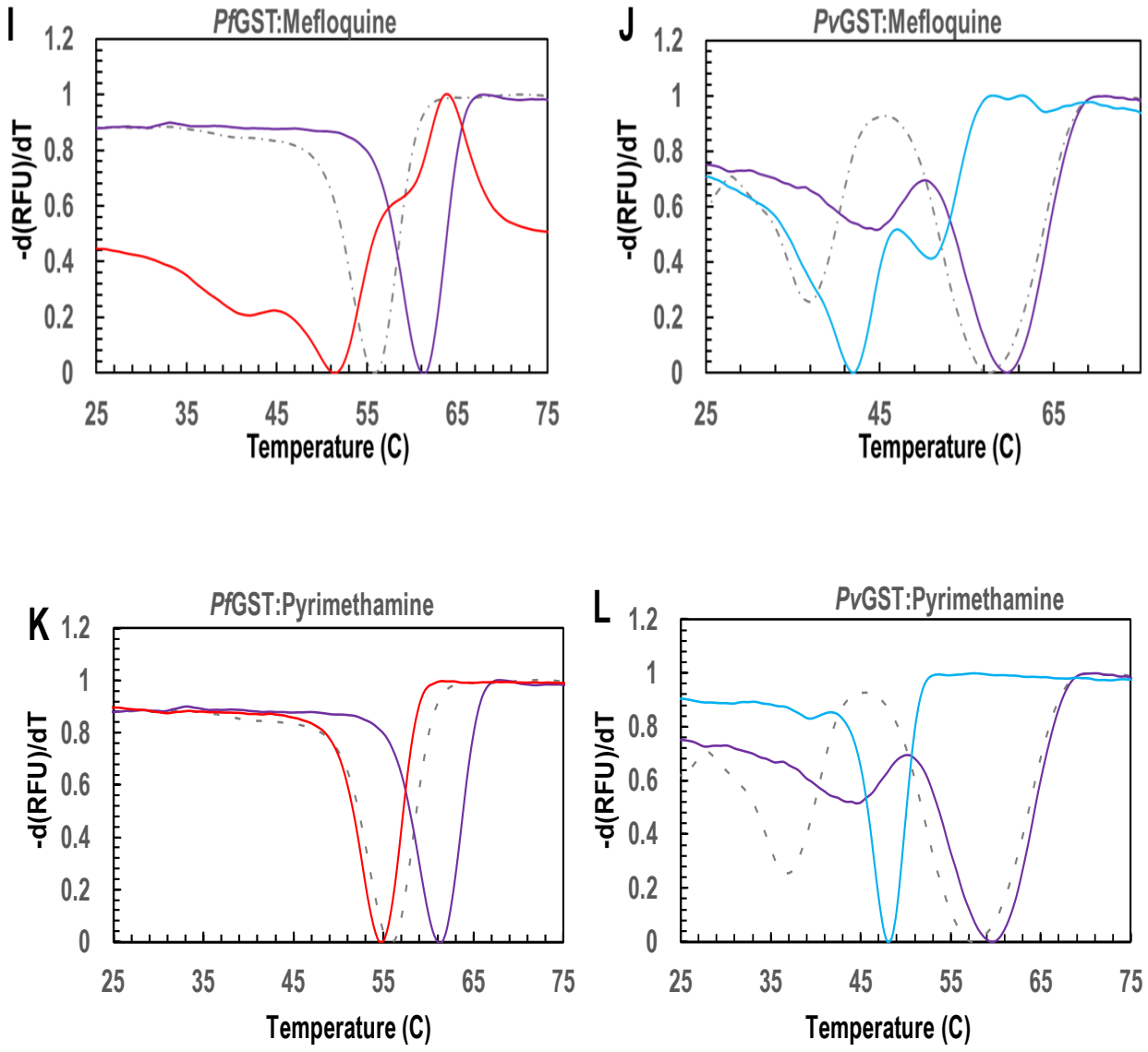


Fig. 4. Thermal stability of *Pf*GST and *Pv*GST using a CFX96 Touch-Real-Time qPCR detection system towards artemisinin (**A** and **B**), artemether (**C** and **D**), artesunate (**E** and **F**), amodiaquine (**G** and **H**), mefloquine (**I** and **J**), and pyrimethamine (**K** and **L**), and their effect on *Pf*GST and *Pv*GST's thermal stability. A naturally quenched fluorescent dye (SYPRO Orange dye) as a probe was used for the thermal denaturation evaluation of sypro orange bound *Pf*GST **(grey dotted lines),** antimalarial complexed **(red),** sypro orange bound *Pf*GST:GSH (**purple**), sypro orange bound *Pv*GST **(grey dotted lines),** sypro orange bound *Pv*GST:GSH **(purple),** and sypro orange bound *Pv*GST:GSH when complexed with the respective antimalarials **(blue).**

## 4. Conclusion

This enzymatic activities inhibition and characterization of *Pf*GST and *Pv*GST towards the seven antimalarials were evaluated and found not to be significant enough to bring a halt to the detoxification ability of the enzymes. This is as the GST's catalytic/enzymatic activities as a bi-substrate detoxification enzyme, which primarily catalyzes xenobiotics to its hydrophobic site (H-site) [39,54] were not completely or significantly brought to a halt. This is graphically seen in the highest inhibitory potency observed in artemisinin inhibiting *Pv*GST specific enzymatic activities at approximately 27 %. While *Pf*GST and *Pv*GST have been recognized as a critical target for the development of potent antimalarials, however the existing antimalarials do not prove potent enough to inhibit them. *Pf*GST and *Pv*GST's ability as biotransformation and detoxification enzymes through GSH conjugation process is herein confirmed. The various observable, blue-shifted excitation fluorescence emission maxima and the significant quenching of the fluorescence intensity of the ANS-extrinsically probed ligandin properties of *Pf*GST and *Pv*GST were evaluated towards the antimalarials. While all the results indicated binding and inhibition, they were however not in correlation with other characterization techniques employed as seen in all the antimalarials eliciting binding and causing differential thermally conformational instability.

**Funding information**

This research received funding support from National Research Foundation (NRF), South Africa.

**Author declaration**

The authors that no ethical permission was required for the experimental work undertaken.

**CRediT authorship contribution statement**

Olalekan Onisuru: Manuscript writing, editing, review and all experimental work performed.

Ikechukwu Achilonu: Research conceptualization, supervision, guidance, and funding support.

**Declaration of Competing Interest**

The authors declare no conflicting interest

## References


[1] M. Kotepui, A. Mahittikorn, P. Wilairatana, F.R. Masangkay, K. Wangdi, K.U. Kotepui, Methemoglobin levels in malaria: a systematic review and meta-analysis of its association with Plasmodium falciparum and Plasmodium vivax infections and disease severity, Sci. Rep. 14 (2024) 3276.

[2] J.Y. Won, E. Mazigo, S.H. Cha, J.-H. Han, Functional characterization of Plasmodium vivax hexose transporter 1, Front. Cell. Infect. Microbiol. 13 (2024) 1321240.

[3] W.-C. Lee, F.W. Cheong, A. Amir, M.Y. Lai, J.H. Tan, W.K. Phang, S. Shahari, Y.-L. Lau, Plasmodium knowlesi: the game changer for malaria eradication, Malar. J. 21 (2022) 1–24.

[4] V. Joste, J. Bailly, V. Hubert, C. Pauc, M. Gendrot, E. Guillochon, M. Madamet, M. Thellier, E. Kendjo, N. Argy, Plasmodium ovale wallikeri and P. ovale curtisi Infections and Diagnostic Approaches to Imported Malaria, France, 2013–2018, Emerg. Infect. Dis. 27 (2021) 372.

[5] J.P. Manata, M. Brochado, B. Silva, J. Chinchila, J.M. Costa, M. Brochado Sr, B. Silva Sr, Chronic Infection by Plasmodium falciparum, Cureus. 16 (2024).

[6] D.E. Loy, W. Liu, Y. Li, G.H. Learn, L.J. Plenderleith, S.A. Sundararaman, P.M. Sharp, B.H. Hahn, Out of Africa: origins and evolution of the human malaria parasites Plasmodium falciparum and Plasmodium vivax, Int. J. Parasitol. 47 (2017) 87–97.

[7] B. Larson, Origin of Two Most Virulent Agents of Human Malaria: Plasmodium falciparum and Plasmodium vivax, Malaria. 4 (2019) 1–16.

[8] S. Tiwari, N. Sharma, G.P. Sharma, Redox interactome in malaria parasite Plasmodium falciparum, (2021) 423–434.

[9] M.R. Rosenthal, C.L. Ng, Plasmodium falciparum Artemisinin Resistance: The E ff ect of Heme, Protein Damage, and Parasite Cell Stress Response, 6 (2020) 1599–1614.

[10] Y. Yuthavong, B. Tarnchompoo, T. Vilaivan, P. Chitnumsub, S. Kamchonwongpaisan, S.A. Charman, D.N. McLennan, K.L. White, L. Vivas, E. Bongard, Malarial dihydrofolate reductase as a paradigm for drug development against a resistance-compromised target, Proc. Natl. Acad. Sci. 109 (2012) 16823–16828.

[11] N. Fisher, B. Meunier, G.A. Biagini, The cytochrome bc1 complex as an antipathogenic target, Febs Lett. 594 (2020) 2935–2952.

[12] T.N. de Sousa, F.S. Kano, C.F.A. de Brito, L.H. Carvalho, The Duffy binding protein as a key target for a Plasmodium vivax vaccine: lessons from the Brazilian Amazon, Mem. Inst. Oswaldo Cruz. 109 (2014) 608–617.

[13] M. Mishra, V. Singh, S. Singh, Structural insights into key Plasmodium proteases as therapeutic drug targets, Front. Microbiol. 10 (2019) 394.

[14] K. Fritz-Wolf, A. Becker, S. Rahlfs, P. Harwaldt, R.H. Schirmer, W. Kabsch, K. Becker, X-ray structure of glutathione S-transferase from the malarial parasite Plasmodium falciparum, Proc. Natl. Acad. Sci. U. S. A. 100 (2003) 13821–13826.

[15] N. Hiller, K. Fritz-Wolf, M. Deponte, W. Wende, H. Zimmermann, K. Becker, Plasmodium falciparum glutathione S -transferase-Structural and mechanistic studies on ligand binding and enzyme inhibition , Protein Sci. 15 (2006) 281–289.

[16] R. Mangoyi, R. Hayeshi, B. Ngadjui, F. Ngandeu, M. Bezabih, B. Abegaz, S. Razafimahefa, P. Rasoanaivo, S. Mukanganyama, Glutathione transferase from Plasmodium falciparum - Interaction with malagashanine and selected plant natural products, J. Enzyme Inhib. Med. Chem. 25 (2010) 854–862.

[17] E.E. Colón-Lorenzo, D.D. Colón-López, J. Vega-Rodríguez, A. Dupin, D.A. Fidock, A. Baerga-Ortiz, J.G. Ortiz, J. Bosch, A.E. Serrano, Structure-Based Screening of Plasmodium berghei Glutathione S-Transferase Identifies CB-27 as a Novel Antiplasmodial Compound, Front. Pharmacol. 11 (2020) 1–17.

[18] I. Quesada-Soriano, C. Barón, R. Téllez-Sanz, F. García-Maroto, L. García-Fuentes, Asn112 in Plasmodium falciparum glutathione S-transferase is essential for induced reversible tetramerization by phosphate or pyrophosphate, Biochim. Biophys. Acta - Proteins Proteomics. 1844 (2014) 1427–1436.

[19] T.M. Belete, Recent progress in the development of new antimalarial drugs with novel targets, Drug Des. Devel. Ther. (2020) 3875–3889.

[20] World Health Organization, WHO guidelines for malaria, 3 June 2022.

[21] C. Rasmussen, P. Alonso, P. Ringwald, Current and emerging strategies to combat antimalarial resistance, Expert Rev. Anti. Infect. Ther. 20 (2022) 353–372.

[22] W. Shibeshi, A.M. Baye, G. Alemkere, E. Engidawork, Efficacy and Safety of Artemisinin-Based Combination Therapy for the Treatment of Uncomplicated Malaria in Pregnant Women: A Systematic Review and Meta-Analysis, Ther. Clin. Risk Manag. 17 (2021) 1353–1370.

[23] S. Akash, G. Abdelkrim, I. Bayil, M.E. Hosen, N. Mukerjee, A.F. Shater, F.M. Saleh, G.M. Albadrani, M.Q. Al-Ghadi, M.M. Abdel-Daim, Antimalarial drug discovery against malaria parasites through haplopine modification: an advanced computational approach, J. Cell. Mol. Med. 27 (2023) 3168–3188.

[24] B.A. Darko, C.M. Owusu-Asenso, A. Mensah, A.C. Seyram, G.B. Dzotefe, T.B. Ebobabaara, F. Opoku-Gyebi, B.Y. Gordor, B.C. Obeng, Global trends in the burden of malaria: Contemporary diagnostic approaches, and treatment strategies, World J. Adv. Res. Rev. 20 (2023) 258–272.

[25] C. Naing, M.A. Whittaker, N.H. Htet, S.N. Aye, J.W. Mak, Efficacy of antimalarial drugs for treatment of uncomplicated falciparum malaria in Asian region: A network meta-analysis, PLoS One. 14 (2019) 1–16.

[26] World Health Organization, World malaria report 2023.

[27] M.S. Issa, M. Warsame, M.H.T. Mahamat, I.D.M. Saleh, K. Boulotigam, H. Djimrassengar, A.H. Issa, O. Abdelkader, M. Hassoumi, M. Djimadoum, Therapeutic efficacy of artesunate–amodiaquine and artemether–lumefantrine for the treatment of uncomplicated falciparum malaria in Chad: clinical and genetic surveillance, Malar. J. 22 (2023) 240.

[28] World Health Organization, World malaria report 2022, World Health Organization, 2022.

[29] M.A. Shibeshi, Z.D. Kifle, S.A. Atnafie, Antimalarial drug resistance and novel targets for antimalarial drug discovery, Infect. Drug Resist. 13 (2020) 4047–4060.

[30] C. Severini, M. Menegon, Resistance to antimalarial drugs: An endless world war against Plasmodium that we risk losing, J. Glob. Antimicrob. Resist. 3 (2015) 58–63.

[31] T. Yang, S. Ottilie, E.S. Istvan, K.P. Godinez-Macias, A.K. Lukens, B. Baragaña, B.

Campo, C. Walpole, J.C. Niles, K. Chibale, K.J. Dechering, M. Llinás, M.C.S. Lee, N. Kato, S. Wyllie, C.W. McNamara, F.J. Gamo, J. Burrows, D.A. Fidock, D.E. Goldberg, I.H. Gilbert, D.F. Wirth, E.A. Winzeler, MalDA, Accelerating Malaria Drug Discovery, Trends Parasitol. 37 (2021) 493–507.

[32] B. Forte, S. Ottilie, A. Plater, B. Campo, K.J. Dechering, F.J. Gamo, D.E. Goldberg, E.S. Istvan, M. Lee, A.K. Lukens, C.W. McNamara, J.C. Niles, J. Okombo, C.F.A. Pasaje, M.G. Siegel, D. Wirth, S. Wyllie, D.A. Fidock, B. Baragaña, E.A. Winzeler, I.H. Gilbert, Prioritization of Molecular Targets for Antimalarial Drug Discovery, ACS Infect. Dis. 7 (2021) 2764–2776.

[33] P.M. Cheuka, P. Njaria, G. Mayoka, E. Funjika, Emerging Drug Targets for Antimalarial Drug Discovery: Validation and Insights into Molecular Mechanisms of Function, J. Med. Chem. 67 (2024) 2, pp 838-865.

[34] I. Quesada-Soriano, C. Barón, F. García-Maroto, A.M. Aguilera, L. García-Fuentes, Calorimetric studies of ligands binding to glutathione S-transferase from the malarial parasite Plasmodium falciparum, Biochemistry. 52 (2013) 1980–1989.

[35] B.K. Na, J.M. Kang, T.S. Kim, W.M. Sohn, Plasmodium vivax: Molecular cloning, expression and characterization of glutathione S-transferase, Exp. Parasitol. 116 (2007) 414–418.

[36] T. Tripathi, B.-K. Na, W.-M. Sohn, K. Becker, V. Bhakuni, Structural, functional and unfolding characteristics of glutathione S-transferase of Plasmodium vivax, Arch. Biochem. Biophys. 487 (2009) 115–122.

[37] J.R. Beck, C.-M. Ho, Transport mechanisms at the malaria parasite-host cell interface, PLoS Pathog. 17 (2021) e1009394.

[38] S. Müller, Redox and antioxidant systems of the malaria parasite Plasmodium falciparum, Mol. Microbiol. 53 (2004) 1291–1305.

[39] H.H. Makumbe, R. Pandian, A. Valli, Y. Sayed, I. Achilonu, Biophysical characterization, crystallization, and solution of the first crystal structure of the 28 kDa-Schistosoma bovis glutathione transferase, J. Mol. Struct. 1298 (2024) 136979.

[40] M. Pawłowska, C. Mila-Kierzenkowska, J. Szczegielniak, A. Woźniak, Oxidative Stress in Parasitic Diseases—Reactive Oxygen Species as Mediators of Interactions between the Host and the Parasites, Antioxidants. 13 (2023) 38.

[41] W.H. Habig, W.B. Jakoby, Assays for differentiation of glutathione S-Transferases, in: Methods Enzymol., Elsevier, 1981: pp. 398–405.

[42] J. Vašková, L. Kočan, L. Vaško, P. Perjési, Glutathione-related enzymes and proteins: A review, Molecules. 28 (2023) 1447.

[43] A. Potęga, Glutathione-mediated conjugation of anticancer drugs: an overview of reaction mechanisms and biological significance for drug detoxification and bioactivation, Molecules. 27 (2022) 5252.

[44] B. Ivanescu, A. Miron, A. Corciova, Sesquiterpene lactones from Artemisia genus: Biological activities and methods of analysis, J. Anal. Methods Chem. 2015 (2015).

[45] F.W. Muregi, A. Ishih, Next-generation antimalarial drugs: hybrid molecules as a new strategy in drug design, Drug Dev. Res. 71 (2010) 20–32.

[46] K. Pooe, M. Thulo, H. Makumbe, B. Akumadu, O. Otun, C. Aloke, I. Achilonu, Biophysical description of Bromosulfophthalein interaction with the 28-kDa glutathione transferase from Schistosoma japonicum, Mol. Biochem. Parasitol. 252 (2022) 111524.

[47] Y. Sayed, L.A. Wallace, H.W. Dirr, The hydrophobic lock-and-key intersubunit motif of glutathione transferase A1-1: implications for catalysis, ligandin function and stability, FEBS Lett. 465 (2000) 169–172.

[48] H. Li, T.-Z. Xie, Z. Liang, D. Dahal, Y. Shen, X. Sun, Y. Yang, Y. Pang, T. Liu, Conformational change due to intramolecular hydrophobic interaction leads to large blue-shifted emission from single molecular cage solutions, Chem. Commun. 55 (2019) 330–333.

[49] L. Zhu, C. Yang, J. Qin, An aggregation-induced blue shift of emission and the self-assembly of nanoparticles from a novel amphiphilic oligofluorene, Chem. Commun. (2008) 6303–6305.

[50] W. Ki, K. Ngo, P. Ghosh, B. Averkiev, G.T. Reeves, I. Ailes, B.C. Pemberton, K. Zhu, J.

Li, Blue-shifted aggregation-induced enhancement of a Sn (iv) fluoride complex: the role of fluorine in luminescence enhancement, Chem. Commun. 56 (2020) 9648–9650.

[51] O.K. Gasymov, B.J. Glasgow, ANS fluorescence: potential to augment the identification of the external binding sites of proteins, Biochim. Biophys. Acta (BBA)-Proteins Proteomics. 1774 (2007) 403–411.

[52] W.A. Lea, A. Simeonov, Differential scanning fluorometry signatures as indicators of enzyme inhibitor mode of action: case study of glutathione S-transferase, PLoS One. 7 (2012) e36219.

[53] M. Redhead, R. Satchell, C. McCarthy, S. Pollack, J. Unitt, Thermal Shift as an Entropy-Driven Effect, Biochemistry. 56 (2017) 6187–6199.

[54] M.N. Al-Qattan, M.N. Mordi, S.M. Mansor, Assembly of ligands interaction models for glutathione-S-transferases from Plasmodium falciparum, human and mouse using enzyme kinetics and molecular docking, Comput. Biol. Chem. 64 (2016) 237–249.

# CHAPTER 5

This chapter has been published as manuscript entitled "**Describing the ligandin properties of *Plasmodium falciparum* and *vivax* glutathione transferase towards Bromosulfophthalein from empirical and computational modelling viewpoints**" by Olalekan Onisuru and Ikechukwu Achilonu as an article in **Journal of Biomolecular Structure and Dynamics**. This manuscript insightfully and novelly describe for the first time via an empirical and computational modelling studies, the ligandin ability of bromosulfophthalein (BSP) in Glutathione S-Transferase enzyme (GST) (that detoxify many substances intracellularly by inactivating and converting diverse exogenous and endogenous toxic molecules to less toxic soluble compounds) present in the two main malaria-causing agents in Africa and Asia continent. The manuscript employed several empirically biophysical techniques and computational modelling studies to show BSP's ability to tightly bind and inhibit *Plasmodium falciparum* GST (*Pf*GST) and *Plasmodium vivax* GST (*Pv*GST), a condition which will consequently disrupt both target's detoxification ability and also reduce their antioxidant capacity, which are critical features of potent antimalarials. To the best of our knowledge, there has not been a published article that integrated empirical and computational findings to describe the ligandin properties of *Pf*GST and *Pv*GST towards bromosulfophthalein. We belief this work will benefit all readers of Journal of Biomolecular Structure and Dynamics

# Describing the ligandin properties of *Plasmodium falciparum* and *vivax* glutathione transferase towards Bromosulfophthalein from empirical and computational modelling viewpoints

Olalekan Onisuru and Ikechukwu Achilonu*

Protein Structure-Function and Research Unit, School of Molecular and Cell Biology, Faculty of Science, University of the Witwatersrand, Braamfontein, Johannesburg 2000, South Africa

***Correspondence to Ikechukwu Achilonu*** (Ikechukwu.Achilonu@wits.ac.za): Protein Structure-Function and Research Unit, School of Molecular and Cell Biology, Faculty of Science, University of the Witwatersrand, Braamfontein, Johannesburg 2000, South Africa

**Authors**

Olalekan Onisuru: 2430435@students.wits.ac.za

Ikechukwu Achilonu: Ikechukwu.Achilonu@wits.ac.za

## Abstract

Research has spotlighted glutathione transferase (GST) as a promising target for antimalarial drug development due to its pivotal role in cellular processes, including metabolizing toxins and managing oxidative stress. This interest arises from GST's potential to combat multidrug resistance in existing antimalarial drugs. *Plasmodium falciparum* GST (*Pf*GST) and *Plasmodium vivax* GST (*Pv*GST) are key targets; inhibiting them not only disrupt detoxification but also reduce their antioxidant capacity, a critical feature for potent antimalarials. Bromosulfophthalein (BSP), a clinical liver function dye, emerged as a potent cytosolic GST inhibitor. This study explored BSP's inhibitory properties on *Pf*GST and *Pv*GST, showcasing its binding capabilities through empirical and computational analyses. The study revealed BSP's ability to significantly inhibit GST activity, altering the proteins' structures and stability. Specifically, BSP binding induced spectral changes and impacted the proteins' thermal stability, reducing their melting temperatures. Computational simulations highlighted BSP's strong binding to *Pf*GST and *Pv*GST at their dimer interface, stabilized by various interactions, including hydrogen bonds and van der Waals forces. Notably, BSP's binding altered the proteins' compactness and conformational dynamics, suggesting a potential non-competitive, allosteric inhibition mechanism. This study provided novel insights into BSP's candidacy as an antimalarial drug by targeting *Pf*GST and *Pv*GST. Its ability to disrupt crucial functions of these enzymes' positions BSP as a promising candidate for further drug development in combating malaria

**Keywords:** Glutathione S-Transferase, *Plasmodium*, BSP, inhibition, ligand, Molecular Dynamics Simulation

# 1. Introduction

The parasitic protozoan's glutathione *S*-transferase (GST) enzyme has gained researchers' attention as a potential drug target. It has continued to be studied, especially in *Plasmodium falciparum* and *Plasmodium vivax*, which are the two main malaria-causing agents in Africa and Asia, respectively (McQueen et al., 2021; Naing et al., 2019; Van Dorp et al., 2020). This is as the GST's primary functions are seen in the nucleophilic addition of glutathione (GSH) to toxic compounds, reduction of hydroperoxides, and ultimately acts as a carrier protein (ligandin) of specific organic molecules. This process results in the inactivation and immobilization of these molecules (Colón-Lorenzo et al., 2020). The protective role in the form of detoxification of xenobiotics being exerted by *Plasmodium falciparum* glutathione *S*-transferase (*Pf*GST) and *Plasmodium vivax* glutathione S-Transferase (*Pv*GST) is thus one main reason they are both considered a unique drug targets towards the development of novel and potent antimalarials (Dasari et al., 2018; Dasari et al., 2018a; Mangoyi et al., 2010; Quesada-Soriano et al., 2013, 2014). Glutathione *S*-transferase's importance, as seen in *Plasmodium* species, is being an intra-erythrocytic relieving enzyme when it comes to oxidative stress stages in the parasite. This, coupled with the fact that it's ubiquitously implicated in increased chloroquine resistance cells, makes their target an unexplored antimalaria drug therapy imperative. This is because these GSTs (*Pf*GST and *Pv*GST) intracellularly detoxify many hydrophobic and electrophilic substances as chemotherapeutic agents implicated in drug resistance evolution (Ahmed et al., 2021; Bhagat et al., 2019; Mohring et al., 2017, 2019).

Since the discovery of resistant and multidrug-resistant malaria-causing *Plasmodium*, first to the traditional quinolone, antifolate antibiotics, and later to the gold standard artemisinin combination therapy (ACTs) approved by the WHO, the search for a new and effective antimalaria and new drug target in *Plasmodium* has never been more compelling to researchers (Chigorimbo-Murefu et al., 2012; Zhan et al., 2015). This is because understanding the drug target mechanism has become pivotal to every scientific effort to develop target-based, novel, and potent antimalarials. This becomes imperative as insight into this mechanism will help to elucidate possible structural modifications of late-stage preclinical development of antimalarials or even postulate possible structural modifications to existing antimalarials that have hitherto been confronted with resistance and rendered ineffective (Calic et al., 2020; Shibeshi et al., 2020). Given the importance of malaria parasites' GST in the detoxification of endogenous and xenobiotic compounds, among other functionalities which has been shown to enhance drug resistance ability to anti-parasitic and

insecticides, the inhibition of this detoxification ability is thus worth targeting as a novel and effective antimalarial (Pawłowska et al., 2023). Also, studies have shown that aside from being identified as the major cause of DDT resistance to a human malaria parasite, GSTs have proven to be the most significant enzyme in chloroquine resistance (Lumjuan et al., 2005; Pawłowska et al., 2023; Sujitha et al., 2017).

Over time, traditional drug discovery and development processes have been bogged down in effectiveness due to exorbitancy and delayment. Computer-aided drug discovery (CADD) using computational modelling approaches to simulate drug receptor/ligand interactions has now been increasingly embraced and deployed for research and pharmacology (Chandel et al., 2018; Leelananda & Lindert, 2016). This drug receptor/ligand interaction is intended to be evaluated for the target's binding and affinity. In addition, this study approach leverages the understanding that ligands can varyingly bind to the receptor or protein targets, with the binding either being hydrophobic, electrostatic, or hydrogen bonding (Bhunia et al., 2021; Choudhuri et al., 2023; Fu et al., 2018). This multidisciplinary technique is based on structure prediction, target identification, binding site prediction, and protein-ligand interaction. Understanding ligandin properties and binding abilities to drug targets have been employed in computational-aided drug design to change drug discovery processes and circumvent associated bottlenecks to traditional drug design approaches (Sabe et al., 2021; Sadybekov & Katritch, 2023).

There has been a paradigm shift in focus towards finding and utilizing cost-effective, safe, and potent small molecules for malaria treatment. To this end, this research novel employed bromosulfophthalein as an effective compound for malaria treatment in the face of resistance being confronted by the artemisinin-based combination therapy (ACT) imperative. Bromosulfophthalein (BSP) is an anionic phthalein, triphenylmethane dye having two sulfonic acid groups often greatly used in diagnosing liver injury through a liver function test. It has also been utilized to study transporters' membranes which are responsible for the movement of reduced glutathione (GSH) as well as organicanions across cell membranes (Cui et al., 2020; Kolobe et al., 2004; Plaa, 2010; Valli & Achilonu, 2022, 2023). BSP's disadvantage is first in its' solubility, as it's insoluble in water, slightly soluble in ethanol, and some polar solvents. This solubility challenge is however solvable as BSP is found to be highly soluble in dimethyl sulfoxide (DMSO), a polar, aprotic solvent. DMSO's miscibility with water and ability to dissolve an enormous catalogue of polar and nonpolar small molecules has made it a choice of solvent for many applications. Hence, its use in

dissolving BSP. BSP with a molecular weight of 838 Da, which is well above the threshold weight for biliary excretion could also be another drawback. However, the many diverse applications of BSP as a drug have continued to gain attention (Cui et al., 2020; Soto et al., 2002; Szabo et al., 2013). While bromosulfophthalein (a purple phthalein dye)'s use transcends liver function clinically diagnostic, it has however not been explored as a potent inhibitor in malaria parasites. To this end and here in this study, BSP is empirically and computationally investigated as an essential ligandin for *Pf*GST and *Pv*GST. The findings in this study will ultimately position BSP as a novel drug candidate for malaria treatment. To the best of our knowledge, no study has either empirically or computationally investigated BSP in this regard.

## 2. Materials and Methods

### 2.1. Materials

The BL21(DE3) vectors used were from New England BioLabs while both *Pf*GST_pET11a and *Pv*GST_pET11a plasmids were synthesized by and purchased from GenScript Biotech, USA. The following materials like glutathione reduced (GSH), bromosulfophthalein (BSP), 1-chloro-2,4-dinitrobenzene (CDNB), and 8-anilino-1-naphthalenesulfonic acid (ANS) were all purchased from Sigma-Aldrich (St. Louis, Missouri, USA). Similarly, the other materials which were equally purchased from Sigma-Aldrich include isopropyl β-D-1-thiogalactopyranoside (IPTG), dimethyl sulfoxide (DMSO), ampicillin, and GSH-agarose. On the other hand, SYPRO Orange dye was purchased from Thermo Fisher Scientific, USA. High-performance gaming computers with Maestro algorithm configurations were used for the computational studies.

### 2.2. Methods

#### 2.2.1. Recombinant overexpression of *Pf*GST, *Pv*GST in *E.coli* and purification

High transformation efficient chemically competent *E.coli* BL21(DE3) cells were respectively used to transform *Pf*GST_pET11a and *Pv*GST_pET11a vectors (GenScript), using a heat shock treatment procedure. The transformation process was concluded by spreading 100 µL of the resuspended recombinant solution on a Luria-Bertani (LB) agar plate supplemented appropriately with 100 µL of ampicillin. A singularly distinct colony from the respective overnight (16 hours)

incubated plates were separately inoculated into a 2 × yeast tryptone (2YT) media [1% (v/v) yeast, 1.6% (w/v) tryptone, 0.5% (w/v) NaCl] which has been appropriately supplemented with 100 µL ampicillin and then incubated overnight (37 ºC, 250 rpm). An optical density ($OD_{600}$) of 0.6 was allowed before adding 0.5 mM IPTG, 6 hrs to induce protein overexpression. An immobilized metal affinity chromatography (IMAC) purification procedure was employed for the purification of the two proteins using a separate 5 mL (1.6 × 2.5 cm) cobalt [Co(II)] charged HisTrap® column, GE Healthcare, Sweden connected to the ÄKTA Start Purifier, Cytiva Life Sciences, USA. A one-step elution method using 50 mM sodium phosphate, 500 mM imidazole, 0.01 % (w/v) NaN3, and pH 7.2 was employed to obtain purified *Pf*GST and *Pv*GST used for the various empirical studies.

### 2.2.2. Enzymatic and inhibitory assay of *Pf*GST and *Pv*GST

Employing GSTs' conjugation ability exhibitable by reduced glutathione toward l-chloro-2,4-dinitrobenzene (CDNB), *Pf*GST and *Pv*GST's enzymatic specific activity was spectrophotometrically determined (Habig & Jakoby, 1981). This is by measuring the conjugation product formed, which is 1-(S-glutathionyl)-2,4 dinitrobenzene. This dinitrophenyl thioether chromophore product formed was measured using a Jasco V-730 BIO spectrophotometer with a 3 mL glass quartz cuvette. The $\varepsilon_{340}$ of 9600 $M^{-1}.cm^{-1}$ and 340 nm absorbance were parameters observed when this activity was monitored spectrophotometrically. The activity assay was carried out at 20 ºC for 60 s. It was equally carried out in triplicate using a reaction buffer containing 100 mM sodium phosphate, 5 mM GSH, 1 mM CDNB (3% (v/v) ethanol), 1 mM EDTA, 5 mM DTT, 0.02% $NaN_3$, pH 6.5.

This assay was carried out using different concentrations of *Pf*GST and *Pv*GST in the presence and absence of 0.5 mM BSP. The results were subsequently corrected for linear progress curves and background non-enzymatic reaction rates.

### 2.2.3. Extrinsic ANS fluorescence spectroscopic analysis of *Pf*GST, *Pv*GST, and BSP complex

The apo proteins and their respective complexes' tertiary structure conformation were evaluated using a JASCO FP-6300 spectrofluorometer machine with installed Spectra Manager software v1.5.00 (Jasco Inc., Tokyo, Japan). Utilizing 8-anilino-1-naphthalenesulfonic acid (ANS)'s ability as an extrinsic probe to fluorescently bind to protein's hydrophobic pockets, the structural conformation and interaction of *Pf*GST and *Pv*GST in the presence and absence of BSP as a ligand

was carried out. The apo *Pf*GST and *Pv*GST samples 5 µM each, in 10 mM sodium phosphate, 200 µM ANS, 1 mM EDTA, 2 mM DTT, 0.02 % (w/v) NaN3, pH 7, were spectroscopically analyzed using a 10 mm pathlength quartz cuvette at 20°C. Their fluorescence emission spectra were at an excitation of 395 nm and between 400 and 650 nm wavelength. A 1 cm path length, excitation bandwidth of 5 nm, 2.5 nm emission with data pitch of 1 nm, and scanning speed of 200 nm/min were recorded in triplicate. The buffer was corrected before being averaged. This procedure was repeated in the presence of reduced glutathione (GSH), a GST substrate.

Bromosulfophthalein's ligandin and binding effect on both *Pf*GST and *Pv*GST's hydrophobic cleft was also carried out. Before spectra measurement, 1 mM BSP was separately incubated with 5 µM *Pf*GST and *Pv*GST in the presence and absence of GSH for 30 min. In this monitored spectroscopic analysis, spectra signals at three accumulations were averaged and recorded. Recorded spectra were buffer-corrected before the fluorescence intensities in the presence of BSP were also corrected for the inner filter effect to account for any absorption of excitation (primary) and emission (secondary) light.

2.2.4. Stability elucidation of *Pf*GST, *Pv*GST, and BSP complex by thermal shift assay

The apo *Pf*GST and *Pv*GST's protein stability in the presence of glutathione (substrate) and their interaction with bromosulfophthalein (ligand) was tested through a thermal shift assay (TSA). Employing the use of a CFX96 Touch-Real-Time qPCR detection system (Bio-Rad Laboratories, Inc., Hercules, CA, USA), the thermal denaturation of *Pf*GST, *Pv*GST, *Pf*GST:GSH, *Pv*GST:GSH, *Pf*GST:BSP, *Pv*GST:BSP, *Pf*GST:GSH:BSP, and *Pv*GST:GSH:BSP were elucidatorily studied. They were studied with respect to their stability using a naturally quenched fluorescent dye (SYPRO Orange dye) as a probe on an environment-sensitive 96-well PCR plate. The 96-well plate was prepared with each well containing a sample mix of 1.5 mg/mL *Pf*GST or *Pv*GST in 100 mM $NaH_2P0_4$, 1 mM DTT, 1 mM EDTA, ± 5 mM GSH, ± 1 mM BSP. Equally, 5 µL diluted SYPRO Orange dye was added before it was briefly spun down on a microplate centrifuge to ensure mixing. This was done before placing it in the qPCR machine. At a set temperature range of 20 ºC – 90 ºC, with 0.5 ºC increments for 10 s each, the dye interacts with the sample's hydrophobic core. This interaction becomes visible upon denaturation leading to the dye's fluorescence quantum yield increasing when bound to exposed hydrophobic patches on a thermally denatured protein. Each sample's melting curve and melt peak were resolved using the CFX

Maestro software and plotted as relative fluorescence unit (RFU) vs temperature (ºC). Replicates were averaged and corrected with buffer blanks. The sample's melting temperature (*Tm*) which represents the lowest point of the melting curve was then derived from the plot (-d(RFU)/dT).

### 2.2.5. *Pf*GST and *Pv*GST's Steady-state kinetics determination

*Pf*GST and *Pv*GST's steady-state kinetics parameters in the presence of GSH and BSP were spectrophotometrically determined. Utilizing the CDNB-GSH conjugation activity assay procedure, the following steady-state kinetic parameters $V_{max}$, $K_M$, $k_{cat}$ and $k_{cat}/K_M$ were determined. The assays were performed with the addition of 100 µL of varying GSH concentration to 2900 µL of reaction buffer separately containing 1.5 mg/mL of *Pf*GST or *Pv*GST, 100 mM $NaH_2P0_4$, 1 mM DTT, 1 mM EDTA, and 1 mM CDNB. $V_{max}$ and $K_m$ were determined from a non-linear regression Michaelis-Menten plot. The slope of a Lineweaver-Burke linear plot of substrate concentration versus activity was used to determine the catalytic efficiency ($k_{cat}/K_M$)

## 2.3. Computational modelling studies

### 2.3.1. Computational software and hardware

Two high-performance computing units were used for this study. These computing units were equipped with specialized configurations. They are a 16 CPU Intel core i7 5960x extreme edition (3.3 GHz, 20 M cache 16x cores), Nvidia GTX 750Ti graphics card, 32 GB DDR4-2133 MHz memory on an MSI X99 motherboard and a 264 GB RAM. Also, an implementable Schrödinger Maestro v13.0 Windows OS desktop was used for a part of the computational study. The study components that use the Windows OS desktop include protein-ligand preparation and induced fit ligand docking. While a similar computing unit was used for the molecular dynamics simulations studies, on the other hand, the post-dynamic analyses were carried out on an equipped Linux computing unit.

### 2.3.2 Apo *Pf*GST, *Pv*GST, and ligand preparation

Protein structure processing is essential before molecular docking. This is to put the protein into a dockable conformation. In achieving this, the *Pf*GST crystal structure with PDB ID 2AAW was retrieved from a Research Collaboration for Structural Bioinformatics Protein Data Bank (RCSB

PDB) repository. For *Pv*GST, the computed alpha fold structure with UniProtKB ID Q0ZS46 was similarly retrieved in the absence of a solved crystallographic structure. Both structures were submitted to the Maestro v13.0 molecular modelling algorithms' protein preparation wizard module. They were subsequently pre-processed by allotting them bond orders, adding hydrogen atoms, making zero bond orders to metals, and disulphide bonds before water molecules (having 5 Å) and solvent molecules were removed from hydrogen atoms as well as deleting $Na^+$ from the coordinates. They were further processed by optimizing the hydrogen bonding network with water orientation sampling with the use of the PROKA algorithm, pH 7.0, after which non-water molecules in comparison with water molecules which are less than 3 hydrogen bonds, were deleted. In concluding the protein preparation for docking studies, the respective structures were subsequently refined, and refrains were placed on the heavy atoms with the use of the OPLS_2005 force field. The converging of heavy atoms to an RMSD value of 0.3 Å was set as the cut-off to terminate the minimization process with the stoichiometry of the side chain checked for no induced perturbations which may happened in the course of structure preparation. The minimized structures were then saved as Maestro (.mae) files for subsequent prediction analysis.

The ligand (BSP) was also prepared by first extracting its structure data files (SDF) from a database, public repository for information on chemical substances and their biological activities (PubChem) with a corresponding ID of CID:6282. This file was then submitted to the Maestro v13.0 module known as LigPrep for ligand preparation involving energy minimization with the use of the OPLS_2005 force field. An Epik module algorithm was used to both generate possible states at pH 7.0 ± 2 and predict the pKa. The ligand was then desalted before generating its possible tautomeric states at pH 7.0 ±2. In addition to this, molecules with multiple chiral centres were either retained or varied so as to return chemically useful structures having low energy states and then saved in Maestro (.mae) files in readiness for the induced fit docking procedure.

### 2.3.3. Computational-based drug-likeness and ADMET predictions

The evaluation of BSP's drug-likeness via a computational-based pharmacological and pharmacokinetic analysis was carried out using a web server known as SwissADME (http://swissadme.ch). This analysis employs the Canonical transformation of BSP's simplified molecular-input entry system (SMILES)' structure according to methods previously discussed (Cheng et al., 2012; Daina et al., 2017). BSP's molecular weight, lipophilicity (MlogP), hydrogen

bond acceptors and hydrogen bond donor number were assessed for drug-likeness (according to Lipinski's rule of five) using SwissADME. Also, the toxicity evaluation of BSP (based on parameters such as hepatotoxicity, carcinogenicity, mutagenicity, cytotoxicity, LD50 (mg/kg) and toxicity class) was predicted using an online server known as ProTox-II (https://tox-new.charite.de/protox_II/) (Banerjee et al., 2018; Lipinski et al., 1997). Similarly, and given the importance of assessing the absorption, distribution, metabolism, and excretion (ADME) properties in drug discovery, these properties are equally evaluated for BSP's pharmacokinetic profile.

### 2.3.4. Induced fit ligand docking

A Schrödinger Maestro v13.0 algorithm is implementable induced fit ligand docking was employed in evaluating BSP's binding to *Pf*GST and *Pv*GST. This is through the protein's ligand-binding site geometry, which is vitally dependable upon the protein's structure-ligand inducible conformational changes at binding. For the binding evaluation and because of the enzymes' two possible binding sites, which include the GSH binding site (G-site) and the xenobiotic binding site (H-site) (Fritz-Wolf et al., 2003), both chains A and B (whole dimer) were selected as the binding site. For this process, an OPLS_2005 force field implicit solvent model was used. For the induced fit ligand docking protocol, both ring conformational sampling with a 2.5 kcal/mol energy barrier and a non-planar conformation penalty on amide bonds were applied.

### 2.3.5. Molecular dynamic simulation

To both increase the reliability of the docking results and gain deeper insight into how BSP affects the functionalities of *Pf*GST and *Pv*GST, further computational studies, and molecular dynamic simulations (MDS) at 500 ns simulations were carried out. This was with the use of a Maestro v13.0 implemented GPU-enabled Desmond molecular dynamics simulation engine. The BSP:*Pf*GST and BSP:*Pv*GST complexes' top-scoring poses were first saved as a PDB file before submission for Desmond MD simulations studies on a Linux (Ubuntu) desktop. A System Builder module implemented in the Desmond algorithm was previously used to build four systems (*Pf*GST, *Pv*GST, BSP:*Pf*GST, and BSP:*Pv*GST) in readiness for the simulation. A transferable intermolecular potential with a three-point (TIP3P) explicit solvent model using the OPLS_2005 force field was then used to solvate the systems. In the same breath, the apo *Pf*GST and *Pv*GST were placed in a periodic orthorhombic box (distance from the box face to the outermost

protein/ligand atom was set at 10 Å, the box angle was $\alpha = \beta = \gamma = 90°$). This is done to initialize the systems. On the other hand, both apo and liganded *Pf*GST and *Pv*GST were first minimized before counter ions were added to neutralize the systems. The addition of 0.15 M NaCl into the solvent box was done to condition the system physiologically. The systems were then submitted for the molecular dynamics production phase subsequent to these explicit solvent model solvation and ionization procedures. The short simulation steps comprise eight distinct steps. These steps are made up of 2 identifiable phases, namely the equilibrium phase (steps 1-7) and the long, final simulation stage, which is step 8. A 500 ns total production stage was performed. While parameters of the solvated system type were detected in step 1, on the other hand in step 2, an NVT-conditioned Brownian Dynamics was performed at 10K and 100 ps simulation, with restraints placed on solute-heavy atoms. Similarly, while restraints were still put on heavy atoms at step 3, a 12 ps simulation was performed under NVT conditions at 10K. Also, while short simulation steps of 12, 12, and 24 ps were performed for steps 4, 6, and 7 respectively, the pocket solvation was omitted for step 5. While that was carried out under NPT conditions at 10K, restraints were only placed on heavy atoms at steps 4 and 6 alone but not on step 7. The long and final stage (Step 8) in concluding the MDS was performed at a constant temperature (300 K) for 500 ns.

### 2.3.6. Post dynamic analyses

The derived trajectories from the MDS studies were further subjected to post-dynamic analyses using a Schrodinger Maestro v13.0 to compare the protein structures. This includes the Simulation Quality Analysis (implemented in Maestro v13.0) of the simulation qualities in terms of average energy, pressure, temperature, and volume of the individual simulated systems. Similarly, the implemented Maestro v13.0 Simulation Interaction Diagram algorithm was used to analyze the alpha carbon atoms (Cα)'s root-mean-square-deviation (RMSD), ligand's RMSD vis-a-vis the receptors. Also, the residues' root-mean-square fluctuations (RMSF), secondary structure element analysis and protein-ligand interaction were equally analyzed. In the same vein, Maestro v13.0 implemented Simulation Events Analysis algorithm was used to analyze the radius of gyration (Rg) and atomic distance calculations. At the same time, the average representative cluster's determination was determined using a Desmond implemented Cα RMSD trajectory clustering algorithm.

### 2.3.7. Post-simulation MM/GBSA binding free energy calculations

In providing valuable insights into the energetics of BSP interactions with *Pf*GST and *Pv*GST and to complement the structural information obtained from the simulations, molecular mechanics/generalized born solvent area (MM/GBSA) calculations were performed. This was done using an MM/GBSA algorithm implementable in Schrodinger Maestro v13.0 and according to previously reported methods (Kollman et al., 2000; Massova & Kollman, 2000; Tsui & Case, 2000; Wang et al., 2019). For each of the *Pf*GST:BSP and *Pv*GST:BSP complexes, 2000 independent snapshots (of the 500 ns molecular dynamics simulations) of binding energies were generated, averaged, and calculated with BSP's binding free energy ($\Delta G_{bind}$) active site calculated following the given equation:

$$\Delta G_{bind}=\Delta G_{RL}-(\Delta G_R+\Delta G_L) \quad (1)$$

Where $\Delta G_{bind}$ in the equation denotes the free energy binding, $\Delta G_{RL}$ represents the free energy of the protein-ligand complex; $\Delta G_R$ denotes the free energy of the receptor, and $\Delta G_L$ the free energy of the ligand. The binding free energy is important to be calculated as it establishes a given protein-ligand binding affinity. Given that, a more negative $\Delta G$ is an indication of better binding of the ligand to the protein (Gilson et al., 1997). In the light above, each state's free energy was calculated with the use of the FF14SB force field, given by the equations:

$$\Delta G_{bind} = \Delta E_{gas} + \Delta G_{sol} - T\Delta S \quad (2)$$

$$E_{gas} = E_{int} + E_{vdW} + E_{ele} \quad (3)$$

$$G_{sol} + G_{GB} + G_{SA} \quad (4)$$

$$G_{SA} = \gamma SASA \quad (5)$$

The gas phase energy ($E_{gas}$) which is the sum of the internal energy ($E_{int}$), Coulomb energy ($E_{ele}$) and the van der Waals energies ($E_{vdW}$) were estimated by the terms of the FF14SB force field. For the solvation free energy ($\Delta G$sol) estimation, the contributions of energy from the polar states ($G_{GB}$) and non-polar states ($G_{SA}$) were accordingly used. While the non-polar solvation energy ($G_{SA}$) was derived using the solvent accessible surface area (SASA in $Å^2$), the contribution from polar solvation ($G_{GB}$) was determined by solving the Generalized Born equation. In the equation above, the solute's total entropy and temperature were represented by S and T respectively. The

total binding free energy profile contributions between BSP:*Pf*GST and BSP:*Pv*GST as per-residue free energy decomposition were estimated at the atomic level residues with the use of MM/GBSA implemented in Maestro v13.0.

#### 2.3.8. Principal component analysis

Further to the knowledge that conformational differences adopted by proteins impact their functions and because protein's total conformational changes are influenced by their collective atom movements, hence a Principal Component Analysis (PCA) was performed (Elseginy, 2023; Ernst et al., 2015; Pérez-Peña et al., 2023). This multivariate statistical technique known as PCA was additionally employed to study BSP's binding effect on *Pf*GST and *Pv*GST's dynamics by deconvoluting their Cα-RMSD, RMSF and Rg simulation trajectories. This analysis was carried out with the imputing of Cα-RMSD and RMSF MD simulation structural datasets into an RStudio statistical program to generate a principal component (PC) phase

## 3. Results and discussion

### 3.1. Recombinantly heterologous overexpression of *Pf*GST, *Pv*GST and purification

In this study, both the *Pf*GST and *Pv*GST constructs, which were purchased from GenScript (New Jersey, USA), were transformed in *E. coli* BL 21(DE3) cells. This was followed by recombinantly and heterologously overexpressing their separate transformed mix using 0.50 mM IPTG for a period of 6 hours at 30ºC. The overexpressed *Pf*GST and *Pv*GST cells were chromatographically purified using a one-step immobilized metal affinity chromatography (IMAC) method on an ÄKTA Start Purifier, Life Sciences, USA. The purification results in 15 mg and 10 mg per litre of uncontaminated, soluble, and active *Pf*GST and *Pv*GST proteins respectively, when spectrophotometrically determined (UV-Vis spectrophotometer V-730, JASCO Europe). The purity of the recombinant *Pf*GST and *Pv*GST were confirmed by sodium dodecyl-sulfate polyacrylamide gel electrophoresis (SDS-PAGE). This is as well as confirming their sizes to be approximately 25 kDa and 24.50 kDa, respectively (Figure 1) which corresponds to their sub-unit's theoretical molecular weights. These results revealed a high-yield soluble and pure protein free from DNA and other contaminants that can be used for further downstream characterization.

## 3.2. Enzymatic and inhibitory assay of *Pf*GST and *Pv*GST

Both *Pf*GST and *Pv*GST were spectrophotometrically assayed for their enzymatic activity according to the method described in section 2.2.2 above. They were found to be catalytically and enzymatically active with their specific activity evaluated to be 38.00 and 37.03 µmol/min/mg respectively in the absence of BSP.

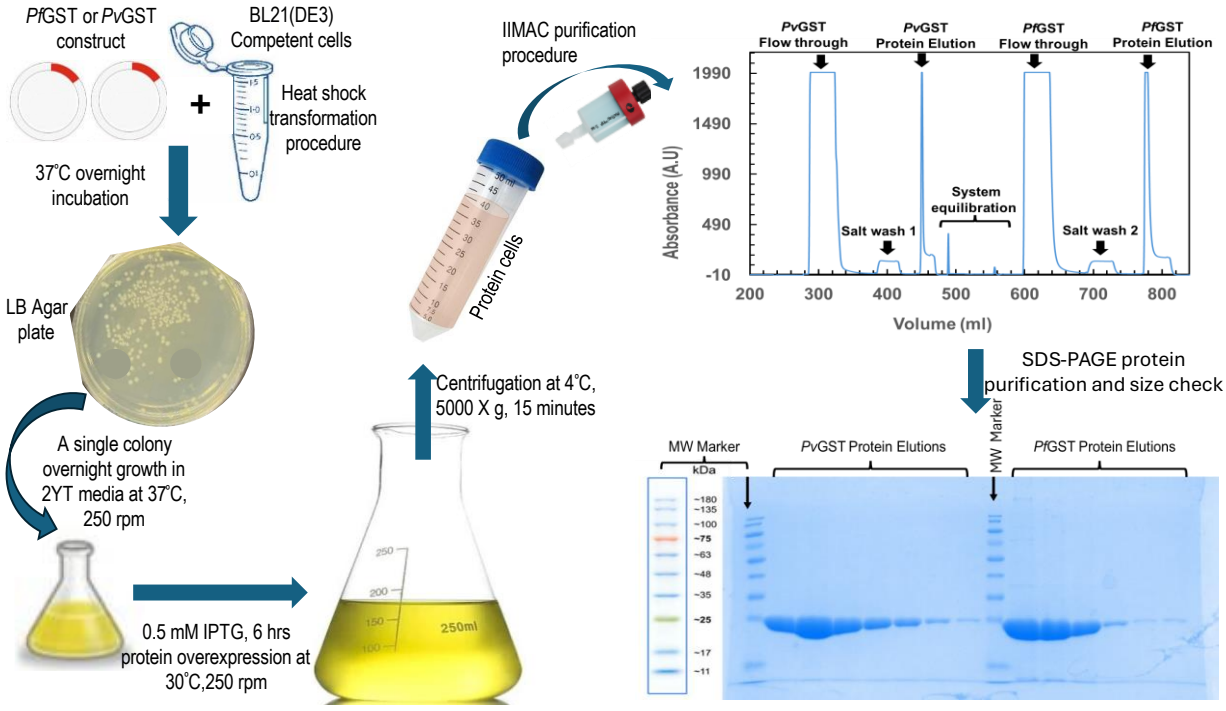


Fig. 1. Schematic description of the recombinant overexpression and purification processes of *Pf*GST and *Pv*GST. The construct's transformation in BL21(DE3) competent cells were successful as evident from the yield of single and distinct colonies on the LB plates. The 0.50 mM overexpressed was successfully purified using a one-step IMAC procedure. The *Pf*GST and *Pv*GST proteins were found to be pure, and their sizes correspond to the approximately 25 kDa theoretical sizes.

Their enzymatic activities were, however, found to be completely inhibited in the presence of BSP as an inhibitor, with their respective specific activity evaluated to be 0.30 µmol/min/mg, which is a 99 % inhibition. This significant inhibition of the enzymatic activities of both *Pf*GST and *Pv*GST is graphically seen in the flattening of the straight line as shown in Figure 2. GST's catalytic/enzymatic activities as a bi-substrate detoxification enzyme, which primarily catalyzes xenobiotics to its hydrophobic site (H-site) (Al-Qattan et al., 2016; Makumbe et al., 2024) were disrupted by the interaction of BSP at the H-site and the dimer interphase. This inhibition of GST in *Plasmodium falciparum* and *Plasmodium vivax* will no doubt make them (*Pf*GST and *Pv*GST)

a critical target for the development of potent antimalarials. This BSP's inhibition propensity on these enzymes agrees with other published results obtained from our research group (Padi et al., 2021; Pooe et al., 2021).

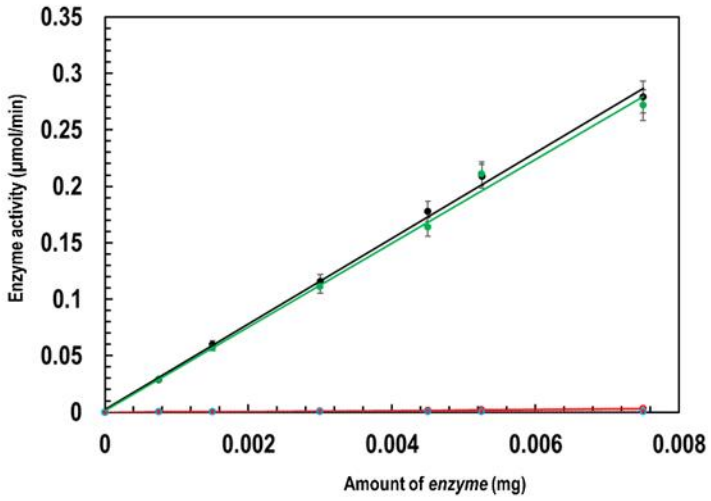


Fig. 2. Characterization of *Pf*GST and *Pv*GST in terms of their enzymatic specific activity in the presence and absence of BSP through a GSH-CDNB conjugation assay (100 mM $NaH_2PO_4$ pH 7.2, 1 mM EDTA, 1 mM DTT, 5 mM GSH pH 6.5, 30 mM CDNB, and 1 mM BSP) monitored spectroscopically showing *Pf*GST's specific activity **(black)**, *Pv*GST's specific activity **(green)**, *Pf*GST:BSP's specific activity **(red)**, and *Pv*GST:BSP's specific activity **(blue)**.

### 3.3. Extrinsic ANS fluorescence spectroscopic analysis of *Pf*GST, *Pv*GST, and BSP complex

The extrinsic anionic dye, 1-anilinonaphthalene-8-sulfonic acid (ANS) was used to probe the ligandin binding of BSP to *Pf*GST and *Pv*GST as shown in Figure 3. An observed emission spectra shifts and changes show protein tertiary structural features with respect to ANS-accessible hydrophobic pockets (Pooe et al., 2022; Sayed et al., 2000). Hence at 395 nm excitation, a fluorescence emission maxima of free ANS from 525 nm to 490 nm and 480 nm for ANS bound *Pf*GST and *Pv*GST respectively can be observed as shown in Figure 3A. ANS bound *Pv*GST however had a higher fluorescence intensity, an indication that *Pv*GST's hydrophobic pockets were more accessible for the ANS than that of *Pf*GST. A slight emission shift with lowered fluorescence intensity to 495 nm and 485 nm for *Pf*GST:GSH:ANS and *Pv*GST:GSH:ANS respectively were equally observed (Figure 3C). This is an indication that GSH does not either bind or displace ANS at the hydrophobic pocket (H-site), but it nonetheless alters the protein's surface hydrophobicity. This result is supported by the established theory of GSH's binding specificity to GST's G-site rather than the H-site (Akumadu et al., 2020). However, BSP-complexed *Pf*GST and *Pv*GST are

blue-shifted to 510 nm and 515 nm respectively (Figure 3B). This is an indication of BSP bounding to the H-site hydrophobic clefts of the protein and causing alteration in the conformational integrity of both *Pf*GST and *Pv*GST's tertiary structure. A decrease in the fluorescence intensity (quenching) however indicates the displacement of ANS upon binding of BSP. On the other hand, BSP complexed *Pf*GST and *Pv*GST in the presence of reduced GSH showed a fluorescence emission maxima at 513 nm for both *Pf*GST:GSH:BSP and *Pv*GST:GSH:BSP and further quenching (Figure 3D). This then shows that while GSH binding to the G-site does not alter the binding of BSP to *Pf*GST and *Pv*GST, it, however, helped to stabilize the surface hydrophobicity of the two proteins for the binding of BSP to the H-site. This result is consistent with other published work which showed BSP bind at GST's H-site (Akumadu et al., 2020; Padi et al., 2021).

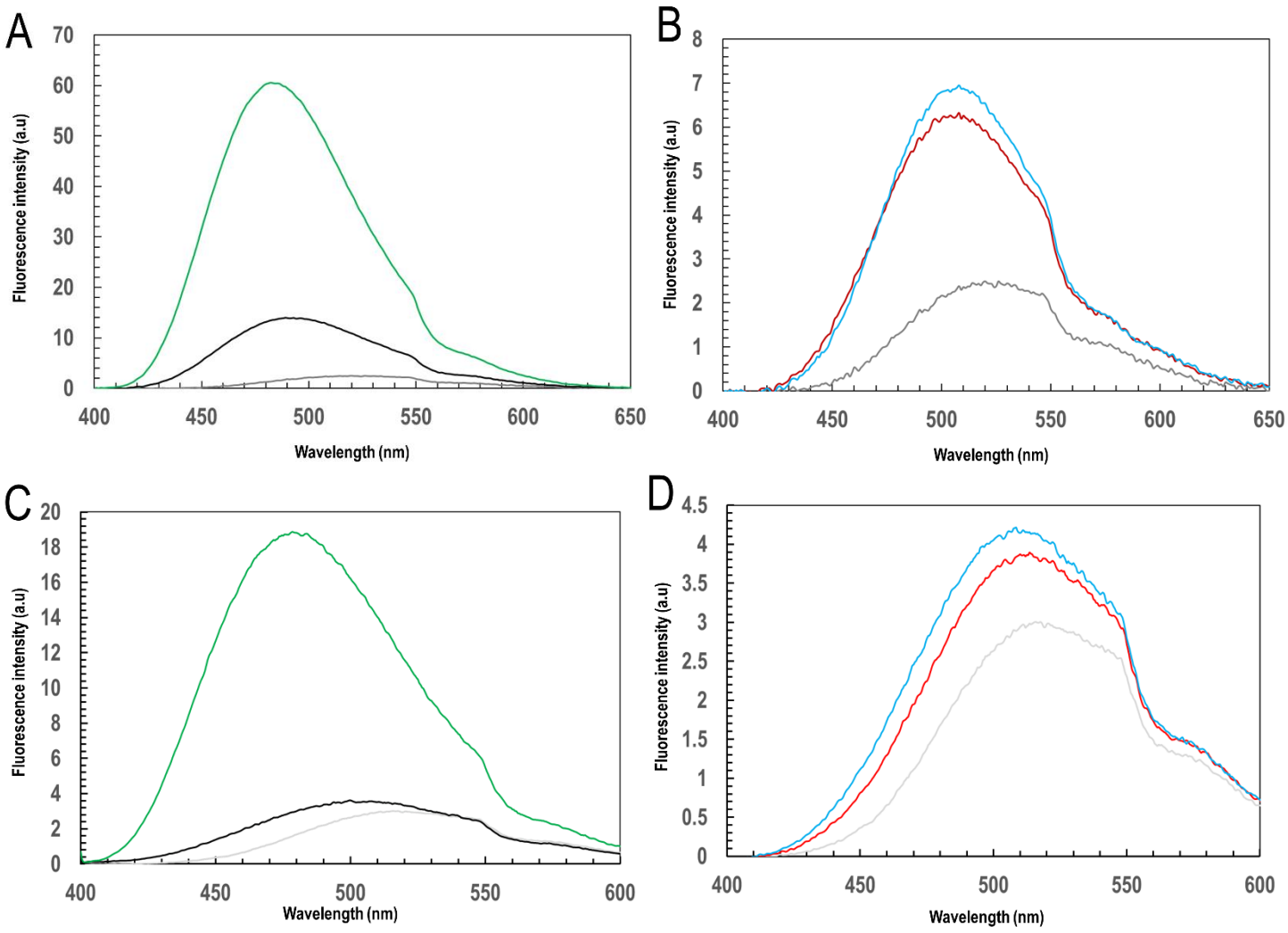


Fig. 3. Ligandin activity of *Pf*GST and *Pv*GST through ANS fluorescence spectroscopy towards BSP and its effect on their tertiary structural conformation. A spectrofluorometric monitored ANS fluorescence emission at 395 nm

excitation showing (A) emission spectrum of free ANS **(grey)**, ANS bound *Pf*GST **(black)** and ANS bound *Pv*GST **(green)**, (B) BSP complexed proteins' emission spectrum of *Pf*GST:BSP **(red)** and *Pv*GST:BSP **(blue)**, (C) reduced GSH incubated protein's emission spectrum of *Pf*GST-GSH **(black)** and *Pv*GST-GSH **(green)**, and (D) BSP complexed and GSH incubated proteins' emission spectrum for *Pf*GST:GSH:BSP **(red)** and *Pv*GST:GSH:BSP **(blue)**

### 3.4. Stability elucidation of *Pf*GST and *Pv*GST in the presence of BSP and/or GSH by thermal shift assay

The protein's thermal stability measurement and the detection of protein-ligand interaction were carried out using the fluorescence thermal shift assay technique with CFX96 Touch Real-Time PCR Detection System (BIO-RAD). The stability of native *Pf*GST and *Pv*GST, *Pf*GST:GSH, and *Pv*GST:GSH *Pf*GST:BSP, *Pv*GST:BSP, *Pf*GST:GSH:BSP, and *Pv*GST:GSH:BSP's were all evaluated. This was through denaturation with increasing temperature from 25 ºC to 65 ºC which was in conjunction with the binding of SYPRO Orange dye as shown in Figure 4.

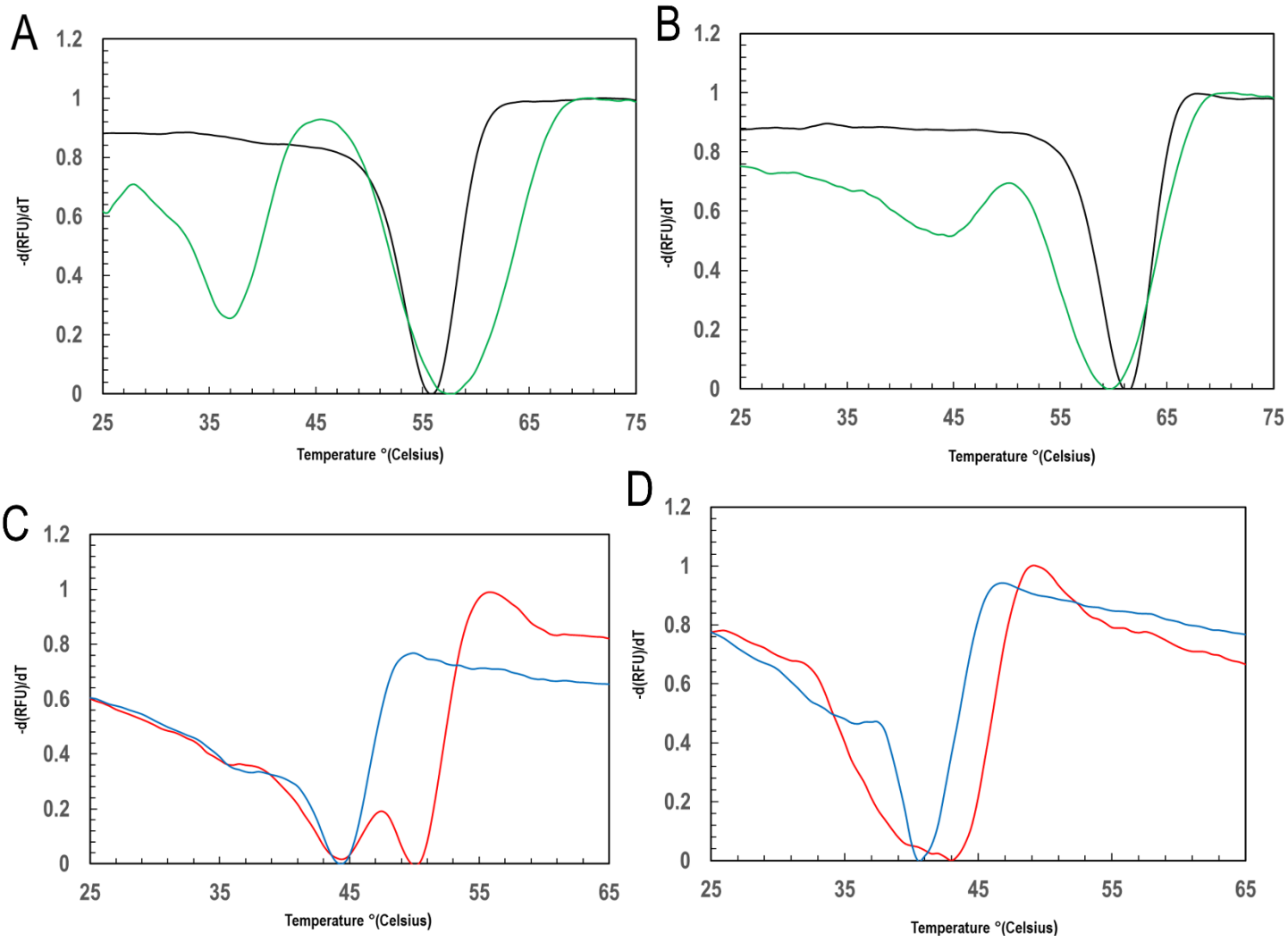

Fig. 4. Profiles for the thermal stability using melting peak temperature of *Pf*GST and *Pv*GST in the presence and absence of GSH and BSP at temperature between 25 – 65 °C using a qPCR differential scanning fluorimetry evaluation. The fluorescence thermal shift assay was carried out in 100 mM $NaH_2P0_4$, 1 mM DTT, and 1 mM EDTA, pH ± 1 mM GSH, ± BSP, with sample monitored in triplicate. The derived -d(RFU)/dT against temperature (◦C) plots showing melting peak temperature *Tm* in ºC of (A) *Pf*GST (**black**) and *Pv*GST (**green**), (B) *Pf*GST:GSH (**black**) and *Pv*GST:GSH (**green**), (C) *Pf*GST:BSP (**red**) and *Pv*GST:BSP (**blue**), and (D) *Pf*GST:GSH:BSP (red) and *Pv*GST:GSH:BSP (**blue**).

Utilizing the dye's propensity for hydrophobic patches, which is seen in increased quantum yield, the apo *Pf*GST's $T_m$ of 56 ± 0.5 ºC and *Pv*GST's $T_m$ of 58 ± 0.5 ºC was observed (Table 1). This is so as the room temperature stable apo protein begins to unfold, thereby making the hydrophobic regions more accessible to the dye. On the one hand, the substrate GSH's specificity and binding to the proteins' G-site do not displace the SYPRO Orange dye (which binds to the H-site) enhancing the stability of the two proteins. BSP significantly and expectedly makes *Pf*GST and *Pv*GST less stable.

Table 1. Summary of the melt peaks showing the stability of PfGST and PvGST in the Presence of GSH and BSP

| | **Melt Peak ( °C)** | |
|---|---|---|
| **Sample** | ***Pf*GST** | ***Pv*GST** |
| Apo | 56.00 | 58.00 |
| Protein:GSH | 61.00 | 59.50 |
| Protein:BSP | 43.00 | 40.50 |
| Protein:GSH:BSP | 44.50*/50 | 44.50 |

### 3.5. *Pf*GST and *Pv*GST's Steady-state kinetics studies

Following the similarly performed CDNB-GSH conjugation activity assay, steady-state kinetic parameters of *Pf*GST and *Pv*GST in the presence and absence of BSP were determined and graphically represented in Figure 5. The parameters summarized in Table 2 were deduced from the steady-state kinetics of *Pf*GST and *Pv*GST towards GSH using the Michaelis-Menten sigmoidal curve and the Lineweaver-Burk straight line plots.

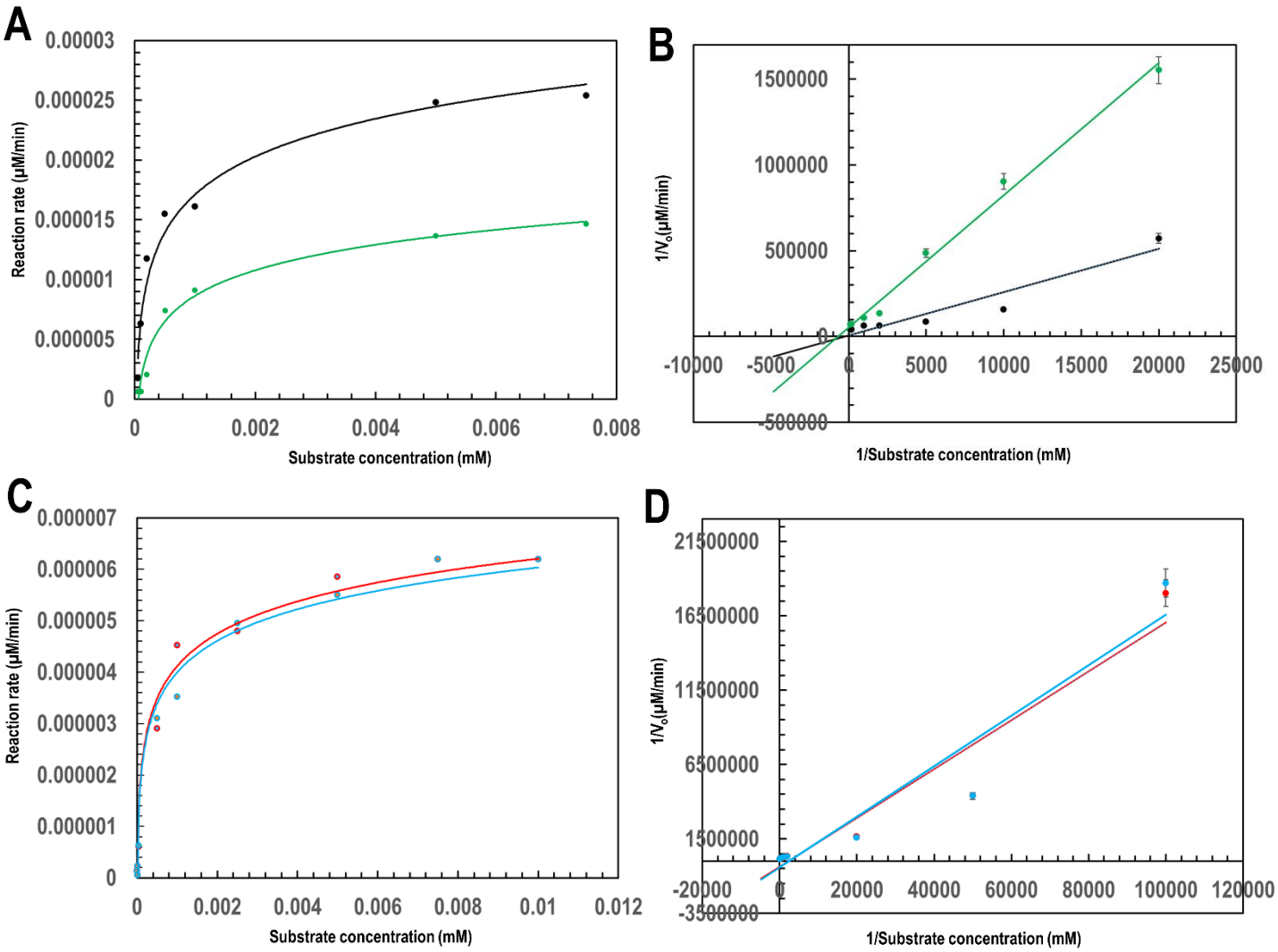


Fig. 5. Plots towards the determination of the steady-state kinetic parameters of *Pf*GST and *Pv*GST towards GSH in the presence and absence of BSP using Michaelis-Menten and Lineweaver-Burke models at varying GSH concentrations. (A). A Michaelis-Menten plot of 300 nM *Pf*GST (**black**) and *Pv*GST (**green**), (B). A Lineweaver-Burke straight line steady-state kinetics plot of *Pf*GST (**black**) and *Pv*GST (**green**), (C). Michaelis-Menten plot of 300 nM *Pf*GST in the presence of 0.5 mM BSP (**red**) and *Pv*GST in the presence of 0.5 mM BSP (**blue**), and (D). A Lineweaver-Burke straight line steady-state kinetics plot of *Pf*GST in the presence of 0.5 mM BSP (**red**) and *Pv*GST in the presence of 0.5 mM BSP (**blue**),

The steady-state kinetic parameters revealed the *Pf*GST and *Pv*GST's reaction maximum rate ($V_{max}$) at the point when the enzymes' active sites are GSH-saturated. It also shows the substrate concentration ($K_M$) at 50 % reaction rate ($V_{max}$) and the enzymes' catalytic efficiency. This catalytic efficiency is otherwise known as the reactions' second-order rate constant rate ($k_{cat}/K_M$) towards GSH. These parameters were 97.56 %, 84.67%, and 85.10 % respectively decreased for *Pf*GST in

the presence of 0.5 mM BSP. Similarly, there are 87.10 %, 69.66 %, and 52.91 % respective reductions in the steady-state kinetic parameters of the same 0.5 mM BSP complexed *Pv*GST (Figures 5A and 5C). These reductions of *Pf*GST and *Pv*GST's steady-state kinetics $V_{max}$, $K_M$, and $k_{cat}/K_M$ indicate BSP's uncompetitive inhibition activity in both *Pf*GST and *Pv*GST. The non-linear regression (Michaelis-Menten hyperbolic) plots are shown in Figures 5A and 5C, and the linear reciprocal plots (Lineweaver-Burke plots) are shown in Figures 5B and 5D respectively. The plots have robustly and precisely aided the determination of the kinetic parameters ($V_{max}$, $K_M$, $k_{cat}$ and $k_{cat}/K_M$) and the visualization of the mode of inhibition of BSP.

Table 2. Steady-state kinetic evaluation of PfGST and PvGST in the presence and absence of BSP

| | **Kinetic parameters** | ***Pf*GST** | ***Pf*GST:BSP** | ***Pv*GST** | ***Pv*GST:BSP** |
|---|---|---|---|---|---|
| **Steady-state kinetics towards GSH** | $V_{max}$ (μM/min) | 2.05 | 0.05 | 0.31 | 0.04 |
| | $K_M$ (mM) | 3.00 | 0.46 | 1.45 | 0.44 |
| | $k_{cat}/K_M$ | 136,333 | 20,308 | 41,707 | 19,638 |

3.6. Computational studies result and discussion

In light of Lipinski's rule of five which allows for examining the drug-likeness of a drug candidate by delineating the relationship between the compound's pharmacokinetic and physicochemical parameters, a SwissADME and ProTox-II servers were used to predict BSP's drug-likeness and toxicity respectively. Table 3 gives the summary of BSP's ADME and toxicity parameters and shows that BSP only violates one of Lipinski's rule of five (MW>500) and falls within acceptability regions for most toxicity parameters. Other ADME parameters such as a MlogP which is less than 4.15; hydrogen bond acceptors, which is equal to 10; and hydrogen bond donors of less than 5, all validated the drug-likeness of BSP. From the toxicity parameters, BSP was predicted to belong to toxicity class 4 and was inactive for hepatoxicity, carcinogenicity, and mutagenicity, and only active for immunotoxicity. The drug-likeness and crucial information on the pharmacokinetic and toxicological aspects of BSP as predicted shows that BSP can be positioned as a potential drug to be therapeutically employed for the treatment of antimalaria.

Table 3. BSP's predicted physicochemical descriptors, ADMET parameters, pharmacokinetic properties, and its' drug-like nature.

| ADMET evaluation of BSP | |
|---|---|
| **Physicochemical properties** | **Parameters/score** |
| Formula | $C_{20}H_8Br_4Na_2O_{10}S_2$ |
| Molecular weight (g/mol) | 838 |
| Number of heavy atoms | 38 |
| Number of aromatic heavy atoms | 18 |
| Rotatable bonds | 4 |
| Fraction Csp3 | 0.05 |
| Hydrogen bond acceptor | 10 |
| Hydrogen bond donor | 2 |
| TPSA (Å2) | 197.92 $Å^2$ |
| Molar refractivity | 135.48 |
| **Lipophilicity** | **Value/score** |
| Log $P_{o/w}$(ILOGP3) | -16.89 |
| Log $P_{o/w}$(XLOGP3) | 5.18 |
| Log $P_{o/w}$(WLOGP) | 6.47 |
| Log $P_{o/w}$(MLOGP) | 4.12 |
| Log $P_{o/w}$(SILICOS-IT) | 3.31 |
| Consensus Log $P_{o/w}$ | 0.44 |
| **Water solubility** | **Prediction/score** |
| Solubility (mg/mL) | 3.45e-06 mg/ml; 4.12e-09mol/l |
| Log *S* (ESOL) | -8.39 |
| Class | Poorly soluble |
| **Pharmacokinetics** | **Prediction** |
| GI absorption | Low |
| BBB permeant | No |
| P-gp substrate | Yes |
| CYP1A2 inhibitor | No |
| CYP2C19 inhibitor | No |
| CYP2C9 inhibitor | No |
| CYP2D6 inhibitor | No |
| CYP3A4 inhibitor | No |
| Log $K_p$ (permeation) | -7.73 cm/s |
| **Drug-likeness** | **Parameters/Prediction** |
| Lipinski | Yes/1 violation (MW>500) |
| Bioavailability | 0.55 |
| Distribution | VDss (human) (log L/kg)/No |
| Metabolism | CYP2D6 substrate/No |
| | CYP3A4 substrate/No |
| | CYP2D6 inhibitor/No |
| | CYP3A4 inhibitor/No |
| **Toxicity model report** | **Prediction/Probability** |

| | |
|---|---|
| Hepatotoxicity | Inactive/0.56 |
| Carcinogenicity | Inactive/0.72 |
| Immunotoxicity | Active/0.94 |
| Mutagenicity | Inactive0.78 |
| Cytotoxicity | Inactive/0.55 |

Also, given the richness of information MDS can provide at the atomistic level, especially in terms of ligand-receptor interactions, mobility, and stability, we, therefore, employed this computational tool to computationally evaluate and validate the ligandin properties of *Pf*GST and *Pv*GST towards BSP. From the induced fit docking results, BSP strongly binds exergonically with *Pf*GST and *Pv*GST (Figure 6) in an interaction process that is accompanied with protein-ligand complex negative Emodel energy and Glide gscores.

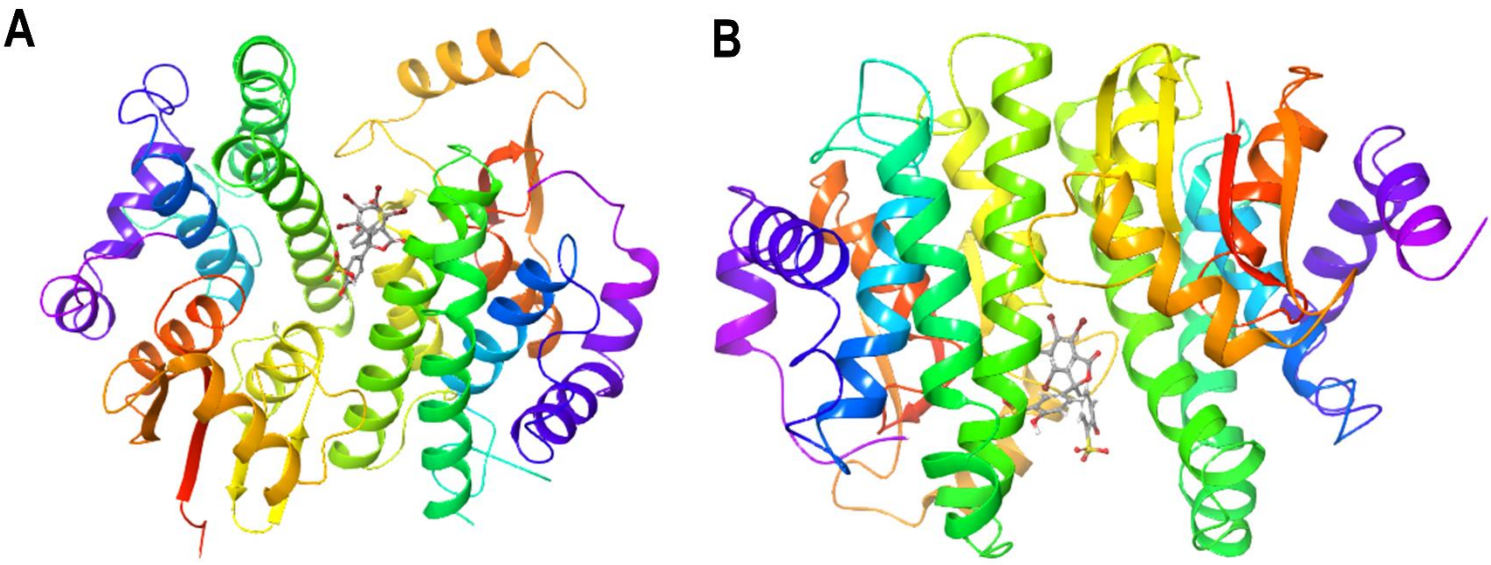


Fig. 6. Protein-Ligand complex ribbon representation of the induced fit docking best pose for (A) *Pf*GST:BSP complex, (B) *Pv*GST:BSP, showing BSP binding at the dimer interphase of *Pf*GST and *Pv*GST. The image is a snapshot from the induced fit ligand docking algorithm implemented in Schrodinger Maestro v13.0.

Although the docking poses, docking score, Glide gscore and IFD score of *Pf*GST:BSP are 17, –8.771, –126.314, and –827.860 respectively and for *Pv*GST:BSP are 35, –8.330, –9.657, and –915.770 respectively, however, the docking with best Emodel energy, which are –126.314 and –130.735 for *Pf*GST:BSP and *Pv*GST:BSP, respectively were submitted for the molecular dynamic simulations.

Predictably, and preferentially too, the IFD shows that BSP binds at the dimer interphase of both *Pf*GST and *Pv*GST as shown in Figure 6, with amino acids side chains from the protein subunits contributing to the binding. Polar side chains (namely Gln73, Gln 71, Gln 104, Ser72, Asn 111) were mostly involved in the binding interaction in both *Pf*GST and *Pv*GST (Figure 7). Additionally, side chains with charged functional groups such as Asp105 and Lys15 in *Pf*GST and Lys109, Lys15 in *Pv*GST were also involved. However, Tyr108 is seen to be involved in π-π* interaction with BSP's phenyl moiety in both *Pf*GST and *Pv*GST (Figure 7) and this agrees with other published results from our research group (Padi et al., 2021; Valli & Achilonu, 2023).

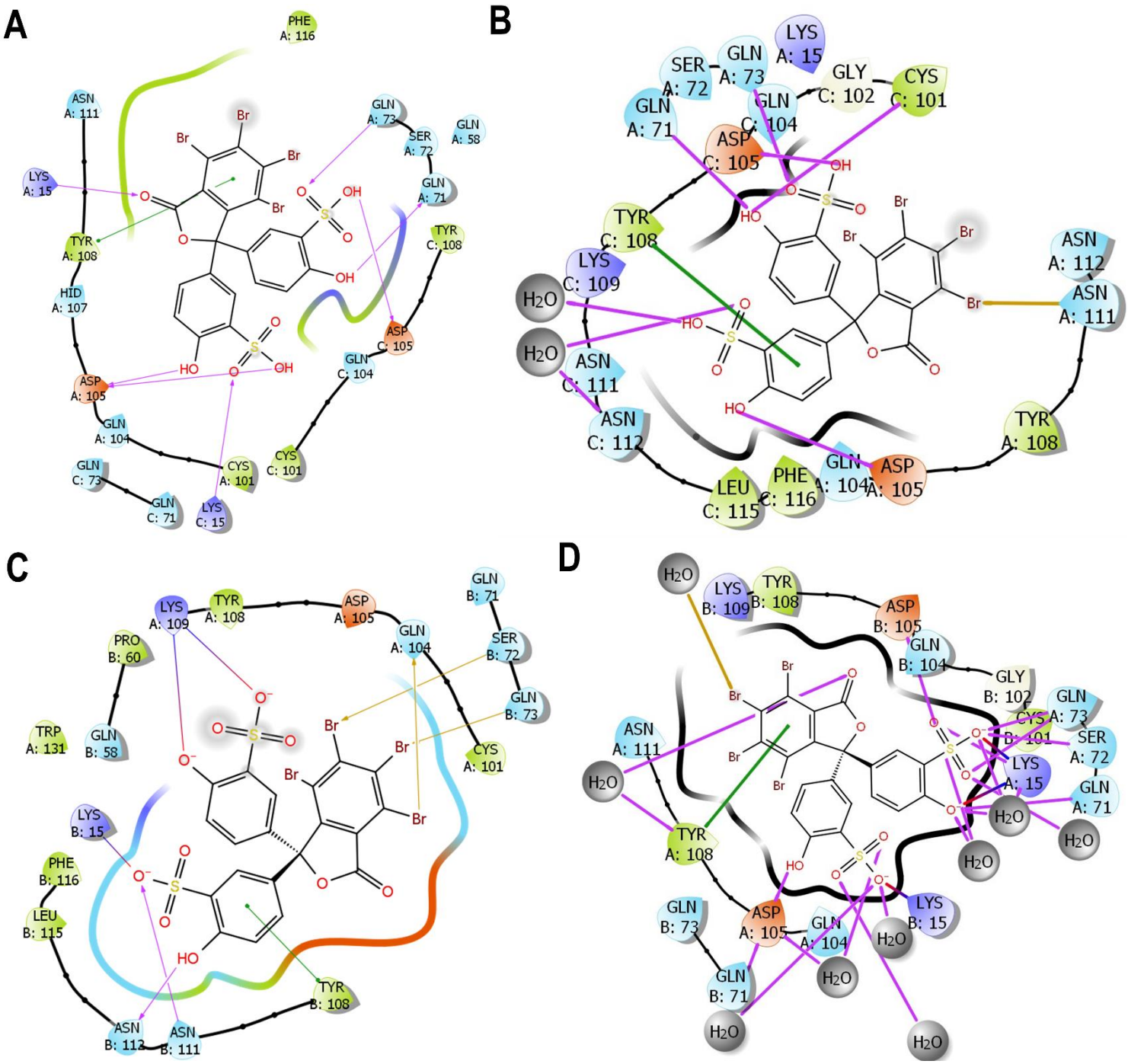


Fig. 7. 2-D ligand interaction plot highlighting the side chains involved in the binding between the interaction of (A) IFD docking pose of BSP with *Pf*GST and (B) amino acid residue's position of BSP with *Pf*GST over 500 ns simulation. (C) IFD docking of BSP with *Pv*GST and (D) amino acid residue's position of BSP with *Pv*GST over 500 ns simulation. Tyr108 is seen as the only non-polar amino side chains (**green**) involved in π-π* interaction with BSP's phenyl moiety in both *Pf*GST and *Pv*GST, while similar amino residues' involvement were seen during docking and the average simulation time. These Images were snapshots from the Maestro 2D interaction diagram implemented in Schrödinger Maestro 13.0

Also, while utilizing an online multiple sequence alignment algorithm package known as T-Coffee Expresso (Expresso™), having its server hosted by the Centre for Genomic Regulation (Barcelona), the *Pf*GST (Q8ILQ7) sequence and that of *Pv*GST (Q0ZS46) were structurally aligned for similarity specific consensus amino acids residues involved in the binding interaction of BSP with *Pf*GST and *Pv*GST (Figure 8). Lys15,105, Gln71,73, Cys101, Asp 105, and Tyr108 were all involved in this binding interaction, an indication of similar atomistic binding interaction in both proteins.

Fig. 8. *Pf*GST and *Pv*GST's structural alignment and sequence analysis reveal the similarity in positions of the amino acid residues taking part in the bonding and simulation interactions using Expresso™. Lys15, Gln 71, Gln 73, Ser72, Cys101, Asp105, Tyr108, and Asn111 were all conserved in both proteins.

Following that, the interactions' stability between *Pf*GST:BSP and *Pv*GST:BSP was evaluated using MDS. Data obtained using the Simulation Quality Analysis algorithm reveals the simulated systems' overall quality. From the results (Table 4), the four systems were adequately equilibrated. This is because there is no significant variation with respect to the simulated systems' (*Pf*GST vs *Pf*GST:BSP and *Pv*GST vs *Pv*GST:BSP) energy, volume, pressure, and temperature throughout the 500 ns simulation. Since the radius of gyration (Rg) measures the degree of structural compactness during the MD simulation, hence with the use of the Simulation Event Analysis algorithm, the average Rg (±SD) of the Cα atoms during the 500 ns MD simulations time of the four systems were evaluated. They are 17.80 ± 0.35 and 21.40 ± 0.35 for the apo *Pf*GST and *Pv*GST respectively and 21.75 ± 0.25 and 21.65 ± 0.25 for the *Pf*GST:BSP and *Pv*GST:BSP respectively. Given that previous studies have established that lower Rg values indicate a

structurally compact system, which translates to system stability, while higher Rg values suggest less compactness and potential instability, hence the results becomes deductible.

Table 4. Simulation Quality Analysis parameters and data of the four systems the 500 ns MD

| Simulated systems | Parameter | Average | ±SD | Slope ($ps^{-1}$) |
|---|---|---|---|---|
| **Apo-*Pf*GST** | Total energy, Et (kcal/mol) | –123300.28 | 41.45 | –0.000 |
| | Potential energy, Ep (kcal/mol) | –151605.96 | 39.58 | –0.000 |
| | Temperature (K) | 298.73 | 0.15 | 0.000 |
| | Pressure (bar) | 1.37 | 16.01 | –0.000 |
| | Volume ($Å^3$) | 456221.84 | 188.16 | 0.000 |
| **Apo-*Pv*GST** | Total energy, Et (kcal/mol) | –121002.36 | 41.43 | –0.000 |
| | Potential energy, Ep (kcal/mol) | –148685.19 | 39.35 | –0.000 |
| | Temperature (K) | 298.73 | 0.15 | 0.000 |
| | Pressure (bar) | 1.79 | 16.22 | 0.000 |
| | Volume ($Å^3$) | 446418.40 | 179.07 | –0.000 |
| ***Pf*GST:BSP** | Total energy, Et (kcal/mol) | –123293.56 | 44.96 | –0.000 |
| | Potential energy, Ep (kcal/mol) | –151650.01 | 42.97 | –0.000 |
| | Temperature (K) | 298.73 | 0.15 | 0.000 |
| | Pressure (bar) | 1.05 | 15.97 | 0.000 |
| | Volume ($Å^3$) | 457136.60 | 204.93 | 0.000 |
| ***Pv*GST:BSP** | Total energy, Et (kcal/mol) | –121084.96 | 42.91 | –0.000 |
| | Potential energy, Ep (kcal/mol) | –148741.01 | 40.99 | –0.000 |
| | Temperature (K) | 298.74 | 0.15 | 0.000 |
| | Pressure (bar) | 0.86 | 16.90 | 0.000 |
| | Volume, Et (kcal/mol) | 445934.53 | 179.12 | 0.000 |

Meanwhile, the Rg profile across *Pv*GST and *Pv*GST:BSP systems shows comparability, as there were no significant deviations in the average Rg throughout the 500 ns simulation time. This shows that there were moderate conformation changes throughout the simulation time, Figures 9A and B compared. However, there is a significant deviation (of 3.95 Å) between *Pf*GST and *Pf*GST:BSP systems, an indication that BSP impacts the compactness of *Pf*GST upon binding. This might be unconnected to the bulky molecule-like size of BSP which is capable of altering the overall confirmation of the very dynamic *Pf*GST. However, the apo 's (*Pf*GST and *Pv*GST) Rg profiles were not closely alike, an indication of different structural compactness or conformational stability and dynamics of these two systems. On the other hand, the Rg profile of the two BSP complexed systems (*Pf*GST:BSP and *Pv*GST:BSP) are comparable, which is an indication that BSP's bulky molecule-like size has a similar effect on the structural compactness of both *Pf*GST and *Pv*GST

during the simulation time. The highest Rg is observed in *Pf*GST:BSP, followed by *Pv*GST:BSP, *Pv*GST, and *Pf*GST. While the mobility pattern obtained for BSP bound *Pv*GST did not show significant mobility difference, though the *Pv*GST:BSP's system exhibited a Rg pattern that is higher than that of *Pv*GST. But with respect to BSP bound *Pf*GST, there is a clear show of mobility difference between the *Pf*GST:BSP and the apo *Pf*GST, indicating a higher conferment of inactivity. This is in the face of the established fact that a lower Rg values is indicative of a structurally compact system, which translates to system stability. On the other hand, a higher Rg values is suggestive of a less compactness and potential instability. This will impact inactivity on the protein.

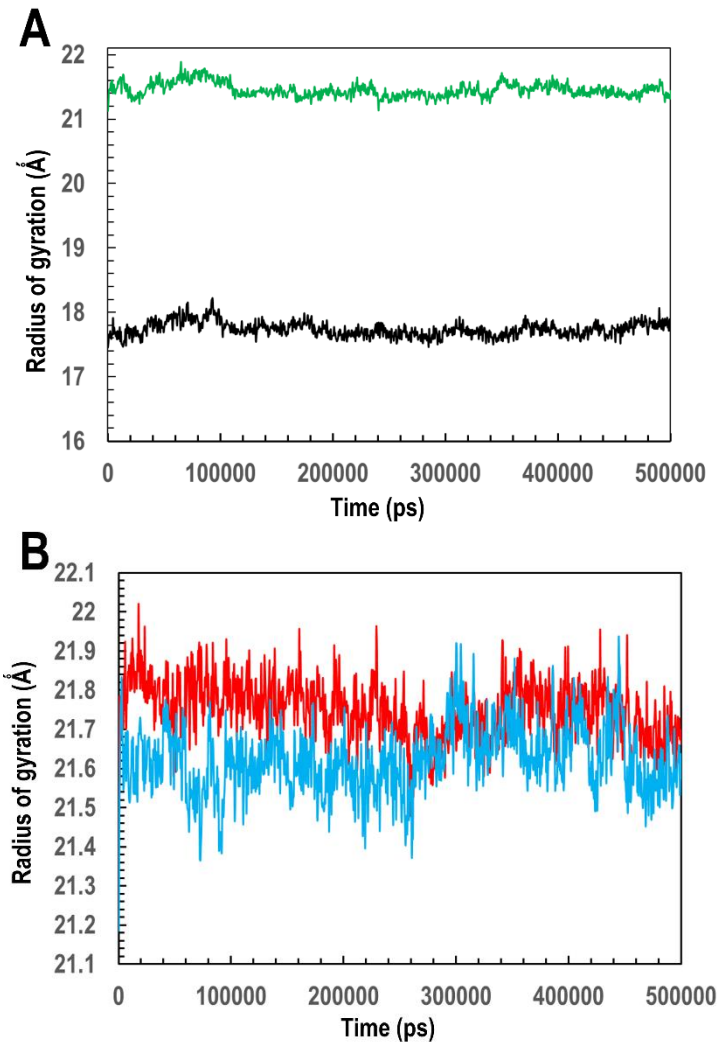


Fig. 9. Simulation event analysis generated profile showing (A) the radius of gyration (Rg) of the apo systems of *Pf*GST (black) and *Pv*GST (green). (B) the radius of gyration (Rg) of the protein-ligand complex *Pf*GST:BSP (red) and *Pv*GST:BSP (blue) throughout the 500 ns simulation time plotted in picoseconds (ps)

After that, the trajectory frames of the four systems' Cα RMSD were calculated. This measurement gives the average distance of the atom's Cα for a specific frame per reference frame. The four systems' Cα RMSD plotted against the 500 ns simulation time is seen in Figure 10A. The four system's global average trajectories are 2.25 ± 0.75 (apo-*Pf*GST), 2.65 ± 0.35 (apo-*Pv*GST), 2.23 ± 0.75 (*Pf*GST:BSP), and 2.77 ± 0.25 (*Pv*GST:BSP). These trajectories reveal not more than 3 Å fluctuations in the simulated systems, an indication of well-equilibrated systems and that the data generated are reliably usable for downstream analysis. Relatedly, the plot also reveals the ligand's RMSD with respect to the two proteins (*Pf*GST and *Pv*GST), which expressed the ligand's degree of motion within the dimer interphase. It also helps to extrapolate the ligand's stability with respect to the proteins and their binding sites. Although BSP was stably bound to *Pf*GST and *Pv*GST throughout the 500 ns simulation, it showed a higher degree of motion in *Pf*GST than in *Pv*GST.

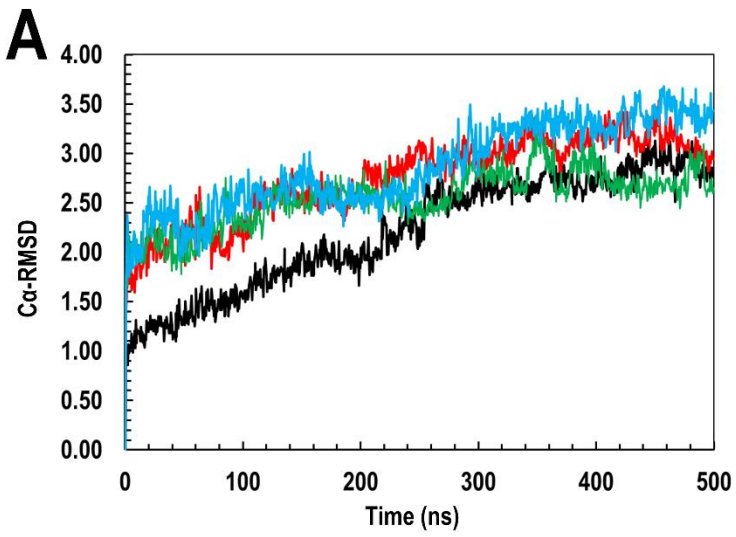

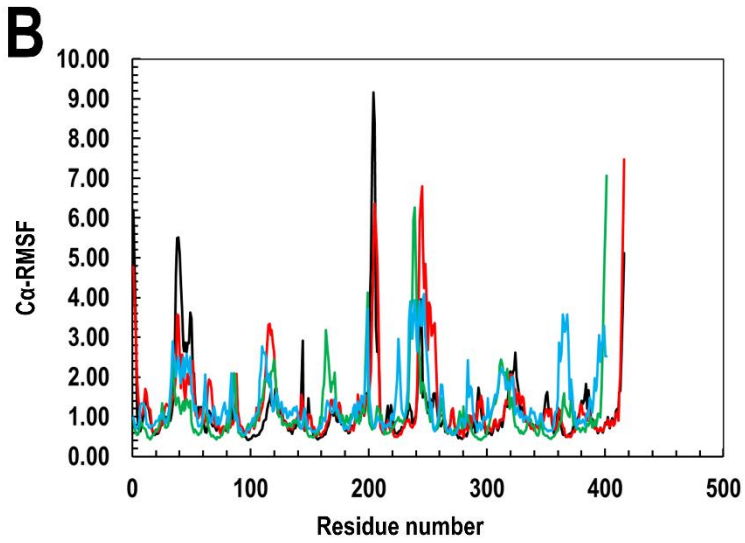


Fig. 10. Analysis of the simulation trajectory showing (A) the RMSD of the Cα atoms and (B) the RMSF of the side chains as a function of the 500 ns simulation time for apo-*Pf*GST (black), apo-*Pv*GST (green), *Pf*GST:BSP complex (red), *Pf*GST:BSP complex (blue).

Similarly, plots of the four systems' side chain root-mean-square-fluctuation (RMSF) values against the residue numbers based on the 500 ns simulation trajectory data was made. In Figure 10B, the RMSF plot shows residues 1-211 and 212-424 correspond to both protein subunits A and B respectively. Also, the side chain fluctuations' general profiles across the four systems and their sub-units were seen to be comparable with little or no deviation in the protein-ligand complexes vis-à-vis their apo structures all through the simulation period with the ligand remaining bound at both *Pf*GST and *Pv*GST's dimer interphase. Furthermore, the degree of compactness of each protein-ligand complexes (*Pf*GST:BSP) and *Pv*GST:BSP) were accessed using the global solvent accessible surface area (SASA) and molecular surface area (MolSA). While MolSA as a technique quantitatively reveals BSP's interaction at both protein's molecular environment, the technique however shows that *Pf*GST:BSP's system (with higher MolSA) is more stable compared to that of *Pv*GST:BSP. This is because, in the 500 ns simulations trajectory, *Pf*GST:BSP shows a greater MolSA which is noted at an average of 422.50 $Å^2$ than *Pv*GST:BSP which is observed at an average of 416.50 $Å^2$ as can be seen in Figure 11A. Although the stable interaction during the 500 ns simulations time reveals that BSP established interaction in both *Pf*GST and *Pv*GST, but the higher MolSA as seen in *Pf*GST's system shows that BSP cause more functional inactivity in *Pf*GST compared to *Pv*GST. This result is in tandem with the protein's enzymatic specific activities carried out during the empirical study. In quantitatively describing the binding dynamics of BSP to *Pf*GST

and *Pv*GST's hydrophobic core, the global SASA trajectories of the protein complexes as shown in in Figure 11B shows a similar binding dynamics of BSP in *Pf*GST and *Pv*GST. Similarly, while *Pf*GST:BSP's SASA is greater than that of *Pv*GST:BSP with *Pf*GST:BSP's average SASA at 150 $Å^2$ while that of *Pv*GST:BSP at 125 $Å^2$, the binding dynamics of the two systems however shows similarities. The increase in *Pf*GST:BSP's average SASA implied that *Pf*GST assumed a more exposed conformation upon binding and during the 500 ns simulations than *Pv*GST, a confirmation that *Pf*GST is more dynamic in comparison to *Pv*GST. These findings are in tandem with the kinetic and stability studies profile earlier reported just as the MolSA results correlates with the SASA of the two protein-ligand complexes.

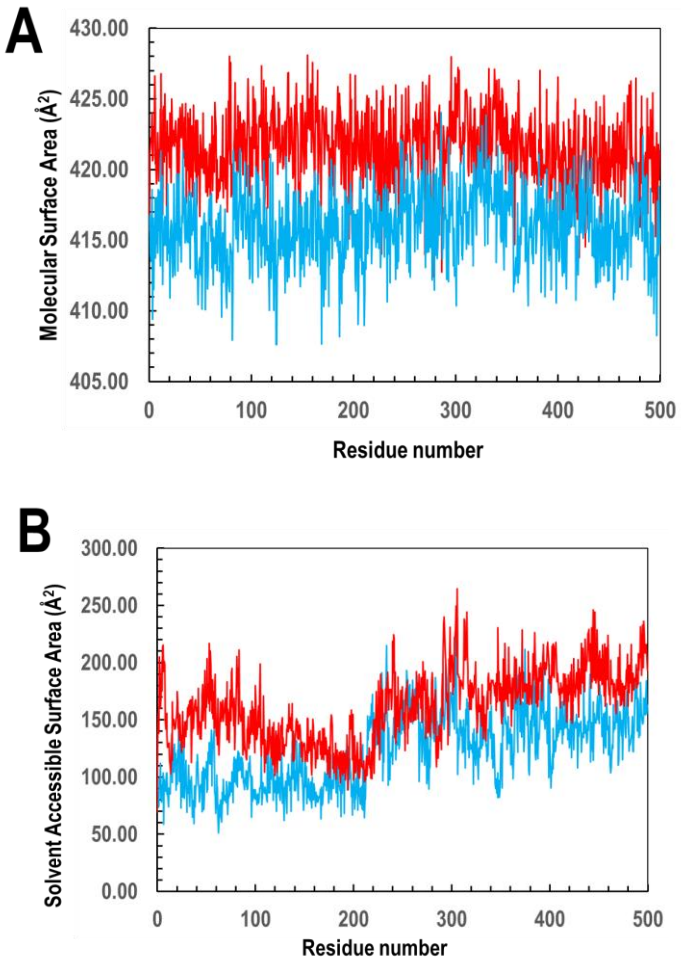


Fig. 11. The interaction of BSP with *Pf*GST and *Pv*GST in respect of their (A) MolSA quantitatively revealing BSP's interaction at both protein's molecular environment, with *Pf*GST:BSP's trajectory (red) showing a higher MolSA than *Pv*GST:BSP (blue) and (B) global SASA showing similar binding dynamics of BSP in the two proteins. The *Pf*GST:BSP's SASA (red) is however higher than that of *Pv*GST:BSP (blue).

Furthermore, from Figure 12 which summarizes the 500 ns simulations monitored protein-ligand interactions, it reveals that a combination of interactions namely hydrophobic, hydrogen, ionic, and salt bridges held and stabilized the ligand (BSP) within the proteins' dimer interphase.

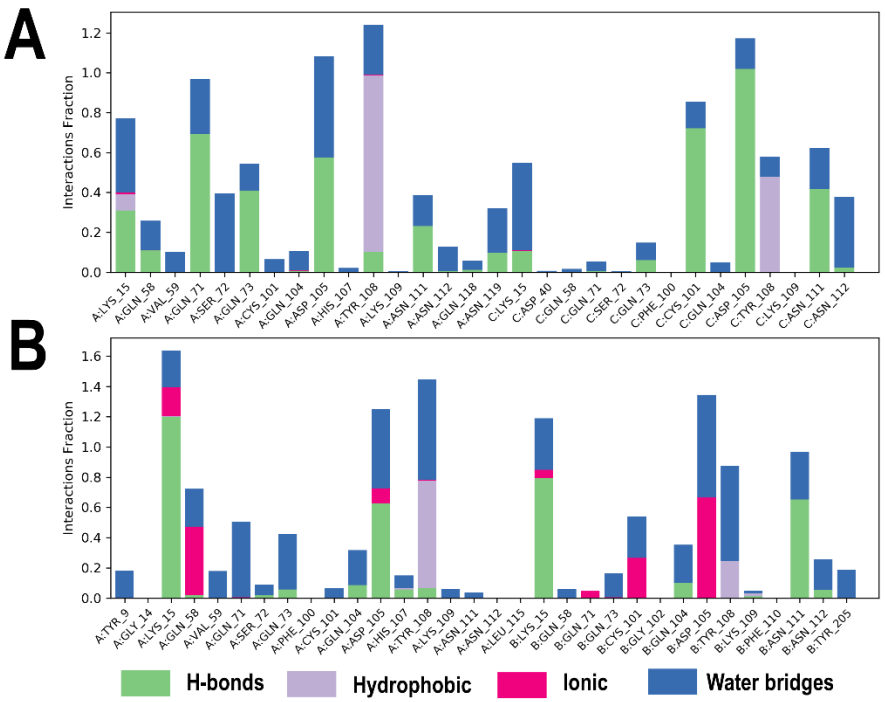


Fig. 12. Amino acid side chains interactions and types of interactions stacked bar charts between (A) *Pf*GST:BSP and (B) *Pv*GST:BSP, throughout the 500 ns simulation. The interaction diagram showed H-bonds are categorized into backbone acceptor; backbone donor; side-chain acceptor; side-chain donor. Hydrophobic interactions are categorized into π-cation; π-π*; and other, non-specific interactions. The stacked bar charts are normalized throughout the 500 ns trajectory. The images were obtained with the use of the Ligand Interaction Algorithm implemented in Maestro v13.0.

There is the understanding that the binding energy of molecule's interaction (vis-à-vis the ligand-protein interaction) that takes place in a biological system gives the descriptive estimate of the thermodynamics/energetics in the biological system. In this regard, the MM/GBSA free energy binding of BSP and the receptors (*Pf*GST and *Pv*GST) were then determined using the MM/GBSA algorithm implementable in Schrodinger Maestro v13.0. The MM/GBSA calculated energy components of the interactions are succinctly tabularized (Table 5). The calculated $\Delta G_{bind}$ of BSP towards *Pf*GST and *Pv*GST are similar, being -13.59 and -16.39 kcal/mol. This negative $\Delta G_{bind}$ is indicative of the possibility of spontaneity in the binding reaction in both *Pf*GST and *Pv*GST. With that in mind, this result also shows that the interaction of BSP with *Pf*GST and *Pv*GST is thermodynamically favorable. The results also indicated that, although the gas phase energy acted

opposite to the solvation free energy, it however contributed chiefly to the overall $\Delta G_{bind}$. In addition, the result also presents that the binding of BSP with *Pf*GST and *Pv*GST is primarily brought about by van der Waals interactions.

Table 5. MM/GBSA calculated binding energy of BSP interaction with *Pf*GST and *Pv*GST

| **Protein Complex** | **Energy components (kcal/mol)** | | | | |
|---|---|---|---|---|---|
| | $\Delta E_{vdW}$ | $\Delta E_{ele}$ | $\Delta E_{gas}$ | $\Delta E_{sol}$ | $\Delta G_{bind}$ |
| *Pf*GST | −52.51 | −10.69 | −65.37 | 53.08 | −13.59 |
| *Pv*GST | −48.84 | 45.49 | −6.46 | −7.13 | −16.59 |

Furthermore, in deconvoluting the Cα atoms' dynamics as a function of ligand binding, PCA was used to expand the conformational changes of the RMSD and RMSF metrics. This is as all singular mode of *Pf*GST and *Pv*GST in relation to their complexes are related to an eigenvalue. This eigenvalue corresponds to their fluctuations' degree along a mode containing different Cα atoms contributions. With PC1 and PC2, sufficient atomistic description of the conformation's fluctuation were revealed. These two PCs (PC1 and PC2) were used to analyze the transitions in conformations of the RMSD and RMSF simulated systems by deconvoluting their trajectories onto a two-dimensional subspace (Figure 13). The unnoticeable color changes from black to red and green to blue scale (Figures 13A and 13B) is an indication of spontaneous conformational transition of *Pf*GST and *Pv*GST respectively, upon the binding of BSP. Also, the scattered dots of PCA of the RMSF of the apo *Pf*GST and *Pv*GST with BSP's system (Figures 13C and 13D respectively) shows it's a liganded system.

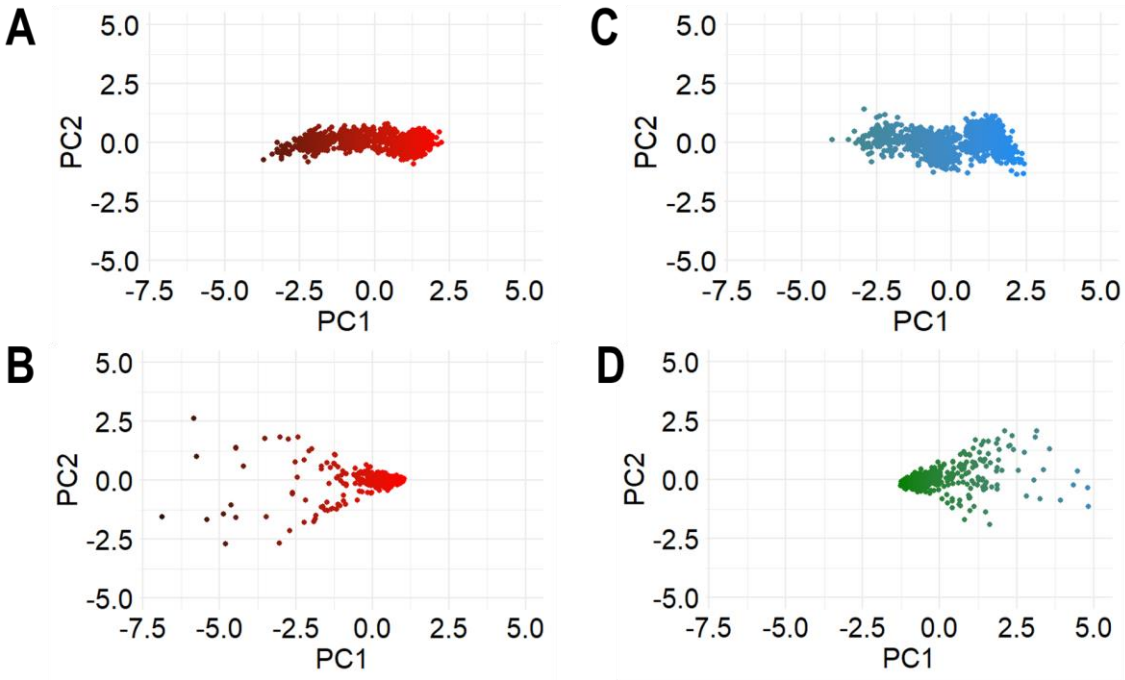


Fig. 13. The subspace trajectories projections of the first two principal components (PC1 and PC2) in respect of their (A) Cα RMSD of *Pf*GST and *Pf*GST:BSP and (B) Cα *Pv*GST and *Pv*GST:BSP, (C) Cα RMSF of *Pf*GST and *Pf*GST:BSP and (D) Cα *Pv*GST and *Pv*GST:BSP.

## 4.0 Conclusion

The combinatory empirical and molecular dynamics simulation studies employed in this article insightfully describes the ligandin properties of *Pf*GST and *Pv*GST towards BSP. The various empirical characterizations and computational modelling studies showed that BSP (as a ligand) binds tightly to *Pf*GST and *Pv*GST and showed good inhibitory abilities to their functionalities in a similar way. Specifically, the potency of BSP to alter the conformational stability and inhibit the enzymatic activities of these enzymes was fully described empirically and validated through the computational modelling approaches employed. The MDS correctly simulated *Pf*GST and *Pv*GST for drug-receptor/ligand interactions towards BSP, and consequently validating the druggability of *Pf*GST and *Pv*GST as a critical drug targets. The different empirical studies and computational modelling approaches strongly positioned BSP as a druggable candidate to be further studied and developed as a potent antimalarial.

## Disclosure statement

The authors declare no potential conflict of interest.

## References


Ahmed, A., Khogali, R., Elnour, M.-A. B., Nakao, R., & Salim, B. (2021). Emergence of the invasive malaria vector Anopheles stephensi in Khartoum State, Central Sudan. *Parasites & Vectors*, *14*(1), 1–5. https://doi.org/10.1186/s13071-021-05026-4

Akumadu, B. O., Pandian, R., Olfsen, J., Worth, R., Thulo, M., Mentor, T., Fanucchi, S., Sayed, Y., Dirr, H. W., & Achilonu, I. (2020). Molecular basis of inhibition of Schistosoma japonicum glutathione transferase by ellagic acid: Insights into biophysical and structural studies. *Molecular and Biochemical Parasitology*, *240*(August), 111319. https://doi.org/10.1016/j.molbiopara.2020.111319

Al-Qattan, M. N., Mordi, M. N., & Mansor, S. M. (2016). Assembly of ligands interaction models for glutathione-S-transferases from Plasmodium falciparum, human and mouse using enzyme kinetics and molecular docking. *Computational Biology and Chemistry*, *64*, 237–249. https://doi.org/10.1016/j.compbiolchem.2016.07.007

Banerjee, P., Eckert, A. O., Schrey, A. K., & Preissner, R. (2018). ProTox-II: a webserver for the prediction of toxicity of chemicals. *Nucleic Acids Research*, *46*(W1), W257–W263. https://doi.org/10.1093/nar/gky318

Bhagat, S., Gahlawat, A., & Bharatam, P. V. (2019). Structure-Based Drug Design of Pf DHODH Inhibitors as Antimalarial Agents. *Structural Bioinformatics: Applications in Preclinical Drug Discovery Process*, 177–220. https://doi.org/https://doi.org/10.1007/978-3-030-05282-9

Bhunia, S. S., Saxena, M., & Saxena, A. K. (2021). Ligand-and structure-based virtual screening in drug discovery. In *Biophysical and Computational Tools in Drug Discovery* (pp. 281–339). Springer. https://doi.org/10.1007/7355_2021_130

Calic, P. P. S., Mansouri, M., Scammells, P. J., & McGowan, S. (2020). Driving antimalarial design through understanding of target mechanism. *Biochemical Society Transactions*, *48*(5), 2067–2078. https://doi.org/10.1042/BST20200224

Chandel, T. I., Zaman, M., Khan, M. V., Ali, M., Rabbani, G., Ishtikhar, M., & Khan, R. H. (2018). A mechanistic insight into protein-ligand interaction, folding, misfolding, aggregation and

inhibition of protein aggregates: An overview. *International Journal of Biological Macromolecules*, *106*, 1115–1129.

Cheng, F., Li, W., Zhou, Y., Shen, J., Wu, Z., Liu, G., Lee, P. W., & Tang, Y. (2012). *admetSAR: a comprehensive source and free tool for assessment of chemical ADMET properties*. ACS Publications. https://doi.org/10.1021/ci300367a

Chigorimbo-Murefu, N. T. L., Njoroge, M., Nzila, A., Louw, S., Masimirembwa, C., & Chibale, K. (2012). Biotransformation and biocatalysis: roles and applications in the discovery of antimalarials. *Future Medicinal Chemistry*, *4*(18), 2325–2336. https://doi.org/10.4155/fmc.12.173

Choudhuri, S., Yendluri, M., Poddar, S., Li, A., Mallick, K., Mallik, S., & Ghosh, B. (2023). Recent Advancements in Computational Drug Design Algorithms through Machine Learning and Optimization. *Kinases and Phosphatases*, *1*(2), 117–140. https://doi.org/https://doi.org/10.3390/kinasesphosphatases1020008

Ciardiello, F., Ciardiello, D., Martini, G., Napolitano, S., Tabernero, J., & Cervantes, A. (2022). Clinical management of metastatic colorectal cancer in the era of precision medicine. *CA: A Cancer Journal for Clinicians*, *72*(4), 372–401. https://doi.org/10.3322/caac.21728

Colón-Lorenzo, E. E., Colón-López, D. D., Vega-Rodríguez, J., Dupin, A., Fidock, D. A., Baerga-Ortiz, A., Ortiz, J. G., Bosch, J., & Serrano, A. E. (2020). Structure-Based Screening of Plasmodium berghei Glutathione S-Transferase Identifies CB-27 as a Novel Antiplasmodial Compound. *Frontiers in Pharmacology*, *11*(March), 1–17. https://doi.org/10.3389/fphar.2020.00246

Cui, F., Sequeira, S. B., Huang, Z., Shang, G., Cui, Q., & Yang, X. (2020). Bromosulfophthalein suppresses inflammatory effects in lipopolysaccharide-stimulated RAW264. 7 macrophages. *Immunopharmacology and Immunotoxicology*, *42*(5), 456–463. https://doi.org/https://doi.org/10.1080/08923973.2020.1808985

Daina, A., Michielin, O., & Zoete, V. (2017). SwissADME: a free web tool to evaluate pharmacokinetics, drug-likeness and medicinal chemistry friendliness of small molecules. *Scientific Reports*, *7*(1), 42717. https://doi.org/10.1038/srep42717

Dasari, S., Ganjayi, M. S., Yellanurkonda, P., Basha, S., & Meriga, B. (2018). Role of glutathione S-transferases in detoxification of a polycyclic aromatic hydrocarbon, methylcholanthrene. *Chemico-Biological Interactions*, *294*(January), 81–90. https://doi.org/10.1016/j.cbi.2018.08.023

Dasari, S., Swamy, M., Yellanurkonda, P., & Basha, S. (2018). Chemico-Biological Interactions Role of glutathione S-transferases in detoxi fi cation of a polycyclic aromatic hydrocarbon , methylcholanthrene. *Chemico-Biological Interactions*, *294*(August), 81–90. https://doi.org/10.1016/j.cbi.2018.08.023

Elseginy, S. A. (2023). Exploring binding mechanisms of omicron spike protein with dolutegravir and etravirine by molecular dynamics simulation, principal component analysis, and free binding energy calculations. *Journal of Biomolecular Structure and Dynamics*, 1–14. https://doi.org/10.1080/07391102.2023.2293278

Ernst, M., Sittel, F., & Stock, G. (2015). Contact-and distance-based principal component analysis of protein dynamics. *The Journal of Chemical Physics*, *143*(24). https://doi.org/10.1063/1.4938249

Fritz-Wolf, K., Becker, A., Rahlfs, S., Harwaldt, P., Schirmer, R. H., Kabsch, W., & Becker, K. (2003). X-ray structure of glutathione S-transferase from the malarial parasite Plasmodium falciparum. *Proceedings of the National Academy of Sciences of the United States of America*, *100*(SUPPL. 2), 13821–13826. https://doi.org/10.1073/pnas.2333763100

Fu, Y., Zhao, J., & Chen, Z. (2018). Insights into the molecular mechanisms of protein-ligand interactions by molecular docking and molecular dynamics simulation: A case of oligopeptide binding protein. *Computational and Mathematical Methods in Medicine*, *2018*. https://doi.org/10.1155/2018/3502514

Gilson, M. K., Given, J. A., Bush, B. L., & McCammon, J. A. (1997). The statistical-thermodynamic basis for computation of binding affinities: a critical review. *Biophysical Journal*, *72*(3), 1047–1069. https://doi.org/10.1016/S0006-3495(97)78756-3

Habig, W. H., & Jakoby, W. B. (1981). Assays for differentiation of glutathione S-Transferases. In *Methods in enzymology* (Vol. 77, pp. 398–405). Elsevier. https://doi.org/https://doi.org/10.1016/S0076-6879(81)77053-8

Kollman, P. A., Massova, I., Reyes, C., Kuhn, B., Huo, S., Chong, L., Lee, M., Lee, T., Duan, Y., & Wang, W. (2000). Calculating structures and free energies of complex molecules: combining molecular mechanics and continuum models. *Accounts of Chemical Research*, *33*(12), 889–897. https://doi.org/10.1021/ar000033j

Kolobe, D., Sayed, Y., & Dirr, H. W. (2004). Characterization of bromosulphophthalein binding to human glutathione S-transferase A1-1: thermodynamics and inhibition kinetics. *Biochemical Journal*, *382*(2), 703–709. https://doi.org/10.1042/BJ20040056

Leelananda, S. P., & Lindert, S. (2016). Computational methods in drug discovery. *Beilstein Journal of Organic Chemistry*, *12*(1), 2694–2718. https://doi.org/https://doi.org/10.3762/bjoc.12.267

Lipinski, C. A., Lombardo, F., Dominy, B. W., & Feeney, P. J. (1997). Experimental and computational approaches to estimate solubility and permeability in drug discovery and development settings. *Advanced Drug Delivery Reviews*, *23*(1–3), 3–25. https://doi.org/10.1016/S0169- 409X(96)00423-1

Lumjuan, N., McCarroll, L., Prapanthadara, L., Hemingway, J., & Ranson, H. (2005). Elevated activity of an Epsilon class glutathione transferase confers DDT resistance in the dengue vector, Aedes aegypti. *Insect Biochemistry and Molecular Biology*, *35*(8), 861–871. https://doi.org/10.1016/j.ibmb.2005.03.008

Makumbe, H. H., Pandian, R., Valli, A., Sayed, Y., & Achilonu, I. (2024). Biophysical characterization, crystallization, and solution of the first crystal structure of the 28 kDa-Schistosoma bovis glutathione transferase. *Journal of Molecular Structure*, *1298*, 136979. https://doi.org/10.1016/j.molstruc.2023.136979

Mangoyi, R., Hayeshi, R., Ngadjui, B., Ngandeu, F., Bezabih, M., Abegaz, B., Razafimahefa, S., Rasoanaivo, P., & Mukanganyama, S. (2010). Glutathione transferase from Plasmodium falciparum - Interaction with malagashanine and selected plant natural products. *Journal of Enzyme Inhibition and Medicinal Chemistry*, *25*(6), 854–862. https://doi.org/10.3109/14756366.2010.486793

Massova, I., & Kollman, P. A. (2000). Combined molecular mechanical and continuum solvent approach (MM-PBSA/GBSA) to predict ligand binding. *Perspectives in Drug Discovery and*

*Design*, *18*, 113–135. https://doi.org/10.1023/A:1008763014207

McQueen, N., Gomes, K. V., McCormick, C., Blumanthal, K., Pisciotta, M., & Wilcox, J. (2021). A review of direct air capture (DAC): scaling up commercial technologies and innovating for the future. *Progress in Energy*, *3*(3), 032001. https://doi.org/10.1088/2516-1083/abf1ce

Mohring, F., Hart, M. N., Rawlinson, T. A., Henrici, R., Charleston, J. A., Clark, C. J., Baker, D. A., Draper, S. J., & Moon, R. W. (2019). *Rapid and iterative genome editing in the zoonotic malaria parasite Plasmodium 2 knowlesi: New tools for P. vivax research 3*. BioRxiv. https://doi.org/10.1101/590976

Mohring, F., Rahbari, M., Zechmann, B., Rahlfs, S., Przyborski, J. M., Meyer, A. J., & Becker, K. (2017). Determination of glutathione redox potential and pH value in subcellular compartments of malaria parasites. *Free Radical Biology and Medicine*, *104*, 104–117. https://doi.org/10.1016/j.freeradbiomed.2017.01.001

Naing, C., Whittaker, M. A., Htet, N. H., Aye, S. N., & Mak, J. W. (2019). Efficacy of antimalarial drugs for treatment of uncomplicated falciparum malaria in Asian region: A network meta-analysis. *PLoS ONE*, *14*(12), 1–16. https://doi.org/10.1371/journal.pone.0225882

Padi, N., Akumadu, B. O., Faerch, O., Aloke, C., Meyer, V., & Achilonu, I. (2021). Engineering a pseudo-26-kda schistosoma glutathione transferase from bovis/haematobium for structure, kinetics, and ligandin studies. *Biomolecules*, *11*(12). https://doi.org/10.3390/biom11121844

Pawłowska, M., Mila-Kierzenkowska, C., Szczegielniak, J., & Woźniak, A. (2023). Oxidative Stress in Parasitic Diseases—Reactive Oxygen Species as Mediators of Interactions between the Host and the Parasites. *Antioxidants*, *13*(1), 38. https://doi.org/10.3390/antiox13010038

Pérez-Peña, H., Abel, A.-C., Shevelev, M., Prota, A. E., Pieraccini, S., & Horvath, D. (2023). Computational Approaches to the Rational Design of Tubulin-Targeting Agents. *Biomolecules*, *13*(2), 285. https://doi.org/10.3390/biom13020285

Plaa, G. L. (2010). Evaluation of Hepatotoxicity: Physiological and Biochemical Measures of Hepatic Function in Animals. In *Comprehensive Toxicology* (pp. 129–140). Elsevier. https://doi.org/10.1016/B978-0-08-046884-6.01006-X

Pooe, K., Thulo, M., Makumbe, H., Akumadu, B., Otun, O., Aloke, C., & Achilonu, I. (2022).

Biophysical description of Bromosulfophthalein interaction with the 28-kDa glutathione transferase from Schistosoma japonicum. *Molecular and Biochemical Parasitology*, *252*, 111524. https://doi.org/10.1016/j.molbiopara.2022.111524

Pooe, K., Worth, R., Iwuchukwu, E. A., Dirr, H. W., & Achilonu, I. (2021). An empirical and theoretical description of Schistosoma japonicum glutathione transferase inhibition by bromosulfophthalein and indanyloxyacetic acid 94. *Journal of Molecular Structure*, *1223*, 128892. https://doi.org/10.1016/j.molstruc.2020.128892

Quesada-Soriano, I., Barón, C., García-Maroto, F., Aguilera, A. M., & García-Fuentes, L. (2013). Calorimetric studies of ligands binding to glutathione S-transferase from the malarial parasite Plasmodium falciparum. *Biochemistry*, *52*(11), 1980–1989. https://doi.org/10.1021/bi400007g

Quesada-Soriano, I., Barón, C., Téllez-Sanz, R., García-Maroto, F., & García-Fuentes, L. (2014). Asn112 in Plasmodium falciparum glutathione S-transferase is essential for induced reversible tetramerization by phosphate or pyrophosphate. *Biochimica et Biophysica Acta - Proteins and Proteomics*, *1844*(9), 1427–1436. https://doi.org/10.1016/j.bbapap.2014.04.017

Sabe, V. T., Ntombela, T., Jhamba, L. A., Maguire, G. E. M., Govender, T., Naicker, T., & Kruger, H. G. (2021). Current trends in computer aided drug design and a highlight of drugs discovered via computational techniques: A review. *European Journal of Medicinal Chemistry*, *224*, 113705. https://doi.org/10.1016/j.ejmech.2021.113705

Sadybekov, A. V., & Katritch, V. (2023). Computational approaches streamlining drug discovery. *Nature*, *616*(7958), 673–685. https://doi.org/10.1038/s41586-023-05905-z

Sayed, Y., Wallace, L. A., & Dirr, H. W. (2000). The hydrophobic lock-and-key intersubunit motif of glutathione transferase A1-1: implications for catalysis, ligandin function and stability. *FEBS Letters*, *465*(2–3), 169–172. https://doi.org/10.1016/S0014-5793(99)01747-0

Shibeshi, M. A., Kifle, Z. D., & Atnafie, S. A. (2020). Antimalarial drug resistance and novel targets for antimalarial drug discovery. *Infection and Drug Resistance*, *13*, 4047–4060. https://doi.org/10.2147/IDR.S279433

Soto, A., Foy, B. D., & Frazier, J. M. (2002). Effect of cadmium on bromosulfophthalein kinetics

in the isolated perfused rat liver system. *Toxicological Sciences*, *69*(2), 460–469. https://doi.org/10.1093/toxsci/69.2.460

Sujitha, V., Murugan, K., Dinesh, D., Pandiyan, A., Aruliah, R., Hwang, J.-S., Kalimuthu, K., Panneerselvam, C., Higuchi, A., & Kumar, S. (2017). Green-synthesized CdS nano-pesticides: toxicity on young instars of malaria vectors and impact on enzymatic activities of the non-target mud crab Scylla serrata. *Aquatic Toxicology*, *188*, 100–108. https://doi.org/10.1016/j.aquatox.2017.04.015

Szabo, M., Veres, Z., Baranyai, Z., Jakab, F., & Jemnitz, K. (2013). Comparison of human hepatoma HepaRG cells with human and rat hepatocytes in uptake transport assays in order to predict a risk of drug induced hepatotoxicity. *PloS One*, *8*(3), e59432. https://doi.org/10.1371/journal.pone.0059432

Tsui, V., & Case, D. A. (2000). Theory and applications of the generalized Born solvation model in macromolecular simulations. *Biopolymers: Original Research on Biomolecules*, *56*(4), 275–291. https://doi.org/10.1002/1097-0282(2000)56:4<275::AID-BIP10024>3.0.CO;2-E

Valli, A., & Achilonu, I. (2022). Comparative structural analysis of the human and Schistosoma glutathione transferase dimer interface using selective binding of bromosulfophthalein. *Proteins: Structure, Function and Bioinformatics*, *90*(8), 1561–1569. https://doi.org/10.1002/prot.26338

Valli, A., & Achilonu, I. (2023). Molecular dynamics-derived pharmacophores of Schistosoma glutathione transferase in complex with bromosulfophthalein: Screening and analysis of potential inhibitors. *Journal of Molecular Graphics and Modelling*, *122*, 108457. https://doi.org/10.1016/j.jmgm.2023.108457

Van Dorp, L., Gelabert, P., Rieux, A., De Manuel, M., De-Dios, T., Gopalakrishnan, S., Carøe, C., Sandoval-Velasco, M., Fregel, R., & Olalde, I. (2020). Plasmodium vivax malaria viewed through the lens of an eradicated European strain. *Molecular Biology and Evolution*, *37*(3), 773–785. https://doi.org/10.1093/molbev/msz264

Wang, E., Sun, H., Wang, J., Wang, Z., Liu, H., Zhang, J. Z. H., & Hou, T. (2019). End-point binding free energy calculation with MM/PBSA and MM/GBSA: strategies and applications in drug design. *Chemical Reviews*, *119*(16), 9478–9508.

https://doi.org/10.1021/acs.chemrev.9b00055

Zhan, Y., Liu, H., Wu, Y., Wei, P., Chen, Z., & Williamson, J. S. (2015). Biotransformation of artemisinin by Aspergillus niger. *Applied Microbiology and Biotechnology*, *99*, 3443–3446. https://doi.org/10.1007/s00253-015-6464-x

# Chapter 6

## Discovery of probable inhibitors of *Plasmodium falciparum* and *vivax* glutathione transferase through high-throughput virtual screening of a flavonoid library using bromosulfophthalein as the benchmark ligand

Olalekan Onisuru and Ikechukwu Achilonu*

Protein Structure-Function and Research Unit, School of Molecular and Cell Biology, Faculty of Science, University of the Witwatersrand, Braamfontein, Johannesburg 2000, South Africa

***Correspondence to Ikechukwu Achilonu*** (Ikechukwu.Achilonu@wits.ac.za): Protein Structure-Function and Research Unit, School of Molecular and Cell Biology, Faculty of Science, University of the Witwatersrand, Braamfontein, Johannesburg 2000, South Africa

**Authors**

Olalekan Onisuru: 2430435@students.wits.ac.za

Ikechukwu Achilonu: Ikechukwu.Achilonu@wits.ac.za

**Abstract**

The justifiable attention researchers have given to *Plasmodium falciparum* Glutathione *S*-Transferase (*Pf*GST) and *Plasmodium vivax* Glutathione *S*-Transferase (*Pv*GST) is unconnected to their role in detoxification, essentiality in malaria parasites' survival, and drug mechanism, making them an important drug target. Hence, these targets holds promise for the development of novel antimalarial therapies with improved efficacy, reduced drug resistance, and minimal toxicity. This is because inhibiting these targets represents a novel approach for the development of effective antimalarial using structure-based drug design and hence making the discovery of new chemical entities with potent and selective inhibitory activity against parasite GSTs. The pharmacological effects exerted by natural compounds such as flavonoids with antiplasmodial activities have potentials explorable as likely scaffold towards the development of new antimalarials. This is owing to the limitations associated with the various treatment options currently employed to treat malaria and the fact that flavonoids' high bioavailability and low toxicity efficiently position them as drug candidate of choice. Hence this research computationally screened and probed baicalin (BA) and 5,7,3'-Trihydroxy-6,4',5'-trimethoxyflavone (TTMF) as the potential inhibitor with improved binding and inhibitory ability than BSP against *Pf*GST and *Pv*GST respectively. BA and TTMF did respectively show they have the ability to significantly impact the targets compactness while strongly bound to them at their respective dimer interface more than bromosulfophthalein, which has shown excellent binding. The molecular dynamics simulations and post-dynamic analysis carried out revealed that various interactions, including hydrogen bonds and van der Waals forces stabilize these bindings. Notably, BA and TTMF's binding altered the proteins' compactness and conformational dynamics, suggesting a potential non-competitive, allosteric inhibition mechanism. This study opened up the need to insightfully look into BA and TTMF's candidacy as probable antimalarial drugs that will target *Pf*GST and *Pv*GST, given their binding ability to disrupt crucial functions of these enzymes.

## 1. Introduction

The infectivity of malaria as an annual three million people-killing disease have continued to necessitate the search for new therapeutics with swift efficacy, affordability, and having minimal toxicity. This is as malaria remains both a health burden, economically challenging, causing significant morbidity cum mortality and leading to grave economic loss (Singh and Rathi, 2023; Siqueira-Neto et al., 2023). The sub-Saharan Africa remains malaria worst hit region health-wise housing 94% of the global 249 million cases recorded and accounting for 96% of the attributed global death. Economically, this disease is associated with an annual economic loss and activity estimated to be US$ 12 billion (Siqueira-Neto et al., 2023; World Health Organization, 2022). A number of artemisinin (ART)-based combination therapies and chloroquine alongside either primaquine or tafenoquine have been used for the treatment of uncomplicated *Plasmodium falciparum* and *Plasmodium vivax*. However, the emergence and development of resistance and multi-drug resistance occurrence has reversed the hitherto once celebrated gains of antimalarial fight and effort towards effective treatment and eradication (Rasmussen et al., 2022; Wicht et al., 2020). While efforts towards the development of new antimalarial drug have been momentously accelerated in the last decade, there is still need to innovatively find new antimalarial drugs that do not only treat *Plasmodium falciparum* but also bring about complete elimination of *Plasmodium vivax* (Yang et al., 2021). These efforts are necessitated by the established resistance of *Plasmodium falciparum* and *Plasmodium vivax* to all the clinically proven and effective antimalarials including the WHO approved frontline artemisinin-based combination therapies (ACTs) (Haldar et al., 2018; Lucy et al., 2020).

Historically, natural products have often been used as a source of antimalarials. This is because researchers recognize their potency, which is attributable to their structural diversity and complexities (Conrad and Rosenthal, 2019; Kingston and Cassera, 2022; Tse et al., 2019). Although, many natural products have been isolated and structurally modified for use as prime antimalarials but not without challenges. These challenges have made the continuous uncomplimentary high-throughput phenotypic screening and unexplored target-based screening of natural products less attractive as scaffold families to pursue (Guantai and Chibale, 2011; Siqueira-Neto et al., 2023; Tse et al., 2019). Researchers have shown that drug target mechanism's understanding will be significant in bringing about a dramatic acceleration from the early-stages to late-stages structural modifications of target-based antimalarials. This understanding becomes

pivotal as it helps to circumvent the limitations associated with other drug discovery approaches including the quintessential phenotypic-based high-throughput screening. Also, this target based research approach becomes critical to designing new inhibitors with the understanding of the target structure, function, and mechanism of action (Calic et al., 2020; Gilbert et al., 2011; Swinney, 2013; Sykes and Avery, 2013). This has led to a new paradigm shift which focuses on targeting the parasite's (*Plasmodium falciparum* and *Plasmodium vivax*) metabolic pathway for drug development. *Plasmodium falciparum* glutathione *S*-transferase (*Pf*GST) and *Plasmodium vivax* glutathione *S*-transferase (*Pv*GST) have come to the fore as new targets for the development of novel antimalarials (Al-Qattan and Mordi, 2023; Forte et al., 2021; CHINNAPPANNA et al., 2023; Sarma et al., 2023).

Flavonoids are natural compounds belonging to the phenolic class of phytochemicals that are commonly found in fruits and vegetables as secondary metabolites. They have been proven to exert pharmacological effects as antiplasmodial agents and with potentials explorable as likely scaffold towards the development of new antimalarials (Boniface and Ferreira, 2019; Chepkirui et al., 2021; Penna-Coutinho and Aguiar, 2018; Song et al., 2021; Zothantluanga et al., 2023). Research interest in the use of flavonoids continues to gain momentum. This is owing to the limitations associated with the various treatment options currently employed to treat malaria and the fact that flavonoids' high bioavailability and low toxicity efficiently position them as drug candidate of choice (Boniface and Ferreira, 2019; Rameshkumar et al., 2021). Given the therapeutic relevance of flavonoids, this research explores a high-throughput virtual screening (HTVS) technique to probe a 506 collection of natural compounds from MedChemExpress (*MCE*) database of flavonoids compounds (Cat. No.: HY-L068). This is for the identification of lead compound that could bind and inhibit *Pf*GST and *Pv*GST targets as inhibitors. In doing this, bromosulfophthalein (BSP), an anionic phthalein, triphenylmethane dye which has been computationally and empirically explored as a potent inhibitor of *Pf*GST and *Pv*GST (in our research group) is added to the library as a benchmark. This is as the findings related to its strong binding and superb inhibitory potentials of the functionalities of *Pf*GST and *Pv*GST has been published (Onisuru & Achilonu, 2024). Similarly, ellagic acid (EA), a natural product which has shown to inhibit parasitic GSTs (in researches conducted in our group) was included in the library as a reference (Akumadu et al., 2020; Pooe et al., 2022, 2021; Valli and Achilonu, 2022). The hit compound(s) from the HTVS study with more binding and inhibitory effect on the targets than BSP and EA is expected to be

better drug candidate. This research approach of benchmarking and referencing the library is expected to give a deeper insight into the probe. The research becomes necessary as *in silico* (HTVS) computational studies continues to play significant role as an employable technique in designing new inhibitors against targets such as *Pf*GST and *Pv*GST. Baicalin, derived from the roots of *Scutellaria baicalensis* and *5,7,3′-Trihydroxy-6,4′,5′-trimethoxyflavone, found in plants such as Artocarpus communis*, have been reported through *in vivo* studies to exhibit strong antimalarial activity primarily through their ability to inhibit the growth and proliferation of the *Plasmodium* parasite in its asexual blood stage. This they achieve by interfering with essential metabolic pathways within the parasite. To this end, and here in this study, a *MCE* flavonoid library with BSP and EA included as benchmarks is computationally probed and studied for binding and inhibitory effect of *Pf*GST and *Pv*GST using molecular dynamics simulation. This will ultimately position the top-ranking flavonoids as novel drug candidates for malaria treatment. To the best of our knowledge, no study has been computationally undertaken to probe such a rich flavonoid library against these unique drug targets (*Pf*GST and *Pv*GST) in this regard.

## 2. Materials and Methods

### 2.1. Computational studies

#### 2.1.1. Computer hardware

This computationally intensive study employed the use of two high performance desktop servers having specialized configurations such as an Extreme Edition 16 CPU Intel core i7 5960x (3.3 GHz, 20 M cache 16x cores), Nvidia GTX 750Ti graphics card, 32 GB DDR4-2133 MHz memory on an MSI X99 motherboard and a 264 GB RAM. While for the HTVS and ligand docking component of the study, an implementable Schrödinger Maestro v13.0 Window OS desktop was employed, a Linux server equipped with the 2019 GPU-enabled Schrödinger Desmond version was used for the molecular dynamics simulation studies. A similarly configured computer hardware was used to perform all the post-dynamic analysis.

### 2.2. Ligand and protein preparation

A collection of 506-sized natural flavonoid library from the *MCE* repository serving as a useful tool for drug discovery and other applications was utilized to source for lead compounds. A two-

dimensional (2D) structure data file (SDF) format of the flavonoids were retrieved from the MCE library after which they were exported to Maestro (Schrödinger suite) to be prepared as ligands for HTVS. The flavonoids SDF file were then submitted to the Maestro v13.0 module known as LigPrep for ligand preparation. This preparation becomes imperative in order to generate structures of high quality forms and having an appropriate ionization state, tautomers, ring conformation, and stereochemistry (Madhavaram et al., 2019). This process involves energy minimization with the use of the OPLS_2005 force field. An Epik module algorithm was used to generate possible ionization states at pH 7.0 ± 2 and predict the pKa. The flavonoid ligands were then desalted before generating their possible tautomeric states at pH 7.0 ±2. In addition to this, molecules with multiple chiral centers were either retained or varied so as to return chemically useful structures having low energy states and then saved in Maestro (.mae) files in readiness for the HTVS. *Pf*GST atomic coordinate with PDB ID 2AAW and *Pv*GST's computed alpha fold structure with UniProtKB ID Q0ZS46 were retrieved from a Research Collaboration for Structural Bioinformatics Protein Data Bank (RCSB PDB) repository. They were subsequently submitted to Maestro v13.0 implementable molecular modelling algorithms' protein preparation wizard module. Both structures were energy-minimized (using the optimized potentials for liquid simulations (OPLS) 2005 force field to a root-mean-square-deviation (RMSD) of 0.30 Å) by assigning precise protonation state at physiological pH. This was followed by the addition of hydrogen atoms using default parameters before their side chains stereochemistry were checked in order to prevent inducement of major perturbations in the preparation of the structure.

### 2.3. High-throughput virtual screening

A Maestro prepared 506-natural flavonoid molecules and BSP ligand receptor grid file prepared by the LigPrep algorithm were submitted to Maestro 13.0 implementable Glide module Ligand Receptor docking for HTVS. The filtering/screening workflow followed three phases as earlier reported by (Achilonu et al., 2020; Madhavaram et al., 2019) and this include the HTVS, standard protocol or precision (SP), and the extend protocol or extra precision (XP). The HTVS procedure was first to be carried out and this involved the ligand docking step of the 506 flavonoid molecules alongside BSP and ellagic acid. This was done without the option of MM/GBSA and Lipinski ADME filtering applied, only the application of QikProp filtering and the OPLS 2005 force field parameters were applied for the HTVS phase and docking calculations respectively. This phase was subsequently followed by the SP phase, which is a rigorous and systematic phase which

subjects 10% of the HTVS-docked ligands to further docking to generate Glide docking scores potential hits. The screening was done separately for *Pf*GST and *Pv*GST and was completed with an extended protocol (XP) phase with the visual inspection and selection of molecules having the best Glide score and Glide energy for further analysis.

### 2.4. Induced-fit ligand docking

Given the need to understand the proteins' dynamic nature vis-à-vis their conformational changes inducible upon ligand binding, an induced-fit docking (IFD) was performed using a Schrödinger Maestro v13.0 algorithm implementable induced-fit ligand docking. This was carried out to evaluate the top scoring ligands with least binding energy (selected for *Pf*GST and *Pv*GST) using the protein's ligand-binding site geometry, which is vitally dependable upon the protein's structure-ligand inducible conformational changes at binding. For the binding evaluation, both chains A and B (whole dimer) were selected as the binding site given the enzymes' possible binding sites, which include the GSH binding site (G-site), the xenobiotic binding site (H-site), and the dimer interface (Fritz-Wolf et al., 2003). For this process, an OPLS_2005 force field implicit solvent model was used with both ring conformational sampling having a 2.5 kcal/mol energy barrier and a non-planar conformation penalty on amide bonds were also applied. The proteins' receptor and ligand scaling were both set at 0.5 with 20 maximal limits permitted poses per ligand. At the end of the IFD, a top-scoring pose of *Pf*GST complexed with baicalin (BA), a flavonoid glycoside which is also an allosteric carnitine palmityl transferase 1 (CPT1) activator (Hu et al., 2024) was selected and saved as a system file for the MDS. Similarly, the corresponding top-scoring pose of *Pv*GST complexed with 5,7,3'-Trihydroxy-6,4',5'-trimethoxyflavone (TTMF), a naturally occurring flavonoid (Yazdiniapour et al., 2021), was also selected, and saved as a system file in readiness for further computational studies.

### 2.5. Molecular dynamics simulations and post-dynamic analyses

To gain deeper insight into the proteins interactions with the docked ligands which will further provide deeper understanding of the parasites drug target's structure-function relationship, a molecular dynamics simulations (MDS) was performed using a GPU-enabled Desmond engine (Bergdorf et al., 2014; Release, 2014) implementable in Maestro v13.0. A 500 ns simulations were performed on *Pf*GST:BA and *Pv*GST:TTMF complexes previously saved as PDB files. In doing this, a System Builder module implemented in the Desmond algorithm was used to build two

systems (*Pf*GST:BA and *Pv*GST:TTMF) which were consequently submitted to the Linux (Ubuntu) desktop for MDS. The systems were first solvated using a transferable intermolecular potential with a three-point (TIP3P) explicit solvent model having the OPLS_2005 force field. Furthermore, the *Pf*GST:BA and *Pv*GST:TTMF systems were first minimized before counter ions were added to neutralize the systems. The addition of 0.15 M NaCl into the solvent box was done to condition the system physiologically. The systems were then submitted for the molecular dynamics production phase subsequent to the explicit solvent model solvation and ionization procedures. In concluding the MDS phase, a series of short simulation steps (equilibration) and a 500 ns simulation at a constant temperature of 300 K was carried out placed at least 20 Å from the ligands. Afterwards, the derived trajectories from the MDS studies were further subjected to post-dynamic analyses using a Schrodinger Maestro v13.0 to compare the protein structures' system. This was done using the Simulation Quality Analysis algorithm (implemented in Maestro v13.0). The analysis puts into consideration the simulation qualities in terms of average energy, pressure, temperature, and volume of the individual simulated systems. Specifically, the implemented Maestro v13.0 Simulation Interaction Diagram algorithm was used to analyze the alpha carbon atoms (Cα)'s root-mean-square-deviation (RMSD), ligand's RMSD vis-à-vis the receptors. Also, the residues' root-mean-square fluctuations (RMSF) and protein-ligand interaction were equally analyzed.

### 2.6. Molecular mechanics/generalized born and surface area solvation (MMGBSA) calculations

In order to estimate the relative binding energies of BA to *Pf*GST and TTMF to *Pv*GST, a molecular mechanics/generalized born solvent area (MM/GBSA) calculations were performed using previously reported methods (Kollman et al., 2000; Massova and Kollman, 2000; Tsui and Case, 2000; Wang et al., 2019). This MM/GBSA calculation method implemented in Maestro v13.0 is intended to provide further insight into *Pf*GST:BA and *Pv*GST:TTMF complexes binding interactions. For each of the *Pf*GST:BA and *Pv*GST:TTMF complexes, 2000 independent snapshots (of the 500 ns molecular dynamics simulations) binding energies were generated, averaged, and calculated with each ligand's $\Delta G_{bind}$ active site calculated following the given equation:

$$\Delta G_{bind}=\Delta G_{RL}-(\Delta G_R+\Delta G_L) \quad (1)$$

Where $\Delta G_{bind}$ in the equation denotes the free energy binding, $\Delta G_{RL}$ represents the free energy of protein-ligand complex; $\Delta G_R$ denotes the free energy of receptor, and $\Delta G_L$ the free energy of ligand. The binding free energy is important to be calculated as it establishes a given protein-ligand binding affinity. Given that, a more negative ΔG is an indication of better binding of the ligand to the protein (Gilson et al., 1997). In the light above, each state's free energy was calculated with the use of FF14SB force field, given by the equations:

$$\Delta G_{bind} = \Delta E_{gas} + \Delta G_{sol} - T\Delta S \quad (2)$$

$$E_{gas} = E_{int} + E_{vdW} + E_{ele} \quad (3)$$

$$G_{sol} + G_{GB} + G_{SA} \quad (4)$$

$$G_{SA} = \gamma SASA \quad (5)$$

The gas phase energy ($E_{gas}$) which is the sum of the internal energy ($E_{int}$), Coulomb energy ($E_{ele}$) and the van der Waals energies ($E_{vdW}$) were estimated by the terms of the FF14SB force field. For the solvation free energy ($\Delta G$sol) estimation, the contributions of energy from the polar states ($G_{GB}$) and non-polar states ($G_{SA}$) were accordingly used. While the non-polar solvation energy ($G_{SA}$) was derived using the solvent accessible surface area (SASA in $Å^2$), the contribution from polar solvation ($G_{GB}$) was determined by solving the Generalized Born equation. In the equation above, the solute's total entropy and temperature are represented by S and T respectively. The total binding free energy profile contribution between BA, TTMF and *Pf*GST, *Pv*GST respectively as per-residue free energy decomposition were estimated at the atomic level residues with the use of MM/GBSA implemented in Maestro v13.0.

## 3. Results and discussion

### 3.1. HTVS analysis of flavonoid compound's potential inhibitor of *Pf*GST and *Pv*GST

Molecular docking and molecular dynamics simulation studies' valuableness in drug discovery process has enhanced the performance of systematic prediction of ligand's ideal pose and

conformation at the binding site of a protein. Here in this study, HTVS's computational and transformative approach in screening large libraries of compounds against specific protein targets was employed to screen for natural compounds. Specifically, and with the use of Maestro v13.0 implementable LigPrep algorithm, a 506 collection of natural compounds flavonoids from MedChemExpress (*MCE*) database alongside BSP and EA were screened against *Pf*GST and *Pv*GST. Procedurally, this step utilizes the Maestro's HTVS and Standard Protocol (SP) Glide Docking algorithm for the library screening with respect to their affinity for *Pf*GST and *Pv*GST. The QikProp analysis filtering produces 5% of the 4698 compounds which are made up of the 506 natural compounds, bromosulfophthalein, ellagic acid, and their respective conformers. This is as this phase quickly identify compounds that possess desirable physicochemical properties and pharmacokinetic profiles, while filtering out those that are less likely to be successful. After this, the HTVS ligand docking was carried out, 56 and 1 compounds were shortlisted for *Pf*GST and *Pv*GST respectively. Afterwards, the filtering made by the SP and XP phase of the remaining compounds, baicalin (BA) and 5,7,3'-Trihydroxy-6,4',5'-trimethoxyflavone (TTMF) compounds were selected for *Pf*GST and *Pv*GST respectively. Fig. 1 gives the 2D chemical structure description of BA and TTMF with $C_2H_{18}O_{11}$; 446 g/mol and $C_{18}H_{16}O_8$; 360.3 g/mol respectively as their molecular formula and molecular weight. Table 1 gives the summary of the HTVS XP top-scoring selected compound for *Pf*GST and *Pv*GST on the basis of the lowest Glide Emodel energy values and docking score. These compounds were then submitted for docking against *Pf*GST and *Pv*GST using a Schrödinger Maestro v13.0 algorithm implementable induced-fit ligand docking algorithm.

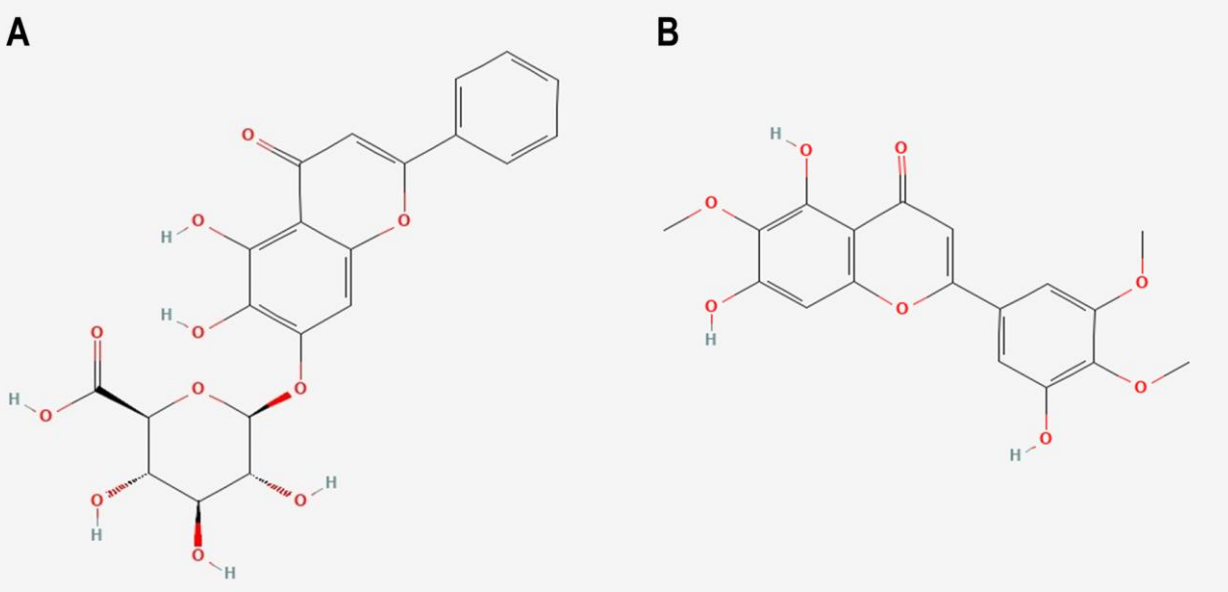


Fig. 1. The 2D chemical structure description of (A) Baicalin, BA and (B) 5,7,3'-Trihydroxy-6,4',5'-trimethoxyflavone, TTMF respectively obtained from PubChem database with CID number 64982 for BA and 5496475.

Table 1. HTVS computed binding affinity scores of the BA and TTMF to *Pf*GST and *Pv*GST's binding site

| System | Docking score | XP_Gscore | Glide energy | Glide emodel |
|---|---|---|---|---|
| PfGST:BA | -9.4006 | -9.4077 | -55.0821 | -73.3101 |
| PvGST:TTMF | -3.8526 | -3.8886 | -31.4576 | -26.5815 |

While the docking score succinctly predicts the assigned energy or score of BA and TTMF's conformation respectively to *Pf*GST and *Pv*GST, the XP_Gscore (Extra Precision Glide score specifically gives high-accuracy docking and virtual screening. This is as XP_Gscore takes into consideration interactions from van der Waals interactions, hydrogen bonding, desolvation energy, and ligand strain (Choudhry, 2021; Rehman et al., 2019). The similarly observed low docking score and XP_Gscore values, implies that BA and TTMF's respectively possess a strong affinity for the binding conformation with specificity within *Pf*GST and *Pv*GST's binding site in a manner that is energetically favorable. On the other hand, the Glide energy and Glide emodel complimentarily reveals the energy associated with BA and TTMF's binding as calculated by the Glide docking algorithm implemented in Schrödinger's Maestro Glide software suite (Friesner et al., 2004; Kaur et al., 2019). Similarly, their low score is an indication of the flavonoids strong binding affinity or fitness within the respective sites of the proteins.

### 3.2. Induced fit docking of BA and TTMF respectively to *Pf*GST and *Pv*GST

Given the rich information MDS provides at atomistic level vis-à-vis ligand-receptor interactions, mobility, and stability, a computational tool with fitted algorithm was hence employed to evaluate and validate the binding of BA and TTMF to *Pf*GST and *Pv*GST respectively. The Schrödinger Maestro v13.0 algorithm implementable induced-fit ligand docking reveals that both BA and TTMF respectively binds tightly and sit at the dimer interphase of *Pf*GST and *Pv*GST (Fig. 2A and B). From the induced fit docking results, BA and TTMF strongly binds exergonically with *Pf*GST and *Pv*GST in an interaction process that is accompanied with protein-ligand complex negative Emodel energy and Glide gscores.

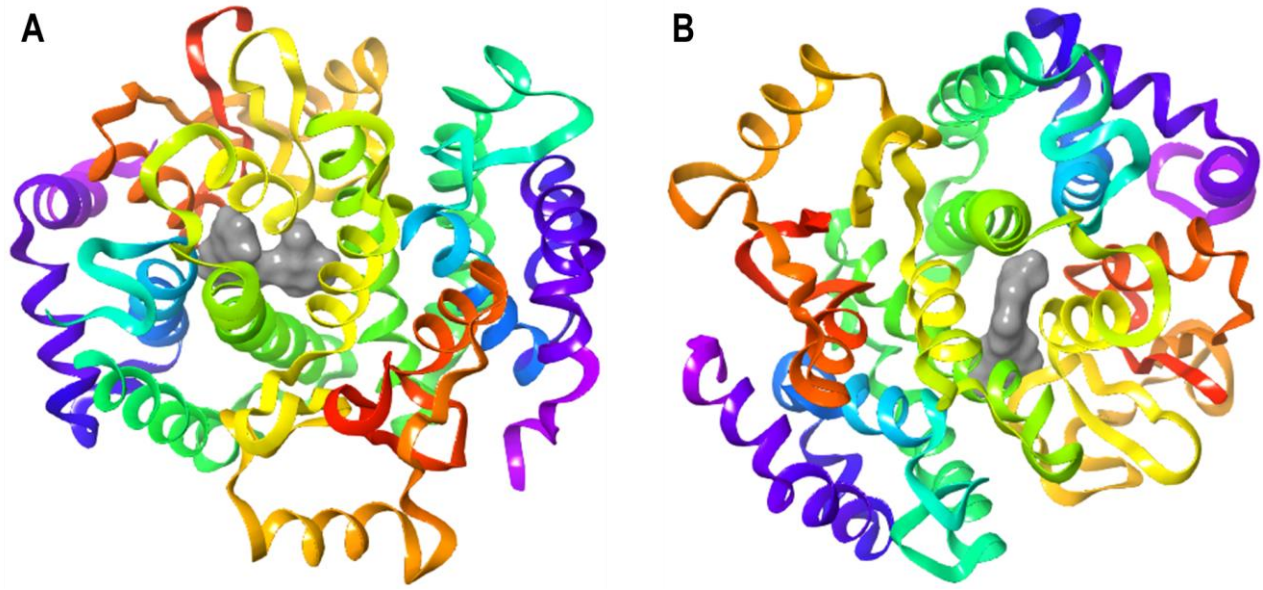


Fig. 2. Induced fit docking analysis of the protein-ligand complex ribbon representation of (A) *Pf*GST:BA complex, (B) *Pv*GST:TTMF, showing BA and TTMF respectively binding and sitting tightly at the dimer interphase of *Pf*GST and *Pv*GST. The image is a snapshot from the induced fit ligand docking algorithm implemented in Schrodinger Maestro v13.0.

The IFD also shows the amino acids side chains from the protein subunits contributing to the binding. Polar side chains that are positively charged (Lys15, Arg13), negatively charged (Asp105, Asp171), and neutrally charged (Ser72, Tyr108) were mostly involved in the binding interaction of BA with *Pf*GST (Fig. 3A). However, HID107 is seen to be involved in π-π* interaction with BA's phenyl moiety with none in involved TTMF's interaction with *Pv*GST. Similarly, polar side chain(s) that are positively charged (Lys109), negatively charged (Glu127,Asp 105), and neutrally

charged nonpolar Gly 102 were involved in the binding interaction of TTMF with *Pv*GST (Fig. 3B). There is however the involvement of more polarly charged amino acid residues in the binding interaction of BA with *Pf*GST than that of TTMF with *Pv*GST, and this explains why there is lower Glide emodel in BA with *Pf*GST than TTMF with *Pv*GST. This is as the involvement of these polar charged amino acid residues are essential in improving binding affinity while also achieving specificity and stability, thereby contributing to the accuracy of the docking process (Zhou and Pang, 2018).

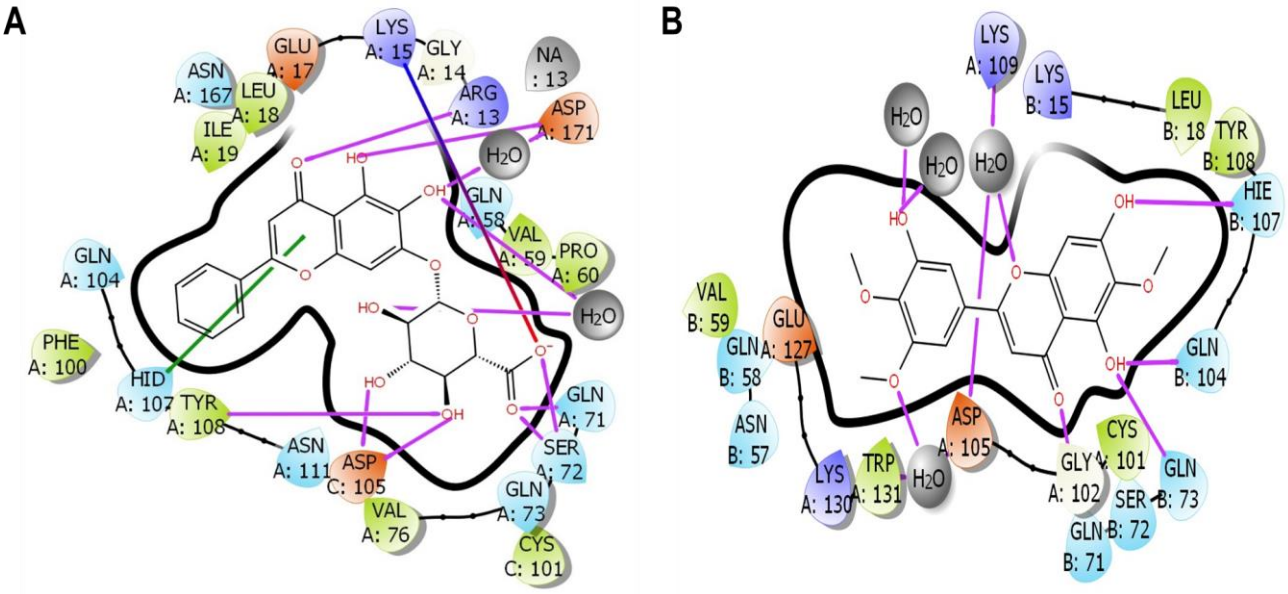


Fig. 3. 2-D ligand interaction plot highlighting the side chains involved in the binding between the interaction of (A) IFD docking pose of BA with *Pf*GST and (B) IFD docking of TTMF with *Pv*GST. HID107 is seen as the only amino side chains involved in π-π* interaction with BA's phenyl moiety in *Pf*GST and not in TTMF interaction with *Pv*GST. Not too similar amino residues' involvement were seen in the induced fir docking process. These Images were snapshots from the Maestro 2D interaction diagram implemented in Schrödinger Maestro 13.0

### 3.3. Molecular dynamics simulation and post-dynamic analysis of *Pf*GST, *Pv*GST, *Pf*GST:BA, and *Pv*GST:TTMF

After that, the trajectory frames of *Pf*GST:BA and *Pv*GST:TTMF systems' Cα RMSD were analyzed for the average distance of the atom's Cα for a specific frame per reference frame. Both

systems' Cα RMSD were plotted against the 500 ns simulation time (Fig. 3A and B). While the *Pf*GST and *Pf*GST:BA's system global average trajectories are 2.25 ± 0.75 and 3.20 ± 0.70 respectively, those of (apo-*Pv*GST) is 2.25 ± 0.50 and 30.50 ± 30.00 (*Pv*GST:BSP). For the *Pf*GST and *Pf*GST:BA's system, the trajectories reveal not more than 1.5 Å fluctuations in the simulated systems (Fig. 3A), an indication of well-equilibrated systems and that the data generated are reliably usable for downstream analysis. This low RMSD fluctuation also reveals the stability of *Pf*GST:BA during the 500 ns simulation time. This is as low RMSD fluctuations indicate that BA maintains a relatively stable conformation with *Pf*GST. However, the high fluctuations observed between *Pv*GST and *Pv*GST:TTMF systems' Cα RMSD (Fig. 3B) suggest that TTMF induces significant conformational dynamics within the dimer interphase of *Pv*GST. This is as the Cα RMSD helps to extrapolate the ligand's stability with respect to the proteins and their binding sites. Although TTMF was stably bound to *Pv*GST throughout the 500 ns simulation, it showed a higher degree of motion in comparison with *Pf*GST:BA.

Similarly, plots of the *Pf*GST, *Pf*GST:BA, *Pv*GST, and *Pv*GST:TTMF systems' side chain root-mean-square-fluctuation (RMSF) values against the residue numbers based on the 500 ns simulation trajectory data was made. This is to give the measure of the average atomic fluctuations and thereby provide valuable information about the flexibility and dynamics of individual atoms or residues within the systems. In Fig. 3C, the RMSF plot shows the typical GST residues 1-211 and 212-424 correspond to both protein subunits A and B respectively. Also, the side chain fluctuations' general profiles across the four systems and their sub-units were seen to be comparable with little or no deviation in the protein-ligand complexes (Fig. 3C and D). compared with their apo structures all through the simulation period. In Fig 3C, the Cα-RMSF pattern is *Pf*GST (black) and *Pf*GST:BA (red), while in Fig. 3D the *Pv*GST (green), and *Pv*GST:TTMF (blue) are represented. The significantly low Cα-RMSF values indicate that the proteins' amino acid residues are relatively stable and have minimal fluctuations around their average positions. This is also an indication that these regions where BA and TTMF binds are structurally well-defined and that both BA and TTMF maintain a stable conformation throughout the simulation period.

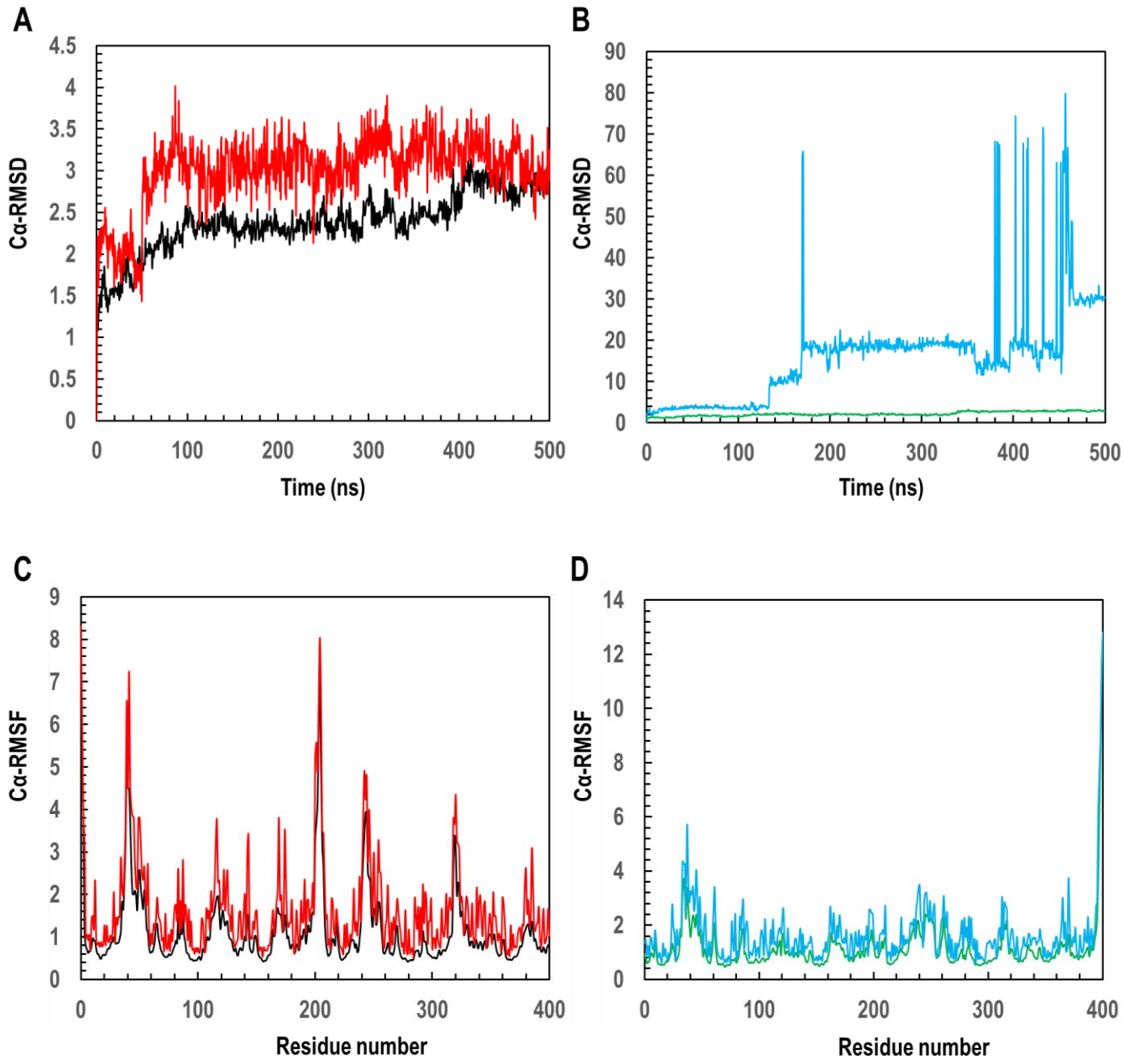


Fig. 4. Analysis of the simulation trajectory showing (A) the Cα-RMSD of *Pf*GST (**black**), *Pf*GST:BA (**red**) and (B) Cα-RMSD of *Pv*GST (**green**), and *Pv*GST:TTMF (**blue**). Also, the RMSF of the side chains as a function of the 500 ns simulation time for (C) apo-*Pf*GST (**black**), *Pf*GST:BA complex (**red**), and (D) apo-*Pv*GST (**green**), *Pv*GST:TTMF complex (**blue**).

Furthermore, in view of the understanding of the need to analyze the interactions which are essential for understanding the mechanisms of protein-ligand recognition, binding, and specificity,

the protein-ligand interactions was monitored and presented in Fig. 5. This knowledge is particularly useful in rational drug design, especially in the early stages Given that, the 500 ns simulations summarized and monitored protein-ligand interactions reveals that a combination of interactions namely hydrophobic and ionic interactions, hydrogen bond, and water bridges held and stabilized the two ligands within the proteins' dimer interphase. The hydrophobic interactions (which occur between nonpolar residues of the protein and hydrophobic regions of the ligand) played more role in the binding than the ionic (which occur between charged residues of the protein and oppositely charged groups of the ligand) interactions. While the role played by water bridges were significant, that of ionic interactions were insignificant in the binding and stability of BA with *Pf*GST (Fig. 5A) and TTMF with *Pv*GST (Fig. 5B).

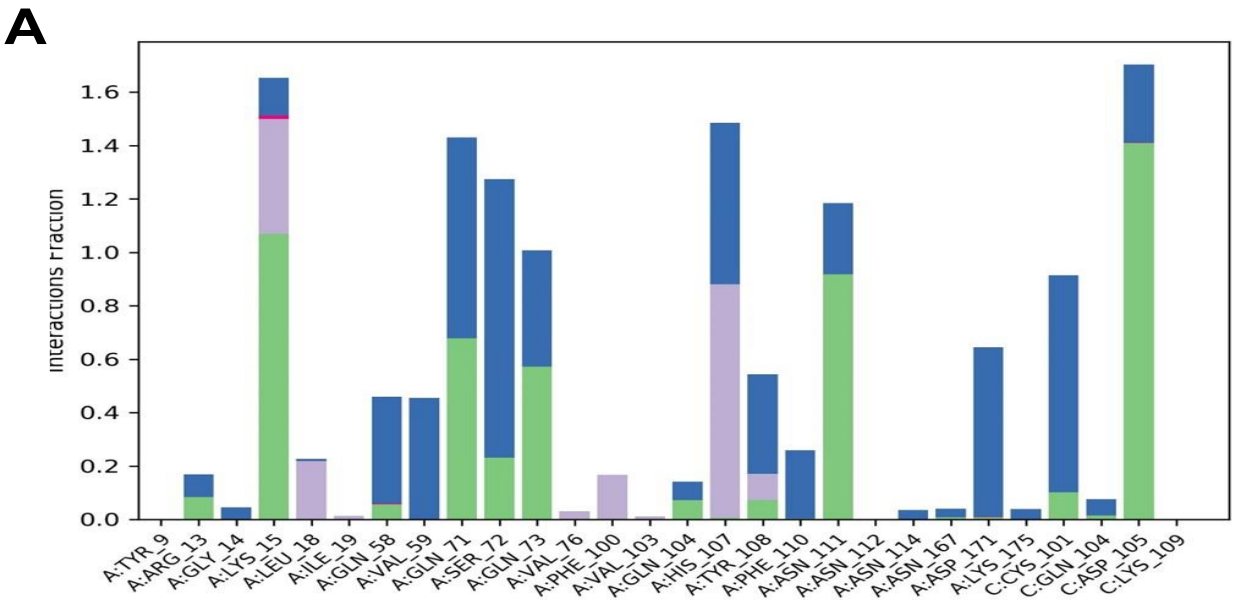

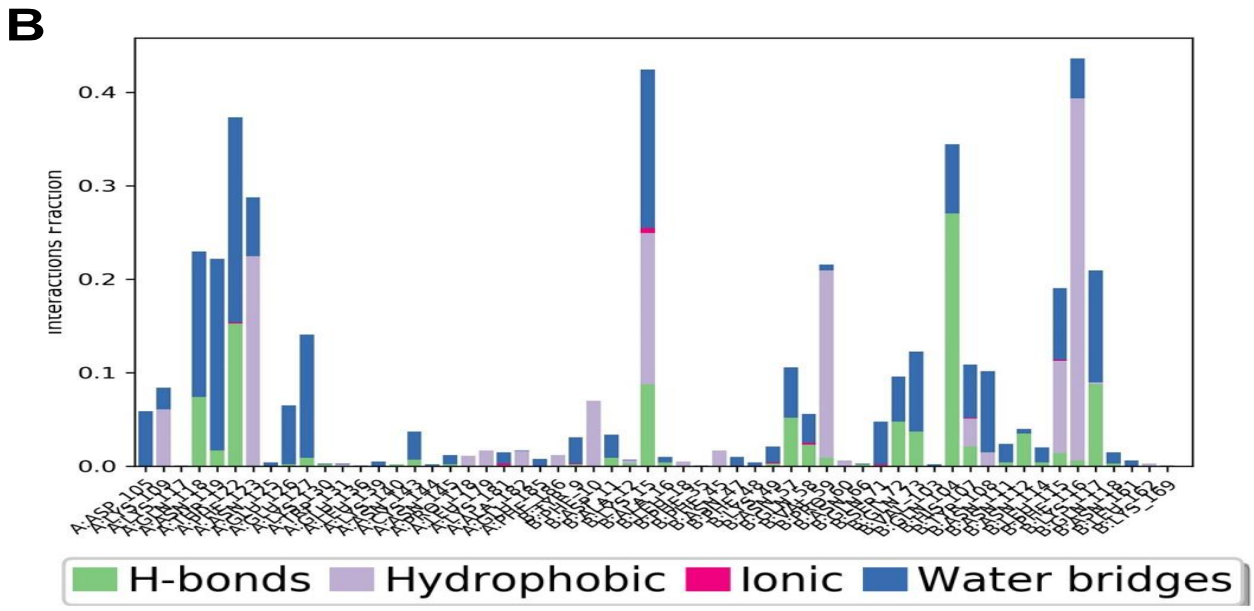


Fig. 5. Amino acid side chains interactions and types of interactions stacked bar charts between (A) *Pf*GST:BA and (B) *Pv*GST:TTMF, throughout the 500 ns simulation. The interaction diagram showed H-bonds are categorized into backbone acceptor; backbone donor; side-chain acceptor; side-chain donor. Hydrophobic interactions are categorized into π-cation; π-π*; and other, non-specific interactions. The stacked bar charts are normalized throughout the 500 ns trajectory. The images were obtained with the use of the Ligand Interaction Algorithm implemented in Maestro v13.0.

### 3.4. Molecular mechanics/generalized born and surface area solvation (MMGBSA) Analysis

The integral role of binding energy involved in molecule's interaction vis-à-vis the ligand-protein interaction that takes place in a biological system is seen in the descriptive estimate of the thermodynamics/energetics of the different components of the interaction energy that contribute to the binding. In this regard, the MM/GBSA free energy binding of BA and TTMF to the respective receptors *Pf*GST and *Pv*GST were then determined using the MM/GBSA algorithm implementable in Schrodinger Maestro v13.0. The calculated MM/GBSA energy components of the *Pf*GST:BA and *Pv*GST:TTMF interactions are presented in Table 2. The calculated $\Delta G_{bind}$ of BSP towards *Pf*GST and *Pv*GST are similar, being -13.59 and -16.39 kcal/mol. This negative $\Delta G_{bind}$ is indicative of the possibility of spontaneity in the binding reaction in both *Pf*GST and *Pv*GST. With that in mind, this result also shows that the interaction of BSP with *Pf*GST and *Pv*GST is thermodynamically favorable. The results also indicated that, although the gas phase energy acted opposite to the solvation free energy, it however contributed chiefly to the overall

$\Delta G_{bind}$. In addition, the result also presents that the binding of BSP with *Pf*GST and *Pv*GST is primarily brought about by van der Waals interactions.

Table 2. Calculated MM/GBSA energy binding of BA and TTMF's respective interaction with *Pf*GST and *Pv*GST

| **Protein Complex** | **Energy components (kcal/mol)** | | | | |
|---|---|---|---|---|---|
| | $\Delta E_{vdW}$ | $\Delta E_{ele}$ | $\Delta E_{gas}$ | $\Delta E_{sol}$ | $\Delta G_{bind}$ |
| *Pf*GST | −38.92 | 25.88 | −0.19 | 0.60 | −23.05 |
| *Pv*GST | −21.40 | -21.07 | −29.76 | 35.82 | −4.05 |

## 4. Conclusion

High-throughput virtual screening robustness as a computational tool to identify potential drug candidates against specific protein targets was employed to screen for natural compounds efficiently and reliably from vast libraries of compounds has been demonstrated in this research. Despite the inclusion of bromosulfophthalein and ellagic acid (with reported efficient binding and inhibitory activities against *Pf*GST and *Pv*GST) in the screened library, BA and TTMF showed best binding respectively with *Pf*GST and *Pv*GST. This is as they both came out as compounds with best top-scoring poses and with the lowest Glide Emodel energy values and docking score while docked with *Pf*GST and *Pv*GST. This result showed that BA and TTMF are predicted to bind tightly to *Pf*GST and *Pv*GST with lowest total energy associated with binding interaction. This is desirable for drug discovery and design identifying BA and TTMF as promising drug candidates as effective antimalarials targeting *Pf*GST and *Pv*GST. The results also showed that polar charged amino acid residues involvement in the binding interactions were essential in improving the binding affinity while also contributing to the specificity and stability of the bound complexes. The respective Cα RMSD and Cα RMSF revealed that the regions where BA and TTMF binds are structurally well-defined and that both BA and TTMF maintain a stable conformation throughout the simulation period. This is significant in that the various results positioned the two natural compounds as having better binding capabilities (than BSP and EA) to be explored as a potent antimalarials. While these results needs to be empirically validated, it has however spotlighted BA and TTMF for further studies as novel flavonoids to be developed as effective antimalarials.

**References**

Achilonu, I., Iwuchukwu, E.A., Achilonu, O.J., Fernandes, M.A., Sayed, Y., 2020. Targeting the SARS-CoV-2 main protease using FDA-approved Isavuconazonium, a P2–P3 α-ketoamide derivative and Pentagastrin: An in-silico drug discovery approach. J. Mol. Graph. Model. 101, 107730. https://doi.org/10.1016/j.jmgm.2020.107730

Akumadu, B.O., Pandian, R., Olfsen, J., Worth, R., Thulo, M., Mentor, T., Fanucchi, S., Sayed, Y., Dirr, H.W., Achilonu, I., 2020. Molecular basis of inhibition of Schistosoma japonicum glutathione transferase by ellagic acid: Insights into biophysical and structural studies. Mol. Biochem. Parasitol. 240, 111319. https://doi.org/10.1016/j.molbiopara.2020.111319

Al-Qattan, M.N.M., Mordi, M.N., 2023. Development and application of fragment-based de novo inhibitor design approaches against Plasmodium falciparum GST. J. Mol. Model. 29, 281. https://doi.org/10.1007/s00894-023-05650-0

Bergdorf, M., Kim, E.T., Rendleman, C.A., Shaw, D.E., 2014. Desmond/GPU Performance as of November 2014. Shaw Res. Tech. Rep. DESRES/TR—2014-01.

Boniface, P.K., Ferreira, E.I., 2019. Flavonoids as efficient scaffolds: Recent trends for malaria, leishmaniasis, Chagas disease, and dengue. Phyther. Res. 33, 2473–2517. https://doi.org/10. 1002/ptr.6383

Calic, P.P.S., Mansouri, M., Scammells, P.J., McGowan, S., 2020. Driving antimalarial design through understanding of target mechanism. Biochem. Soc. Trans. 48, 2067–2078. https://doi.org/10.1042/BST20200224

Chepkirui, C., Ochieng, P.J., Sarkar, B., Hussain, A., Pal, C., Yang, L.J., Coghi, P., Akala, H.M., Derese, S., Ndakala, A., 2021. Antiplasmodial and antileishmanial flavonoids from Mundulea sericea. Fitoterapia 149, 104796. https://doi.org/10. 1016/j.fitote.2020.104796

Choudhry, H., 2021. High-throughput screening to identify potential inhibitors of the Zα domain of the adenosine deaminase 1 (ADAR1). Saudi J. Biol. Sci. 28, 6297–6304. https://doi.org/10.1016/j.sjbs.2021.06.080

Conrad, M.D., Rosenthal, P.J., 2019. Conrad, M. D., & Rosenthal, P. J. (2019). Antimalarial drug resistance in Africa: the calm before the storm? The Lancet Infectious Diseases, 19(10),

e338–e351.Antimalarial drug resistance in Africa: the calm before the storm? Lancet Infect. Dis. 19, 338–351. https://doi.org/10.1016/S1473-3099(19)30261-0

Forte, B., Ottilie, S., Plater, A., Campo, B., Dechering, K.J., Gamo, F.J., Goldberg, D.E., Istvan, E.S., Lee, M., Lukens, A.K., 2021. Prioritization of molecular targets for antimalarial drug discovery. ACS Infect. Dis. 7, 2764–2776.

Friesner, R.A., Banks, J.L., Murphy, R.B., Halgren, T.A., Klicic, J.J., Mainz, D.T., Repasky, M.P., Knoll, E.H., Shelley, M., Perry, J.K., 2004. Glide: a new approach for rapid, accurate docking and scoring. 1. Method and assessment of docking accuracy. J. Med. Chem. 47, 1739–1749. https://doi.org/10.1021/jm0306430

Fritz-Wolf, K., Becker, A., Rahlfs, S., Harwaldt, P., Schirmer, R.H., Kabsch, W., Becker, K., 2003. X-ray structure of glutathione S-transferase from the malarial parasite Plasmodium falciparum. Proc. Natl. Acad. Sci. U. S. A. 100, 13821–13826. https://doi.org/10.1073/pnas.2333763100

Gilson, M.K., Given, J.A., Bush, B.L., McCammon, J.A., 1997. The statistical-thermodynamic basis for computation of binding affinities: a critical review. Biophys. J. 72, 1047–1069. https://doi.org/10.1016/S0006-3495(97)78756-3

Guantai, E., Chibale, K., 2011. How can natural products serve as a viable source of lead compounds for the development of new/novel anti-malarials? Malar. J. 10, 1–8. https://doi.org/10.1186/1475-2875-10-S1-S2

H Gilbert, I., Leroy, D., A Frearson, J., 2011. Finding new hits in neglected disease projects: target or phenotypic based screening? Curr. Top. Med. Chem. 11, 1284–1291. https://doi.org/10.2174/156802611795429176

Haldar, K., Bhattacharjee, S., Safeukui, I., 2018. Drug resistance in Plasmodium. Nat. Rev. Microbiol. 16, 156–170. https://doi.org/10.1038/nrmicro.2017.161

Hu, H., Li, W., Hao, Y., Peng, Z., Zou, Z., Liang, W., 2024. Baicalin ameliorates renal fibrosis by upregulating CPT1α-mediated fatty acid oxidation in diabetic kidney disease. Phytomedicine 122, 155162. https://doi.org/10.1016/j.phymed.2023.155162

Kaur, T., Madgulkar, A., Bhalekar, M., Asgaonkar, K., 2019. Molecular docking in formulation

and development. Curr. Drug Discov. Technol. 16, 30–39. https://doi.org/10.2174/1570163815666180219112421file:///C:/Users/Administrator/Downloads/scholar - 2024-03-21T133232.509.ris

Kingston, D.G.I., Cassera, M.B., 2022. Antimalarial natural products. Springer. https://doi.org/10.1007/978-3-030-89873-1_1

Kollman, P.A., Massova, I., Reyes, C., Kuhn, B., Huo, S., Chong, L., Lee, M., Lee, T., Duan, Y., Wang, W., 2000. Calculating structures and free energies of complex molecules: combining molecular mechanics and continuum models. Acc. Chem. Res. 33, 889–897. https://doi.org/10.1021/ar000033j

Lucy, D., Zhang, L., Tate, E.W., 2020. A Natural Product Puts Malaria on a Low-Fat Diet. Cell Chem. Biol. 27, 137–139. https://doi.org/10.1016/j.chembiol.2020.02.001

Madhavaram, M., Nampally, V., Gangadhari, S., Palnati, M.K., Tigulla, P., 2019. High-throughput virtual screening, ADME analysis, and estimation of MM/GBSA binding-free energies of azoles as potential inhibitors of Mycobacterium tuberculosis H37Rv. J. Recept. Signal Transduct. 39, 312–320. https://doi.org/10.1080/10799893.2019.1660895

Massova, I., Kollman, P.A., 2000. Combined molecular mechanical and continuum solvent approach (MM-PBSA/GBSA) to predict ligand binding. Perspect. drug Discov. Des. 18, 113–135. https://doi.org/10.1023/A:1008763014207

Penna-Coutinho, J., Aguiar, A.C.C., 2018. Commercial drugs containing flavonoids are active in mice with malaria and in vitro against chloroquine-resistant Plasmodium falciparum. Mem. Inst. Oswaldo Cruz 113, e180279. https://doi.org/10.1590/0074-02760180279

Pooe, K., Thulo, M., Makumbe, H., Akumadu, B., Otun, O., Aloke, C., Achilonu, I., 2022. Biophysical description of Bromosulfophthalein interaction with the 28-kDa glutathione transferase from Schistosoma japonicum. Mol. Biochem. Parasitol. 252, 111524. https://doi.org/10.1016/j.molbiopara.2022.111524

Pooe, K., Worth, R., Iwuchukwu, E.A., Dirr, H.W., Achilonu, I., 2021. An empirical and theoretical description of Schistosoma japonicum glutathione transferase inhibition by bromosulfophthalein and indanyloxyacetic acid 94. J. Mol. Struct. 1223, 128892.

https://doi.org/10.1016/j.molstruc.2020.128892

Rameshkumar, M.R., Indu, P., Arunagirinathan, N., Venkatadri, B., El-Serehy, H.A., Ahmad, A., 2021. Computational selection of flavonoid compounds as inhibitors against SARS-CoV-2 main protease, RNA-dependent RNA polymerase and spike proteins: A molecular docking study. Saudi J. Biol. Sci. 28, 448–458. https://doi.org/10.1016/j.sjbs.2020.10.028

Rasmussen, C., Alonso, P., Ringwald, P., 2022. Current and emerging strategies to combat antimalarial resistance. Expert Rev. Anti. Infect. Ther. 20, 353–372. https://doi.org/10.1080/14787210.2021.1962291

REDDY CHINNAPPANNA, N.K., Yennam, G., Chaitanya, C.B.H.N.V., Pottathil, S., Borah, P., Venugopala, K.N., KISHORE DEB, P., PRASAD MAILAVARAM, R., 2023. Recent approaches in the drug research and development of novel antimalarial drugs with new targets. Acta Pharm. 73, 1–27. https://doi.org/10.2478/acph-2023-0001

Rehman, M.T., AlAjmi, M.F., Hussain, A., Rather, G.M., Khan, M.A., 2019. High-throughput virtual screening, molecular dynamics simulation, and enzyme kinetics identified ZINC84525623 as a potential inhibitor of NDM-1. Int. J. Mol. Sci. 20, 819. https://doi.org/10.3390/ijms20040819

Release, S., 2014. 1: Desmond molecular dynamics system, version 3.7. Shaw Res. New York, NY, Maest. Interoperability Tools, version.

Sarma, M., Abdalla, M., Zothantluanga, J.H., Abdullah Thagfan, F., Umar, A.K., Chetia, D., Almanaa, T.N., Al-Shouli, S.T., 2023. Multi-target molecular dynamic simulations reveal glutathione-S-transferase as the most favorable drug target of knipholone in Plasmodium falciparum. J. Biomol. Struct. Dyn. 1–17. https://doi.org/10.1080/07391102.2023.2175378

Singh, A.P., Rathi, B., 2023. Advances in Anti-Malarial Drug Discovery. Front. Drug Discov. 3, 1–2. https://doi.org/10.3389/fddsv.2023.1335842

Siqueira-Neto, J.L., Wicht, K.J., Chibale, K., Burrows, J.N., Fidock, D.A., Winzeler, E.A., 2023. Antimalarial drug discovery: progress and approaches. Nat. Rev. Drug Discov. 22, 807–826. https://doi.org/10.1038/s41573-023-00772-9

Song, M., Liu, Y., Li, T., Liu, X., Hao, Z., Ding, S., Panichayupakaranant, P., Zhu, K., Shen, J.,

2021. Plant natural flavonoids against multidrug resistant pathogens. Adv. Sci. 8, 2100749. https://doi.org/10.1002/advs.202100749

Swinney, D.C., 2013. Phenotypic vs. target-based drug discovery for first-in-class medicines. Clin. Pharmacol. Ther. 93, 299–301. https://doi.org/10.1038/ clpt.2012.236

Sykes, M.L., Avery, V.M., 2013. Approaches to protozoan drug discovery: phenotypic screening: miniperspectives series on phenotypic screening for antiinfective targets. J. Med. Chem. 56, 7727–7740. https://doi.org/10. 1021/jm4004279

Tse, E.G., Korsik, M., Todd, M.H., 2019. The past, present and future of anti-malarial medicines. Malar. J. 18, 1–21. https://doi.org/10.1186/s12936-019-2724-z

Tsui, V., Case, D.A., 2000. Theory and applications of the generalized Born solvation model in macromolecular simulations. Biopolym. Orig. Res. Biomol. 56, 275–291. https://doi.org/10.1002/1097-0282(2000)56:4<275::AID-BIP10024>3.0.CO;2-E

Valli, A., Achilonu, I., 2022. Comparative structural analysis of the human and Schistosoma glutathione transferase dimer interface using selective binding of bromosulfophthalein. Proteins Struct. Funct. Bioinforma. 90, 1561–1569. https://doi.org/10.1002/prot.26338

Wang, E., Sun, H., Wang, J., Wang, Z., Liu, H., Zhang, J.Z.H., Hou, T., 2019. End-point binding free energy calculation with MM/PBSA and MM/GBSA: strategies and applications in drug design. Chem. Rev. 119, 9478–9508. https://doi.org/10.1021/acs.chemrev.9b00055

Wicht, K.J., Mok, S., Fidock, D.A., 2020. Molecular mechanisms of drug resistance in Plasmodium falciparum malaria. Annu. Rev. Microbiol. 74, 431–454. https://doi.org/10.1146/annurev-micro-020518- 115546

World Health Organization, 2022. World malaria report 2022. World Health Organization.

Yang, T., Ottilie, S., Istvan, E.S., Godinez-Macias, K.P., Lukens, A.K., Baragaña, B., Campo, B., Walpole, C., Niles, J.C., Chibale, K., Dechering, K.J., Llinás, M., Lee, M.C.S., Kato, N., Wyllie, S., McNamara, C.W., Gamo, F.J., Burrows, J., Fidock, D.A., Goldberg, D.E., Gilbert, I.H., Wirth, D.F., Winzeler, E.A., 2021. MalDA, Accelerating Malaria Drug Discovery. Trends Parasitol. 37, 493–507. https://doi.org/10.1016/j.pt.2021.01.009

Yazdiniapour, Z., Yegdaneh, A., Akbari, S., 2021. Isolation and characterization of methylated

flavones from Artemisia kermanensis. Adv. Biomed. Res. 10, 1–4. https://doi.org/10.4103/abr.abr_1_21

Zhou, H.-X., Pang, X., 2018. Electrostatic interactions in protein structure, folding, binding, and condensation. Chem. Rev. 118, 1691–1741. https://doi.org/10.1021/acs.chemrev.7b00305

Zothantluanga, J.H., Chetia, D., Rajkhowa, S., Umar, A.K., 2023. Unsupervised machine learning, QSAR modelling and web tool development for streamlining the lead identification process of antimalarial flavonoids. SAR QSAR Environ. Res. 34, 117–146. https://doi.org/10.1080/1062936X.2023.2169347

# Chapter 7

## Summary and conclusion of the study

There has been extensive research into the targetability of Glutathione *S*-Transferase (GST) as a potential drug target in *Plasmodium falciparum* (*Pf*GST) and *Plasmodium vivax* (*Pv*GST). The literature review put together in this study has insightfully and novelly provided the scientific significance of targeting the inhibition of phase II detoxification enzymes in *Plasmodium* parasite vis-à-vis in *Pf*GST and *Pv*GST. The significance and different approaches employed in targeting GST's inhibition in both *Plasmodium falciparum* and *Plasmodium vixax*, which are two most responsible malaria causing parasites in Africa and Asia respectively, have been sufficiently presented in this study. The *Pf*GST and *Pv*GST enzymes was successfully and recombinantly overexpressed and purified to high purity, thereby making the suitable for the various biophysical characterizations carried out in this study. All techniques employed in this study were according to standard protocols previously reported and are done with reproducibility quality in view.

The effective management and drug treatment of malaria using glutathione-conjugation and biotransformation enzyme inhibition pathway, vis-à-vis the binding by antimalarial drugs, has not been fully explored till date. This study, therefore, systematically characterize *Pf*GST and *Pv*GST's ligandin properties towards artemisinin, artemether, artesunate, amodiaquine, lumefantrine, mefloquine, and pyrimethamine. While various characterizations techniques employed in this study show not all the antimalarials used in this study are glutathionylated, all are however biotransformed by *Pf*GST and *Pf*GST. This result is not totally unexpected given the reported inefficiency and resistance associated with the antimalarial drugs. This result therefore led to the search towards the discovering potent drug candidates that could be positioned as an alternative effective antimalarial. Given that background, a first time insightful and novel description via an empirical and computational modelling studies of the ligandin ability of bromosulfophthalein (BSP) towards *Pf*GST and *Pv*GST was there carried out in this study. Through the systematic integration of different biophysical techniques and computational modelling studies, the study shows BSP's ability to tightly bind and inhibit *Plasmodium falciparum* GST (*Pf*GST) and *Plasmodium vivax* GST (*Pv*GST). This result further reveals BSP's excellent ability to disrupt both target's detoxification ability and also reduce their antioxidant capacity. This result ultimately positions BSP as a potent antimalarial having critical features expected of an effective antimalarial.

In the face of natural compounds' vis-à-vis flavonoid's pharmacological effects as antiplasmodial, with potentials explorable as likely scaffold towards the development of new antimalarials, this study further explore a high-throughput virtual screen to probe a large library of flavonoids for potent compound. Hence this research computationally screened and probed baicalin (BA) and 5, 7,3'-Trihydroxy-6,4',5'-trimethoxyflavone (TTMF) as potential inhibitor with improved binding and inhibitory ability than BSP against *Pf*GST and *Pv*GST respectively. Both Baicalin and 5,7,3'-Trihydroxy-6,4',5'-trimethoxyflavone results validated their reported antioxidant properties, which help mitigate the oxidative stress induced by *Plasmodium* infection. This additional therapeutic benefit will contribute to their overall antimalarial efficacy. Given these reported mechanisms of action and the results obtained in this study, flavonoids indeed represent a promising class of compounds for developing new antimalarial drugs, particularly in the face of growing drug resistance. Justifiably, the attention as potential antimalarial agents due to their significant effectiveness against the *Plasmodium* parasite has been scientifically proven. These naturally occurring polyphenolic compounds, commonly found in various plants, have unique biochemical properties that disrupt the malaria parasite's life cycle, making them promising candidates for antimalarial drug development and need to be positioned as future antimalarial.

The systematic integration and use of empirical and computational studies to investigate protein-ligand interactions is critical and has proven effective in this study in the search for effective antimalarial treatments. These approaches provide complementary insights that significantly enhance our understanding of how potential drug candidates interact with specific protein targets within the malaria parasite. The empirical methods provide detailed insights into the binding affinities, kinetics, and structural conformations of the protein-ligand complexes. By empirically determining/affirming the binding site and interaction strength, the study assesses the potential efficacy of the ligands as antimalarial agents. Additionally, these studies help identify key amino acids involved in the interaction, validating the design of ligands with improved binding efficiency and specificity. On the other hand, the computational studies employed in this study with advanced algorithms and simulations, help predict and analyze protein-ligand interactions on a molecular level. Techniques like molecular docking, molecular dynamics simulations, and molecular mechanics/generalized born solvent area (MM/GBSA) calculations offer valuable insights into the dynamic behaviour and energetics of these interactions. High throughput virtual screening allows for the screening of large libraries of compounds rapidly, predicting their binding modes and

affinities before empirical testing. This combinatorial approach will, in no doubt help accelerate the drug discovery process by focusing experimental efforts on the most promising candidates. Conclusively, the following probable inhibitors discovered in this study, namely BSP, BA and TTMF, need to be further investigated so as to be validated as antimalarial.

**Limitation of the study**

Despite the successful completion of this study, the following limitations are however worthy of note and they include

a. Unavailability of the synthesizable flavonoid compounds (BA and TTMF) from *MedChemExpress* as at the time this study was nearing completion. This led to inability to empirically validate the results of the HTVS and MDS results component of the study.
b. The insufficiency of time to solve a crystal structure of BSP complexed *Pf*GST. While preliminary attempts showed successful crystallization and diffraction at 1.7 Å resolution, however the data collection were not as good as expected.
c. The lack of time to crystalize and solve for the first time, the crystal structure of *Pv*GST. This is as no crystal structure of *Pv*GST has been deposited in the Protein Data Bank as at the time of submitting this study for examination.

**Future Perspective.**

The limitations itemized above form the basis for the work to be carried out relating to this study. This will include

a. Empirical studies through biophysical characterizations to validate BA and TTMF's ability as an effective inhibitor of the functionalities of the ligandin properties of *Pf*GST and *Pv*GST.
b. Putting together the systematic integration of the empirical validation of (a) above with the theoretical studies already carried out, and submit the important findings as manuscript for publication in a peer-reviewed journal
c. *in vitro*, *in vivo*, and *ex vivo* studies will be conducted to ascertain the efficacy of these three identified compounds on malarial cell and animal models.

d. Based on the study's results, some of the compounds may be derivatized from theoretical chemistry perspectives to give compounds with better pharmacokinetics and pharmacodynamics properties.
e. Crystallization of BSP complexed *Pf*GST, Apo *Pv*GST and complexed with any other discovered ligands.